Modelling and measurement of diode rectifiers and their interaction with shunt active filters

Hamish Duncan Laird, B.E.(Hons), M.E.

A thesis presented for the degree of
Doctor of Philosophy
in
Electrical and Electronic Engineering
at the
University of Canterbury,
Christchurch, New Zealand.

August 2001

ABSTRACT

The use of power conditioning equipment, such as the shunt active filter, is becoming more popular to remedy power quality problems associated with non-linear rectifier loads. Typically in the shunt active filter situation the non-linear load is considered to be insensitive to the terminal voltage variation. This assumption is made tacitly by modelling the non-linear load as a constant current source. In fact all loads, including non-linear rectifier type loads, are sensitive to voltage variation at their terminals. Since a shunt active filter changes the terminal voltage when it operates by changing the current flowing in the AC system, the shunt active filter can change the current in the non-linear load. The interaction of the non-linear load with the shunt active filter has implications for the power quality delivered by and to that load.

In order to determine the interaction of the non-linear load with the shunt active filter and the AC system a control system approach is taken. This shows that the non-linear load contributes to the control behaviour of the shunt active filter because it forms part of the forward control transfer. A suitable model for the non-linear load is required because classical linear system cannot accurately represent the non-linearity.

A small-signal frequency domain model is used to represent the non-linear load. This model completely and accurately includes the modulation with a frequency transfer matrix by including the phase dependent nature of the modulation results. The frequency domain model ensures that modulation is represented in a linear way. This means the evaluation of the non-linear load response is achieved by the solution of the linear equation set given by its frequency transfer matrix.

The very common single-phase rectifier is analysed using this frequency domain approach. The two rectifier small signal transfer mechanisms, by which it connects its AC and DC sides, are the base switching and the switching instant modulation. Partitioning the rectifier into appropriate partial transfers and then using the small signal approach allows both these mechanisms to be analysed. The effect of the switching instant modulation is found to be second order and so is ignored in this analytic model. The component transfers and the total transfer are validated by time domain simulation. The model shows excellent accuracy.

Experimental measurements of the single-phase rectifier are made by injecting AC current perturbations with a DSP controlled converter and measuring the small signal

load current response. These measurements show good correlation to those predicted by the analytic model. The analytic model also allows the calculation of the effect of shunt active filter operation on the single-phase rectifier current. Measurements of a three-phase rectifier are made and the first order sequence coupling nature of this device for both continuous and discontinuous DC side current conduction is demonstrated. This shows that the three-phase rectifier behaviour can be modelled and analysed using the same frequency transfer matrix approach as used for the single-phase rectifier.

To martyr yourself to caution is not going to help at all, because there is no safety in numbers when the right one walks out the door.

Pink Floyd, 1994.

ACKNOWLEDGEMENTS

I must thank my supervisor, Dr Simon Round, for his encouragement, support and calm good humour throughout my studies. His commitment and enthusiasm have been invaluable inspirations. Thanks also to Dr Richard Duke for his help with this work and also with previous graduate work.

There have been other postgraduate students who have helped with discussions covering both work and other non related subjects such as rugby, drinking, tramping and life in general. These people include Dave Hume, Chris Osauskas, Phil Talacek, Karen Kennedy, Dr. Rick Liew, Matt O'Neil, Dr. Graeme Bathurst, Dr. Simon Todd, Dr. Bruce Smith, Dr. Tom Keppler, Dave Ingram, Paul Sinclair, Adam Taylor, Dr. Cressida Harding, Valerie Leung, and Dr. Sharee McNab. I wish all of them well for the future.

Thanks to the other staff who have helped especially Ron Battersby, Dermot Sallis, Scott Lloyd, Steve Weddel, Jack Woudberg, Dudley Berry, Ken Smart, Mike Shurety, Dave van Leeuwan, Florin Predan, Pieter Kikstra and Dr. Alan Wood.

The financial support from the FRST through Industrial Research made my study possible and to Alister Gardiner and Roger Brough I owe many thanks. A special thanks to Roger his technical support.

The other people in my life who I owe thanks to are all my family and friends. A special thanks to the Dragons Ice Hockey team, the Redbacks Inline Hockey people, especially the under ten team and their supporters, and the Inline referees. These people have all contributed to my happiness during the course of this work. I also like to thank Dr. Tim Jones for his advice, support and help. I must acknowledge also Shane Crimp for his friendship, advice, support and good company.

Finally I must thank Nicola, my partner. Her support has been great and her company an honour. At times she must have presumed me insane and I thank her for accepting that situation without too much fuss. I am sure that the 310ers curse will not apply to her.

I have spent about twenty one and a half of my almost thirty three years studying. I am just now getting the feeling that I am ready to do something else.

PUBLISHED PAPERS

The following papers were published as a result of the work associated with that presented in this thesis.

Power quality observations at a light industrial site.
H.D. Laird, S.D. Round, R.M. Duke, and A. Gardiner.
8th International Conference on Harmonics and Quality of Power.
October 1998, Athens, Greece. pp 88-93.

The transient and steady state performance of a shunt active filter using measured site data.
S.D. Round, H.D. Laird, R.M. Duke and A. Gardiner.
8th International Conference on Harmonics and Quality of Power.
October 1998, Athens, Greece. pp 395-400.

A robust controller for a shunt active filter.
B.C. Cooper, S.D. Round, H.D. Laird and R.M. Duke
Australasian Universities Power Engineering Conference.
1998 Hobart, Tasmania, Australia. pp 566-571.

An improved three level shunt active filter.
S. D. Round, H. D. Laird, R. M. Duke, and C. Tuck
International Conference on Power Electronics Drives and Energy Systems for Industrial Growth.
December 1998, Perth, Western Australia. pp 12 -20.

A frequency domain model of an uncontrolled single-phase voltage source rectifier.
H. D. Laird, S. D. Round, and R. M. Duke.
IEEE Transactions on Industrial Electronics.,
Vol. 47, No. 3, June 2000. pp 525–532.

Incorporating non-linear load characteristics into the control transfer of a shunt active filter.
H. D. Laird, S. D. Round, and R. M. Duke.
International Power Engineering Conference.
April 2000, Tokyo, Japan. pp 2180–2186

Incorporating the characteristics of a non-linear load into the control transfer of a shunt active filter.
H. D. Laird, S. D. Round, and R. M. Duke.
Submitted to *IEEE Transactions on Industrial Electronics.*

GLOSSARY

Symbols

α	Two phase stationary signal component
β	Two phase stationary signal component
$\Delta\theta_1$	Change in turn on switching instant
$\Delta\theta_2$	Change in turn off switching instant
ΔV_{AC}	AC side perturbing voltage or change in AC side voltage
ΔV_{DC}	DC side perturbing voltage or change in DC side voltage
ΔI_{AC}	Change in AC side current
ΔI_{DC}	Change in AC side current
$\Delta I_{DC_{Part}}$	Change in DC side current due to base switching
ΔI_{PSSC}	Pseudo steady state current
ΔI_L	Change in the load current
ΔV_{DCBUS}	Change in DC bus voltage
δ_k	Perturbing voltage phase
θ_1	Angle of turn on switching instant
θ_2	Angle of turn off switching instant
a	A phase quantity
b	B phase quantity
c	C phase quantity
C	Capacitance
$Cont$	Shunt active filter controller transfer
C_{PFC}	Power factor correction capacitance
d	Direct rotating component
$diff_{real}$	Real part of difference term phasor
$diff_{imag}$	Imaginary part of difference term phasor
f_0	Fundamental frequency in Hz
f_{step}	Frequency step in FTM
h	Arbitrary amplitude
I_{AC}	Base AC side current
I_{Base}	Base case current
I_{DC}	Base DC side current

I_{AF}	Active filter current
I_{Inj}	Experimentally injected perturbing current
I_L	Load current
I_S	Supply current
I_{System}	Current in AC system
in_{real}	Real part of example input phasor
in_{imag}	Imaginary part of example input phasor
j	$\sqrt{(}-1)$
kf_0	Frequency of perturbing voltage in Hz
$k\omega_0$	Frequency of perturbing voltage in rads/s
l	FTM index
L	Inductance
$m\omega_0$	Harmonic frequencies for $m = 1, 2, 3, ...$
M	Fundamental supply voltage magnitude
ω_0	Fundamental frequency in rads/s
$\omega_0 t$	Angular time
out_{real}	Real part of example output phasor
out_{imag}	Imaginary part of example output phasor
q	Quadrature rotating component
R	DC side load resistance
R_{Load}	AC Load resistance
R_{Sys}	AC System resistance
sum_{real}	Real part of sum term phasor
sum_{imag}	Imaginary part of sum term phasor
t	Time
V_{AC}	Supply voltage at load terminal
V_{Drop}	Voltage drop in AC system
V_{PC}	Point of coupling voltage
V_{DCBUS}	DC bus voltage
V_{DC}	Rectifier DC side voltage
Ψ	Rectifier switching function Fourier series.
Ψ_{Simod}	Switching modulation function Fourier series.
V_k	Perturbing voltage magnitude
V_{Base}	Base case voltage
V_S	AC Supply voltage
$x + jy$	Arbitrary complex number
X_k	Sinusoidal signal
Y_m	Sinusoidal signal
$\mathbf{X_k}$	Phasor form of X_k
$\mathbf{Y_m}$	Phasor form of Y_m

Y_{PFC}	Admittance of power factor correction capacitor
Y_{Load}	Load admittance
Z_{Load}	Load impedance
Z_{Sys}	AC system impedance
$\mathbf{A}$	V_{AC} to I_{AC} transfer Frequency Transfer Matrix
$\mathbf{B}$	V_{DC} to I_{AC} transfer FTM
$\mathbf{C}$	V_{AC} to I_{DC} transfer FTM
Cont	Shunt active filter controller FTM
$\mathbf{D}$	V_{DC} to I_{DC} transfer FTM
$\mathbf{I}$	Identity matrix
$\mathbf{Y_{DCFilter}}$	DC side filter admittance FTM
$\mathbf{Y_{Load}}$	Load admittance FTM
$\mathbf{Z_{Sys}}$	System Impedance FTM

Abbreviations

AC	Alternating Current
ADC	Analogue to Digital Converter
DC	Direct Current
DSP	Digital Signal Processor
DVR	Dynamic Voltage Restorer
EMC	Electromagnetic Compatibility
EMTDC	Electro-Magnetic Transients for Direct Current
EMTP	Electro-Magnetic Transients Program
FFT	Fast Fourier Transform
FPGA	Feild Programmable Gate Array
FTM	Frequency Transfer Matrix
HVDC	High Voltage Direct Current
IEC	International Electrotechnical Commission
IEEE	Institute of Electrical and Electronic Engineers
IGBT	Insulated Gate Bipolar Transistor
IGCT	Integrated Gate Commutated Thyristor
IRPT	Instantaneous Reactive Power Theory
LCM	Load Current Measurement
LTI	Linear Time Invariant
MIMO	Multiple Input Multiple Output
PAM	Pulse Amplitude Modulation
PC	Personal Computer
PLL	Phased Locked Loop
PSCAD	Power System Computer Aided Draughting program

PSSC	Pseudo Steady State Current
RAM	Random Access Memory
RMS	Root Mean Square
RTDS	Real Time Digital Simulator
SAF	Shunt Active Filter
SCL	Serial Communications Link
SCM	Supply Current Measurement
SIV	Switching Instant Variation
SIMO	Single Input Multiple Output
SISO	Single Input Single Output
SRF	Synchronous Reference Frame
STATCOM	Static Compensator
SVC	Static VAr Compensator
SVM	Supply Voltage Measurement
TCSC	Thyristor Controlled Series Capacitor
TCR	Thyrustor Controlled Reactor
THD	Total Harmonic Distortion
VAr	Volt Amp Reactive (Unit of reactive power)
VCO	Voltage Controlled Oscillator

CONTENTS

LIST OF FIGURES

LIST OF TABLES

Chapter 1

INTRODUCTION

1.1 POWER QUALITY

The concept of electrical power quality is a subject currently attracting a large amount of interest [Heydt 1991]. As the power system of a number of countries moves from a highly regulated utility industry to one where a market is created with the intention of forcing behaviour that maximises total benefit on market participants, power quality is becoming increasingly important. The main reason for this is that market orientation forces the most efficient use of equipment at times operating near or at its physical limits. The principal difficulty in defining and measuring power quality is that the focus of the electric power industry has, for a long time, been the generation, transmission and distribution parts of the industry. However power quality implicitly involves the customer and as with all consumer or end user involvement there is much variability in the customers' needs, expectations and desires. This makes power quality a very difficult area to analyse in a totally deterministic way in anything other than a case by case manner.

In purchasing goods other than electrical power customers require products that are fit for purpose. It is difficult to make a fit for purpose determination with electrical power by analysing only the network or waveform. That is, for a customer who uses electric power for lighting and heating, a variability, such as a sag or dip in the supply voltage may have little effect while the same power incident may be catastrophic for a manufacturer using some continuous process such as extrusion, winding or wafer processing. This means that the sensitivity of the load and the process are, if not determining factors, at least contributing factors for the power quality as seen by the customer [Abi-Samra *et al.* 1996a, Abi-Samra *et al.* 1996b]. Attempts to determine the number of sags and dips in electrical power systems have been made. These surveys typically survey the number of sags and produce a statistical distribution with sags categorised by magnitude [Bollen *et al.* 1997, Koval and Hughes 1997]. The determination of the cost of a sag or interruption has also been surveyed by analysing customer loads and processes and by asking the customer to estimate the cost of an

interruption or sag [Sullivan *et al.* 1997]. This approach allows utilities to determine which, if any, customer has high sensitivity to the quality of the power delivered from the network. However analytic methods to determine the sensitivity of the customer's plant are not presently available.

The network centric approach to power quality means that the network operator or owner treats the network as an area that should not be overly contaminated. Other authors [Round 1992, Redl *et al.* 1996] have noted that power system disturbances, be they steady state or transient in nature, are a pollution of the power system. Such a concept is very useful for steady state disturbances in the power system as they are generally cumulative. Steady state disturbances are typically harmonic currents generated by non-linear loads [Arrillaga *et al.* 1985], the use of which has increased so that between 50% to 60% of all electric power used in industrialised countries now flows through some power electronic system [Redl *et al.* 1996]. This increase in harmonic current producing loads causes a corresponding increase in the harmonic voltage in the network. An example of this is the network in Switzerland where the harmonic content of the 230V supply level system has increased from 3.6% in 1979 to 4.7% in 1991 [Redl *et al.* 1996].

The effects of the increasing voltage and current harmonic content of power systems have been surveyed [Arrillaga *et al.* 1985, IEEE 1983, Shaughnessy 1997]. They include increased losses in rotating machines, torque ripple in rotating machines, overvoltages from system resonances which can cause insulator breakdown, zero crossing detection errors in phase angle control systems, ripple control interference, power line communication problems, errors in power metering and interference in telecommunications systems. Methods to diagnose and correct these problems have been developed [Michaels 1997]. One estimate of the amount presently spent on "cleaning up" the power supply in the USA is $ 1.2 billion per year [Bernard 1997]. This figure is said to be rising. Typically there are limits put on the permissible network harmonic voltages and the harmonic currents allowed to flow from a load. Standards such as the IEEE-519 [IEEE 1992] limit the harmonic current a load may inject with regard to the short circuit ratio and also the allowable terminal voltage harmonics. This allows the network operator to limit harmonic currents and the customers are supplied with a voltage below a set distortion level. The IEC approach to the problem is to include the load harmonic current behaviour in EMC requirements, making generic current limits for each individual piece of electrical equipment [IEC 1995]. This approach aims to prevent problems occurring by keeping the harmonic current of the network low. In order to move away from a regulated approach the possibility of charging consumers for the harmonic current has been proposed and possible methods to do this have been explored [McEachern *et al.* 1995]. The marginal pricing of harmonics is also being investigated, however the operation of such a system depends somewhat on the allocation of property rights in the network [Talacek and Watson 1999]. This property right de-

cision which is whether the customers own the right to pollute or the right to a clean supply, is a political decision which seems far removed from the typically deterministic engineering traditionally associated with power networks.

Traditionally the power system has been viewed as a means to transfer power from generator to load effectively completing the transfer of a good in return for compensation. As deregulation is used there is the possibility that a number of people will own the electric power as it is transfered from generator to end user. In these situations the responsibility for ensuring that the power quality delivered to a customer is yet to be well defined [Arrillaga *et al.* 2000]. The market approach brings possibility of problems because the power system is typically operated at or near to physical limits which makes the marginal cost of connecting the next load high. In other words, the AC power system operates transmitting maximum allowable power thus ensuring maximum return on invested capital. A physical limit such as a line current rating or voltage limit can prevent increased power being transfered. This means that the next load to connect cannot be supplied, effectively making its marginal price the cost of the necessary line upgrade. In the harmonic current injection case, the analogous situation is that the customer that causes another customer or the network a cost must pay that cost.

In attempting to quantify the cost or benefit of power quality the market approach differs from the traditional network centric power quality definitions where low voltage and current distortion levels and low numbers of sags and interruptions mean high power quality. When the customer is considered these traditional definitions struggle to provide blanket assurances of power quality.

1.1.1 Power quality measures

The traditional measures used in power quality studies reflect the network centric focus of power quality study. The total harmonic distortion (THD) of the voltage or current is often quoted as a measure of power quality with lower THD being better. THD is defined in equation (1.1).

$$THD = \frac{\sqrt{\sum_{h=2}^{\infty} I_h}}{I_1} \tag{1.1}$$

Other measures include weighted THD type measurements with emphasis at frequencies used in telecommunications [Arrillaga *et al.* 1985] and the crest factor which gives a measure of the peak of a waveform to its RMS. However as with all power quality measures, the construction of a figure of merit removes information. It is apparent that the THD measurement removes all phase information because only magnitude information is retained. It is possible that the phase of the distortion could be relevant to the power quality for a certain customer. Power quality is therefore not able to be

described completely by THD or any other single number. Statistical reliability, availability and force outage approaches may be end up being the appropriate frameworks to view power quality [Arrillaga *et al.* 2000].

In summary, measuring power quality is difficult because it must involve the customers needs and expectations. This means that the traditional measures of power quality are difficult to use as indicators of power quality. This lack of measurability does not mean that power quality does not exist. In fact as with all quality considerations *people know it when they see it, but find it difficult to measure.* Perhaps the best and most appropriate way to measure or quantify power quality is to use a cost and benefit approach giving the economic value of power quality more emphasis. Accepting that power quality is difficult to measure does not however prevent using methods or devices, such as power conditioners, to improve power quality.

The area of power conditioning is recieving a large amount of research effort. The local solution of power quality problems is, it seems, an appealling approach. This is born out by the commercial power conditioners that are now available, most of which are shunt active filters (SAF). The justification of power conditioners is that they prevent or suppress power quality problems and their succesful application bares this out. However as the character of the AC power system changes with more and more electrical power being utilised by power electronic rectifiers there is the chance that the power conditioner may interact with the AC system and load in an unforseen and perhaps even power quality lowering way. The interaction of power conditioners with the AC system and loads is an area that requires exploration. While it is possible to intuitively describe these interactions such qualitative descriptions are generally unsuitable for use in design and analysis so the interaction needs to be described in a quantitative or numeric way.

1.2 THESIS SCOPE AND OUTLINE

The principal aim of this thesis is to quantitatively describe the interaction of the shunt active filter power conditioner with non-linear loads and the AC system. This area of SAF research has been largely ignored as the non-linearity of the load is very difficult to incorporate into analysis attempted in a linear systems framework. As a result this has meant that typically non-linear loads in the SAF context have been modelled as having no sensitivity to voltage disturbance. Chapter 2 presents a review of shunt active filtering. In it the present state of the art of SAF operation, SAF control systems and SAF power converters are surveyed and described. SAF connection to AC systems and non-linear loads is discussed and the lack of research effort into the interaction between the SAF, the AC system and the load described.

In order to provide a framework for the interaction analysis, the customer or supply end of the AC power system is viewed as a control system and formulated in block

diagram form. This approach shows how the behaviour of the total combined system is dependent on both the AC system and the non-linear load. Chapter 3 describes this control system approach and presents some initial results that can be deduced without accurately modelling the non-linear load behaviour. The control system approach shows that the non-linear load forms part of the forward transfer of the SAF and so must be modelled accurately.

Chapter 4 describes an experimental system capable of performing the shunt active filter function. It can also make measurements of the non-linear load behaviour by causing small disturbances and measuring the resulting changes.

A frequency domain approach is useful in describing the way in which non-linear rectifier loads transfer voltages and currents from their AC sides to the DC sides and back. This is because the non-linear device can be represented in a linear fashion in the frequency domain. Chapter 5 details the frequency domain modelling of non-linear rectifier loads using a constant matrix that accurately represents modulation. This method is then used in the analysis of the single-phase rectifier which is detailed in Chapter 6. The analysis of the single-phase rectifier is confirmed by time domain simulation and a number of experimental measurements in Chapter 7 in order to show that the analysis is accurate. It also shows that it is possible for accurate experimental measurements of the single-phase rectifier load characteristics to be made. The predicted effect of SAF operation on single-phase rectifier operation is also validated.

In order to show that the same modelling and analysis methods used for the single-phase rectifier are valid and appropriate for three-phase rectifiers the experimental system is used to measure the characteristics of a three-phase rectifier. The results are presented in Chapter 8. Future work possibilities are described in Chapter 9 and final conclusions presented in Chapter 10.

Chapter 2

A REVIEW OF SHUNT ACTIVE FILTER POWER CONDITIONING

2.1 INTRODUCTION

The active filter concept originated in the 1970s when the idea of using magnetic amplifier technology to prevent harmonics from entering the power system was proposed [Sasaki and Machida 1971]. Since then there has been considerable effort into research and development of these shunt active filters (SAF) [Al-Haddad *et al.* 1999] which are the most commercially available power conditioning device. The SAF is used to improve power quality, typically by reducing the hamonic level in the power system.

This review chapter firstly introduces the shunt active filter by describing operating principles and the intention of the user when they install an SAF. The present state of the SAF art is then established. A survey of the available control methods is presented followed by a discussion on the power converters used to produce currents and voltage at the level of the AC system. Non-linear rectifier load interaction with the SAF is discussed because this is an area where there are few published research findings. To find the total combined system behaviour it is necessary to accurately model the rectifier load. This has not yet done for the SAF situation. In order to model the rectifier loads, techniques used in other power system models of non-linear rectifier loads are presented specifically those for three-phase HVDC converters. The existence of three-phase rectifier models that are adaptable to the uncontrolled rectifier situation is discussed along with the almost total lack of investigation of the single-phase rectifier.

2.2 ACTIVE FILTERS

One way to prevent or remove the power quality problem is to use some form of power conditioner. These devices operate to prevent the cause of or suppress the symptoms of the power quality problem and exist in a number of variants including the static compensator (STATCOM), thyristor control reactor (TCR), dynamic voltage restorer (DVR), thyristor controlled series capacitor (TCSC), series active filter, and the shunt

active filter (SAF).

Active filters have two principal variants these being the shunt form and the series form. The series form, Figure 2.1, is connected in the AC network in series between the AC system and the load. It functions by creating a harmonic voltage to harmonically isolate the load from the AC system. Although the converter size necessary for the series active filter is smaller than that for shunt active filter [Akagi *et al.* 1986], the use of series active filters is not as common as shunt active filters [Akagi 1996a].

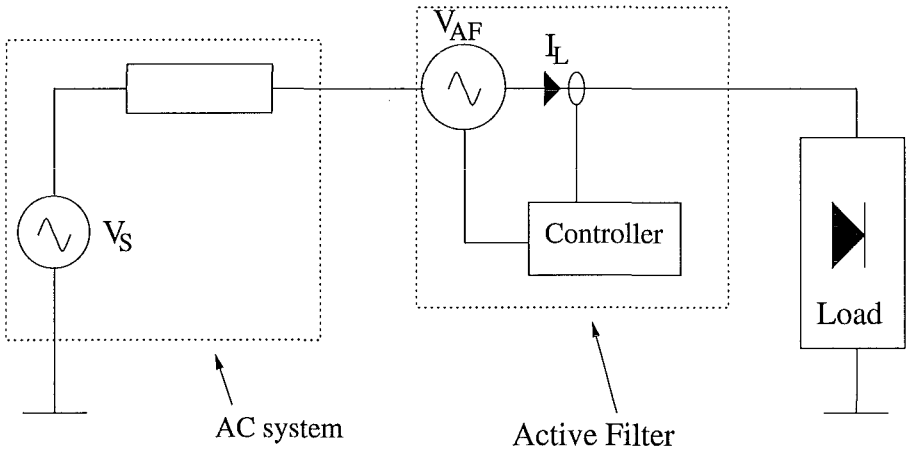

Figure 2.1 Series active filter system.

The shunt active filter typically operates as a harmonic compensator in the manner shown in Figure 2.2. The load current I_L is measured, the controller rejects the fundamental frequency and produces a compensating current I_{AF} that is the negative harmonic or non-fundamental current components of the load current. The compensating current is then added to the load current meaning that the harmonic currents sum to zero and so the supply current has no harmonic content [Round 1992]. This is called a load current measurement SAF. It is also possible to measure the supply current and by a feedback action force the harmonic current to be zero [Round *et al.* 1998a]. The use of active filter technology is becoming technically and economically feasible as the power switching device technology improves with 500 (mainly shunt) active filter systems operating in Japan performing harmonic compensation and reactive power compensation [Akagi 1996a]. Commercial three-phase shunt active filter units are available from motor speed control manufacturers [Sonnenschein *et al.* 1996].

The improvement in power quality that shunt active filters give for commercial office buildings measured by the improvement in the voltage THD is reported as being low [Lai and Key 1997] but this is perhaps an inappropriate indicator of power quality rather than an indictment of the shunt active filter. In fact the amount of research into shunt active filtering [Al-Haddad *et al.* 1999, Grady *et al.* 1990] shows that the research community believes there is significant value in the technology. Also the adoption of the technology in Japan for both harmonic compensation and voltage

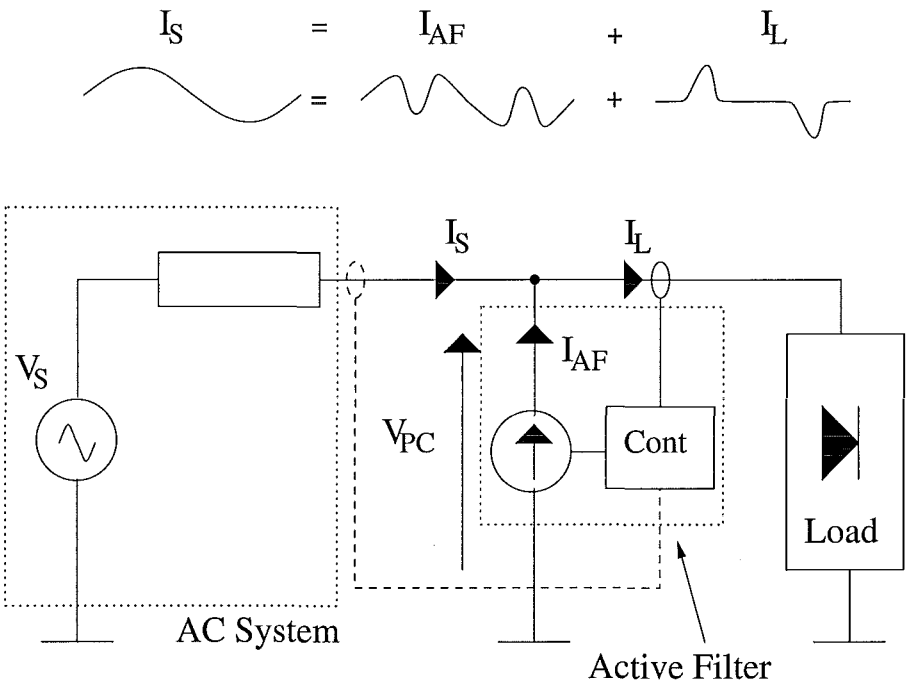

Figure 2.2 Shunt active filter system.

impact-drop compensation show the benefits of shunt active filters [Akagi 1996a].

2.2.1 Uses of shunt active filters - intention of users

Shunt active filters and other power conditioning devices are intended to improve the power quality of the network where they are installed. The assumption that the SAF can and does do this is the driving force in their use and this assumption is tacitly made by the large number of manufacturers who sell SAFs and researchers who investigate them. The SAF can prevent current harmonics flowing into the AC system network thereby lowering the RMS current and the current distortion level in the network. This may allow the customer to meet a requirement imposed by the utility company or may allow the utility to prevent excessive harmonic voltages occurring at other customers points of connection. Therefore the use of the SAF depends on the intention of the user and the users intention depends on whether they are a consumer or transporter of electrical power [Akagi 1996a]. This again reinforces the view that from the customers viewpoint the AC system in fact brings pollution, in the form of voltage harmonics and disturbances, into the site along with useful AC power. The network company sees the customer's *dirty* load as injecting pollution into the AC network. However, the generally held view is that the shunt active filter can provide benefit to both the network operator and the customer by removing harmonic currents or providing harmonic damping.

2.2.2 Harmonic current removal

It is possible to remove harmonic currents from the AC system by providing a low impedance path for them to flow through, thus preventing them flowing into the AC network. The passive filter approach to harmonics does just this using a tuned passive LC circuit to ensure the filter has lower impedance than the network at the harmonic frequency. This low impedance can cause harmonic currents from other parts of the network to flow to and into passive filters [Arrillaga *et al.* 1985] perhaps exceeding their rating. Current measurement shunt active filters, which use a power converter to generate the current to compensate for the measured load harmonic currents, do not suffer from the problems associated with presenting a low impedance to the AC network and so cannot attract harmonics from other harmonic sources. The connection of shunt active filters to high voltage networks is problematic in that the switching device voltage is high. With the increase in the voltage ratings of integrated gate bipolar transistors (IGBTs) and the development of fast switching gate turn off thyristors with integrated gate commutation (IGCTs) [Linder *et al.* 1997] means that this is becoming less of a problem. It is however possible to create hybrids of active filters and passive filters. One variant has a series active filter in the AC line and the passive filter connected in shunt [Akagi 1996a]. Another variant has the active filter in series with a shunt passive filter so both together form a shunt branch [Akagi 1996a]. This allows the voltage rating of the converter to be relatively small because voltage is dropped across the passive filter components. Considering the effect of the passive filter components on the controller transfer ensures the system is stable [Hafner *et al.* 1997]. It is also possible to combine passive filters connected as shunt branches with shunt active filters effectively connecting the two in parallel. The connection of a shunt active filter and a series active filter to a common DC bus leads to the so called unified power quality conditioner [Akagi 1996a]

2.2.3 Harmonic damping

The SAF was first applied at the source of the harmonic current with the intention of removing that harmonic current [Akagi *et al.* 1986]. However there is the possibility of applying the active filter at an arbitrary point throughout the network to improve the power quality of the entire network. The optimal point to install the shunt active filter in the network with the aim of having the lowest total network distortion level can be found with optimisation techniques [Berizzi *et al.* 1996, Grady *et al.* 1991].

The proposed use of shunt active filters as a solution to excessive harmonic propagation in 6.6kV distribution networks in Japan led to the SAF terminal voltage being used as the input to the control system [Akagi 1997a]. This approach makes the SAF operate as a voltage to current transfer device meaning that the the SAF appears as an impedance or admittance in exactly the same way as a passive filter. The voltage

measurement system means that the SAF can contribute damping to the AC system and prevents the propagation of harmonic currents. The use of a current-measurement current-output SAF in the distribution network is not possible as it leads to increased harmonic current flow and there is the possibility of instability if a capacitor or capacitive component is connected downstream of the SAF [Akagi 1997a].

The use of the voltage as the control input with a current output gives a SAF that has the same type of transfer as a passive filter. The stability of the voltage measurement SAF means that it has been proposed that this type of SAF can be used without significant consideration of the network or load [Sato *et al.* 2000]. This makes its application like that of an appliance in that the user simply plugs it in and turns it on. The price of this convenience of operation is that the filter does not remove harmonic currents but rather provides system damping [Sato *et al.* 2000], so it may or may not improve the power quality for the user.

2.2.4 Transient suppression

The AC network is subject to constant change and at times the change can be extremely fast due to the switching of a load. Any such transient excites the natural or transient response of the SAF control system filter. In effect the filter used to determine the harmonic or non-fundamental components of the measured load current treats transient excitation as a non-fundamental component. This means that the SAF attempts to counter the transient. In the event that the transient response is larger than the current rating of the SAF converter then the converter must current limit, potentially causing more distortion in the short term [Round *et al.* 1998b]. The speed of the transient response of the control system can be traded for signal rejection or retention bandwidth. That is, the natural response of a narrow band notch filter is longer in time than a notch filter with a wider notch. However no matter the width of the notch, transient load current changes are always measured as non-fundamental frequencies and so the shunt active filter attempts to compensate for them. This means that the SAF is really only effective in the steady state or for relatively small transient changes unless there is significant excess rating in the converter.

2.3 CONTROL SYSTEMS

A large number of shunt active filter control systems have been proposed and tested. All these schemes have the goal of removing or retaining a certain frequency or group of frequencies from or within the power system so all implement some kind of filtering operation. Control systems can use the voltage or current as an input and can produce a voltage or a current as an output. Typically a shunt active filter measures either the

current or terminal voltage and produces a current. Control systems can be based on three-phase or single-phase concepts.

2.3.1 Single-phase control systems

The single phase AC system presents a conceptually simple starting point for active filter control systems. The active filter measures the load current, determines the harmonic content of the current and injects the antiphase current to cancel the load harmonic currents. There are a number of ways to determine the harmonic content of the load current. It is possible to construct a sinusoidal signal that has the same power as the load current and then by subtraction to determine the harmonic content. As it is necessary to provide real power to overcome losses in the power converter the size of the sinusoidal signal can be used to ensure power balance by regulating the energy stored in the DC bus. This method is termed the synthetic sinewave method [Duke and Round 1990, Duke *et al.* 1990].

The harmonic content can also be found by filtering the load current signal either with a notch or high pass filter to remove or keep the harmonic content [Quinn *et al.* 1993, Choe and Park 1988]. It is important to note that high pass filters can be synthesised from low pass filters by subtracting the original signal from the filtered signal. High pass or low pass systems can suffer from the inability to achieve good rejection between the fundamental and the third harmonic [Ingram 1998].

The FBD method uses signal processing techniques to determine the equivalent resistance and reactance of the load and then makes the supply current exactly match that required to draw the same real power as the equivalent resistance [Staudt 1996]. This and other such equivalent methods [Enslin and Van Harmelan 1990] must measure both voltage and current and can have stability problems if power flow reverses as the equivalent resistance becomes negative, providing negative damping and perhaps destabilising the AC system.

2.3.2 Three-phase control systems

When the power level increases it is typical to use a three-phase electrical supply system. The three-phase system allows motors to generate constant torque and power and therefore avoid problems with pulsating torque that occur in single-phase systems. Three-phase SAF control systems can use one of two methods. One approach makes use of the characteristics of the three-phase system. The other uses three single-phase controllers to control a three-phase active filter which may or may not be built from single-phase units [Round *et al.* 1998a].

It is possible to use what are effectively single-phase techniques to control a three-phase SAF [Quinn *et al.* 1993]. Each load current phase can be filtered with a separate

low pass, high pass or notch filter controller and the resulting compensating currents used to individually control the SAF [Round *et al.* 1998a]. However by combining the information from all three phases and using three-phase techniques the controller can make use of the properties of the three-phase system.

2.3.2.1 Rotating control systems

The rotating reference frame approach to active filter control, Figure 2.3, is based on the three to two transform where a three-phase system with no neutral can be represented by an equivalent two phase system. Typically a rotating reference frame is used to transform the rotating quantities to stationary quantities by performing a frequency shift with a vector rotator. This means that a rotating three-phase system can be

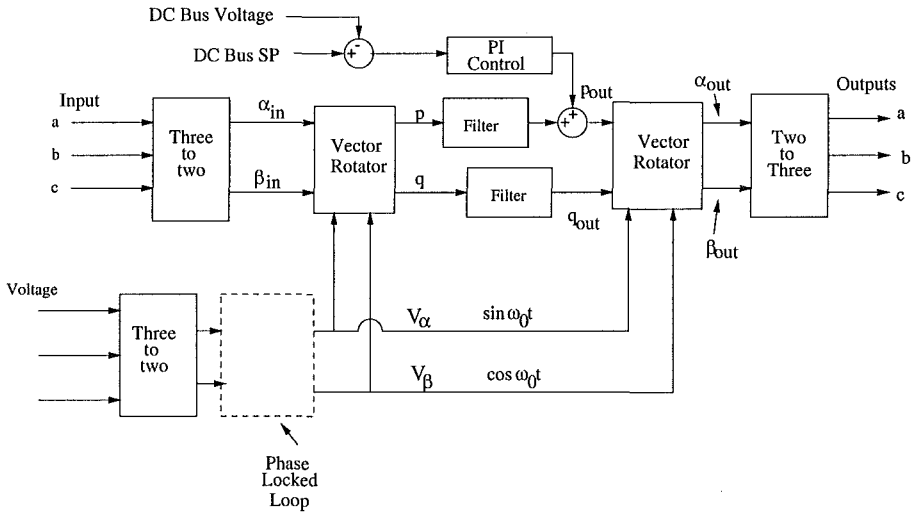

Figure 2.3 Three-phase rotating control system.

transformed to a two phase stationary system where the zero frequency component in one phase represents the real power and the other the reactive power. Control action is performed by filters that operate on the rotated variables and the control outputs created by re-rotating the variable and converting back to the three-phase variables. One variant of a rotating SAF controller is the synchronous reference frame (SRF) approach [Bhattacharya *et al.* 1991]. Another variant uses the instantaneous active and reactive power and is called the instantaneous reactive power theory (IRPT) [Akagi *et al.* 1986]. In this method the three-phase system is decomposed into a p and a q component by a rotating transform formed from the three to two transform of the voltages V_α and V_β. The zero frequency part of the p component represents the real power flow while the non-zero frequency components represent parts of the load current that involve energy absorption and release in the DC bus of SAF converter when compensating. The q component zero frequency part represents the reactive power and the non-zero frequency components can be compensated by the SAF without energy

storage in the DC bus. This means it is possible to use three-phase static power converters to perform active filtering and reactive power compensation without them having DC bus energy storage so long as only the q components are compensated [Akagi *et al.* 1984]. The real power to maintain the SAF converter DC bus voltage can be met by adding the power required to p_{out} in Figure 2.3.

It is also possible to use a phase locked loop (shown dotted in Figure 2.3) to provide the reference frame locking it to the positive sequence fundamental voltage. This ensures that only the positive sequence component of the current is transferred to zero frequency p and q [Watanabe *et al.* 1993]. By contrast the IRPT transfers frequency components that exist in both current and voltage to the representative real p and reactive q power signals. It is possible to extend the IRPT to include the zero sequence components associated with three-phase four-wire systems [Watanabe *et al.* 1993, Aredes and Watanabe 1995]. A number of comparisons between these and other rotating control systems have been presented [Horn *et al.* 1996, Round and Ingram 1997, Cavallini and Montanari 1994] each drawing slightly different conclusions as to which is the best. A large number of papers describing control systems for both single-phase and three-phase SAFs have been published [Al-Haddad *et al.* 1999].

2.3.3 Control filter implementation

There are proposals to use a Fast Fourier Transform (FFT) to perform the signal processing to detect the harmonic or non fundamental components [Ingram 1998]. The rotating systems described in the previous section effectively perform the complex rotation of a complex variable. This is equivalent to the operation of a butterfly in the FFT algorithm [Brigham 1988]. The direct equivalence of the FFT and the rotating filtering then re-rotating approach has been demonstrated by Srianthumrong and Sangwongwanich [Srianthumrong and Sangwongwanich 1988].

2.4 POWER CONVERTERS

The controller function of measurement, detection and isolation of the components to be removed from the supply is only part of the operation of the shunt active filter. The other part is the generation of the compensating current. This operation is an amplification from the low power signal level of the detection system to the voltage and current levels of the AC system. The amplifier must have high fidelity so that the SAF operates to reduce harmonic levels rather than increase them and also must have high efficiency so the ongoing cost of operation is low. The use a switching power electronic converter is typical in SAFs as they have high efficiency and can be made to have high signal fidelity. It is possible to use a current source converter [Williams and Hoft 1991]

but it is more typical to use a voltage source converter as the efficiency is higher and the initial cost lower [Akagi 1996a].

2.4.1 Voltage-source controlled-current systems

The voltage source converter is the most commonly chosen converter configuration for shunt active filtering [Akagi 1996a, Al-Haddad *et al.* 1999]. The converter is typically controlled to produce an output current rather than a voltage [Round 1992]. This current control makes full use of the bandwidth of the switching converter to prevent AC system voltage disturbance having any significant effect on the current [Brod and Novotny 1985]. Both analogue [Round 1992] and completely digital implementations have been successful [Ingram 1998, Ingram and Round 1999] and it is possible to use fixed frequency switching [Moran *et al.* 1995] or spread spectrum switching generated by hysteretic control [Round 1992]. Three-phase power converters have a structure that allows the use of vector switching controllers, making use of the redundancy in the switching states to minimise the output current ripple and number of switchings [Kwon *et al.* 1999]. This three-phase vector control can be extended to include three-phase four-wire systems [Verdelho and Marques 1999]. All these controlled current systems have wide current control bandwidth so long as the DC bus voltage is higher than the peak of the AC system voltage, the output inductors are small enough and the switching frequency is sufficiently high. The design considerations for the converter parameters has been previously documented [Brod and Novotny 1985]. A more thorough and exhaustive review of current control methods can be found in [Kazmierkowski and Dzieniakowski 1994] and a large number of papers on the subject are collected in the October 1998, Volume 45, No 5 issue of the IEEE Transactions on Industrial Electronics [Kazmierkowski and Malesani 1999].

2.5 SHUNT ACTIVE FILTER CONNECTION, THE AC SYSTEM AND THE LOAD

Shunt active filters operate connected to the AC system but that AC system is typically viewed as having little effect on the performance of the SAF. Also the SAF is typically connected near to a non-linear load with the intention of preventing that load causing system disturbances. It is possible that the SAF may be connected away from a non-linear load but as the use of power electronic systems increases the likelihood increases that there will be some non-linear load close to the SAF. Generally little attention has previously been paid to the AC systems effect on the operation of the SAF and vice versa. The instability caused by SAF connection with power factor correction capacitors shows that the AC system can have a large effect on SAF operation [Akagi 1997a]. Control analysis identifies the downstream capacitor and the AC

system impedance as both playing a part in the forward control transfer of an SAF [Malesani *et al.* 1988, Round *et al.* 1998a]. It has not been typical to analyse the SAF system for small signal stability or robustness except where the operation of the control transfer of the SAF is deliberately modified with power system connected passive components [Hafner *et al.* 1997, Staudt 1996]

The load connected near the SAF is generally a non-linear harmonic producing load because it is typically the intention to remove these harmonics. The behaviour of the non-linear load is very much ignored with the load assumed to be a constant current source [Akagi *et al.* 1986, Ingram 1998]. The recent work on current measurement SAFs connected to generic loads shows that there is significant interaction with the SAF when there are capacitors in the load position [Malesani *et al.* 1988]. If the non-linear load can present as a capacitive admittance to the network it may be possible for the SAF to be unstable or inoperative.

The idea that a non-linear load has an admittance or impedance is, at first sight, perhaps a strange one. However the constant current source assumption that is usually used in SAF research is in effect an assumption that the non-linear load has zero admittance or infinite impedance which means that if the AC voltage changes there is no change in the current. It is intuitively apparent that any non-linear load's current is sensitive to AC voltage change and the non-linearity may perhaps make a non-linear load relatively more sensitive than a linear load. As the SAF typically operates near a non-linear load, the sensitivity of that load has implications for the SAF.

There have been attempts to incorporate the sensitivity of non-linear rectifier loads into the analysis of SAF operation. The constant current source load assumption has been replaced by a load having a *low impedance* [Peng and Lai 1996]. This approach can be used to predict the effect of SAF operation on the load current but determining the value of the impedance is difficult. The replacement of a non-linear system with a linear equivalent is also questionable. Other investigations of the interaction of the SAF and the non-linear load have been carried out with time domain simulation [Luor 2000]. However the result is not a description of the interaction, but rather a conclusion that some types of rectifiers are sensitive to SAF operation. Series inductors connected between the load and the SAF are the proposed solution to any problems [Luor 2000]. The present research on non-linear loads in the SAF context does not attempt to quantitatively describe the interaction in any way. There is however a realisation that the non-linear load is an integral part of the power system behaviour and so there is effort to measure the effect of the load on the driving point impedance of the AC system [Palethorpe *et al.* 2000]. This work attempts to use a discontinuous current injection to determine the response of the AC system and the rectifier load. The results are encouraging but the use of a discontinuous current injection means the measurement is the transient response rather than the steady state response. The transient response of a non-linear system does not always relate to the steady state

response in the same way as linear systems. That is, as a result of the uniqueness of the Inverse Laplace Transform, a linear system's frequency response contains enough information to determine the system's transient response [Siebert 1986]. The same is not always true of a non-linear system.

The analysis and modelling of non-linear rectifier loads for use in power systems is relatively advanced in the area of high voltage direct current (HVDC) transmission. The reasons for this are that the HVDC converters have ratings that are comparable to the rating of the AC system and that the cost of the system is so high that almost absolute operational certainty is required. As a result there has been a large amount of research effort into the behaviour of thyristor based naturally commutated controlled current converters. The driving force for this effort has been the occurrence of problems with HVDC systems which cannot be explained or controlled without the accurate representation of the converter [Ainsworth 1967]. Although time domain simulation of these large converters is common [Dommel 1969] the frequency domain is more appropriate to represent and solve control problems [Wood and Arrillaga 1995]. This is because the frequency domain allows the robustness of the system to be described. It is not the aim of this review to list a large number of papers concerning converter models, rather to point to a number of salient papers that influenced the direction taken in the work described in this thesis.

The interaction of low frequencies around the rectifier converter was explored with numeric frequency to frequency transfers developed from time domain simulations [Larson *et al.* 1989]. This is a matrix formulation of the frequency transfer behaviour. A analytic approach to find the frequency transfer for non-harmonic frequencies is described in [Wood 1993, Wood and Arrillaga 1995]. This was used to produce control equivalents for the HVDC system and further extended to show that a describing function, based on the frequency transfer approach, can be used for transient control design [Todd *et al.* 1997]. The HVDC converter behaviour at harmonic frequencies means that frequency transfers or couplings represented by complex numbers cannot be accurate and a tensor representation is required [Smith *et al.* 1998]. The behaviour of back to back HVDC links has been accurately represented with this type of frequency domain tensor matrix coupling [Wood *et al.* 1998]. Other uses of this type of model are in the fast solution using Newton's method of power system load flows when non-linear rectifiers couple harmonic frequencies to the fundamental [Bathurst 1998]. In this case the frequency transfer tensor matrices are used as the Jacobian or sensitivity matrix.

The HVDC converter has controlled firing of its thyristors. This mechanism is used to control the DC side current. Most rectifiers used at the customer or supply level are uncontrolled diode bridges with power levels a number of orders of magnitude lower than HVDC converters. However the same frequency transfer approaches can be used to describe the behaviour of the rectifier. A method for analytically calculating the harmonic currents for an uncontrolled three-phase rectifier has been developed

[Sakui and Fujita 1994]. This gives a solution at harmonic frequencies, but does not describe the non-harmonic frequency behaviour. There is very little research on the non-harmonic behaviour of supply level rectifier loads, the reason for this being that there has been no pressing reason to persue this area. However, when shunt active filters and other power conditoners are used to prevent the effects of the increasing use of three-phase and single-phase non-linear rectifiers, supply level power systems become complicated and the possibility for unforseen interaction increases.

The three-phase rectifier is the main device used to convert AC voltage to DC voltage at power levels above 2kW. It typically utilises the uncontrolled switching of a diode bridge. The three-phase rectifier with uncontrolled switching devices is very much like the HVDC converter in topology. The only difference is the lack of firing angle control. This means that by describing the switching change caused by the circuit conditions for an uncontrolled rectifier and using this as the firing angle control with an existing HVDC type three-phase converter analysis, the model of the three-phase uncontrolled rectifier can be developed. For this reason the three-phase rectifier is not analysed in this thesis.

Probably the most common non-linear rectifier load is the single-phase rectifier with a DC bus capacitor. This device appears in personal computers and most electronic appliances and has a current that has significant harmonic content [Arrillaga *et al.* 1985]. The behaviour of the single-phase rectifier has received less research attention than that of the three-phase rectifier. Third harmonic current it produces flows in the neutral of three-phase four-wire systems [Arthur and Shanahan 1996]. Also the interaction of the single-phase rectifier with the power system has been explored with an iterative solution to find the harmonic transfers [Jalali and Lasseter 1994]. Recently the same type of frequency coupling approach was used to show that a single-phase rectifier could cause the system to be unstable when used in the traction system of an electric train [Mollerstedt and Berhardsson 2000]. This and the previously noted three-phase HVDC rectifier instability [Ainsworth 1967] shows that non-linear rectifiers can at times be the cause of AC system instability.

2.6 SUMMARY

This lack of knowledge and research into the behaviour of the single-phase rectifier means that this is an area that should be explored especially as power conditioners and non-linear devices become a increasing part of the supply level AC system. The behaviour of the single-phase rectifier in the SAF operational situation is the primary focus of the work contained in this thesis. The rectifier behaviour when stimulated with both harmonic and non-harmonic frequencies is explored and analysed with the intention is to develop a model and understanding of how the single-phase rectifier behaves so that this knowledge can be used in the analysis of the interaction of the

single-phase rectifier, the AC system and the shunt active filter.

A framework is required in which the interaction between the SAF, the AC system and the single-phase rectifier can be analysed. In the next chapter a control system approach to the interaction is presented. This allows the interdependence of the three parts of the overall system to be evaluated and analysed.

Chapter 3

A CONTROL SYSTEM APPROACH TO POWER CONDITIONER ANALYSIS AND DESIGN

3.1 INTRODUCTION

The decision to install a power conditioner is typically taken when there are power quality problems. It is self evident that the power conditioner is installed to alleviate the problem. The problem could be excessive voltage fluctuation with load variation, intolerable harmonic voltages and/or currents or perhaps excessive voltage sags or dips. The present thinking on power conditioners has them viewed as almost a panacea for all power quality problems. For example, a non-linear load can have all its harmonic current prevented from reaching the AC system by an SAF. Perhaps the voltage dip due to an induction motor start can be removed by supplying reactive power and if the dip is removed then the power quality is improved. It is this assumption that has driven the use and analysis of power conditioners [Shaughnessy 1997].

Typically the power conditioner is considered almost in isolation from the load. If the conditioner control system is the area of interest then simplifying assumptions are made concerning the non-linear load and the AC system [Moran *et al.* 1995, Akagi 1992]. Recent work on the possible interaction of power conditioners with distribution power factor correction capacitors in Japan [Akagi 1997a] suggests that taking a narrow focus on control systems without considering the AC system and the load could lead to problems in SAF operation. This chapter introduces a systematic method to analyse the power conditioner system concentrating specifically on the shunt active filter situation. However it is sufficiently general that it can be used for all power conditioner situations. An initial analysis of the SAF system is then presented. The control system approach is then used to investigate the interaction of power factor correction capacitors with the SAF using frequency domain robustness and stability techniques.

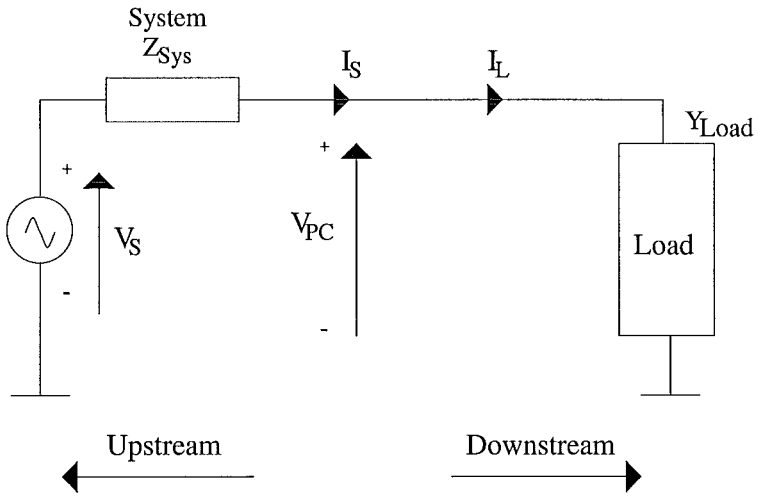

Figure 3.1 Load connection to AC power system.

3.2 LOAD END FEEDBACK LOOP

An AC power system can be divided into three parts. These are generation, transmission/distribution and the loads. Figure 3.1 shows the a schematic of an AC system with the generation[1] shown as a voltage source V_S. The AC system is represented by its impedance Z_{Sys}, the load by its admittance Y_{Load} and the terminal voltage at the point of coupling of the load and system is V_{PC}. The upstream direction is defined as closer to the source and downstream as farther from the source. The load current is I_L and the supply current is I_S. In the situation shown in Figure 3.1 the load and the supply current are the same current. SAF operation, see section 3.3, means that the load and supply current are different. The load is best represented as an admittance because, in AC power systems, voltage is connected to a load and the current flows. That is, the current is the output and the voltage is the input. The admittance is therefore a multiplying transfer that gives the current for an applied voltage (3.1). Multiplying transfers are suitable for block diagram manipulation. If the transfer is not invertible then it is impossible to write the inverse transfer as shown in equation (3.2).

$$I_L = Y_{Load} V_{PC} \tag{3.1}$$

$$V_{PC} = Z_{Load} I_L \tag{3.2}$$

The AC system can be best represented by its impedance because current flowing, the input, in the AC system causes a voltage drop, the output, as shown in equation (3.3).

$$V_{Drop} = Z_{Sys} I_S \tag{3.3}$$

[1]The mechanical governor and automatic voltage regulator behaviour of the generator are ignored but can be included in the system by incorporating these effects into the system impedance.

The voltage at the point of coupling can be determined using the voltage drop and is given by equation (3.4).

$$V_{PC} = V_S - I_S Z_{Sys} \tag{3.4}$$

The impedance is therefore the multiplying transfer from the supply current to system voltage drop. Consider connecting the load to the AC system. The load current I_L flows in the system impedance Z_{Sys} causing a voltage drop as per equation (3.3). This system voltage drop causes a change in V_{PC} changing the load current in turn causing a change in the voltage drop in the system impedance. Both equations (3.1) and (3.4) simultaneously apply so the load current and voltage depend on both the load admittance and the supply impedance. The total effect is a feedback loop. Consider now the fault situation where the AC system impedance is significantly greater than the fault (or load) impedance. It is impossible to achieve a current of $V_S Y_{Load}$ (or equivalently $\frac{V_S}{Z_{Load}}$) because of the voltage drop across the system impedance.

3.2.1 Perturbing sources

The use of perturbing sources is a typical control approach to determining the response or sensitivity of a feedback loop system [Stefani *et al.* 1994] like that described in the previous section 3.2. The load AC system circuit with perturbing or disturbance sources added is shown in Figure 3.2(a). Figure 3.2(b) shows the equivalent block diagram. Notice that in Figure 3.2(a) the perturbing voltage source ΔV is in series with the system source, the system impedance and the load. This means that in this case all perturbing voltages are the same so ΔV is equivalent to a supply voltage perturbation. The current injection perturbation ΔI is subtracted[2] from the load current to make the supply current in Figure 3.2(b). This representation seems to imply that ΔI does not flow into the load at all. This is not the case because any change in the supply current causes a change in the terminal voltage, changing the load current so long as Y_{Load} is not zero.

Consider an example situation where the system impedance and the load are resistors R_{Sys} and R_{Load} respectively. Taking a circuit approach the supply (and load) current is given by equation (3.5)

$$\Delta I_S = \frac{\Delta V_S}{R_{Sys} + R_{Load}} \tag{3.5}$$

This means the load voltage is (3.6)

$$\Delta V_{PC} = \frac{R_{Load}}{R_{Sys} + R_{Load}} \Delta V_S \tag{3.6}$$

[2]This subtraction is the result of the sign conventions of the load and supply current in Figure 3.1

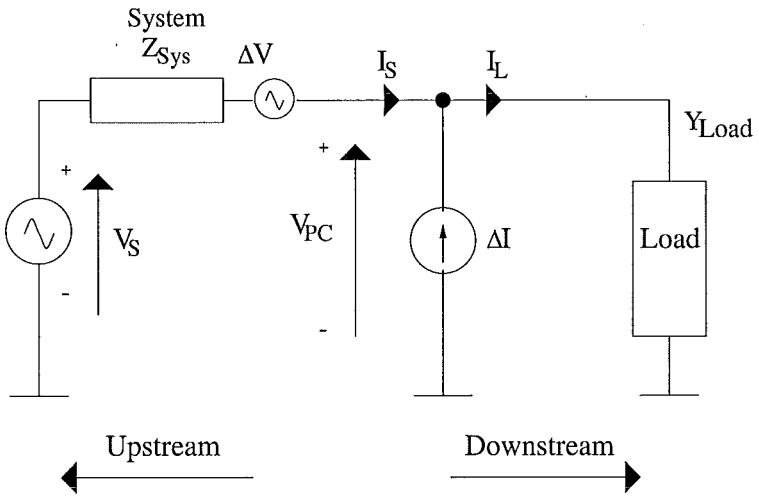

(a) Load connection to AC power system showing possible perturbing sources

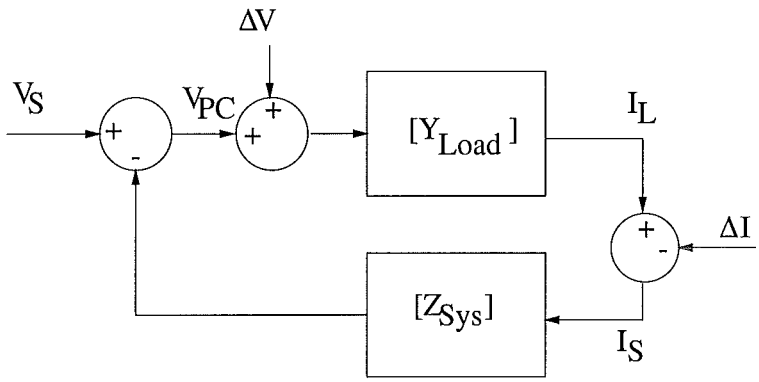

(b) Feedback loop made by the load and AC system

Figure 3.2 AC system showing feedback loop made by the load and AC system.

If the control system approach is taken the transfer of V_{PC} to I_L is $Y_{Load} = \frac{1}{R_{Load}}$ and that of I_L to V_{PC} is R_{Sys}. This means the total transfer is (3.7)

$$\Delta V_{PC} = \frac{1}{1 + \frac{R_{Sys}}{R_{Load}}} \Delta V_S \tag{3.7}$$

which is equivalent to (3.6). This shows that the two approaches are equivalent and give the same result.

Consider now the case where the system impedance is an inductor, $Z_{Sys} = sL$, and the load is a capacitor, $Y_{Load} = sC$. The loop transfer from ΔV_S to ΔV_{PC} is

therefore (3.9).

$$\Delta V_{PC} = \frac{1}{1 + Z_{Sys} Y_{Load}} \Delta V_S \tag{3.8}$$

$$= \frac{1}{1 + s^2 LC} \Delta V_S \tag{3.9}$$

This shows that the connection of a capacitor to an inductive system impedance creates a highly oscillatory system, as would be expected.

3.3 ADDING THE SHUNT ACTIVE FILTER

The shunt active filter (SAF) is used to prevent or limit the flow of harmonic currents in the power system. This can be seen as a control function because some system quantity is measured and then used to form a control action that minimises the harmonic currents flowing into the AC system. The SAF system is therefore the feedback part of a control system and so an appropriate analysis and design approach is a control system approach. The forward part of the control loop is a combination of the AC system and load.

The connection of a typical load current measurement (LCM) SAF is shown in Figure 3.3(a). This shows the SAF measuring the load current, I_L, and generating a injected active filter current I_{AF}. The control system block diagram representation of a LCM SAF is shown in Figure 3.3(b). The harmonic current is detected by the controller *Cont*. The output of the controller is inverted to give the active filter or compensating current. This current is then added to the load current to form the supply current. The effect of the supply current on the load voltage V_{PC} is given by the system impedance Z_{Sys}. Is is usually assumed that the load current is not dependent on the load voltage or this dependence is very small [Akagi 1992]. This assumption is unreasonable because all loads are dependent to some extent on voltage variation. In fact problems with SAF applications have been demonstrated previously [Peng and Lai 1996, Akagi 1997b] that are not predicted when the constant current source load assumption is made. Figure 3.3(b) shows that both the load and system contribute to the forward transfer of the SAF.

3.4 GENERALITY OF THE CONTROL APPROACH AND ITS USE FOR OTHER POWER CONDITIONERS

There are a number of power conditioning approaches that are different in both their intention and implementation. These include the SAF, which removes current harmonics if the load or supply current is used as the control input and damps harmonic propagation if the voltage is used as a control input. The voltage input SAF forms a transfer block from voltage to current. Its transfer function is an admittance and it

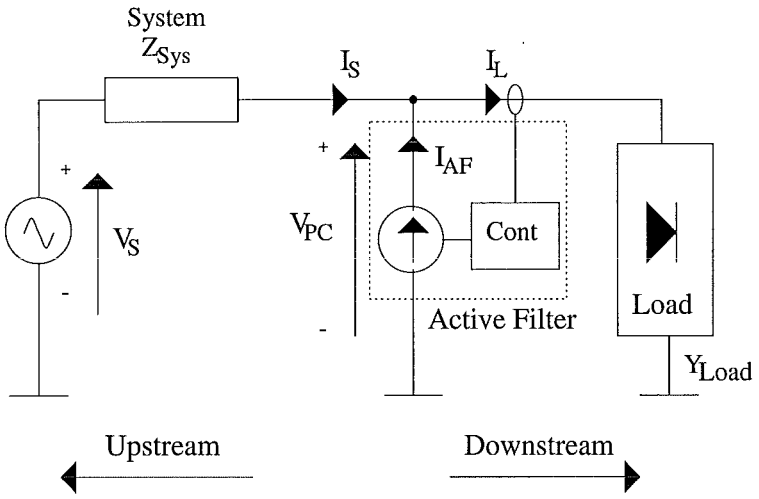

(a) Circuit connection of SAF power conditioner.

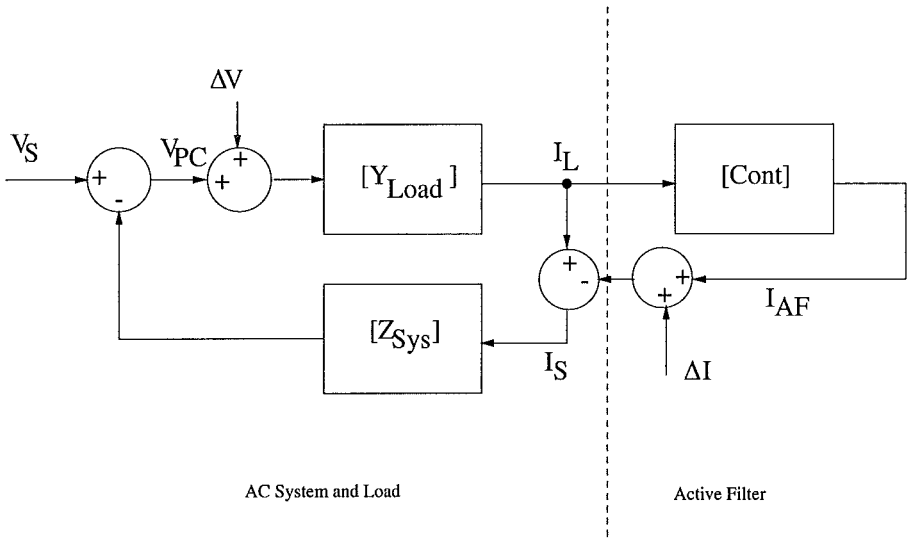

(b) Block diagram form of SAF power conditioner connection.

Figure 3.3 Active filter connection.

connects from the coupling voltage V_{PC} to the current injection ΔI forming a block in parallel with the load. The dynamic voltage restorer (DVR) is a series connected device used to restore the voltage when a voltage dip occurs. This controller measures the terminal voltage V_{PC} and generates ΔV_{PC} so as to eliminate or minimise the disturbance in V_{PC}. A static VAr compensator (SVC) provides reactive power and can be used to regulate the AC voltage. The forward transfer of this power conditioner is ΔI to V_{PC}. It is possible to analyse the forward control transfer of any power conditioner using the control transfer block diagram. This thesis is confined to the analysis of the LCM SAF and all other power conditioners are outside the scope. Table 3.1 summarises the forward transfers of a number of power conditioners.

Device	Function	Forward Transfer
Dynamic Voltage Restorer	Voltage dip elimination	ΔV to ΔV_{PC}
Static VAr Compensator	Reactive power supply or Voltage control	ΔI to V_{PC}
SAF Voltage Measurement	Harmonic damping	ΔI to ΔV_{PC}
SAF Load Current Measurement	Harmonic current removal	ΔI to ΔI_L
SAF Supply Current Measurement	Harmonic current removal	ΔI to ΔI_S

Table 3.1 Forward transfers of power conditioning devices.

3.5 AN INITIAL ANALYSIS OF A SHUNT ACTIVE FILTER SYSTEM

As a first analysis of the LCM SAF assume for the time being that the linear time invariant scalar, Y_{Load}, accurately represents the load and that $Y_{Load}^{-1} = Z_{Load}$. Since the transfers are all scalars, the use of the Δ prefix for the small signal behaviour is not required because the small signal behaviour and the large signal behaviour are the same. The transfer of V_{PC} to I_L is (3.10).

$$I_L = \frac{1}{Z_{Load}} V_{PC} \tag{3.10}$$

Shunt active filter operation means that the supply current is (3.12)

$$I_S = I_L - I_{AF} \tag{3.11}$$

$$= (1 - Cont) I_L \tag{3.12}$$

The terminal voltage

$$V_{PC} = V_S - I_S Z_S \tag{3.13}$$

Solving for the circuit gives (3.14)

$$\begin{aligned} V_S &= V_{PC} + I_S Z_{Sys} \\ &= I_L Z_{Load} + I_S Z_{Sys} \\ &= \frac{I_S}{1 - Cont} Z_{Load} + I_S Z_{Sys} \end{aligned} \tag{3.14}$$

Re-arranging gives (3.15)

$$V_S = I_S\left(\frac{Z_{Load}}{1 - Cont} + Z_{Sys}\right) \tag{3.15}$$

This means that the supply current is 3.16.

$$I_S = \frac{V_S}{\frac{Z_{Load}}{1-Cont} + Z_{Sys}} \tag{3.16}$$

Cont can typically have the form of a notch filter [Quinn *et al.* 1993] with stop band of width $\Delta\omega_0$ at the fundamental frequency ω_0 as shown in Figure 3.4.

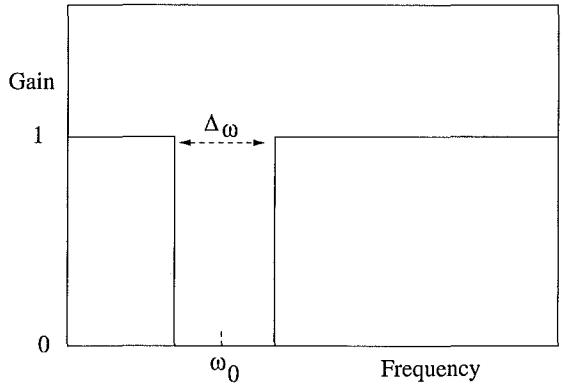

Figure 3.4 Typical SAF notch filter type controller frequency response.

At the fundamental frequency, $Cont = 0$ which means the supply current is given by equation (3.17).

$$\begin{aligned} I_S &= \frac{V_S}{\left(\frac{Z_{Load}}{1-Cont} + Z_{Sys}\right)} \\ &= \frac{V_S}{Z_{Load} + Z_{Sys}} \end{aligned} \tag{3.17}$$

This is the result that would be expected if there were no active filter operating. At a non-fundamental frequency however the supply current is (3.18).

$$\begin{aligned} I_S &= \frac{V_S}{\left(\frac{Z_{Load}}{1-Cont} + Z_{Sys}\right)} \\ &= \frac{V_S}{\infty} \end{aligned}$$

$$= 0 \tag{3.18}$$

This means the SAF removes any non-fundamental current from I_S which is the intention.

Solving similarly for the load current gives (3.19).

$$I_L = \frac{V_S}{(Z_{Sys}(1 - Cont) + Z_{Load})} \tag{3.19}$$

If *Cont* is made zero at all frequencies (effectively turning the SAF off) then the load current is (3.20).

$$I_L = \frac{V_S}{(Z_{Sys} + Z_{Load})} \tag{3.20}$$

At non-fundamental frequency with the SAF running the load current is (3.21).

$$I_L = \frac{V_S}{Z_{Load}} \tag{3.21}$$

This is larger than the load current for the non-active filter situation (3.20). These results have been previously shown [Peng and Lai 1996] and are repeated here. This shows that when the SAF operates, no non-fundamental frequency voltage can be dropped across the system impedance Z_{Sys}. This means that, to the load, the system impedance appears to be zero at non-fundamental frequencies and this increases the current in the load. The analysis illustrates this point but is simplistic in it approach because the impedance Z_{Load} represents a linear time invariant device. The operation of shunt active filters is to eliminate or reduce the level of harmonic currents and so the impedance representation of the load is also simplistic and inaccurate as it is more than likely that the load will be non-linear. This means that a different way of representing or modelling the non-linear load is required.

At times however it is possible that the SAF will be operating when there is no non-linear load connected. In such a situation the analysis of the system can be done using standard linear analytic tools such as the Laplace transform.

3.6 USING THE CONTROL SYSTEM APPROACH TO ANALYSE THE INTERACTION OF POWER FACTOR CORRECTION CAPACITORS AND THE SAF

AC systems commonly have power factor correction capacitors connected. The capacitors provide reactive power locally to prevent it having to flow from the AC system. As reactive power flow requires current and causes system voltage drop, the provision of the reactive power local to the load lowers system losses and improves the voltage

profile of the system. In many countries, such as New Zealand, electric power tariff structures typically include a peak kVA demand charge that financially penalises the customer for having too large an inductive power factor. Alternatively some utility companies regulate the allowable power factor. As a result, customers install switchable banks of power factor correction capacitors at the point of coupling. Typically these banks are switched by a controller to keep the power factor relatively constant. Therefore it is likely there will be power factor correction capacitors installed near the SAF.

3.6.1 Power factor correction capacitor connection downstream of SAF

Power factor correction capacitors downstream of the SAF are connected in parallel with the load. Figure 3.5(a) shows the connection of the capacitor and 3.5(b) the equivalent block diagram. Table 3.2 gives the component values for a hypothetical power system used in the following examples[3]. The system impedance is $Z_{Sys} = sL_{Sys} + R_{Sys}$, the load impedance is $Z_{Load} = sL_{Load} + R_{Load}$ and the power factor correction capacitor connected to provide local VAr support has admittance $Y_{Load} = sC$. By

Component	Value	PU Value
System Resistance, R_{Sys}	0.03Ω	0.13
System Inductance, L_{Sys}	43.5μH	0.05
Load Inductance, L_{Load}	3.3mH	4.5
Load Resistance, R_{Load}	1.34Ω	5.8
Power Factor Correction Capacitor Capacitance, C_{PFC}	1535μF	9.0

Table 3.2 Example system component values. Per unit values on 750KVA, 415V base.

combining the individual component transfers using the block diagram in Figure 3.3(b) the transfer from active filter current to load current can be found. As this transfer is the open loop forward transfer for the SAF the stability and robustness of the total system can be determined using the gain and phase margin [Stefani *et al.* 1994]. Figure 3.6 shows the LCM SAF open loop forward transfer in bode plot form for a power factor correction capacitor connected to the example AC system.[4] The transfer has a gain of 0dB (unity) when the phase is -180^o. This means that the system is very close to instability and will be very sensitive to external disturbances [Stefani *et al.* 1994]. When the SAF operates the closed loop system response will not be well damped and will be subject to transient oscillation. The effect of any load and supply resistance is

[3] As with all example systems there is an air of contrivance. However the example system is chosen to be a realistic as possible in that it uses the estimate of a commercial building's system impedance made from measurements and the building has switchable banks of power factor correction capacitors. The choice of the load is arbitrary but it is not unrealistic for the building.

[4] Representing the system impedance as an inductor and a resistor is a simple approximation. However this does not change the principal result of this analysis because distribution power systems are in general inductive due to the leakage reactance of supply transformers.

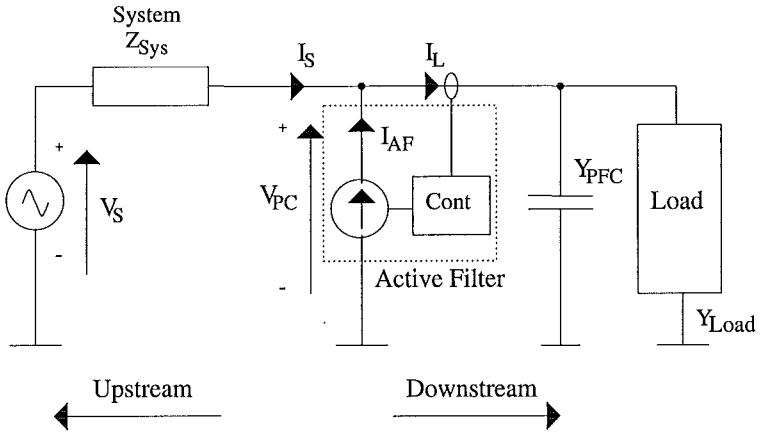

(a) Circuit connection.

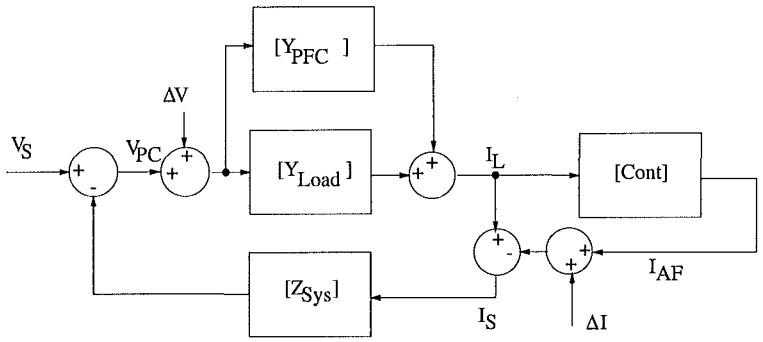

(b) Block diagram.

Figure 3.5 SAF system with power factor correction capacitors downstream.

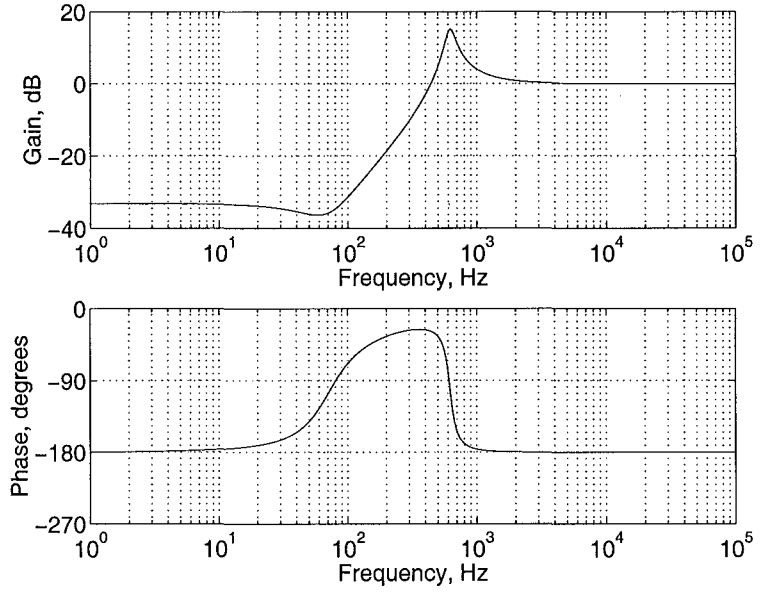

Figure 3.6 Bode plot of SAF system forward transfer with power factor correction capacitors downstream showing that the system has almost zero phase margin.

to provide damping thereby increasing the margin but, as is demonstrated by the bode plot in Figure 3.6, the system transfer has low phase margin.

3.6.2 Capacitor connection upstream of the SAF

Figure 3.7(a) shows connection of a capacitor upstream of the SAF and 3.7(b) shows the equivalent block diagram. Capacitor connection upstream of the shunt active filter does not cause the SAF operation to be unstable as in the previous downstream case. This is shown by the bode plots of the forward transfer in Figure 3.8. This transfer has a gain that is always below 0dB (unity) meaning that closing the loop with the LCM SAF will always be stable. The gain margin is approximately 40dB and the phase margin is undefined as the gain plot never crosses the unity gain line.

However a transfer of interest is the way any disturbance in the system voltage effects the system current I_{System}. When the power factor correction capacitor is connected this is (3.22)

$$I_{System} = \frac{Y_{Load}[1 - Cont] + Y_{PFC}}{1 + (Y_{Load}[1 - Cont] + Y_{PFC})\, Z_{Sys}} V_S \tag{3.22}$$

The transfer is the sensitivity of the SAF load PFC combination as seen from the AC system. The damping that the load contributes by presenting an impedance with some positive real component[5] to the AC system is one mechanism that the energy associated with transient oscillations is removed. In Figure 3.9(a) the bode plot of the effect of the system voltage on the system current is shown for the case when the SAF is not operating. Notice that the transfer, which is of the form of an impedance, is resistive for the low frequencies. When the SAF operates this resistance is removed as can be seen in the bode plot of the transfer in Figure 3.9(b). Therefore with the SAF operating there is less damping in the system for lower frequencies.

3.7 AC SYSTEM EFFECT OF SAF

If the SAF plus load combination is considered from the view of the AC system then the AC system "sees" the situation shown in Figure 3.10. Consider a small non-fundamental change in the voltage at the point of coupling. This voltage change causes the load current to change. However the SAF measures the change in the current and generates the anti-phase current to cancel the initial current. This means that no current change flows out into the AC system. Therefore the effective incremental or small-signal impedance seen by the AC system is the change in the voltage over the change in the voltage $\frac{\Delta V}{\Delta I}$ is ∞ or an open circuit. Thus the connection of SAF can

[5]Positive real impedance has a phase angle of zero and is equivalent to a component having the capability to dissipate energy.

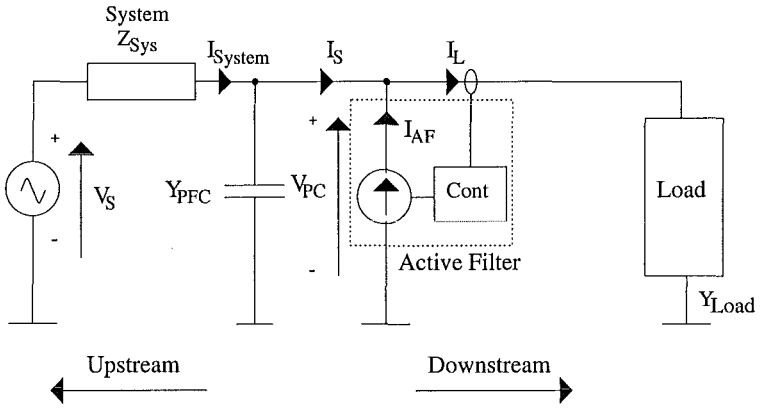

(a) Circuit connection

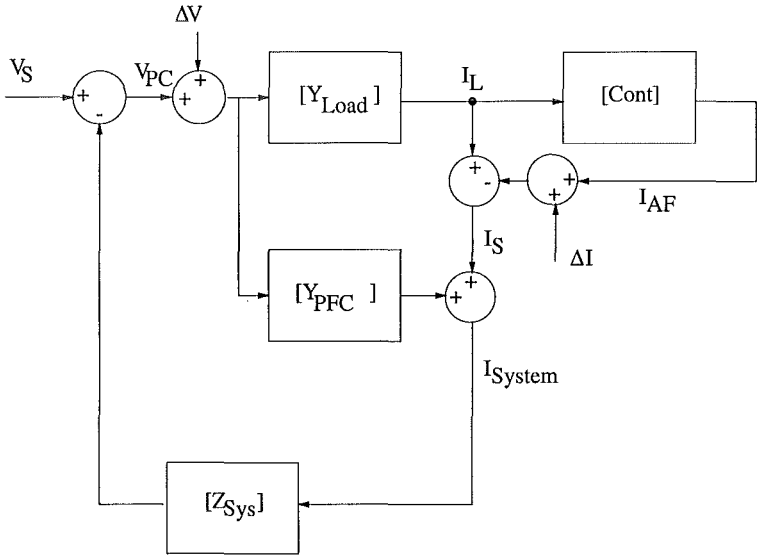

(b) Block diagram

Figure 3.7 SAF system with power factor correction capacitors upstream.

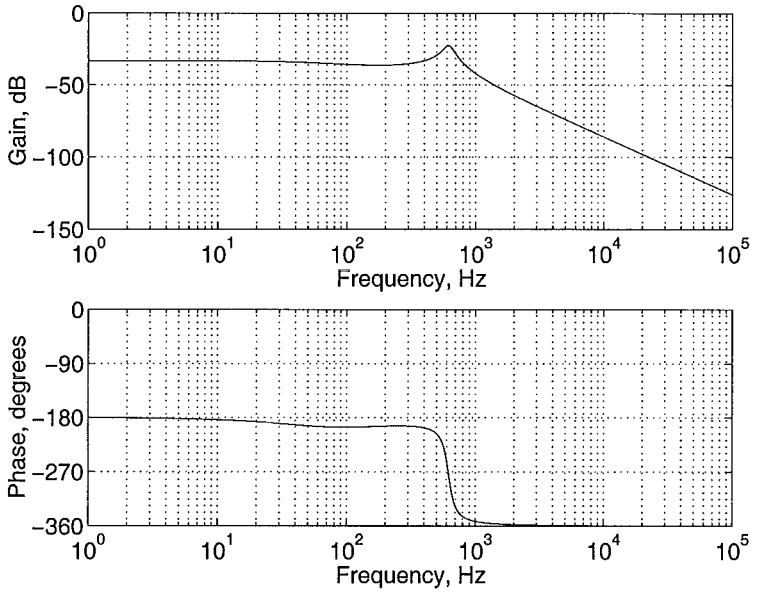

Figure 3.8 Bode plot of SAF transfer when PFC capacitors are connected upstream.

result in the removal of any damping that the load provides to the AC system. Note that this effect does not depend on the connection or otherwise of a capacitor.

3.8 INFLUENCE OF SAF ON THE LOAD

A similar intuitive look at the effect of the SAF can be obtained by taking the load's view of the SAF plus AC system combination as in Figure 3.11. Consider the load injecting a non-fundamental current into the SAF plus AC system combination. This current is measured by the SAF and the SAF current ensures that none of the original current reaches the AC system. This means the terminal voltage does not change. The effective impedance of $\frac{\Delta V}{\Delta I}$ is 0 so the upstream impedance seen by the load at non-fundamental frequencies is zero. From a loads point of view the system impedance has become much reduced at non-fundamental frequencies.

3.9 SUMMARY

The control system approach to power conditioner analysis has been introduced. This allows the analysis of SAF and other power conditioner systems to be placed in a framework to consider how the component parts of the system interact. An initial analysis of the load current measurement (LCM) connected SAF shows that SAF operation changes the current flowing into the load if the load admittance is not zero. The interaction of the SAF with other system components such as power factor correction capacitors causes instability if they are connected electrically downstream of the SAF. The upstream connection of PFC capacitors does not cause instability but the action

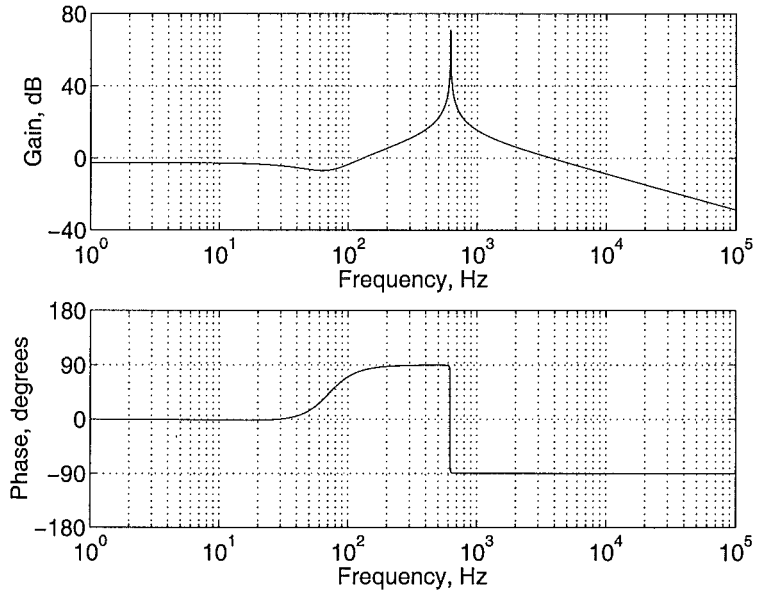

(a) SAF not operating

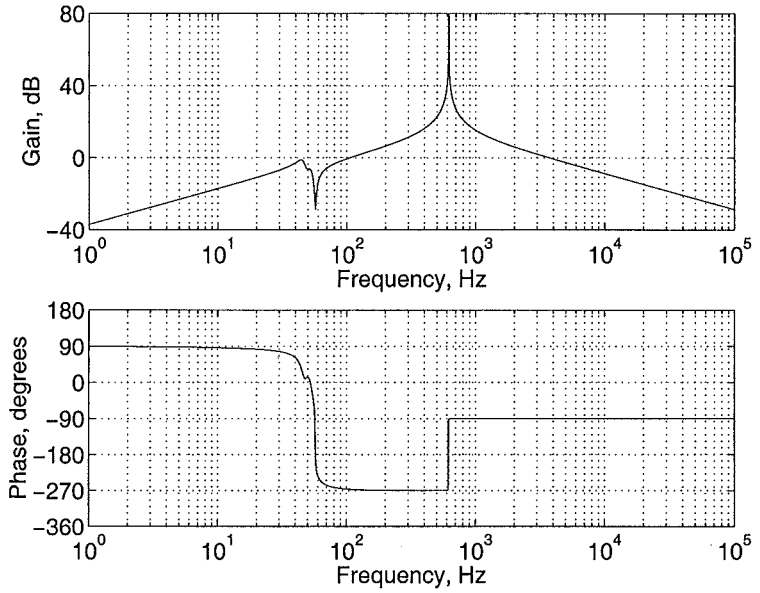

(b) SAF Operating

Figure 3.9 Bode plots of system voltage to system current transfer with power factor correction capacitors connected upstream of the SAF showing how the SAF operation removes damping at low frequencies.

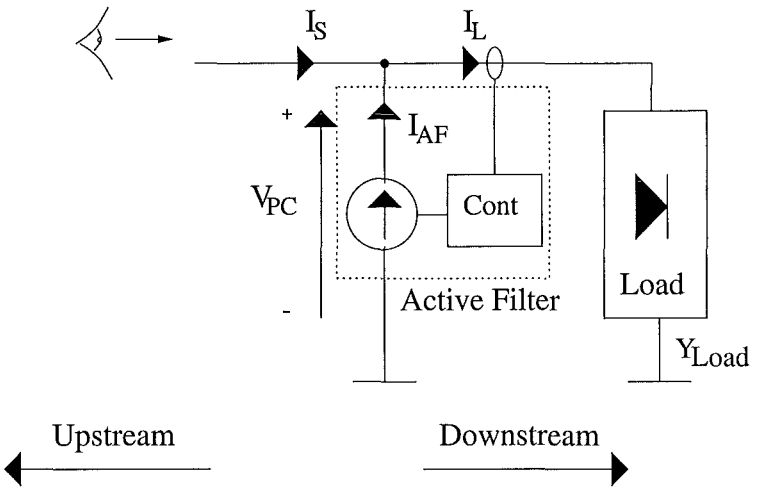

Figure 3.10 Effect of SAF on the response of the load as seen by the AC system.

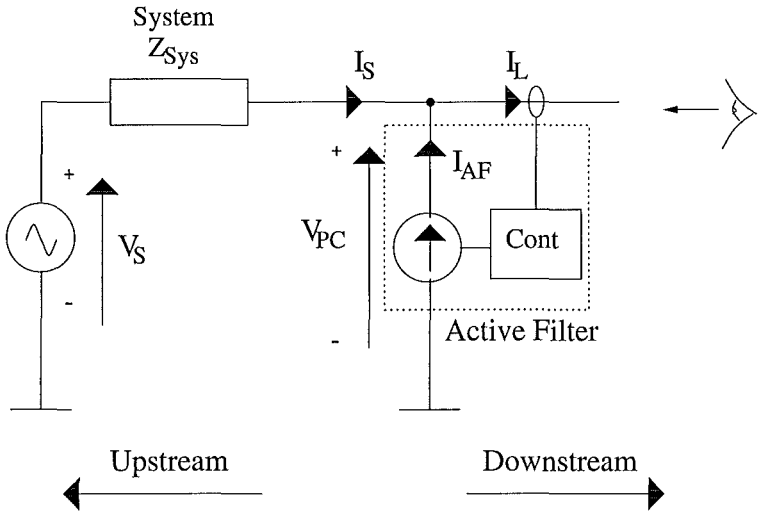

Figure 3.11 Effect of SAF on the effective AC system seen by the load.

of the SAF is to remove the damping provided by the load and this may have an implication for AC system transient damping. The fact that the forward transfer of a LCM SAF depends on the sensitivity of the load and the fact that the load will be in all probability non-linear means that representing or modelling the non-linear load in a way that fits with the SAF operation would be useful. The impedance presented by a non-linear load determines the effectiveness of shunt active filtering and the stability of the SAF-AC system-load combination. In the following chapter the experimental system capable of performing shunt active filtering and measuring the way in which non-linear rectifier loads behave is described. This system will allow the control system approach to power conditioner analysis presented in this chapter to be validated experimentally.

Chapter 4

THE EXPERIMENTAL SYSTEM - HARDWARE, FIRMWARE AND SOFTWARE

4.1 INTRODUCTION

This chapter describes the target test system implementation including all hardware, software and firmware. The system performs the SAF operation and is used to measure the behaviour of non-linear loads. This allows the behaviour and characteristics suggested by the theoretical models to be confirmed.

4.2 FUNCTIONAL OVERVIEW AND DESIGN APPROACH

An overview of the system to perform experiments and take measurements is shown in Figure 4.1. The three-phase AC supply system is connected to a non-linear rectifier load and a three phase current controlled switching converter. A central digital signal processor (DSP) based controller measures voltages and currents and generates current demands. The load current and the voltage are measured by the controller. As the controller is software based, a number of different control strategies can be implemented by changing the software. A three-phase approach is chosen because a single-phase AC system is a sub-set of the three-phase system. This means that single-phase experiments can be performed with three-phase equipment but the converse is not true. Also, the use of a three-phase controlled converter means that the current to provide the real power flow to maintain DC bus voltage does not have significant sub-harmonic content which can occur with single-phase systems [Round 1992].

4.2.1 Operating framework

The experimental system is designed to perform three functions. These are to shunt active filter, to generate and inject perturbing currents for frequency response measurements and to collect and store measurements of the currents and voltages. Figure 4.2 shows the total measurement and acquisition system. The current into the load and the voltage at the load terminals is measured by analogue to digital converters (ADCs).

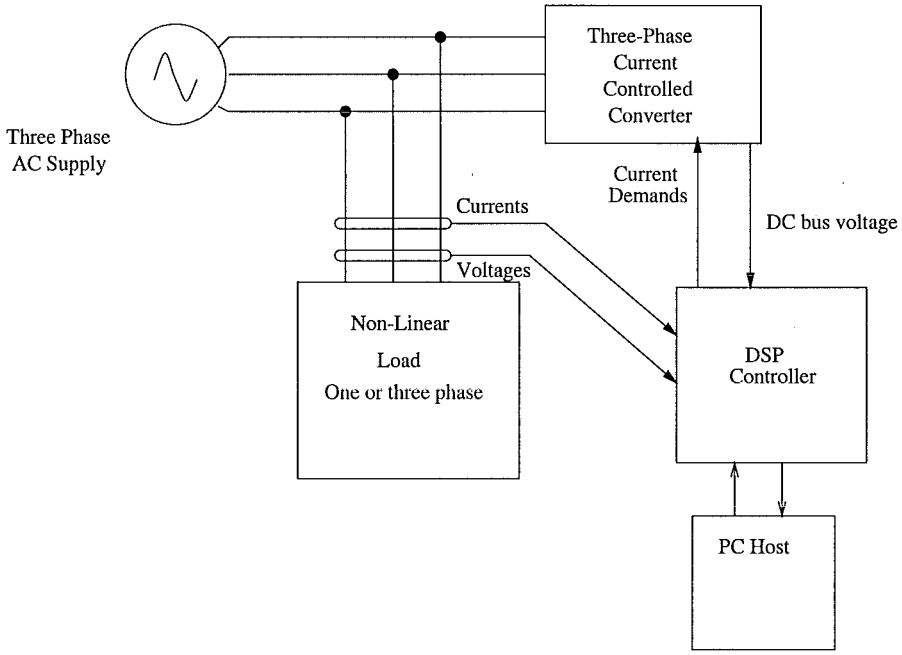

Figure 4.1 Experimental system overview.

These ADCs are connected to the field programmable gate array (FPGA) part of the central controller by serial communication links (SCL). The FPGA provides all the interfacing, handshaking and logic functions for the controller. This is described in more detail in section 4.3. An ADC also measures the load DC bus voltage for completeness. The three-phase converter current is measured along with its DC bus voltage. Switching signals from the FPGA complete the current loop. The DSP provides the processing power for the system and executes the control software. The PC host is used to house and power the controller. Software running on the PC provides supervisory control of the entire system and a user interface. The user interface allows the system to be started, stopped and reset from fault states. It also displays system information and data to the user. In order to facilitate the measurement and collection of experimental data the PC software includes a system that can change the operating condition, record the resulting data, store it to the PC hard drive and then move on to the next operating condition. This allows frequency and phase sweeps to be made automatically.

4.2.2 Control system overview

The control of a SAF requires measurement of the control input, be it the load current, the supply current or the voltage. The harmonic or undesired components of the waveform must be isolated and the output demand sent to the switching controller. With three-phase systems the use of the so called rotating control systems such as the synchronous reference frame (SRF) [Bhattacharya *et al.* 1991], shown in Figure 4.3, or the

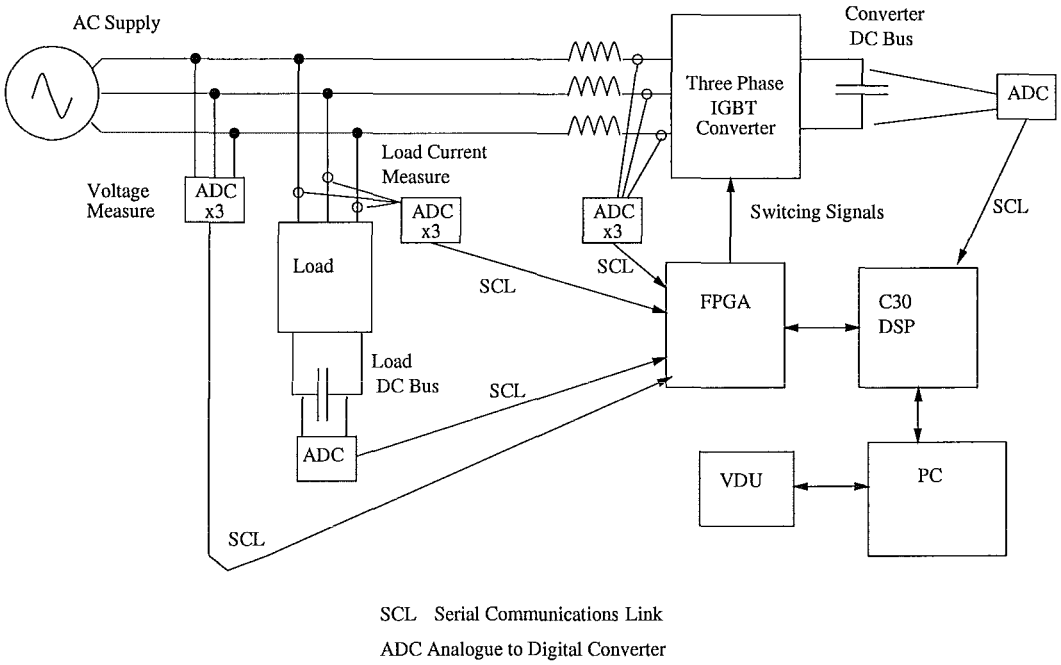

Figure 4.2 Measurement and acquisition function.

instantaneous reactive power theorem (IRPT) is a suitable choice [Akagi *et al.* 1986]. A synchronous reference frame system is used as the base for the experimental control system. The reasons for this are that it provides a stable phase reference for frequency domain analysis and the real power for the maintenance of the SAF power converter's DC bus voltage can be drawn from the supply with only fundamental frequency. As single-phase systems are a sub-set of three phase systems it is possible to implement a single-phase SAF alongside the three-phase framework effectively using the three-phase system as a real power controller. Figure 4.3 shows the three input signals converted to an equivalent two-phase system. Since there is no neutral connection, no zero sequence exists so the three to two transform does not remove any information from the signals. The two-phase signals are then frequency shifted by the vector rotators so that the fundamental frequency real and reactive power producing components are shifted to zero frequency and are the signals, d and q respectively. The d and q components are filtered to remove or retain the desired frequency and sequence components. The DC bus is maintained at a constant set value by the PI controller which produces a real power demand that is added to d_{out}. The total current demands are them formed from the re-rotated two-phase outputs α_{out} and β_{out} by a two to three conversion that is the inverse of the three to two conversion. The entire system is synchronised to the fundamental voltage of the AC system with a phase locked loop that with a lookup table produces sine and cosine waveforms at the fundamental frequency ω_0. These two signals are used to perform the frequency shift with the vector rotators.

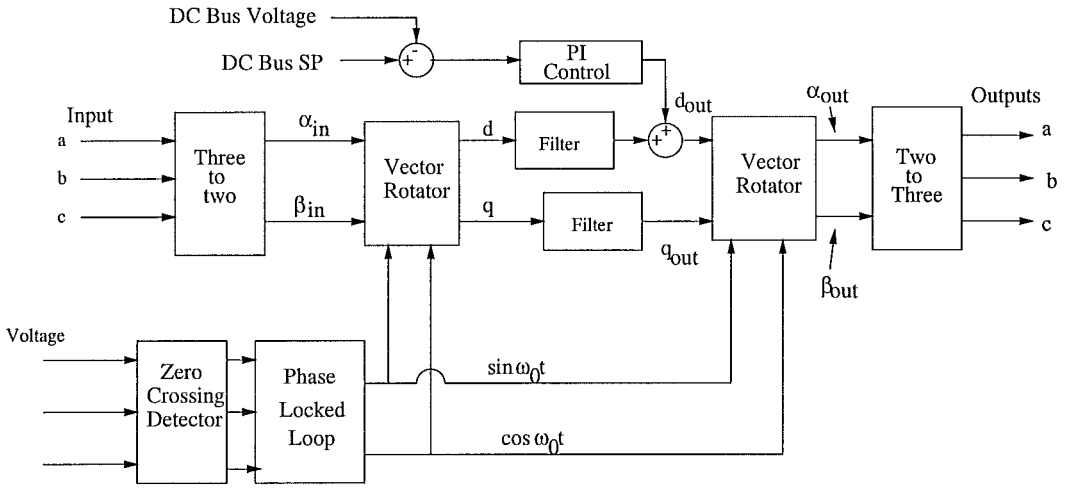

Figure 4.3 Three-phase control system framework.

4.2.3 Use of a current controlled converter

The converter is operated as a hysterisis current-controlled voltage-source converter. This means that the current is controlled with a high bandwidth and the control is robust to system parameter change, disturbances and noise [Brod and Novotny 1985]. As an example of the effectiveness of a current controlled system in rejection of a disturbance, consider the case where an AC power system develops a significant negative sequence voltage. If the converter voltage is controlled and there is no control loop to detect and control negative sequence current it is possible that the converter current will have a large negative sequence component. If, however, the current itself is the control input variable to the converter the converter voltage is adjusted very quickly (within one or two switchings) to ensure there is no negative sequence current. Typically negative sequence voltages in AC systems are small but the sensitivity of the converter current to this voltage can be very large as the output inductors are small. The control of the current in the converter means that the central controller generates current demands. A dedicated switching controller switches the converter to maintain the currents without further intervention from the central controller.

4.3 HARDWARE AND FIRMWARE

In order to minimise the system's data acquisistion overhead and therefore maximise the available processing time for the DSP, the data measurement system is implemented so it requires no software intervention from the DSP. The system is part of the FPGA which provides all necessary interfacing from the ADCs, PLL and IGBT converter to the DSP. FPGA technology provides reconfigurable programmable logic that allows system on chip designs [Xilinx Corporation 1998]. Figure 4.4 shows the external interfacing for the FPGA, the DSP and the PC. The PC communciates with the DSP via dual port

RAM, which the PC accesses via the ISA bus. This RAM is mapped into the DSP's main memory. The FPGA is connected to the DSP via the DSP's expansion bus. Other FPGA connections are the serial communication links (SCLs) to the ADCs, the PLL connections and the switching signals to the converter. Figure 4.5 shows

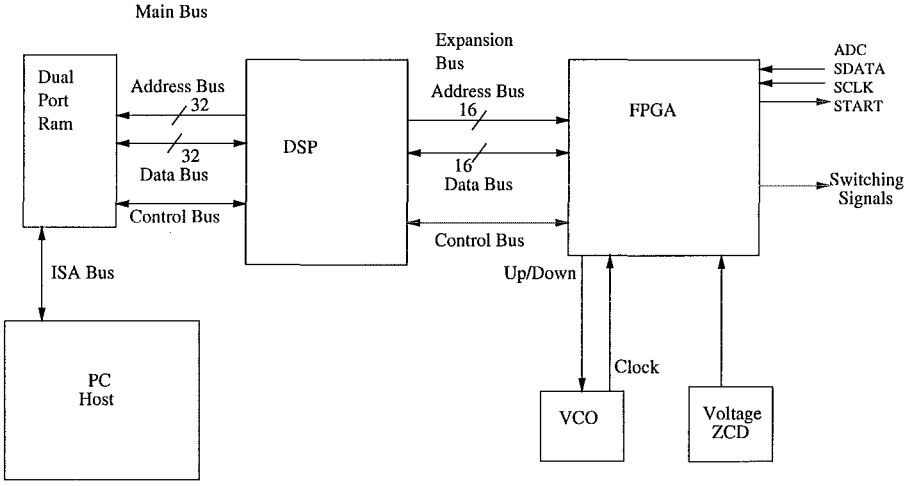

Figure 4.4 Digital interfacing detail for PC, DSP and FPGA.

a functional diagram of the FPGA design used to implement the interfacing for the experimental system. This interface is made by programming an FPGA with the design using circuit capture and design entry tools from Xilinx [Xilinx Corporation 1998]. The internal FPGA design has a bus interface that connects to the DSP expansion bus. This interface produces an internal data, chip select and control bus that connect the subsytems. The ADC subsystem receives serial data from the external ADC boards and stores the data in parallel latched registers. Writeable memory mapped command and control registers allow the DSP to give current demands and other control commands. This allows functions such as starting, stopping and the change of system parameters. The phase lock loop subsystem, described in detail in section 4.3.2, locks the entire control system to the positive sequence fundamental of the AC system voltage and produces a regular sampling clock at 128 times the fundamental frequency. This is used as the sampling clock for the DSP software and it generates the start pulse for the ADC system and also the DSP interrupt. The current control sub-system uses three dedicated ADC sampling at 200kHz to measure the converter current. By comparing these feedback currents to the current demands from the DSP the inverter switch signals are generated. This is described in section 4.3.3.

4.3.1 Analogue to digital converters

The FPGA system connects to ten 14-bit ADCs that measure the system currents and voltages. Three ADCs are used for the current control loop and these sample

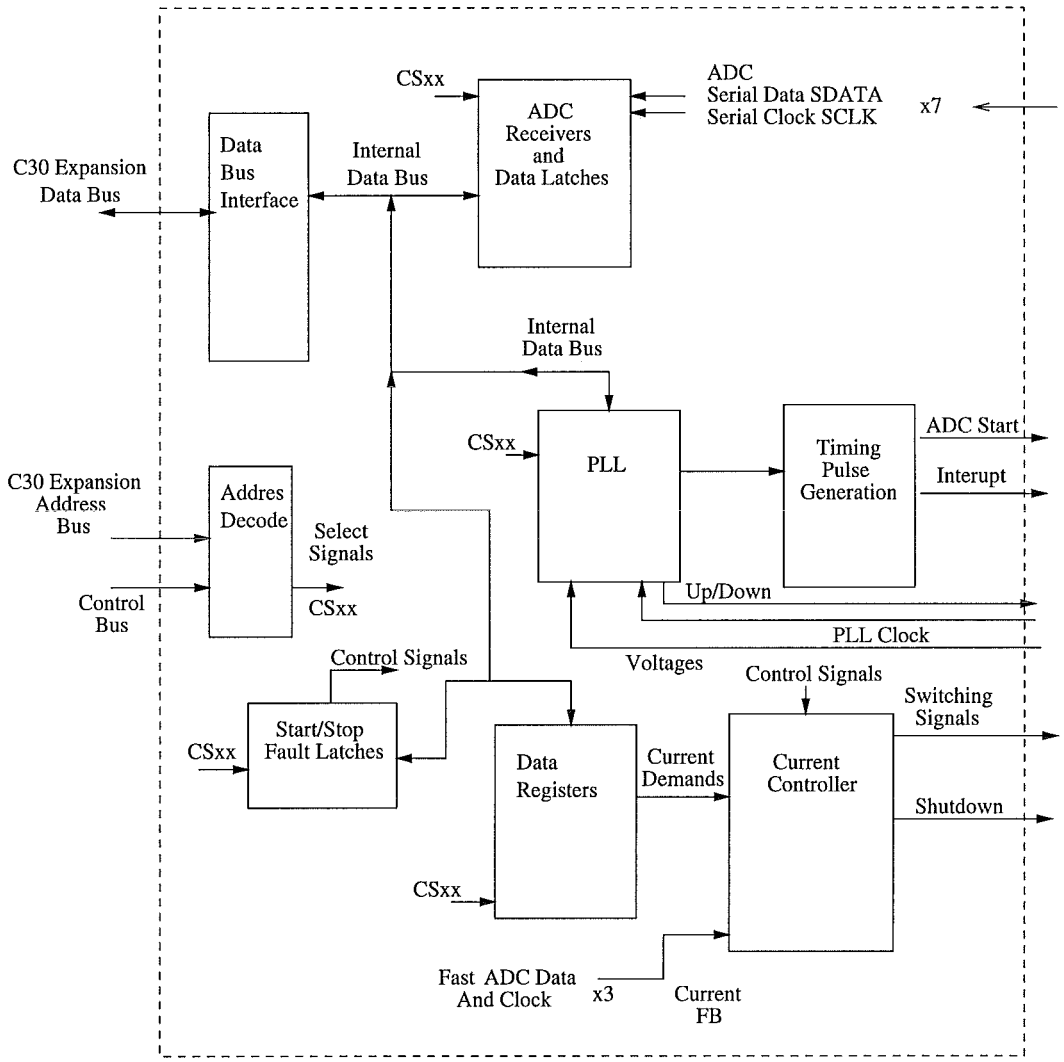

Figure 4.5 Internal Structure of FPGA.

and transmit continuously using a 4MBit/s data stream. The 6.4kHz sampling ADCs transmit the data using a 4MHz serial clock in a period of approximately 8 μs.

4.3.1.1 Analogue signal interfacing

Each ADC has the facility for the use of a low pass anti-aliasing filter. Filters are fitted to each card but to avoid phase shifts causes by filter group delay the filters' cut off frequencies are high so that they do not actually perform the anti-aliasing function. Each of the filters is included only to reduce the sensitivity of the ADC to the switching noise of the converter. Table 4.1 shows the filter orders and cut off frequencies for each ADC depending on its function. In order to measure the system voltages, resistor dividers are used to reduce the voltages to suitable levels for the ADC. Current measurements are made with LEM flux nulling current sensors. These have a bandwidth of 0Hz to 50kHz, which is more than suitable for a converter switching

Function	Cut Off Frequency	Order
Voltage measure ADC	6.4kHz	4th order Bessel
Current measure ADC	80kHz	2nd order Bessel
Current Control ADC	250kHz	2nd order Bessel

Table 4.1 ADC Filter cut off frequencies and orders.

frequency of 10kHz. A suitable burden resistor is used to convert the current output to a voltage suitable for the ADC.

4.3.1.2 Analogue to digital converter control and data reception

The FPGA includes the digital interface serial receiver system for the analogue to digital converters. The serial receiver system is shown schematically in Figure 4.6. Each of the ADCs produces 14-bit serial twos-complement data, SDATA, and a serial clock signal, SCLK. Conversion is initiated by a start pulse which is simultaneously broadcast to all seven measurement system ADCs (see the current control description in section 4.3.3 for information on the other three ADCs). This simultaneous start pulse ensures there is no data skew. Serial data is received by the serial-in parallel-out shift register and then moved into parallel registers mapped into the DSPs expansion bus memory space. A short time before the data has been received an interrupt is sent to the DSP. The delay of the DSP interrupt latency and initial interrupt processing means the ADC data is ready in the FPGA registers when the program reads it. This minimises the delay between sampling and the start of the control processing. The DSP program performs parallel bus reads to move the data into main memory.

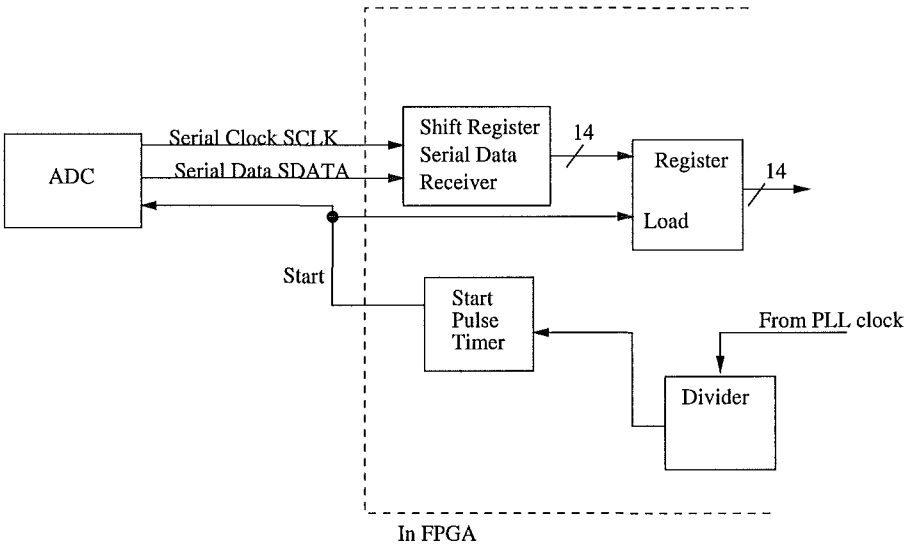

Figure 4.6 ADC serial data receiver and data register system.

4.3.2 Phase locked loop

The DSP software and the control system operate at a rate of 128 times per AC cycle. This means that each cycle has a constant number of cycles which ensures that the signals can be processed with a Fast Fourier Transform without having to use any windowing typically used with unsynchronised sampling (see section 4.3.2.1). Synchronisation is achieved using a three-phase phase locked loop as shown in Figure 4.7. This PLL compares the zero crossings of the low pass filtered three-phase AC line

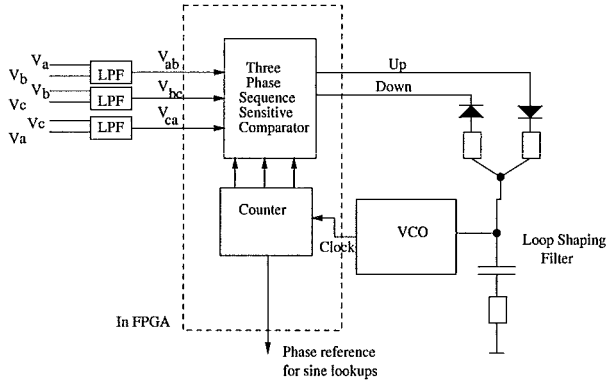

Figure 4.7 Phase locked loop system.

to line voltages with the crossings of a three-phase counter internal to the FPGA. The difference between the two sets of zero crossings, if any, drives the external analogue voltage controlled oscillator (VCO) faster or slower so as to drive the counter to match the zero crossings exactly. The three-phase edge driven phase comparator ensures that the system locks only to positive sequence. The VCO is implemented in analogue circuitry for simplicity. The PLL bandwidth is set to be approximately 3 Hertz using the loop filter [Encinas 1989]. This allows the PLL to lock reasonably fast and also ensures that any noise signals are rejected. The VCO operates at a nominal frequency of 102.4kHz. The sampling rate of one hundred and twenty eight samples per AC cycle is 6.4 kHz at a nominal 50Hz system frequency. This sampling rate gives a Nyquist bandwidth of 3.2kHz which allows measurement up to the 64th harmonic for a 50Hz system.

4.3.2.1 Fast Fourier Transform considerations

In order to determine and display the frequency components of current and voltage signals Fast Fourier Transforms (FFTs) are performed by the DSP. It is important that the data is either windowed or sampled synchronously to avoid spectral bin leakage [Brigham 1988]. The PLL system ensures this synchronisation and so data windowing is not required. Also, the number of samples taken should be made so that the FFT length is a power of two because this allows a fast algorithm [Ramirez 1985]. Two FFT lengths are used in the experimental system. The first uses one AC cycle of 128

samples giving a frequency resolution of 50Hz. The second has length 1024 samples giving frequency resolution of 6.25Hz.

4.3.3 Current control loop

The current control system has three parts (Figure 4.8). The first is the IGBT converter unit which incorporates gate drive and interface circuitry to connect signals from the FPGA. The second is an FPGA subsystem that initiates sampling of the current and performs serial reception of the data. The third is a set of comparators which compare the demand currents with the actual currents. From this comparison a switching decision is made. The switch signals, with suitable deadtime, then travel to the inverter gate drive interface and on to the inverter switches completing the control loop. This completely digital approach has been found to be appropriate for current controlled converters so long as the sampling rate is high [Ingram 1998]. Current control is achieved using hysteretic current control. This system is well suited to active filter applications as it has wide bandwidth and is robust to noise [Brod and Novotny 1985, Ingram 1998]. The incoming demand signal has a small positive and negative value added to form an upper and lower hysteresis bound as in Figure 4.9. The two resulting signals

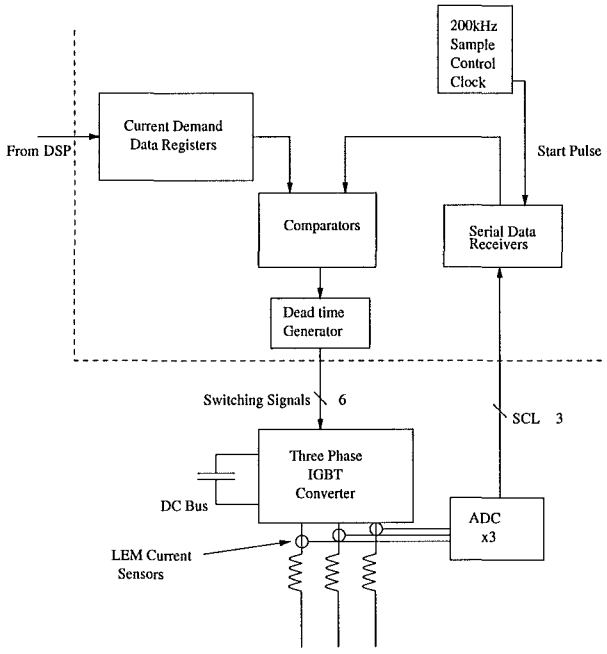

Figure 4.8 Current control system.

are compared to the measured current. If the measured current is greater than the upper bound then a switching decision is made to reduce the current. Conversely the opposite switching decision is made to increase the current if the measured current is less than the lower bound. This results in the behaviour as shown in Figure 4.9 where the current is switched up and down between the upper and lower bounds. As the

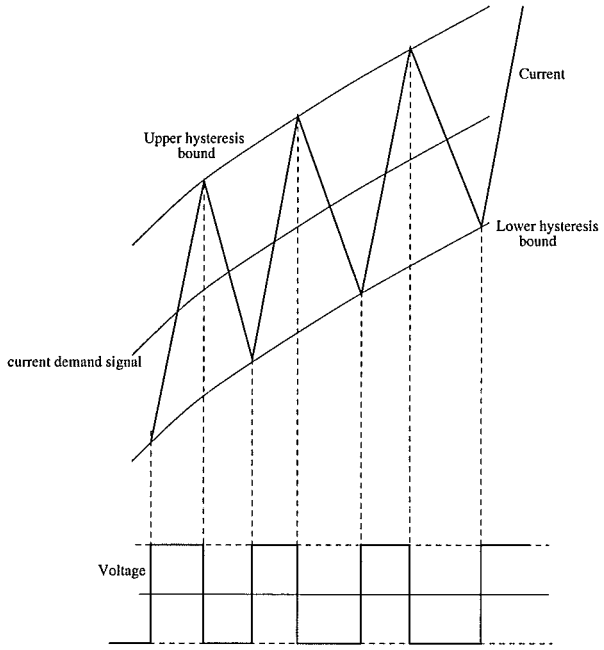

Figure 4.9 Current switching.

current control system operates a three-phase converter bridge there is the possibility of interaction between the phases. The effect of one switch applying the positive DC bus voltage is aways to increase the currrent in that phase. However, if one of the other two switches is also applying positive DC bus voltage then the voltage applied to the inductor is only half that applied if both the other phase switches are applying negative DC voltage. This problem has been previously noted and is a concern in three-phase inverters connected to three-phase voltage sources. Examples of such situations are the induction motor drive and the active filter situtaion. Generally the switching pattern of the three-phase hysteretic current control system, where each phase is individually controlled, is adequate but the switching controller can suffer from high frequency limit cycles due to the effect of switching one phase on another [Brod and Novotny 1985]. In order to eliminate this problem all three switchings can be controlled simultaneously. The intention is to minimise the current ripple and the number of switchings thereby reducing the switching loss. A three-phase current control system [Kwon *et al.* 1999] is implemented in the FPGA along with the simpler individually controlled approach. The use of either the individually controlled or simultaneously controlled switching approach is software selectable.

4.4 DIGITAL SIGNAL PROCESSOR AND SOFTWARE

The digital signal processor forms the heart of the control algorithm implementation for the experimental system. A TMS320C30 DSP from Texas Instruments is used as the controller. This DSP has in-built fixed and floating point data types. This allows

for rapid software development because it avoids the data scaling and normalisation problems which can occur when using fixed point DSPs. The DSP also has a number of other features that include automatic index generation and circular addressing. This allows the fast and efficient implementation of digital filters [Texas Instruments 1989]. The DSP is clocked with a 32MHz clock performing 32 MIPs [Texas Instruments 1994].

4.4.1 Program flow

The DSP software has two main parts. These are the main or supervisory routine and the interrupt service routine and together they implement the control framework described in section 4.2.2. The main routine performs housekeeping such as starting and stopping the converter and communicating with the PC host. The interrupt forms the heart of the control and performs the co-ordinate transforms, filtering and other control functions to produce the current demand signal for the current controller. The software implements a rotating reference frame locked to the local AC bus voltage by the PLL (section 4.3.2) as described in section 4.2.2. The DSP software is written in C code with assembly language routines added to utilise the special features of the DSP when appropriate.

4.4.2 DSP Supervisory Loop

When the DSP is initially started it first performs an initialisation shown on the left of Figure 4.10. This involves reserving a number of data areas, initialising filter coefficients and setting up trigonometric look up tables. The program then ensures that the FPGA is properly programmed. If not the DSP program sends that message to the PC. The DSP then sets a number of control registers in the FPGA. These control registers include start-stop and fault latches, sampling speed control and deadtime selection for the switching controller. The DSP program then branches to the main loop. The main loop of the DSP program (Figure 4.10) is repeated continually. Initially the DSP checks to see if the PC host has issued a new command. This routine allows the operational control of the controller by parsing control commands from the PC. If the command is valid the DSP performs the required action. If the command is not valid the DSP ignores the command. The interrupt service routine (described later in section 4.4.3) collects eight cycles of AC data on command from the PC. If this has occurred and the collection completed then an FFT is performed on this data. When this FFT result is valid the DSP signals the PC. Along side the eight cycle collection, alternate buffers of one AC cycle of data are filled continually by the interrupt service routine. When one of these buffers is full then the DSP signals this to the PC. The PC then uploads and displays this data.

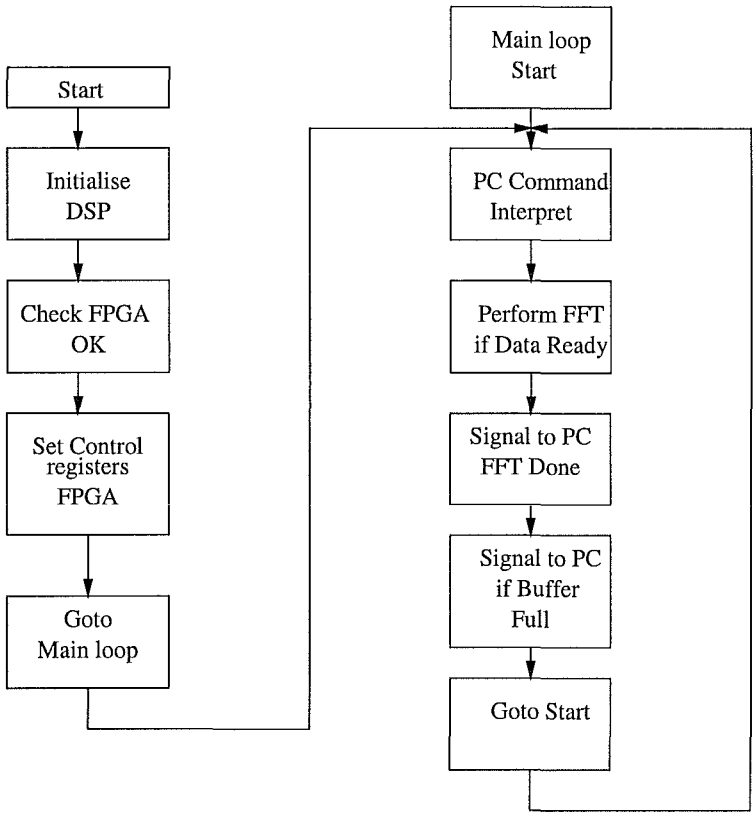

Figure 4.10 DSP software initialisation routine and main loop.

4.4.3 Control interrupt service routine

The main control interrupt is where the measured input data is loaded into the DSP. The first operation in the interrupt routine is to load the counter from the phase locked loop (see section 4.3.2). The counter is used to index and retrieve sine and cosine values from the lookup tables generated during the initialisation. Input data is loaded from dedicated data registers in the FPGA as described in section 4.3. Control calculations are performed and the current demand outputs are generated and written out to the FPGA current control sub-system registers (section 4.3.3). The final operation in the interrupt is to perform the data collection if required (see section 4.4.4). The timing of the interrupt routine is shown in Figure 4.11(b). The analogue to digital converters (ADC) are started before the DSP interrupt occurs. This means that the interrupt latency does not cause any more delay than absolutely necessary. The PLL counter is read and then all the data loaded. This takes approximately 5 μs. The control calculation typically takes 28 μs and the data collection approximately 10 μs for a total interrupt processing time of approximately 43μs. The repetition rate of the interrupt is 156 μs.

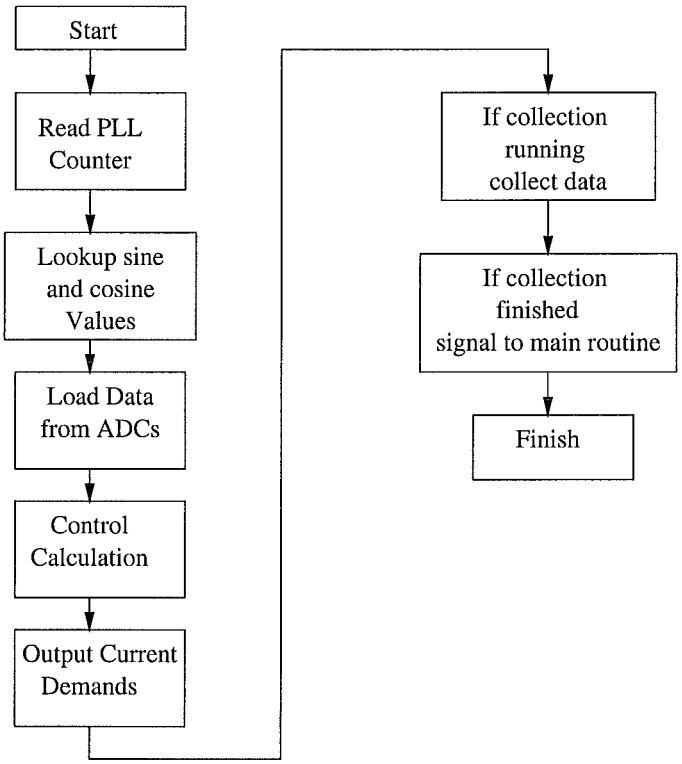

(a) Interrupt service routine flow.

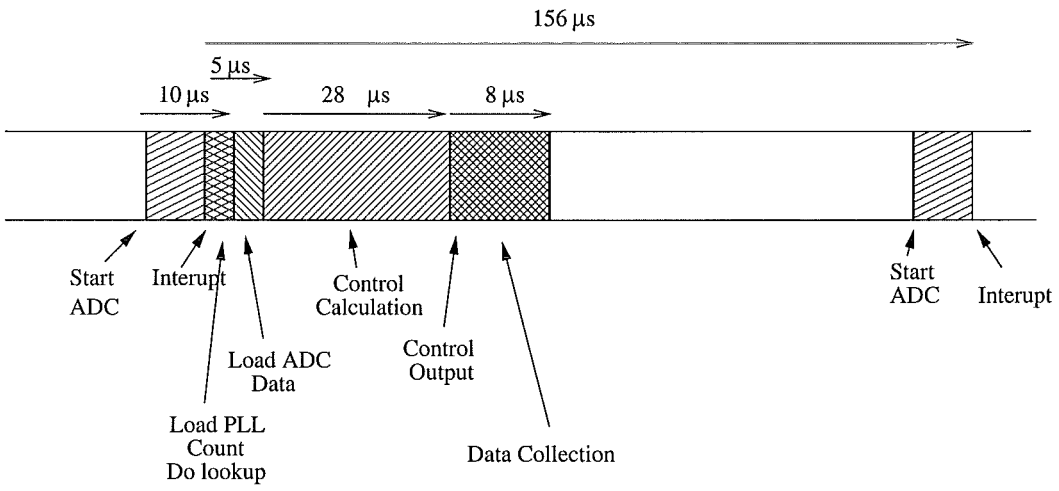

(b) Interrupt service routine timing.

Figure 4.11 DSP interrupt service routine.

4.4.4 Data collection

Along with performing the control, the interrupt routine can collect and store data into memory buffers on a sample by sample basis. This allows the system to measure its own

performance and for the collected data to be uploaded by the PC host. The collection system is overlaid on the interrupt control processing by using a small dedicated routine at the end of the interrupt service. This routine uses a pre-defined list of source variables and a list of destination buffers to, at each sample, collect and store data from each source. The list of source variables can be changed at run time. This allows the data collection system to be used to calibrate the gain and null the offset of each input ADC.

Two different variants of the data collection routine are used. The first collects floating point data and converts to integer form and moves it to one of a double buffer set. This "floating to integer system" collects one AC cycle of data (128 samples) and then signals the PC that the buffer is full. The integer storage allows the PC to upload the data and operate on it without having to do any format conversion while the double buffering ensures that the PC upload does not cause a memory clash with the DSP. This integer data is used by the PC for real time on screen display. An FFT of length 128 is also performed on the data buffer and the result converted to integer format allowing the PC to display this information. Floating point data can be uploaded by the PC but due to format differences, the DSP uses a propriety floating point format, the PC must process tha data before it is useful. The floating point collection system is used to provide data for FFT analysis and so is configured to collect eight AC cycles of data when signaled by the PC host. This floating point version is the system used to collect data to measure the response of the load or the system impedance. When the FFT is performed the DSP indicates that the results are ready and the PC uploads, converts and stores the data for post processing.

4.5 SUMMARY

This chapter has described the experimental system. The system is a three-phase system with an IGBT switching converter. This converter is controlled with a current control loop to produce the current demands generated by the control software running on the DSP. The system also measures the load current allowing the load's characteristics to be measured. A stable phase reference is provided by a phase locked loop and this ensures that the sampling is synchronised with the AC system frequency. The DSP software is interrupt driven and is capable of collecting data and performing FFTs on the data. This data can be uploaded by the PC host for storage and post processing. The PC also provides a user interface and the ability to control the system. The system is used to perform experiments measuring the response of rectifier loads. It also performs the shunt active filtering.

In the next chapter the frequency domain modelling of non-linear loads such as the single-phase rectifier is presented. Chapter 6 details the use of the frequency domain in developing an accurate model of the single-phase rectifier. In chapter 7 the experimental system described in this chapter is used to make measurements to confirm the rectifier

model.

Chapter 5

FREQUENCY DOMAIN REPRESENTATION OF RECTIFIER LOADS

5.1 INTRODUCTION

When represented in the frequency domain, signals are described by the sum of a number of sinusoids. The Fourier and Laplace transforms link the time domain, which is the familiar waveform representation of a signal that can be viewed on an oscilloscope, to the frequency domain where the spectrum is the visualisation method. In the case of non-linear power electronic rectifier loads the application of an AC voltage at one frequency causes a current that contains a number of frequencies. For a single-phase rectifier, applied fundamental voltage at 50Hz produces currents at 50Hz, 150Hz, 250Hz and all the continuing odd harmonics. This one frequency to many frequency response makes the device non-linear in a classical time domain sense because a classically linear system has a single frequency to single frequency transfer.

When system behaviour is considered, the small-signal response is important as it determines absolute stability and relative stability or robustness. The frequency domain allows the robustness of systems to be quantitatively examined and this is the reason for pursuing a frequency domain representation of a non-linear load.

This chapter describes non-linear rectifier load modelling using the frequency domain. It first outlines the reasons for developing frequency domain models of non-linear loads and then shows that a small-signal approach is useful and suitable for the modelling and analysis of rectifier type loads connected to an AC power system and SAF. The approaches to modelling rectifiers are surveyed and the switching function model is found to be the most appropriate. Modulation, as it applies to rectifier loads, is described along with the phasor representation of sinusoidal signals. The Frequency Transfer Matrix (FTM) method to represent the modulation is then detailed. A number of examples of the accuracy and suitability of this method are shown. The FTM are interpreted as the frequency domain partial differentials of the two variables they connect and the usefulness of this is demonstrated.

5.2 APPROPRIATENESS OF THE FREQUENCY DOMAIN

The key operational requirement of any piece of equipment connected to the AC power system is that the device operates correctly and does not prevent other devices from doing the same. Generally, whether a device will function or not is very difficult to establish in the time domain. This is because the methods to allow for component variability, variation and modelling inaccuracies do not exist in the time domain. Concepts such as robustness of performance exist only in the frequency domain. Time domain analysis, which is effectively repeated time domain simulation, cannot ever explore the entire operating space of a device and cannot intrinsically account for the variability and modelling inaccuracies [Mollerstedt and Berhardsson 2000]. Almost all control design techniques including open loop bode design and root locus techniques rely on the frequency domain.

The frequency domain is perhaps less intuitive than the time domain. The representation of physical phenomena with a number of frequency components is difficult for humans to perceive or visualise. This is because the time domain is the one in which humans live and it is perhaps this preference for the time domain that has lead to large numbers of time domain simulation based investigations of both linear and non-linear systems. In fact, time domain simulation of AC power systems is generally accepted as a suitable and robust method of analysis.

5.3 SMALL-SIGNAL MODELLING OF RECTIFIERS

The AC power system is defined largely by its fundamental frequency voltage which is generally close to sinusoidal. This voltage drives the switching of rectifier type loads. In the case where the rectifier has uncontrolled switching devices the actual instant at which the devices switch depends on the voltage. For thyristor controlled switching rectifiers the voltage does not determine the switching instants but does drive the switching action. Therefore the fundamental voltage establishes a periodic repetitive response in the rectifier load.

Any voltage disturbance in the AC system is superimposed on the fundamental frequency voltage. A non-linear load's response to a disturbance depends on both the disturbance and the periodic effects of the fundamental voltage driven switching. This situation, where the fundamental voltage establishes the switching pattern, means that the device's operating conditions can be considered constant. Therefore, a small-signal approach is suitable. The small-signal approach divides the excitation and response into two parts as shown in Figure 5.1. The first is the base case response, I_{Base}, and this is the response caused by the base case voltage, V_{Base}, which is typically a fundamental voltage. The second is the small-signal response ΔI which is the change in the response caused by the disturbance ΔV. This small-signal approach has been

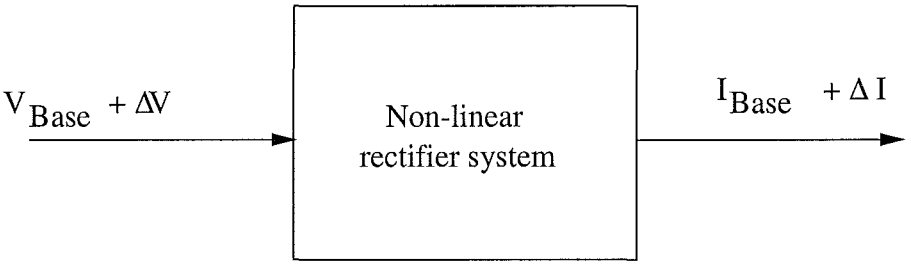

Figure 5.1 Rectifier system showing both the base case response and the small-signal response (Labeled with Δ).

used with rectifiers to characterise the devices in a way that is useful for control design or analysis [Todd *et al.* 1997, Wood 1993].

The usefulness of a small-signal approach in the SAF application is apparent when the SAF operation is considered. The LCM SAF can be seen to cause a small change in the voltage at the point of coupling because harmonic currents from the load no longer flow into the system. In other words the SAF changes the voltage drop in the system impedance. The small change in voltage causes a change in the load current. Accurately predicting the change in the load current would be useful as it allows the effectiveness or otherwise of the SAF to be determined. Steady state stability of the SAF system depends on the small-signal response. The response of the total system, including the non-linear load, to a small perturbation in the active filter output current will indicate if the system is stable or not. In chapter 3 the instability caused by power factor correction capacitors connected downstream of the LCM SAF is shown and discussed. If it is possible for a non-linear load to present an capacitive impedance then there may be the possibility of instability when the SAF operates with non-linear loads.[1] The desire to determine that the SAF, load and AC system will operate together in a stable, robust fashion without repeated time domain simulation is the motivation for the accurate modelling of non-linear loads.

5.3.1 Possible non-linear rectifier models

Load and supply current measurement SAF power conditioners are installed with the intention of removing current harmonics, so it is usual that the load is non-linear. As an increasing amount of electrical power is processed by non-linear rectifier devices [Bose 1992] it is probable that all power conditioners will operate connected near or to a non-linear load.

When a model of a non-linear system is generated there is generally a loss of information about the system. Typically the model represents only the dominant charac-

[1]The operation around the world of SAFs in a stable and useful fashion points to the fact that non-linear rectifier loads do not present capacitive impedances. The question then becomes what impedance does a non-linear rectifier load present to the AC system.

teristics of the system. The intention of the model is to represent the switching system with an equivalent linear time invariant (LTI) system [Verghese and Mukherji 1981]. This representative LTI system is then used with frequency domain analysis and design techniques to ensure the overall system operates as expected in a stable fashion. It also allows the system robustness to variations and disturbances to be estimated.

A number of well known methods to model non-linear power electronic switching systems exist. These methods generally involve some kind of averaging. This averaging generates an approximation to the behaviour of the system effectively producing an equivalent transfer function or set of poles and zeros to describe the system. Previous models of non-linear loads used in SAF analysis have been simple and have removed large amounts of information. A constant current source removes all sensitivity to voltage variation effectively making the load small-signal admittance zero. Using a linear time invariant impedance Z_{Load}, as in section 3.5, leads to the questions what is the correct value for Z_{Load}, how does it vary with frequency and how does the non-linearity fit with a linear representation?. The answer to this question lies in the choice of the best modelling approach.

5.3.1.1 Classical averaging

One of the methods used to represent non-linear switching circuits in classical averaging. This involves the replacement of switching functions in system equations with the continuous average of that switching [Verghese and Mukherji 1981]. This system typically produces suitable models when the switching frequency is considerably higher than the natural frequency of any mode of the system [Verghese and Mukherji 1981]. The averaging methods assume that the desired model bandwidth is less than the switching frequency thereby ensuring that the Nyquist sampling limit is obeyed. This means that they do not produce useful models if the switching of the system does not meet the Nyquist sampling criteria.

5.3.1.2 State space averaging

The averaging process has been formalised in the state space averaging approach [Cuk 1984]. This approach provides a formal framework for averaging. A weighted sum of the state transition matrices of the different circuit switching configurations is computed and from here poles and transfer zeros can be calculated. Generally, the switching frequency must be considerably higher than the frequency at which control action is performed or considered [Cuk 1984] but this cannot in itself guarantee that the model behaviour accurately reflects that of the original system [Verghese and Mukherji 1981]. Inaccuracies can also occur if the mode of the system changes.

5.3.1.3 Mode changes and large signal models

The modelling or analysis of non-linear systems in the large signal is often problematic. The principal difficulty is that the mode of operation of the system can change with the amplitude of a disturbance. Consider a voltage source rectifier connected to an AC system and the AC system voltage changing so that its peak is below the DC side voltage of the rectifier. No switching device in the rectifier is ever forward biased so no device can conduct. Effectively, the rectifier disappears from the circuit for some time. Modelling this behaviour is difficult because the system behaviour varies with time in an unpredictable non-periodic way. Mode changes caused by large signal behaviour is outside the scope of this thesis.

5.3.1.4 Non-linear rectifier loads as modulators

One approach to modelling rectifier switching loads is to notice that these loads have a one to many frequency response. This is because the switching makes the device operate as a modulator. For the single-phase rectifier this can be observed when it is connected to the AC system. The fundamental ω_0 equivalent to 50Hz voltage connected to the rectifier causes currents to flow at frequencies $n\omega_0$ where $n = 1, 3, 5, 7...$. This is the normal operation response of the rectifier and it can be viewed as a frequency coupling. Any non-linear switching rectifier type load can be viewed as connecting its AC side to its DC side. It is immediately apparent that fundamental voltage on the AC side of a single-phase rectifier causes zero frequency voltage on the DC side of the device. Zero frequency current on the DC side delivers real power to the load and there is a corresponding fundamental current flowing on the AC side. This is in fact the primary function of a rectifier, to supply DC power while absorbing fundamental power. In order to represent the non-linear load as a modulator its modulation must be accurately represented. This can be achieved by describing the rectifier switching with a switching function.

5.3.2 Switching functions

The switching of non-linear power electronic rectifier loads means that an applied voltage causes current at more than one frequency to flow. This switching can be represented as a switching function with values 1, 0 and -1. These values correspond respectively to direct connection of the AC side to the DC side, no connection and reversed connection. The typical switching function, Ψ, and how it is developed is shown in Figure 5.2 along with the a typical fundamental voltage waveform. The development of the Fourier series of this pulse can be seen by considering the final switching function as the sum of two other functions both of which are based on the pulse waveform that repeats every 2π shown in Figure 5.2(a). The Fourier series of this base pulse is (5.1)

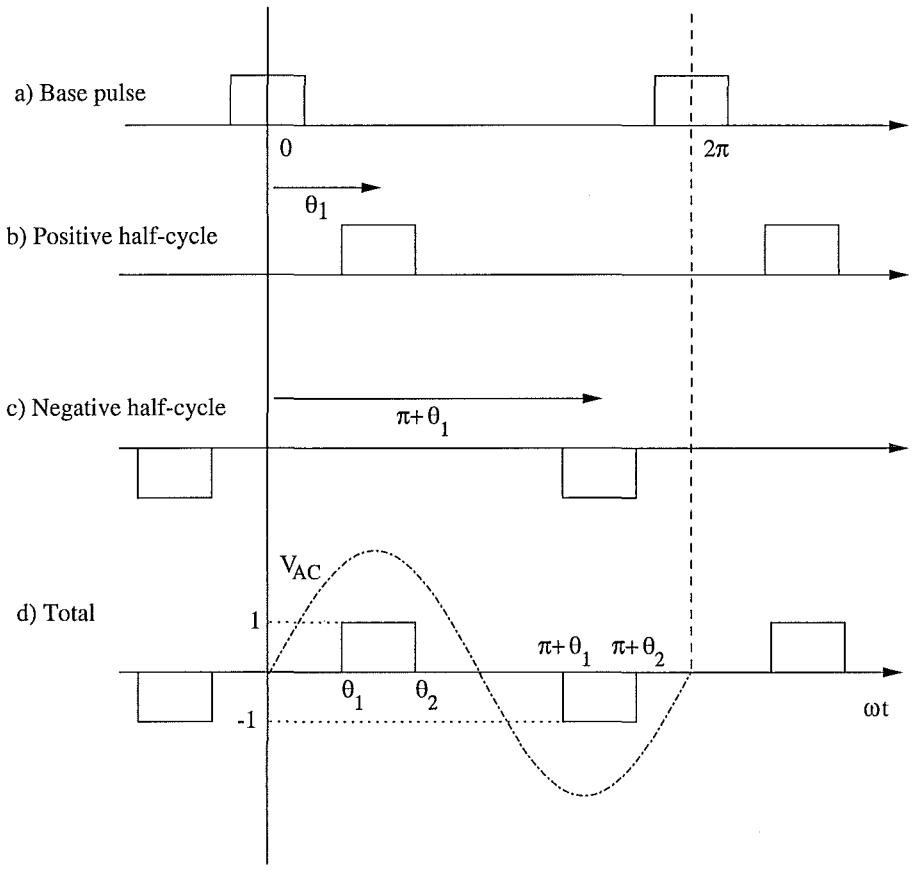

Figure 5.2 Single-phase switching function development showing time shifting and sign change.

where the switching instants are defined by the switching instant angles θ_1 (turn on) and θ_2 (turn off).

$$\begin{aligned}\Psi &= \frac{1}{2\pi}(\theta_2 - \theta_1) \\ &+ \sum_{m=1}^{m=\infty} \frac{2}{m\pi} \sin\left(\frac{m\theta_2 - m\theta_1}{2}\right) \sin(m\omega_0 t + \frac{\pi}{2})\end{aligned} \tag{5.1}$$

In order to time shift the waveform, the new time of $(t - t_0)$ is substituted for t in (5.1) which with $t_0 = \frac{\theta_1+\theta_2}{2\omega_0}$ gives (5.2)

$$\begin{aligned}\Psi &= \frac{1}{2\pi}(m\theta_2 - m\theta_1) \\ &+ \sum_{m=1}^{m=\infty} \frac{2}{m\pi} \sin\left(\frac{m\theta_2 - m\theta_1}{2}\right) \sin(m\omega_0 t - m\frac{\theta_1 + \theta_2}{2} + \frac{\pi}{2})\end{aligned} \tag{5.2}$$

This time shifting produces the Fourier series of the waveform in Figure 5.2(b). The negative half cycle switching pulse, Figure 5.2(c), is created by shifting the base waveform by $\pi + \theta_1$ and multiplying by -1. By adding these two shifted Fourier series the

total switching function series is found (5.3)

$$\begin{aligned}\Psi &= \frac{4}{m\pi}\sin\left(\frac{m\theta_1 - m\theta_2}{2}\right)\sin\left(m\omega_0 t - m\frac{\theta_1+\theta_2}{2} + \frac{\pi}{2}\right)\\ &\quad for\ m = 1,3,5,7...\\ \Psi &= 0\\ &\quad for\ m = 0,2,4,6...\end{aligned} \tag{5.3}$$

The DC side signal (voltage or current), Sig_{DC}, that results from the application of an AC side signal (voltage or current), Sig_{AC}, is the product of the signal and the switching function [Laird *et al.* 2000]. Multiplying the AC side signal by each switching function Fourier series (5.3) frequency component gives the DC side frequencies that are generated (5.5).

$$Sig_{AC} = \sin(k\omega_0 t + \delta_k) \tag{5.4}$$

$$\begin{aligned}Sig_{DC} &= \frac{2}{m\pi}\sin\left[\frac{m\theta_1 - m\theta_2}{2}\right]\cdot\\ &\quad (+\sin\left[(m+k)\omega_0 t + \delta_k - m\frac{\theta_1+\theta_2}{2}\right]\\ &\quad -\sin\left[(m-k)\omega_0 t - \delta_k - m\frac{\theta_1+\theta_2}{2}\right])\\ &\quad \text{for m} = 1,3,5,7...\\ Sig_{DC} &= 0\\ &\quad \text{for m} = 0,2,4,6...\end{aligned} \tag{5.5}$$

It can be seen from (5.5) that the switching function modulates AC side signals to the DC side. It also performs the reverse operation. As the switching function is made up of a number of different frequency components, the result of its operation on a signal is the sum of each of its component frequencies multiplied by the signal.

5.3.3 Representing modulation

The modulation of two signals X_k, equation (5.6) and Y_m, equation (5.7), of frequency $k\omega_0$ and $m\omega_0$ respectively, produces two resultant frequencies. These are commonly called the sum (5.9) and difference (5.8) terms as they occur at frequencies that are

the sum of and difference between the two original frequencies.

$$X_k = A\sin(k\omega_0 t + \delta_k) \tag{5.6}$$

$$Y_m = B\sin(m\omega_0 t + \delta_m) \tag{5.7}$$

$$Y_m * X_k = \frac{AB}{2}\cos\left[(m-k)\omega_0 t + \delta_m - \delta_k\right] \tag{5.8}$$

$$-\frac{AB}{2}\cos\left[(m+k)\omega_0 t + \delta_m + \delta_k)\right] \tag{5.9}$$

If the frequency, $(m-k)\omega_0$, of the difference term is negative then it is neccesary to retain this information. However by noting that (5.10)

$$\cos\left[(m-k)\omega_0 t + \delta_m - \delta_k\right] = \cos\left[(k-m)\omega_0 t - \delta_m + \delta_k\right] \tag{5.10}$$

the use of negative frequencies can be avoided. Replacing the cosines in (5.9) with sines and keeping all frequencies positive gives (5.12) and (5.11).

$$Y_m * X_k = \begin{bmatrix} \frac{AB}{2}\sin\left[(m-k)\omega_0 t + \delta_m - \delta_k + \frac{\pi}{2}\right] \\ \text{if m} \geq \text{k} \\ \frac{AB}{2}\sin\left[(k-m)\omega_0 t - \delta_m + \delta_k + \frac{\pi}{2})\right] \\ \text{otherwise} \end{bmatrix} \tag{5.11}$$

$$-\frac{AB}{2}\sin\left[(m+k)\omega_0 t + \delta_m + \delta_k + \frac{\pi}{2}\right] \tag{5.12}$$

Note the the difference term depends on the conjugate of one of the signals. That is the phase of the $m-k$ term decreases (increases) as the phase of the k signal increases (decreases).

5.3.4 Phasor representation of sinusoidal signals

By removing the explicit frequency information and retaining it implicitly, the phase and magnitude information of sinusoidal signals can be described in complex phasor form. The phasor representation for the sinusoidal signal X_k (5.13) is defined as $\mathbf{X_k}$ (5.14).

$$X_k = A\sin(k\omega_0 t + \delta_k) \tag{5.13}$$

$$\mathbf{X_k} = A\left[\cos(\delta_k) + j\sin(\delta_k)\right] \tag{5.14}$$

This definition sets the zero angle reference to be the real axis of the complex plane so a positive value in the real part is equivalent to a sinewave with zero phase. A positive

number in the imaginary part represents a cosine wave with zero phase or a sinewave with phase of $\frac{\pi}{2}$. Likewise if the real (imaginary) part is negative then the waveform is a negative sine (cosine) wave. Examples of phasor representation of (5.13) for δ_k =0, $\frac{\pi}{4}$, π and $\frac{3\pi}{2}$ are shown in Figure 5.3.

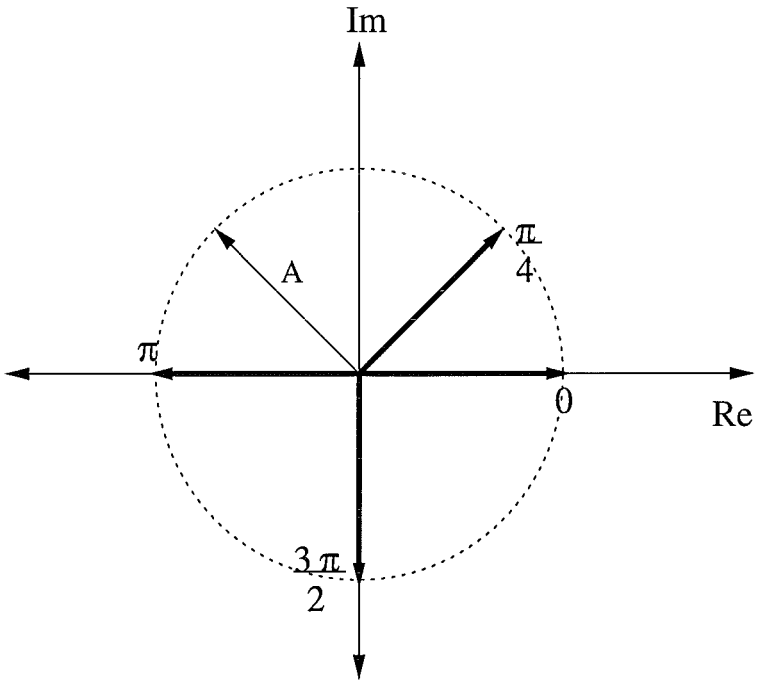

Figure 5.3 Four example phasors

5.3.4.1 Zero frequency signals in phasor form

A DC signal has by definition a frequency of zero.[2] The representation of a zero frequency signal with a phasor is accomplished by noting that if $k = 0$ and $\delta_k = \pi/2$ in equation (5.15), then a constant value with zero frequency arises (5.16).

$$X_k = A\sin(k\omega_0 + \delta_k) \quad (5.15)$$

$$= A \quad (5.16)$$

The angle for δ_k of $\frac{\pi}{2}$ is necessary to ensure that the signal X_k (5.15) has a non-zero value. If $\delta_k = 0$ then $X_k = 0$ as $\sin(0) = 0$ and if $\delta_k \neq \frac{\pi}{2}$ then the magnitude of the phasor does not represent that of the signal, A. To avoid the phasor having a magnitude that is different from A the angle of a zero frequency signal is therefore

[2]Throughout this thesis, to avoid confusion between DC side signals (these being signals on the DC side of a rectifier) and DC signals (these having a frequency of zero Hertz) the former are called *DC side signals* and the latter *zero frequency signals.*

made $\frac{\pi}{2}$. So in phasor form a zero frequency signal is represented as (5.17)

$$\begin{aligned} \mathbf{X_k} &= A\left[\cos(\delta_k) + j\sin(\delta_k)\right] \\ &= A\left[\cos(\frac{\pi}{2}) + j\sin(\frac{\pi}{2})\right] \\ &= jA \end{aligned} \tag{5.17}$$

This means that a zero frequency signal is represented as a phasor that has only an imaginary component. Such a phasor points upward or downward along the imaginary axis of the complex plane.

5.3.4.2 Modulation results as phasors

The phasor representation of the two sinusoidal signals previously shown in equations (5.6) and (5.7), are (5.18) and (5.19)

$$\mathbf{X_k} = A\left[\cos(\delta_k) + j\sin(\delta_k)\right] \tag{5.18}$$

$$\mathbf{Y_m} = B\left[\cos(\delta_m) + j\sin(\delta_m)\right] \tag{5.19}$$

and the phasors of the result of their multiplication $X_k * Y_m$, (5.20) and (5.21).

$$\mathbf{XY_{m-k}} = \frac{AB}{2}\left[\cos(\delta_m + \frac{\pi}{2} - \delta_k) + j\sin(\delta_m + \frac{\pi}{2} - \delta_k)\right] \tag{5.20}$$

$$\mathbf{XY_{m+k}} = -\frac{AB}{2}\left[\cos(\delta_m + \frac{\pi}{2} + \delta_k) + j\sin(\delta_m + \frac{\pi}{2} + \delta_k)\right] \tag{5.21}$$

Consider the situation where Y_m is a phasor representing a single frequency component of the switching function (5.3) and is therefore a constant transfer phasor. X_k is an input signal of which the phase δ_k varies. Figure 5.4(a) shows three input phasors of differing phases and Figure 5.4(b) shows an example arbitrary transfer phasor. The multiplication gives two other phasors that represent the sum and difference terms. The frequency of the results are not explicit in the phasor representation but are implied. The resulting sum frequency phasors are shown in Figure 5.4(c). Notice how the phase of the resulting phasor rotates in the same direction as the phase of the input phasor. Appendix D shows that a complex multiplication can be used to generate the sum term phasor at the correct angle. The difference term phasors have phase angle that decreases as the input phase increases. That is, for the difference term phasor, as the phase angle of the input phasor moves anti-clockwise the phase angle of the output phase moves in a clockwise direction. If the difference term is to be produced using a complex multiplication (see Appendix D) then the negative angle of the input signal X_k must be generated. This is the angle of the conjugate of X_k which is typically written as $X_k{}^*$. Conjugation changes the sign of the complex component of a phasor and it cannot be represented by multiplication of one complex number by another

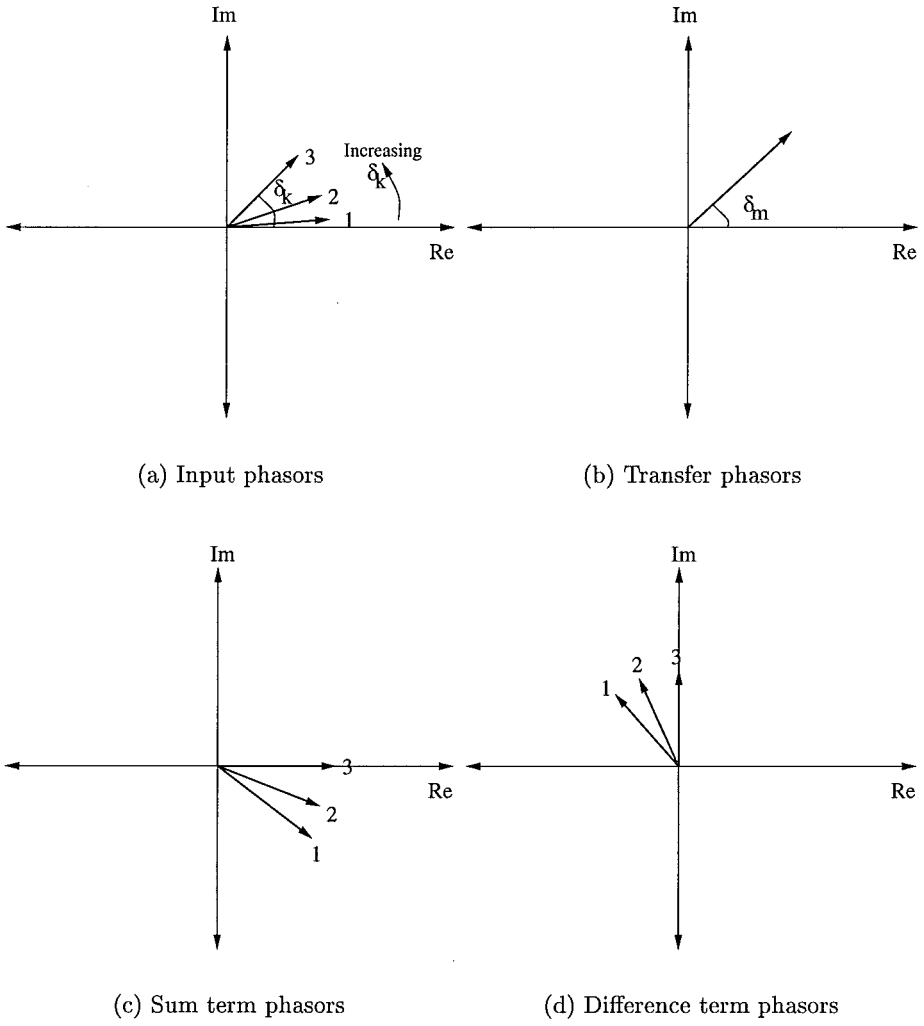

Figure 5.4 Multiplication of phasors showing how the sum term phase depends on the input phase while the difference term phase depends on the conjugate phase of the input

complex number when only positive frequencies are represented [Smith *et al.* 1998]. It is, however, made possible by separately representing the real and imaginary parts of the phasor and using a two by two matrix, (5.22), to perform the conjugation. (*In* and *Out* are example variables.)

$$\begin{bmatrix} out_{real} \\ out_{imag} \end{bmatrix} = \begin{bmatrix} 1 & 0 \\ 0 & -1 \end{bmatrix} \begin{bmatrix} in_{real} \\ in_{imag} \end{bmatrix} \tag{5.22}$$

The rotation and scaling operation, which is equivalent to multiplication in the complex plane by a complex number $x + jy$, has the transformation matrix (5.23).

$$\begin{bmatrix} out_{real} \\ out_{imag} \end{bmatrix} = \begin{bmatrix} x & -y \\ y & x \end{bmatrix} \begin{bmatrix} in_{real} \\ in_{imag} \end{bmatrix} \tag{5.23}$$

Combining these two matrix operations generates the real and imaginary part of difference term phasor, $diff$, (5.20). The development of the total matrix can be seen in (5.24) and (5.25).

$$\begin{bmatrix} diff_{real} \\ diff_{imag} \end{bmatrix} = \frac{A}{2} \begin{bmatrix} \cos(\delta_m + \frac{\pi}{2}) & -\sin(\delta_m + \frac{\pi}{2}) \\ \sin(\delta_m + \frac{\pi}{2}) & \cos(\delta_m + \frac{\pi}{2}) \end{bmatrix} \begin{bmatrix} 1 & 0 \\ 0 & -1 \end{bmatrix} B \begin{bmatrix} \cos(\delta_k) \\ \sin(\delta_k) \end{bmatrix} \tag{5.24}$$

$$= \frac{A}{2} \begin{bmatrix} \cos(\delta_m + \frac{\pi}{2}) & -\sin(\delta_m + \frac{\pi}{2}) \\ \sin(\delta_m + \frac{\pi}{2}) & \cos(\delta_m + \frac{\pi}{2}) \end{bmatrix} B \begin{bmatrix} \cos(-\delta_k) \\ \sin(-\delta_k) \end{bmatrix}$$

$$= \frac{AB}{2} \begin{bmatrix} \cos(\delta_m + \frac{\pi}{2} - \delta_k) \\ \sin(\delta_m + \frac{\pi}{2} - \delta_k) \end{bmatrix} \tag{5.25}$$

The conjugation (5.22) and the rotation (5.23) operations allow the complete modulation process to be described in a linear form. The sum term phasor is generated with the matrix in equation (5.26) giving (5.27).

$$\begin{bmatrix} sum_{real} \\ sum_{imag} \end{bmatrix} = \frac{A}{2} \begin{bmatrix} -\cos(\delta_m + \frac{\pi}{2}) & \sin(\delta_m + \frac{\pi}{2}) \\ -\sin(\delta_m + \frac{\pi}{2}) & -\cos(\delta_m + \frac{\pi}{2}) \end{bmatrix} \begin{bmatrix} \cos(\delta_k) \\ \sin(\delta_k) \end{bmatrix} \tag{5.26}$$

$$= \frac{AB}{2} \begin{bmatrix} -\cos(\delta_m + \frac{\pi}{2} + \delta_k) \\ -\sin(\delta_m + \frac{\pi}{2} + \delta_k) \end{bmatrix} \tag{5.27}$$

Separating a phasor's real and imaginary components allows the classically non-linear modulation operation to be represented as a linear matrix operation. Phasors representing the resulting sum and difference frequency terms can be generated using two by two matrices. This two by two matrix operator accurately describes conjugation allowing the accurate linear modulation representation.

5.3.5 Frequency domain representation format and conventions

Each component frequency of any signal is separately represented as the real and imaginary parts of a phasor in the column vector form as shown in the left column of (5.28). The right hand column shows the index number of the element. The frequency step is arbitrary as is the number of frequency components, l. By setting a constant frequency step, f_{step}, the index of each complex phasor component determines the frequency that the complex phasor represents. That is, the components in the third and fourth positions f_{1real} and f_{1imag} (5.28) represent the real and imaginary parts of the f_{step} frequency phasor. Note that the real part of the zero frequency phasor is retained only for computational convenience in indexing elements. The two components in the lth phasor, which has frequency $(l) * f_{step}$, have indices $2l+1$ and $2l+2$. Thus, a number of signal components in phasor form are stored in a column vector. This means that the

$$\begin{bmatrix} \\ f_{0real} \\ f_{0imag} \\ f_{1real} \\ f_{1imag} \\ . \\ \\ . \\ f_{lreal} \\ f_{limag} \end{bmatrix} \begin{bmatrix} \text{Index} \\ 1 \\ 2 \\ 3 \\ 4 \\ 5 \\ \\ 2l \\ 2l+1 \\ 2l+2 \end{bmatrix} \tag{5.28}$$

signal of magnitude h and phase δ_k, (5.29), is represented as a two element sub-vector, (5.30), at the appropriate position in the vector.

$$h\left[\cos(\delta_k) + j\sin(\delta_k)\right] \tag{5.29}$$

$$\begin{bmatrix} . \\ . \\ h\cos(\delta_k) \\ h\sin(\delta_k) \\ . \\ . \end{bmatrix} \tag{5.30}$$

Conversion from the frequency domain to the time domain is achieved by adding sinusoids at the appropriate frequencies and phases.

5.3.6 Representing frequency coupling - The Frequency Transfer Matrix

The frequency transfer matrix (FTM) is the mechanism used in this thesis to numerically and visually represent the modulation of a non-linear switching device. The vector of input phasors, with separate real and imaginary parts representing the component frequencies, is linked or coupled to the vector of output phasors by the FTM. Figure 5.5 shows the FTM for the AC side to DC side frequency coupling previously shown by the Fourier series in equation (5.3). Non-zero elements are represented by dots. The banded diagonal structure represents the coupling between input frequencies and output frequencies. From Figure 5.5 it can be seen that a 50Hz input signal generates 0Hz, 100Hz and 200Hz and the continuing even harmonics on the DC side.

The two by two structure of the each frequency coupling sub-matrix can be seen in the detailed view of the same FTM in Figure 5.6. The frequency is discretised

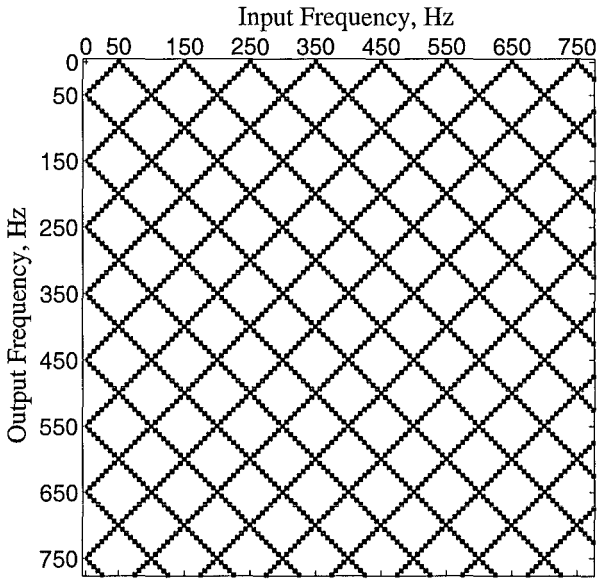

Figure 5.5 FTM for single-phase rectifier AC to DC transfer

to 6.25Hz steps.[3] This step is arbitrary and can be made any value. For example, the harmonic domain where only harmonics of the system frequency are represented [Bathurst 1998] is an FTM with frequency steps of 50Hz. The choice of step size is a trade off between required accuracy and computation speed. Diagonals in Figure 5.6 are labelled to indicate the value of m in the Fourier series, equation (5.3), they arise from. This shows that the $m + k$ sum frequencies have diagonals down with increasing input frequency k and the difference terms have diagonals up when $m - k$ is positive and diagonals down when $m - k$ is negative. If the frequency of the input signal is for example 125Hz, then by tracing down a vertical line from the 125Hz position on the horizontal axis the output frequencies can be seen to be 25Hz, 75Hz, 125Hz, 175Hz... etc. Since the FTM is linear, when more than one frequency occurs in the input signal then the total output can be found as the sum of the FTM multiplied by each of the input components separately or by applying the FTM to the sum of the inputs. Alternatively this means that superposition applies.

5.3.6.1 Generality of the FTM approach

Typically modulation is considered non-linear because an output frequency arises that was not present in the input signal. However, by viewing modulation as a linear operation of frequency domain coupling and extending the transfer operator (using the two by two matrix) to include conjugation the operation of the non-linear device becomes linear. There are non-linear devices where this *non-linear in the time domain*

[3]The experimental system performs an eight cycle data collection (Chapter 4) which gives a frequency resolution of 6.25Hz. For this reason a 6.25Hz frequency step or resolution is generally used in this thesis.

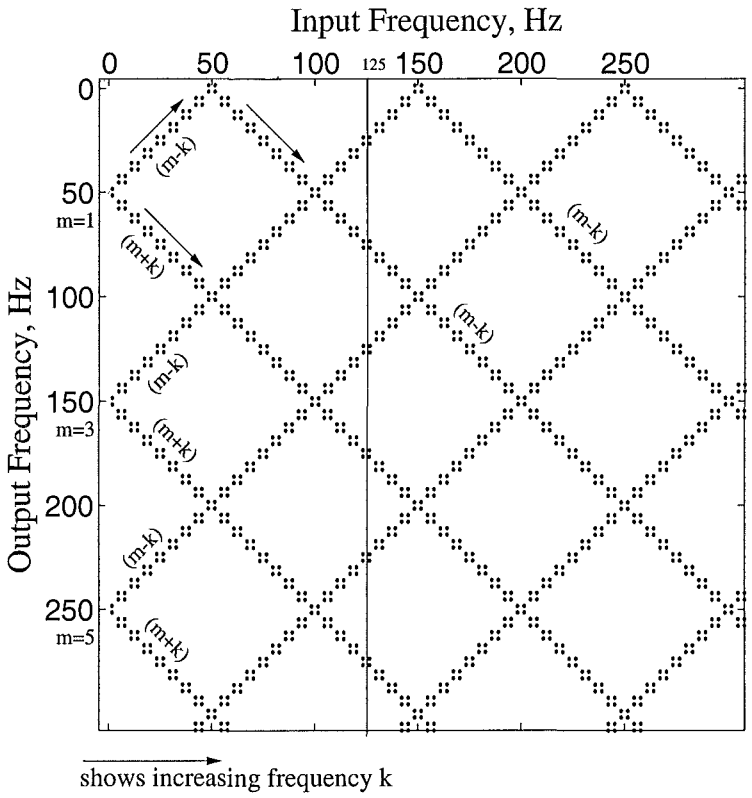

Figure 5.6 FTM for single-phase rectifier AC to DC transfer (detailed view)

becomes linear in the frequency domain concept is not valid. Examples of such non-linear devices include hysteretic systems where the non-linearity depends to some degree on the past state or very strongly on the input magnitude. This type of non-linear system is outside the scope of this thesis. The FTM approach is however suitable for rectifier type loads.

5.3.6.2 FTM examples using uncontrolled rectifiers

As an example of the accuracy of the FTM representation Figure 5.7(a) shows a typical rectifier switching function and a 50Hz signal. The product of these two time domain waveforms is shown in Figure 5.7(b) along with the waveform that results when the FTM frequency domain result is synthesised into a waveform. The time domain waveforms match closely, although not exactly. This is the result of using a limited number of frequencies (in this case 125 steps of 6.25Hz are used giving a maximum frequency of 781.25Hz). The frequency domain accuracy of the approach can be seen in Figures 5.7(c), where the magnitude of the spectrum of the time domain multiplication is shown, and 5.7(d) which shows the magnitude of the spectrum generated using the FTM. These are the same. The phase angle of the spectra (Figure 5.7(e) for the time domain and Figure 5.7(f) for the FTM) are also the same. Another example of the FTM accuracy is shown in Figure 5.8 for an input frequency of 230Hz. The input

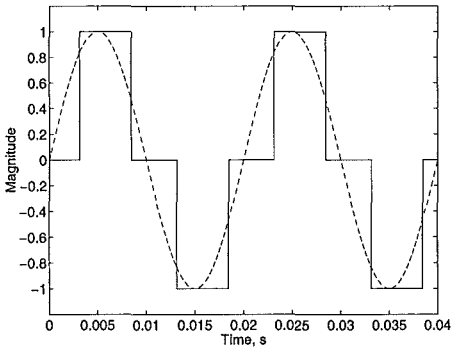

(a) Input signal and switching function

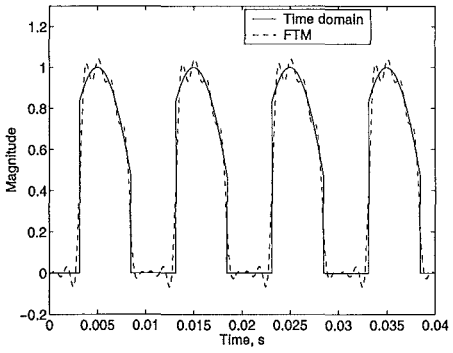

(b) Output signal from time domain multiplication and synthesis of FTM spectrum (FTM result bandwidth limited to 781.25Hz)

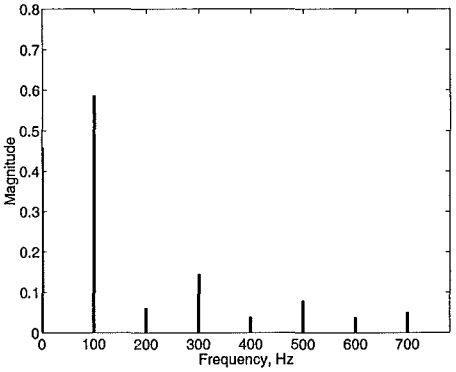

(c) Magnitude of spectrum from FFT of time domain multiplication

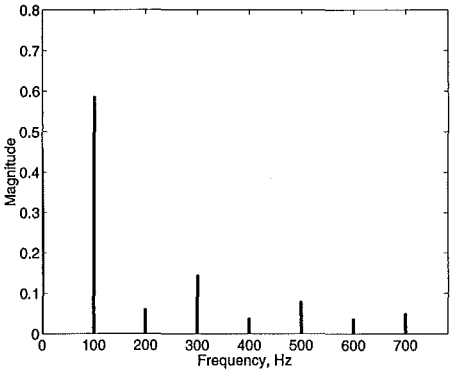

(d) Magnitude of FTM Spectrum(FTM Bandwidth limited to 781.25Hz)

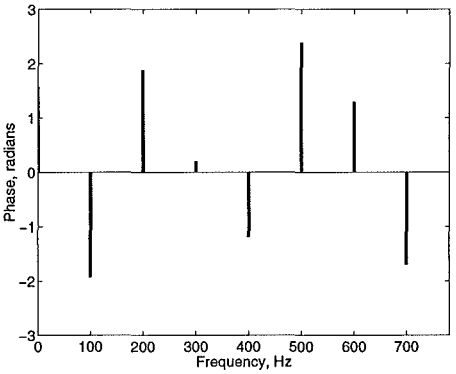

(e) Phase angle of spectrum from FFT of time domain multiplication

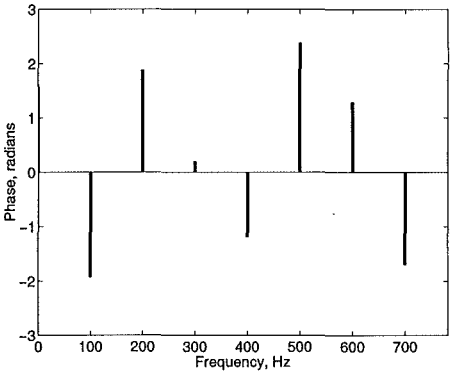

(f) Phase angle of FTM pectrum(FTM Bandwidth limited to 781.25Hz)

Figure 5.7 FTM example of direct transfer with 50 Hz AC side voltage signal and the resulting DC side signal

waveform and switching function are shown in Figure 5.8(a). The spectra for both the FFT of the time domain multiplication and the FTM are shown in Figure 5.8(b). The match is excellent. The phase of the two spectra, which is not shown, match also. The

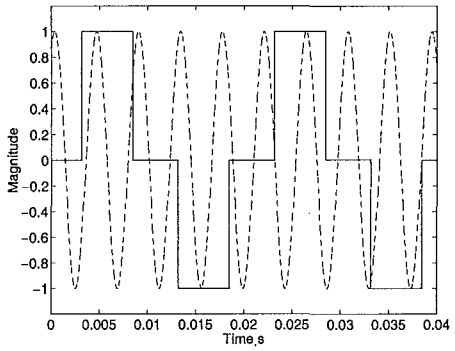

(a) Switching Function and Input Signal.

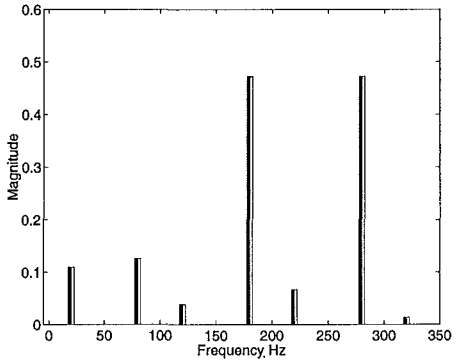

(b) Comparison of time domain (dark) and frequency domain FTM (light) spectra.

Figure 5.8 Input waveforms and output spectra for time domain and FTM with non-fundamental frequency input. (Input frequency 230 Hz, phase $\frac{\pi}{2}$.)

two examples show that the FTM is an excellent accurate method to represent the modulation associated with non-linear rectifier loads in a linear way.

5.3.6.3 Magnitude - Phase dependence

The use of a two by two matrix to couple the real and imaginary phasor components to the output phasor allows the conjugation of the input to produce the correct phase for the difference term. When the output at a certain frequency depends on both the input phasor and the conjugate of the input phasor the effect is that the magnitude of the output becomes dependent on the phase of the input. This dependence on both input and its conjugate occurs when a sum term diagonal and difference term diagonal intersect as in Figure 5.6. This effect is termed magnitude-phase dependence. The importance of accurately representing modulation which can be seen by considering the representative switching function and the third harmonic signals with two different phase angles 90° and 0° shown in Figure 5.9(a). Figure 5.9(b) shows the DC side signals that result when the two signals are each separately multiplied by the switching function. Notice that the average component of the DC side signal (which corresponds to the zero frequency component of the signal) is zero in the 90° case and has a negative value in the 0° case. This operation indicates how the magnitude of a specific frequency component of a signal that results from modulation can depend on the phase of the applied signal. It is precisely this relationship that the conjugation matrix can represent. The implications of the magnitude - phase depedence for a rec-

tifier are the rectifier has a phase dependent characteristic at harmonic frequencies so the response of the load to the SAF is phase dependent. The phase dependence may be important because the odd harmonic frequencies, such as the third in the example of Figure 5.9(a), couple to zero frequency on the DC side of the rectifier which in turn strongly couples to fundamental frequency on the AC side. This indicates that odd harmonics may change the fundamental response of the rectifier and because the SAF generates these harmonics the response may be phase dependent. Accurate modelling and analysis of the behaviour of the rectifier load will indicate the size and importance of the magnitude-phase dependent effect.

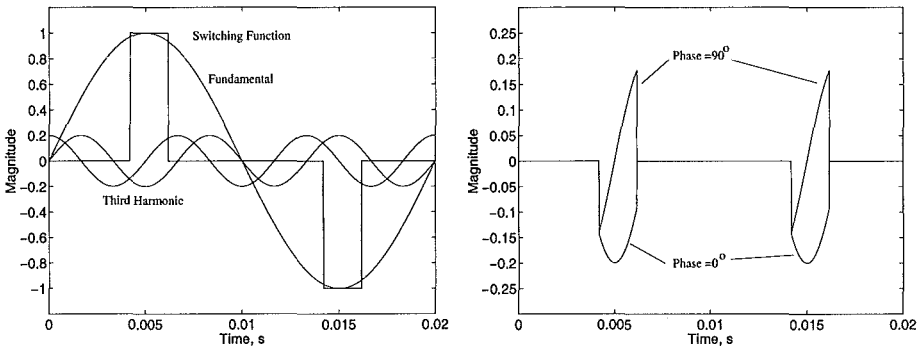

(a) Input AC side signals and switching function

(b) Resulting DC side signals

Figure 5.9 Single-phase rectifier AC to DC transfer magnitude-phase dependency

5.3.6.4 Effect of limited maximum FTM frequency

The use of a limited number of frequencies in the FTM means that the time domain waveforms created with this method have inaccuracies. However this is not a problem when the low pass nature of real physical systems is considered because the magnitude of the response of a physical system falls markedly with increasing frequency. This makes the response at high frequency relatively small so it can be ignored. The choice of a maximum frequency is perhaps not a trivial problem but typically power system characteristics are considered up to approximately the twenty fifth harmonic or 1250Hz.

5.3.6.5 FTMs as partial differentials

When a small-signal perturbation is applied to the single-phase rectifier or any other system the response is the result of a number of things that happen simulataneously. Consider the situation where the magnitude of the AC fundamental voltage increases by a small amount. This increases the fundamental current flowing into the rectifier. As a result the DC side current increases increasing the DC bus voltage in turn. In fact the

effect of the voltage rise on the DC side will act to cancel the effect of the rise on the AC side. From this it can be seen that any change on the AC side causes a change on the DC side and this in turn causes changes on the AC side. One method to determine the behaviour of the entire rectifier is to separate each behaviour mechanism into a partial differential and then combine these differentials to obtain the total system behaviour [Bathurst 1998]. This is a common approach to multi-input multi-output problems such as optimisation.

The partial differentials are found by varying one input while holding the others constant and a matrix of partial differentials describes the way in which system variables are dependent. Such a matrix, usually referred to as the system Jacobian, can be used as the sensitivity matrix in Newton's method for solving non-linear equations [Smith *et al.* 1998].

The FTM is a matrix of partial differentials. It contains the sensitivity of one variable at a certain frequency to the change in another variable at another frequency. If the two variables have no dependence then the sensitivity is zero. This corresponds to the two by two FTM sub-matrices with zero elements that are represented as white space in lattice diagrams like that of Figure 5.5. Sensitivity means that the FTM has non-zero elements in the position where the input column and output row meet, as is shown in Figure 5.6.

5.4 SUMMARY

Rectifier loads present a complex analysis and modelling problem. The representation of these non-linear loads with an equivalent linear system is a typical approach to control and system design and analysis. By representing the modulating effects of the rectifier load accurately with linear frequency transfer matrices, which allow for the conjugation that occurs in the phase of the difference term, the transfer of signals by switching functions can be accurately represented. Because the rectifier's behaviour is driven by the AC system fundamental voltage the response to disturbance can be separated from the base response by the use of small-signals. This representation allows the non-linear effects of the modulation to be represented in a linear way with the Frequency Transfer Matrix (FTM). The FTM approach to frequency coupling or transfer is shown to be accurate in the frequency domain and so long as the maximum frequency represented in the FTM is suitably large the low pass nature of the physical system will ensure accuracy.

The following chapter develops a small-signal model of the single-phase rectifier. The FTM for each partial transfer is found for the device and by combining these partial transfers the total rectifier transfer is developed.

Chapter 6

SINGLE-PHASE RECTIFIER SMALL-SIGNAL MODEL

6.1 INTRODUCTION

The single-phase rectifier is possibly the most widely used static power conversion system in the world. With the proliferation of the personal computer and other small appliances the conversion of AC supply to DC using this converter is very common. The single-phase rectifier operation and characteristics are, as a result of its popularity, well known. The device draws a current that has harmonic components at the third, fifth and continuing odd harmonics [Heydt 1991]. The shape of the single-phase rectifier current waveform is very well known. This can be seen by the existence of the Class D "special wave shape definition" in IEC 61000-3-2 [IEC 1995] which effectively makes specific allowance for the single-phase rectifier [Ingram 1998]. The device is inexpensive, effective and operates connected to the AC system with very few reported problems. Typical problems that do occur are usually solved by increasing neutral conductor size [Arthur and Shanahan 1996]. This lack of problems has meant that investigation of the single-phase rectifier's characteristics and behaviour in the power system has not been attempted or carried out. This is true of most rectifier non-linear loads which are either dismissed as too difficult to analyse or too small to have significant effect.

The accurate representation of rectifier loads in distribution or supply level power systems is an area that has received little attention unless the load has a large power rating. Large transmission level connected loads such as HVDC and smelter converters have always required detailed analysis because the consequences of the system not operating as planned are enormous. However, single-phase rectifiers usually have a low power rating and their behaviour is generally ignored apart from noting that there are harmonic currents generated. These harmonic currents can at times cause problems in the AC supply network as has been noted previously [Heydt 1991, Arrillaga *et al.* 1985]. Filters can be installed to remove these harmonic currents. However it is not typical to install harmonic filters at the low voltage customer level because power quality effects experienced by customers or supply companies that are caused by harmonic currents are uncommon. Such a statement seems to imply that

there is no reason to research or even consider the power quality effects of harmonic currents. However the increased pressure to deliver "better" electric power with existing distribution equipment means it is possible, and perhaps probable, that harmonics in power systems will become significant contributors to bad power quality.

Generally power quality analysis focuses either on the AC network [Arrillaga *et al.* 1985] or on the customers' ability to tolerate the disturbances [Bollen *et al.* 1997] that come from the AC network [Koval and Hughes 1997, Sullivan *et al.* 1997]. The joining of these two approaches requires that a system to describe the interdependence of the AC network and the possibly non-linear load is developed. A cornerstone of such a system is the accurate representation of the non-linear rectifier load. The characteristics of the single-phase rectifier as a power system component are generally not well known. It is typical to represent a rectifier with its power consumption and then to include the harmonic currents as constant current source injections that are in no way dependent on the terminal voltage [Hafner *et al.* 1997, Duke and Round 1993, Round 1992, Akagi *et al.* 1986]. This model is meant to represent the steady state behaviour of the rectifier but gives no indication of the stability or robustness of the device's operation.

A typical approach to system stability and robustness is small-signal analysis. By determining the single-phase rectifier small signal response its behaviour in terms of stability when connected to the AC system can be determined and predicted. Single-phase and other types of rectifiers are connected to power systems in large numbers and typically these devices operate effectively, indicating that there are no stability problems. When a power conditioner is connected to the system to remove harmonic current or minimise the harmonic voltage the load, which is typically a rectifier, forms part of the forward control transfer of the power conditioner (see section 3.3). An accurate small signal analysis of the rectifier is therefore required to determine if stable and robust operation will result. The instability, described in section 3.6.1, caused by connection of capacitors downstream of the current measurement SAF shows that system components connected near to the SAF can have significant influence on effective operation [Akagi 1996b].

The single-phase rectifier operates to transfer real power to its DC side. Therefore at fundamental frequency it presents to the AC system an impedance that dissipates energy. That is, the rectifier has an AC side current that is, to some extent, in phase with the AC side voltage. If a load resistor is connected instead of the rectifier energy is absorbed by the load at all frequencies. This energy absorption provides damping to oscillatory behaviour in the AC system. Having a measure of the single-phase rectifier's energy dissipation ability at non-fundamental frequency gives the rectifier's damping at that frequency. Section 3.6 showed that the load current measurement SAF removes the damping provided by the downstream load. If the load is a rectifier this effect can only be quantified by having a good understanding and an accurate model of rectifier

load behaviour.

In this chapter a small signal frequency domain model of the single-phase rectifier is developed. Firstly, the operation of the rectifier is described and the small signal response separated from the base case operation. A suitable model structure is developed, and then the component transfers for the base switching and the switching instant effects are constructed. The component transfers are compared with time domain simulation of the rectifier. Finally the component transfers are combined to form the complete model and these are confirmed with time domain simulation.

6.2 THE SINGLE-PHASE RECTIFIER

The typical single-phase rectifier is shown in Figure 6.1. The AC side voltage source has two parts. The first is the base fundamental AC system voltage V_{AC}, which is typically sinusoidal. The second is a small perturbing voltage, ΔV_{AC}, which is added to the base voltage V_{AC}. The other rectifier variables are the AC side current I_{AC}, the DC side current I_{DC} and the DC bus voltage V_{DCBUS}. Note that I_{DC} is not the current that flows in the DC side load resistor but rather the current that flows in the DC side circuit of the rectifier itself. The current flowing in the DC side resistor can be calculated as $\frac{V_{DCBUS}}{R}$. When only the base case AC voltage is applied the result is called the base case response or simply the base case. This base case is defined by I_{AC}, I_{DC}, V_{DCBUS} and V_{AC}. Adding the perturbing AC side voltage ΔV_{AC} to the base voltage causes the other variables to change. The difference from the base case is the small signal response defined by ΔI_{AC}, ΔI_{DC}, ΔV_{DCBUS} and ΔV_{AC}. As previously described in section 5.3 this separation of the response is a typical approach used for non-linear systems and is well suited to the AC driven single-phase rectifier because the AC voltage ensures constant operating point that defines the base case operation.

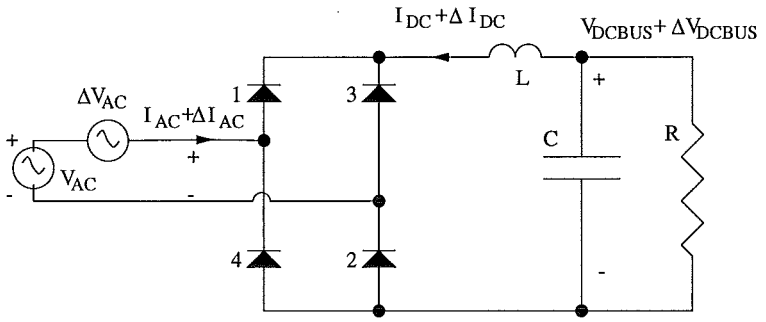

Figure 6.1 Single-phase rectifier showing base operation variables.

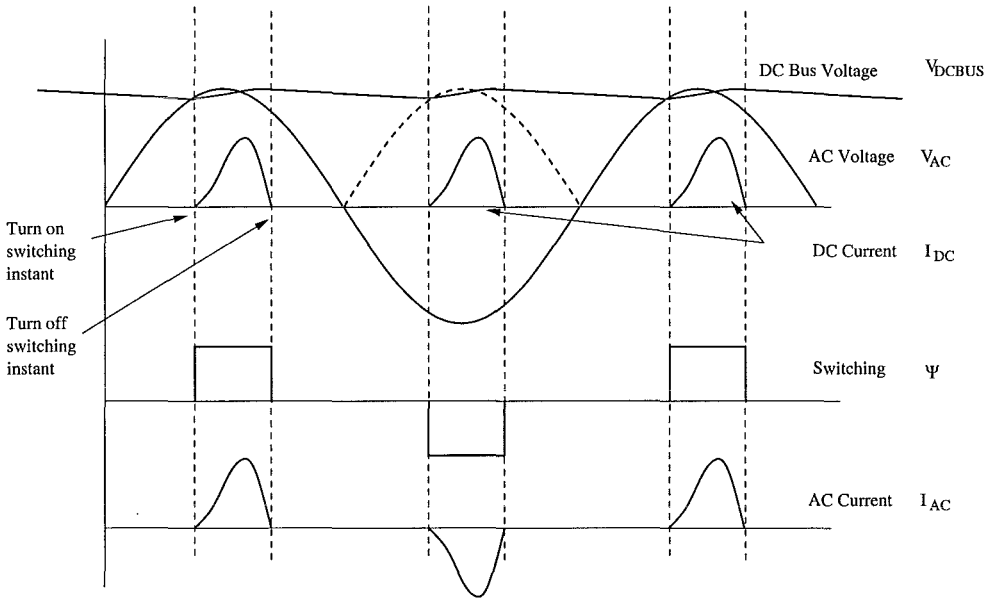

Figure 6.2 Base case operating waveforms for single-phase rectifier.

6.2.1 Base case operation

Normal base case operation of the single-phase rectifier (Figure 6.1) is shown in Figure 6.2. The sinusoidal (or close to it) AC voltage causes the switching of alternate diode pairs, 1+2 and 3+4, to connect the AC side voltage, V_{AC}, to the DC side capacitor and load. The AC side current, I_{AC}, is discontinuous as is the DC side current, I_{DC}. Each alternate DC side current pulse is the negative of the AC side current pulse. The switching waveform, Ψ, shows how the AC side and DC side are connected. The DC bus voltage has a variation, typically called the ripple, which is the result of the DC capacitor supplying energy to the load when the current from the AC side is zero. In the steady state the energy supplied from the AC side is the same as that flowing into the load on the DC side. This means that the DC side voltage has a constant average, or zero frequency component, value. The DC bus ripple voltage that occurs during normal rectifier operation is part of the base case operation. It is also probable that the base case AC voltage will have frequency components at harmonic frequencies of the fundamental frequency. These are caused by either the rectifier's own load current causing harmonic voltage drop in the system impedance or by other non-linear loads causing voltage distortion. It should be noted that the steady state deviations from the ideal sinusoidal AC voltage and the ideal "flat" DC side voltage which occur in the normal unperturbed operation of the rectifier are considered part of the base case operation.

6.2.2 Initial identification of the effects of a small perturbing voltage

Consider the single-phase rectifier when a small perturbing voltage ΔV_{AC} is added to the base supply voltage V_{AC} (Figure 6.1). The AC side perturbing voltage ΔV_{AC} has two principal effects in the single-phase rectifier. Firstly, ΔV_{AC} is modulated by Ψ to the DC side (shown by the arrow labelled **a** in Figure 6.3 with the * indicating a time domain multiplication). That is, ΔV_{AC} is multiplied by the base switching function and the result is a voltage on the DC side. Secondly, ΔV_{AC} causes the changing of the switching instants or angles from their normal unperturbed or base operating values (**c** in Figure 6.3.) The resultant switching instant modulation spectrum forms

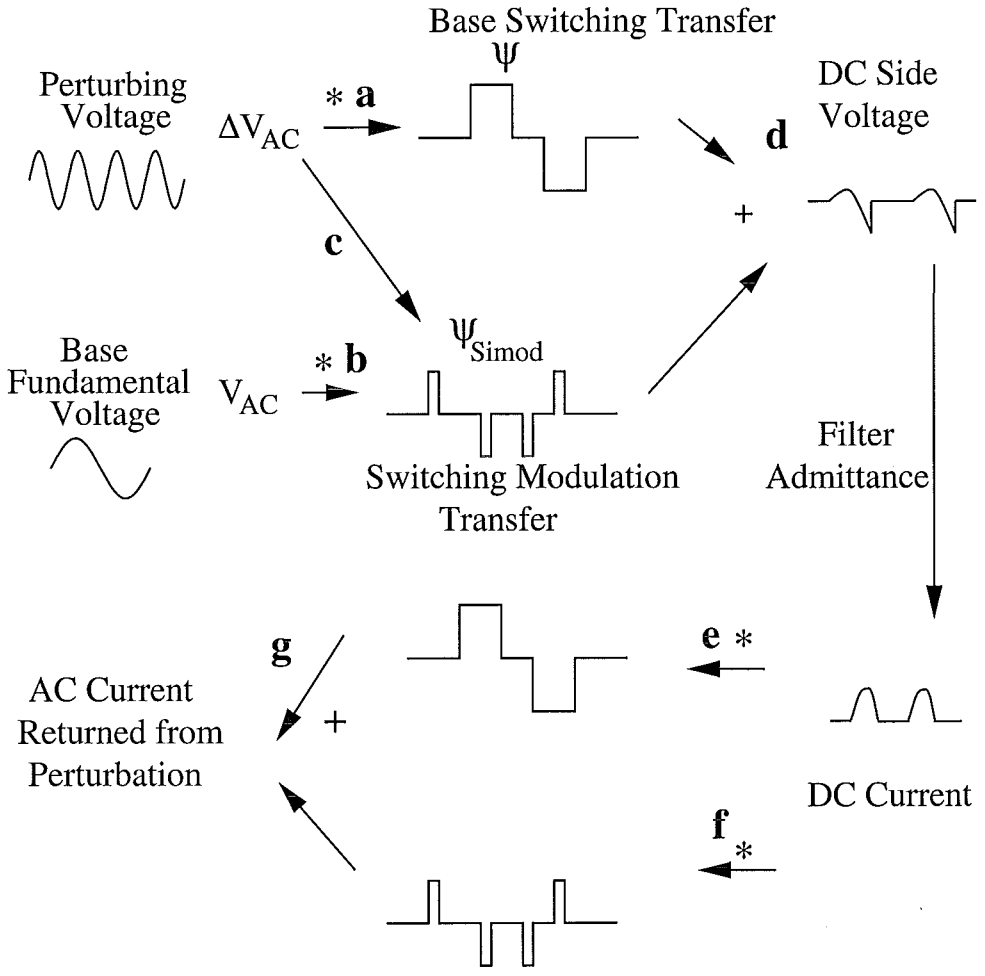

Figure 6.3 Intuitive examination of frequency transfer mechanisms for the single-phase rectifier and representative waveforms. Arrows labelled with * are multiplications. Arrows without * are couplings that do not involve multiplication.

the frequency transfer function, Ψ_{Simod}, which then modulates V_{AC} (**b** in Figure 6.3) in the same way as Ψ modulates ΔV_{AC}. The two modulations, base and switching instant, characterise the response of the single-phase rectifier to ΔV_{AC} and the sum of the two is the DC side voltage (**d** in Figure 6.3). The DC side filter admittance converts this voltage to a current which is then remodulated back to the AC side by

both Ψ (**e** in Figure 6.3) and Ψ_{Simod} (**f** in Figure 6.3). The AC side current that results from the application of ΔV_{AC} is the sum of the two effects (**g** in Figure 6.3). In this analysis it is assumed that ΔV_{AC} is sufficiently small so that the system has an essentially constant operating point and behaves linearly around this point. This assumption ensures that the two frequency transfer effects can be evaluated separately and combined by superposition. The result of ΔV_{AC} modulated by the switching instant modulation Ψ_{Simod} is a second order effect. Second order effects are considerably smaller than the original perturbing signal and are usually negligibly small compared to first order effects.

In summary, two effects make up the transfer of AC side signal to the DC side and the transfer from DC side signal to the AC side. These are the transfer due to the base switching and the transfer due to the switching instant modulation. By determining and combining these two transfers the total behaviour of the rectifier can be ascertained.

6.2.2.1 Base rectifier switching function

The typical switching function (Ψ) of the diode rectifier, as shown in Figure 6.4, represents the switching of the alternate diode pairs (1&2, and 3&4 in Figure 6.1) to connect the supply voltage, V_{AC}, to the DC bus capacitor, C, and the load, R, through the inductor, L. The switching function shows diode pair 1 and 2's turn on switching instant indicated by the angle θ_1 and the turn off switching instant, angle θ_2. The switchings for diode pair 3 and 4 occur in the voltage's V_{AC} negative half cycle at angles $\pi + \theta_1$ and $\pi + \theta_2$. The switching function is given in Fourier series form in equation (6.1)

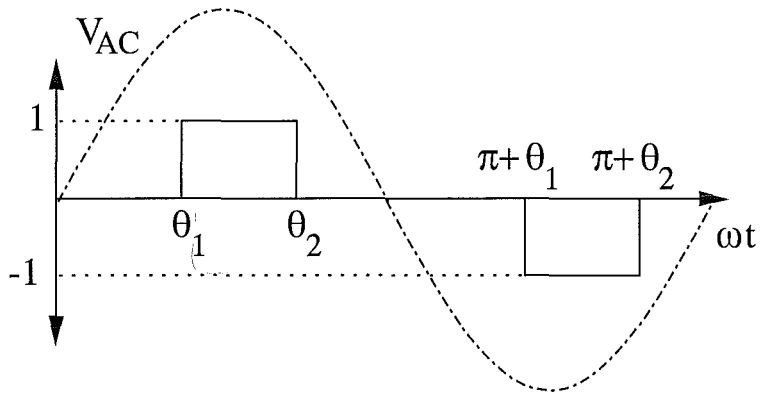

Figure 6.4 Single-phase rectifier base switching function.

and it operates as a frequency transfer function in that it describes the way an AC side frequency is transferred to the DC side. The product of the switching function with a sinusoidal AC side voltage or current signal of arbitrary frequency $k\omega_0 t$ and phase δ_k gives the Fourier series for the resulting DC side voltage or current signal Sig_{DC} (6.2). It can be seen from this Fourier series that there is a time shift of $\frac{m\theta 1 + m\theta_2}{2}$ and the

$$\begin{aligned}\Psi &= \frac{4}{m\pi}\sin\left(\frac{m\theta_1 - m\theta_2}{2}\right)\sin\left(m\omega_0 t - \frac{m\theta_1 + m\theta_2}{2} + \frac{\pi}{2}\right)\\ &\quad for\ m = 1,3,5,7...\\ \Psi &= 0\\ &\quad for\ m = 0,2,4,6...\end{aligned} \tag{6.1}$$

$$\begin{aligned}Sig_{DC} &= \frac{2}{m\pi}\sin\left[\frac{m\theta_1 - m\theta_2}{2}\right]\\ &\quad (+\sin\left[(m+k)\omega_0 t + \delta_k - \frac{m\theta_1 + m\theta_2}{2}\right]\\ &\quad -\sin\left[(m-k)\omega_0 t - \delta_k - \frac{m\theta_1 + m\theta_2}{2}\right])\\ &\quad for\ m = 1,3,5,7...\\ Sig_{DC} &= 0\\ &\quad for\ m = 0,2,4,6...\end{aligned} \tag{6.2}$$

difference term has phase that depends on $-\delta_k$. There are no even harmonic terms because of the symmetry of the switching pulses in the positive and negative fundamental half cycles. The magnitude is of the form of a sinc function $\frac{\sin x}{x}$, although it is not explicitly written as such. This switching transfer result describes the inter-connection of the AC and DC side for the unperturbed base switching instants.

6.2.2.2 Switching instant modulation function

Any AC side voltage perturbation can change or modulate the turn on and turn off switching instants. Figure 6.5(a) shows the front switching instant modulation waveform and Figure 6.5(b) shows rear switching instant modulation waveform. Appropriately signed small rectangular variation waveforms are added to the base switching waveform creating the total switching function. The four example pulses show the switching variation waveforms for positive and negative switching instant angle variations. The frequency components that arise from switching instant modulation can be determined using the spectrum from Swcharz's analysis of the pulse duration modulator [Swcharz *et al.* 1966]. As an example, the Fourier series that results from the modulation $\Delta\theta_1 = b\sin(k\omega_0 t + \delta_k + \frac{\pi}{2})$ of the turn on switching instant θ_1 is given in (6.3). This spectrum gives a complete frequency domain representation of the switching instant modulation which is used as a frequency transfer function Ψ_{Simod} in the same way as the rectifier switching function Ψ (Figure 6.4). A similar Fourier

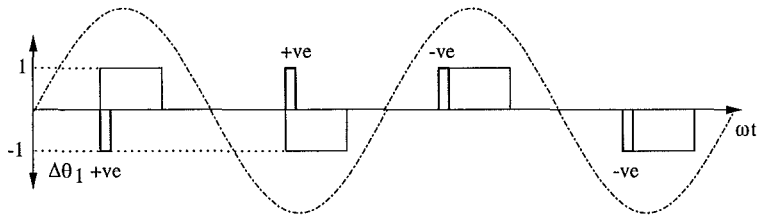

(a) Front switching instant modulation waveform

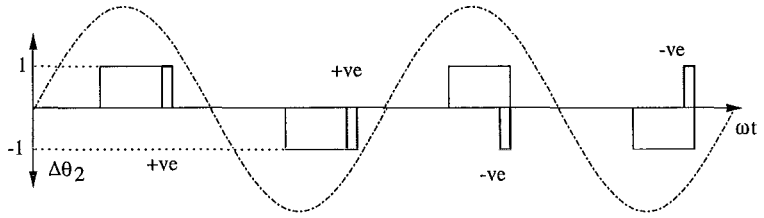

(b) Rear switching instant modulation waveform

Figure 6.5 Switching instant variation waveform for front and rear switching instant variation.

$$\Psi_{Simod} = \frac{2}{m\pi}\left[J_0(mb) - 1\right]\sin(m\omega_0 t - m\theta_1) \tag{6.3}$$
$$- \frac{2}{\pi}\sum_{n=1}^{\infty}\frac{J_n(mb)}{m}\left[\sin(m+nk)\omega_0 t - m\theta_1 + n\delta_k - \frac{n\pi}{2}\right]$$
$$- \frac{2}{\pi}\sum_{n=1}^{\infty}\frac{J_n(mb)}{m}\left[\sin(m-nk)\omega_0 t - m\theta_1 - n\delta_k - \frac{n\pi}{2}\right]$$
$$\text{for } m = 1, 3, 5..$$
$$\Psi_{Simod} = 0$$
$$\text{for } m = 2, 4, 6..$$

series, which is shown in Appendix C, describes the rear switching instant modulation spectrum. Together the rectifier base switching spectrum Fourier series and the switching instant modulation spectrum Fourier series completely characterise the behaviour of the single-phase rectifier by linking the voltages and currents on both sides of the device.

6.3 SELECTING AN APPROPRIATE MODEL STRUCTURE

It is possible to choose any two variables from the two voltages and the two currents as the input variables for the single-phase converter. Choosing two inputs forces the other two variables to be the outputs. The choice can be made with an intuitive approach by assuming that the rectifier has an admittance type transfer from AC voltage to

AC current. This makes the AC side voltage the input and the AC side current the output. This assumption was tacitly made in section 6.2.2. It seems therefore that the natural choice of the perturbing input on the AC side is the voltage. However, voltage input and current output is not the only choice possible. The AC side current can be made the rectifier's input variable and the AC voltage the output. However attempting to connect a continuous current source perturbation to the input terminals of the single-phase rectifier means that the current source connects to an open circuit during the periods when the rectifier does not conduct. This is an impossible situation and indicates that applying a voltage perturbation is the best way to determine the response of the rectifier.

It is however possible to apply a discontinuous current perturbation to the rectifier by matching its discontinuity to that of the rectifier [Palethorpe *et al.* 2000]. A discontinuous current perturbation gives information pertaining to only one part of the rectifier operation, this being the time when the devices conduct. Therefore it cannot completely characterise the rectifier because it may or may not cause switching instant modulation. This makes the AC current an inconvenient and inappropriate choice as an input. The same argument can be applied on the DC side of the rectifier, once again because the current is discontinuous. So, drawing the same conclusion on the DC side of the rectifier indicates that the DC side voltage should be chosen as the input.

The discontinuity in the current can be seen as the result of high harmonic distortion. A general rule is that the least distorted variables should be made the inputs. This also defines the variables that are the outputs, these being the most distorted. This approach has previously been proposed for three-phase rectifiers [Bathurst 1998] when only continuous conduction with continuous DC side current is considered. Application of this maxim to the single-phase rectifier leads to the same choice of the AC and DC side voltages as the inputs that is suggested by both the intuitive choice and the discontinuous current argument.

The choice of inputs will have no bearing on the analysis accuracy but will more than likely effect the complexity of the analysis and so any simplifying assumptions made could influence the accuracy. Considering the fact that the single-phase rectifier connects AC to DC voltage functionally, choosing AC voltage as an input is intuitive. The choice of the DC voltage as an input is perhaps a little less obvious but by examining the operation of the rectifier its suitability will become apparent.

6.3.1 Rectifier conduction modes

The single-phase rectifier operates by cycling through a number of conduction modes. The first of these modes connects the positive half cycle of the fundamental AC voltage to the DC bus. This is shown in Figure 6.6(a). The second conduction mode disconnects the AC side from the DC side as shown in Figure 6.6(b). The final mode is the opposite

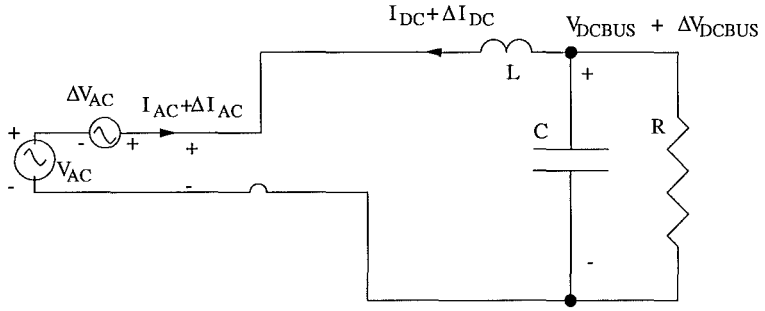

(a) Positive conduction

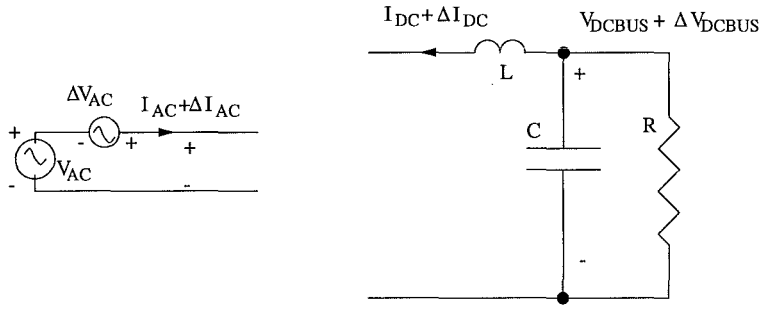

(b) No conduction

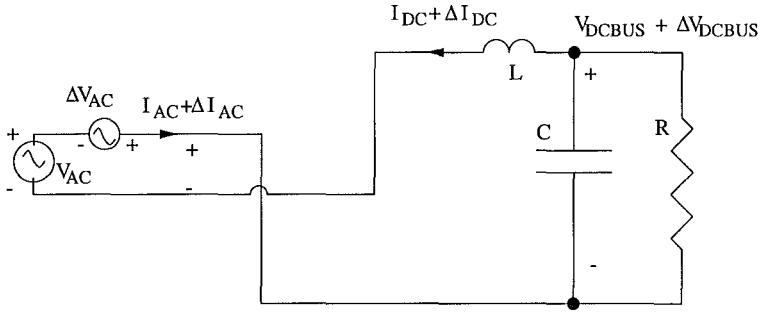

(c) Negative conduction

Figure 6.6 Single-phase rectifier conduction modes.

of the first in that the negative fundamental voltage is connected to the DC side with the alternate pair of diodes. Each of the conduction modes has initial (final) conditions that are the final (initial) conditions of the previous (next) conduction mode. The successive conduction modes, especially the second or non-conduction mode, have an impact on the suitable partitioning of the rectifier.

6.3.2 Partitioning the rectifier

The direct frequency transfer function and the switching instant transfer function describe how the AC side and DC side interconnect. At first sight the single-phase rectifier seems to be a voltage to voltage coupling device. This suggests that separating the rectifier from its AC and DC circuits can be accomplished by partitioning the rectifier in a voltage source to voltage source manner. This rectifier partition is necessary because although the rectifier has been shown as connected to a perfect AC voltage source it will in reality be connected to an AC system with some arbitrary impedance as shown in Figure 6.7. Likewise the DC side has been assumed to be of the form of an

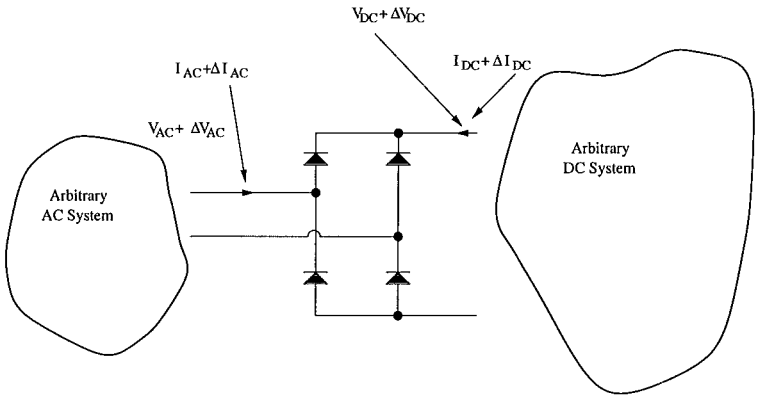

Figure 6.7 Rectifier connected to arbitrary AC and DC systems.

LCR filter but it is possible that the DC side could have a more complex filter circuit and even include a source of some kind. In order to keep the analysis as general as possible it would be useful to have the possibility of connecting arbitrary impedances to both sides of the rectifier. This means that it is necessary to decide where the rectifier begins and where the external circuit begins. An obvious partition is the setting of the rectifier to include only the switching devices producing the voltage partition.

6.3.3 Voltage partition

The voltage partition, Figure 6.8, means that the rectifier has terminals defined so that only the switching diodes are considered part of the rectifier. In this partition the voltage that is applied to the DC side filter circuit is the AC side voltage multiplied by the switching function. Figure 6.8 shows the rectifier partitioned so the inductor is considered part of the DC side filter. The current that flows on the DC side is determined by the integral of the difference between the DC voltage caused by the voltage on the AC side and the voltage on the DC bus capacitor. Consider the example small voltage perturbation ΔV_{AC} waveform, as shown in Figure 6.9(a), applied to the AC side of the single-phase rectifier. The resulting DC side voltage, ΔV_{DC} Figure 6.9(c), is the product of Figure 6.9(a) and Figure 6.9(b). The current that flows on the DC side,

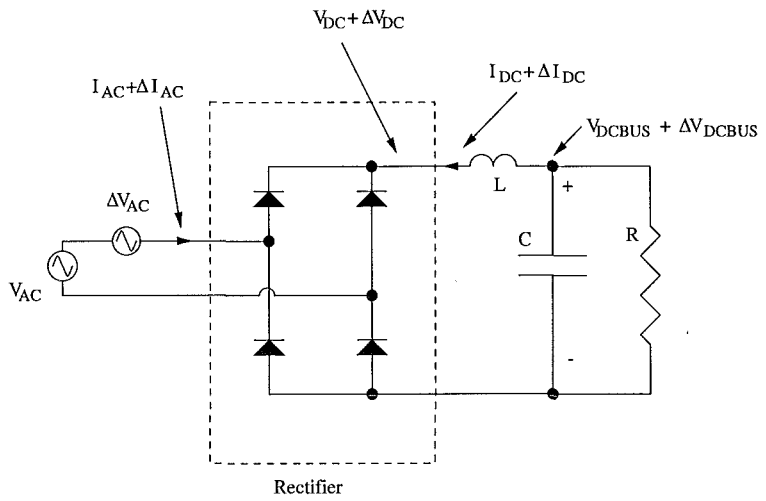

Figure 6.8 Rectifier partitioned in a voltage to voltage manner.

Figure 6.9(e), is required to be zero when the rectifier is in the non-conducting mode. The current can be returned to zero at the turn off switching instant with a voltage impulse of the correct amplitude as shown in Figure 6.9(d). An impulse is a signal that when integrated produces a step waveform[1] [Siebert 1986]. The voltage impulse when integrated by the inductor therefore returns the current to zero. The correct size impulse is discussed in section 6.5.4. The DC voltage waveform, Figure 6.9(c), is

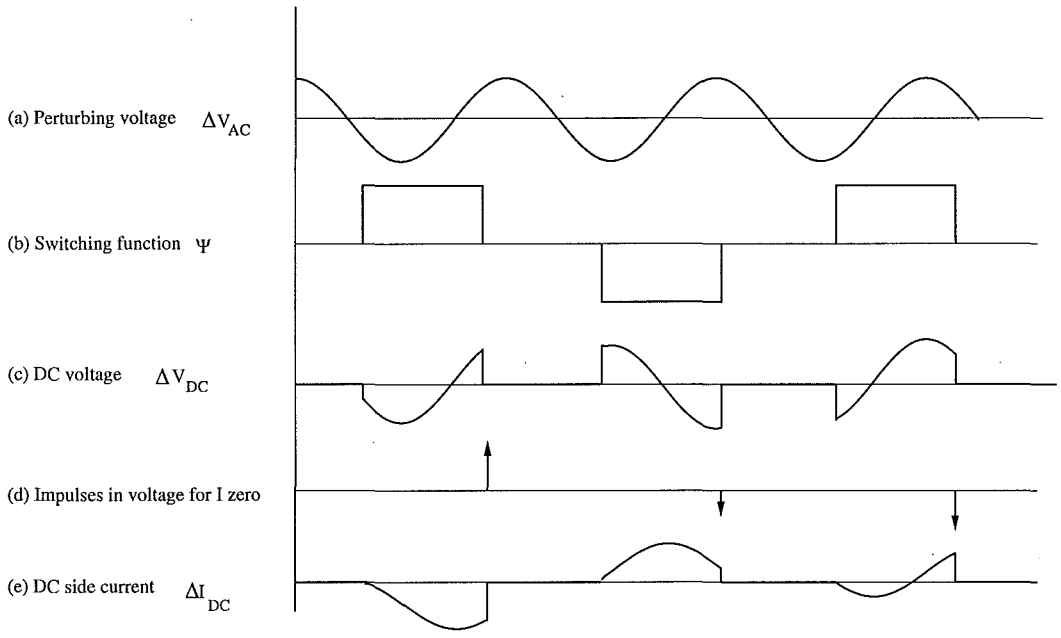

Figure 6.9 Waveforms showing the construction of AC side voltage to DC side voltage transfer (a) Perturbing voltage (b) Switching function (c) DC voltage (d) Impulses to return current to zero (e) DC side current.

[1] An impulse signal cannot exist in a real physical system because the impulse has infinite bandwidth. However because all physical systems are low-pass the impulse can be approximated with a band-limited signal that produces effectively the same response in the actual physical system [Siebert 1986].

zero during the time that the rectifier is not conducting. The no conduction mode, described previously in section 6.3.1 and shown in Figure 6.6(b), is an open circuit. Zero voltage is however, not an open circuit but rather a short circuit. Therefore the conduction mode enforced by the voltage waveform of Figure 6.9(c) is the short circuit of Figure 6.10(a) and not the open circuit required in Figure 6.6(b). In the paper on which this work is based [Laird *et al.* 2000] the analysis of the single-phase rectifier included only the AC side effects and therefore assumed that the DC side voltage was constant. The result of this assumption is that the DC bus connection is a short circuit as shown in Figure 6.10(b). This means that the application of zero voltage during the non-conduction period shorts the rectifier inductor and there is zero applied voltage. Any current flowing in the inductor is therefore maintained constant and because the current has been returned to zero by the impulse at the end of the conduction period the current remains zero during this time.

When zero voltage is connected to the complete DC side filter circuit, as in Figure 6.10(a), the bus capacitor has some non zero voltage. This voltage drives a current through the inductor during a period when the current is required to be zero. The model approach is therefore not accurate. To overcome this problem the best method is to use a current source on the DC side. A current source with its current set to zero has the characteristics of an open circuit. That is, it does not allow any current to flow through it no matter the voltage in the circuit and so appears as an open circuit. The conclusion from this is that the rectifier transfer from AC side voltage to the DC side is best represented with a controlled current source (Figure 6.10(c)).

6.3.4 Voltage to current partition

In making the voltage to current type partition the rectifier inductor is included as part of the rectifier (Figure 6.11). This makes the rectifier a voltage input current output device and ensures that the current will be zero when required no matter the characteristics of the DC side filter or AC side system impedance. The connection of a current source to an inductor removes the inductor current state variable. This means that the inductor no longer has an effect and so no longer exists as a circuit element. As will be seen later in section 6.4, the inductor value is used as the gain of the voltage to current transfer so in effect the inductor has been replaced with a current source of the appropriate gain.

The inductor need not be completely included in the rectifier. That is, any arbitrary small inductance can be made part of the converter. The DC side filter can then be attached. The filter can be of any form so long as the basic switching action of the converter is not changed. However, if all of the inductance is made part of the rectifier then the rectifier model's DC side terminal voltage, ΔV_{DC}, is the same as the DC bus voltage of the rectifier, ΔV_{DCBUS}, as shown in Figure 6.11. If only

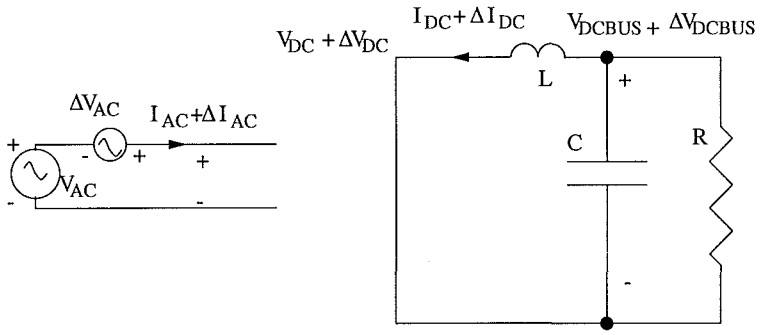

(a) Zero voltage connection to DC filter showing a short circuit.

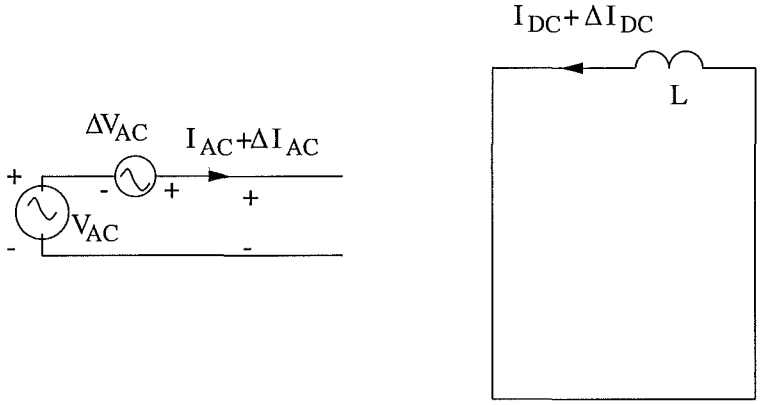

(b) Zero voltage with DC bus voltage source represented as a short circuit.

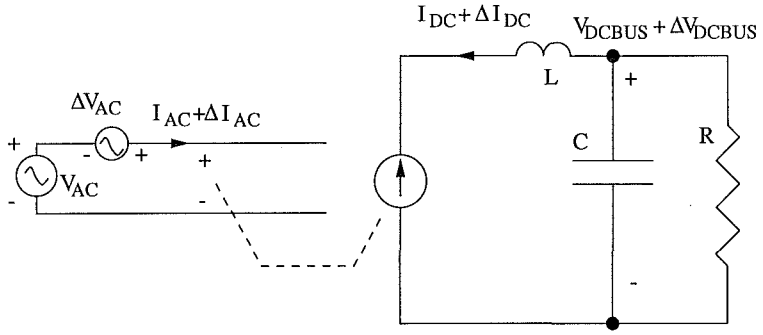

(c) Zero current in a current source is equivalent to an open circuit.

Figure 6.10 Rectifier conduction mode with no connection to DC side showing that the voltage to voltage partition is only valid if the DC bus is a voltage source.

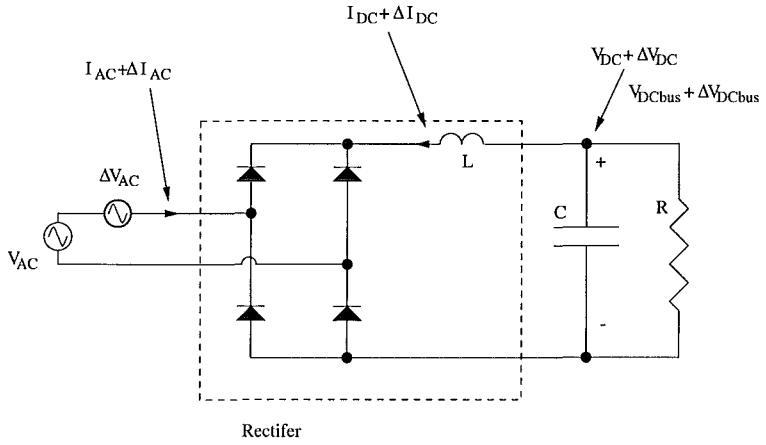

Figure 6.11 Rectifier partitioned in a voltage to current manner.

part of the inductor was included in the rectifier this would not be the case and so for convenience the entire inductor is absorbed into the rectifier. Thus the inputs to the rectifier model are the two voltages ΔV_{AC} and ΔV_{DC} and the outputs are the current ΔI_{AC} and ΔI_{DC}. The rectifier in Figure 6.12 with small perturbation inputs, ΔV_{AC} and ΔV_{DC}, added separately to the AC side and the DC side voltage is modelled as the system shown in Figure 6.13. Each of the transfers from a voltage

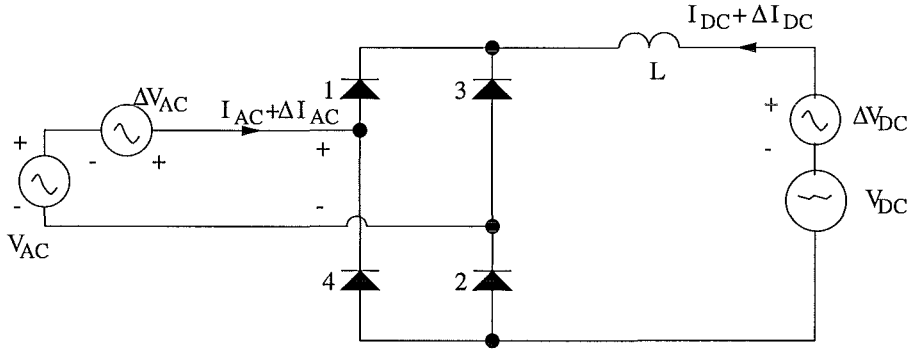

Figure 6.12 Single-phase rectifier circuit to be used for analysis. Circuit shows base case variables and small signal perturbation sources, (marked with Δ) added to those variables.

to a current in Figure 6.13 is the FTM of the partial differential of the current with respect to the voltage. Descriptions of partial differentials have been given previously in section 5.3.6.5. The four partial differentials used to model the single-phase rectifier are given in equation (6.4). The total sensitivity matrix of the single-phase rectifier is obtained by combining the component FTM partial differentials as in equation (6.5)

$$\begin{bmatrix} \Delta I_{AC} \\ \Delta I_{DC} \end{bmatrix} = \begin{bmatrix} \mathbf{A} & \mathbf{B} \\ \mathbf{C} & \mathbf{D} \end{bmatrix} \begin{bmatrix} \Delta V_{AC} \\ \Delta V_{DC} \end{bmatrix} \tag{6.5}$$

This matrix equation links the two input voltages to the two output currents and so describes the complete behaviour of the device.

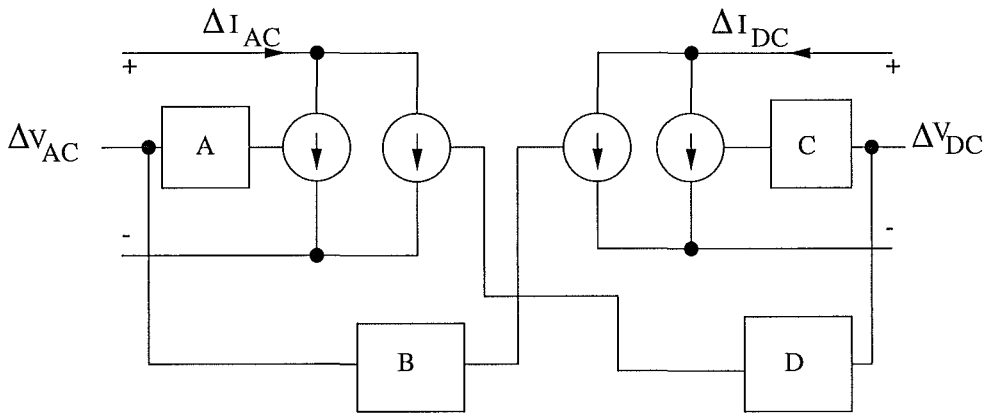

Figure 6.13 Controlled current source representation of the small signal part of the single-phase rectifier.

$$
\begin{aligned}
\mathbf{A} &= \left.\frac{\Delta I_{AC}}{\Delta V_{AC}}\right|_{\Delta V_{DC}=0} \\
\mathbf{B} &= \left.\frac{\Delta I_{AC}}{\Delta V_{DC}}\right|_{\Delta V_{AC}=0} \\
\mathbf{C} &= \left.\frac{\Delta I_{DC}}{\Delta V_{AC}}\right|_{\Delta V_{DC}=0} \\
\mathbf{D} &= \left.\frac{\Delta I_{DC}}{\Delta V_{DC}}\right|_{\Delta V_{AC}=0}
\end{aligned}
\tag{6.4}
$$

6.3.5 Suitability of using undistorted voltage sources in the analysis to generate the model

The single-phase rectifier is typical operated connected to an AC system of some finite impedance and to a DC side filter that has finite bus capacitance. Therefore there are always base case AC voltage harmonics and DC bus voltage ripple. This ripple is the DC side equivalent of AC voltage harmonics. In the analysis of the following sections the voltage on the DC side is assumed to have a constant zero frequency value with no ripple and the voltage on the AC side is assumed to have no harmonic content. The assumptions make the analysis simpler. As always there is the possibility that these simplifying assumptions may lead to inaccuracies in the analysis. The key to producing an accurate model is to ensure that these inaccuracies are small. Unfortunately it is always impossible to determine if the approximating assumptions are correct until the analysis is complete and the results compared. However, the assumptions seem reasonable as AC power systems generally have close to sinusoidal voltages or equivalently low distortion levels. Standards such as IEEE 519 [IEEE 1992] enforce point of supply voltage THD limits of less than 5%. Voltage source rectifiers operate to produce steady

DC side voltage with the ripple level being relatively low. Thus relatively low distortion levels appear on both the AC side and DC side voltages in rectifiers with capacitors on the DC side and so it is more than likely that suitable approximations of distorted base case voltages can be made with undistorted voltages when small signal perturbations are made.

6.4 DEVELOPING THE TRANSFERS FROM BASE SWITCHING

Consider the small signal terminal voltage perturbation in equation (6.6) which is shown in Figure 6.14(a).

$$\Delta V_{AC} = V_k \sin(k\omega_0 t + \delta_k) \tag{6.6}$$

The current that results from this voltage being applied to an inductor is given by integrating the voltage (6.7). This current is called the Pseudo Steady State Current (PSSC) because it is the current that would flow in the inductor in the steady state if ΔV_{AC} were applied directly.

$$\begin{aligned} \Delta I_{PSSC} &= \frac{1}{L}\int \Delta V_{AC} dt \\ &= \frac{-V_k}{k\omega_0 L}\cos(k\omega_0 + \delta_k) + Constant \\ &= \frac{-V_k}{k\omega_0 L}\sin(k\omega_0 + \delta_k + \frac{\pi}{2}) + Constant \end{aligned} \tag{6.7}$$

The PSSC waveform with the *Constant* of integration set to zero is shown in Figure 6.14(b). Multiplying the PSSC in Figure 6.14(b) by the switching function shown in Figure 6.14(c) gives the partial current waveform $\Delta I_{DC_{part}}$ (Figure 6.14(d)). Equation (6.9) gives the Fourier series of this waveform.

$$\begin{aligned} \Delta I_{DC_{part}} &= \frac{-2V_k}{m\pi k\omega_0 L}\sin\left[\frac{m\theta_1 - m\theta_2}{2}\right] \\ &\quad (+\sin\left[(m+k)\omega_0 t + \delta_k - \frac{m\theta_1 + m\theta_2}{2}\right] \\ &\quad -\sin\left[(m-k)\omega_0 t - \delta_k - \frac{m\theta_1 + m\theta_2}{2}\right]) \\ &\quad \text{for } m = 1,3,5,7... \end{aligned} \tag{6.8}$$

$$\begin{aligned} \Delta I_{DC_{part}} &= 0 \\ &\quad \text{for } m = 0,2,4,6... \end{aligned} \tag{6.9}$$

This partial current waveform has the correct shape because the current is the integral of the voltage. However the initial condition requirement that the current be zero at each turn on switching instant is not generally met. In order to meet this condition it is necessary to subtract the value of the $\Delta I_{DC_{part}}$ at the turn on switching instant. This value is the same as the value of the PSSC, Figure 6.14(b), at the turn on switching instant. The result of this is that the constant value in the integral result in equation (6.7) is varied with each successive conduction period and this constant is the negative value of the PSSC at the turn on switching instant. The constant value for each conduction period, shown for negative and positive switchings in Figure 6.14(e) and Figure 6.14(f) respectively, is added to the current in Figure 6.14(d) to produce the final current, Figure 6.14(f), which now has zero value at each turn on instant as required. Notice again that the offset current in Figure 6.14(e) and Figure 6.14(f) has a magnitude which is the value of the PSSC, Figure 6.14(b), at each turn on switching instant. The waveform holds this value during the period from the turn on to the turn off switching instant. Also note that each alternate switching period has a constant value that is the negative value of the PSSC, Figure 6.14(b), sampled at the turn on switching instant. This type of waveform is generally referred to as pulse amplitude modulation (PAM).

The PAM waveforms of Figure 6.14(e) and (f) are both generated as is shown in Figure 6.15. Sampling the PSSC at the turn on switching instant, Figure 6.15(a), with the time shifted sampling function, Figure 6.15(b), gives Figure 6.15(c). The square pulse shape is then added by time domain convolution which is the equivalent of frequency domain spectral multiplication, with a single square wave pulse of the correct width centred around time zero (Figure 6.15(d)). The waveform is then time shifted by half the square pulse width to form the final PAM waveform, the Fourier series of which is shown in (6.10). Appendix B.5 gives the derivation of the PAM spectrum.

$$
\begin{aligned}
PAM(\omega_0 t) = {} & \frac{bd}{2\pi}\mathrm{sinc}(\frac{kd}{2\pi})\cos(k\omega_0 t - k(\frac{d}{2}) + \delta_k) \\
+ {} & \frac{bd}{2\pi}\sum_{m=1}^{\infty}\mathrm{sinc}((m+k)\frac{d}{2\pi})\cos((m+k)\omega_0 t - (m+k)(\frac{d}{2}) - m\theta_1 + \delta_k) \\
+ {} & \frac{bd}{2\pi}\sum_{m=1}^{\infty}\mathrm{sinc}((m-k)\frac{d}{2\pi})\cos((m-k)\omega_0 t - (m-k)(\frac{d}{2}) - m\theta_1 - \delta_k)
\end{aligned}
$$

$$
\begin{aligned}
\text{where } d &= \text{pulse width} \\
&= (\theta_2 - \theta_1)
\end{aligned}
\tag{6.10}
$$

When a zero frequency AC side voltage is applied, the waveform of the resulting

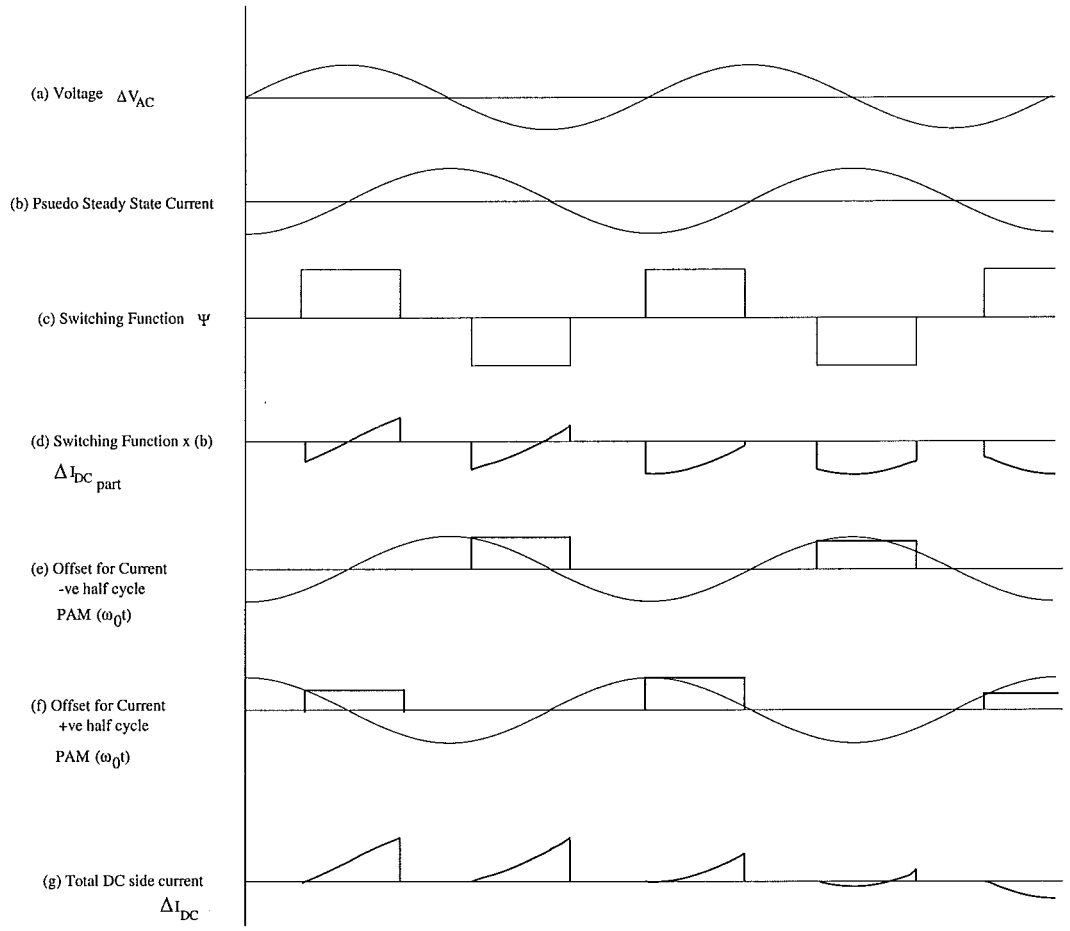

Figure 6.14 Waveforms showing the construction of AC side voltage ΔV_{AC} to DC side current ΔI_{DC} transfer.

DC side current cannot be found in the same way as previously for a non-zero frequency signal. This is because the integral of a constant zero frequency value, that is required for the PSSC, is an ever increasing ramp. Such a waveform is not periodic so its Fourier series cannot be found. To determine the transfer for zero frequency the AC side voltage ΔV_{AC}, Figure 6.16(a), is multiplied by the switching function, Figure 6.16(b), to give the resulting change in the voltage across the rectifier inductor. The current is then calculated for each part of the switching period, see equation (6.11), to give the resulting current waveform of Figure 6.16(d).

$$\begin{aligned} \Delta I_{DC_{k\omega_0=0}} &= \frac{1}{L}\int_{\theta_1}^{\theta_2} V_k dt \\ &+ \frac{1}{L}\int_{\theta_1+\pi}^{\theta_2+\pi} -V_k dt \end{aligned} \tag{6.11}$$

This sum of integral results, waveform Figure 6.16(d), is periodic so its Fourier series can be calculated as the sum of time shifted and scaled copies of (6.12). The Fourier

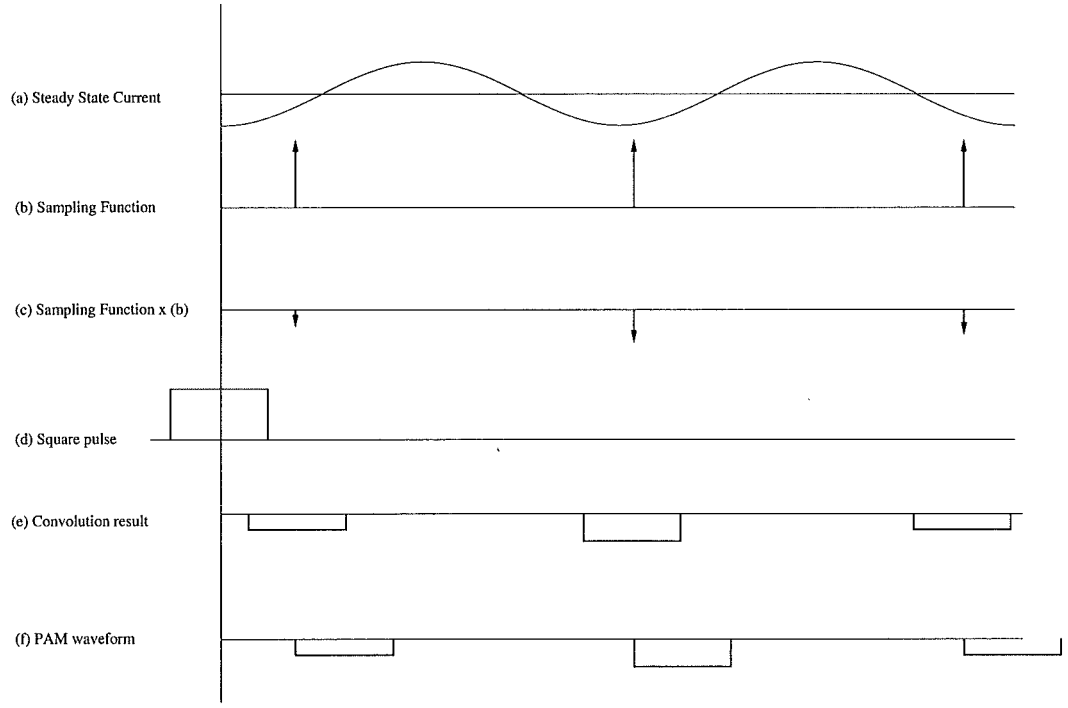

Figure 6.15 Construction of the pulse amplitude modulation waveform.

series in (6.12) is a ramp waveform of width $\theta_2 - \theta_1$ with zero value at time zero.[2]

$$\begin{aligned}\Delta I_{DC_{k\omega_0=0}} &= \frac{V_k}{2\pi L} \\ &+ \frac{V_k}{L\pi}\sum_{m=1}^{\infty}\frac{1}{m^2}\left[\sin(m\theta_2 - m\theta_1) - m(\theta_2 - \theta_1)\cos(m\theta_2 - m\theta_1)\right]\sin(m\omega_0 t) \\ &+ \frac{V_k}{L\pi}\sum_{m=1}^{\infty}\frac{1}{m^2}\left[\cos(m\theta_2 - m\theta_1) + m(\theta_2 - \theta_1)\sin(m\theta_2 - m\theta_1)\right]\cos(m\omega_0 t)\end{aligned} \tag{6.12}$$

6.4.1 Transfer construction

To construct the FTM for each transfer from the voltage perturbation to the resultant current the Fourier series of six component waveforms must be combined. These six are the PSSC, the positive half cycle switching function, the negative half cycle switching function, the two PAM waveforms that make the current zero at the turn on instant and the two component parts of the zero frequency transfer described by equation (6.12). The component transfers for ΔV_{AC} to ΔI_{DC} are summarised in Table 6.1. Each component waveform is described along with the Figure number where the waveform can be seen. Also, the equation number of the Fourier series is given along with the time shift and sign multiplier. As detailed in section 6.4, the PSSC is multiplied by the

[2]The time shift of the waveform is performed by substituting the shifted time for the time variable t.

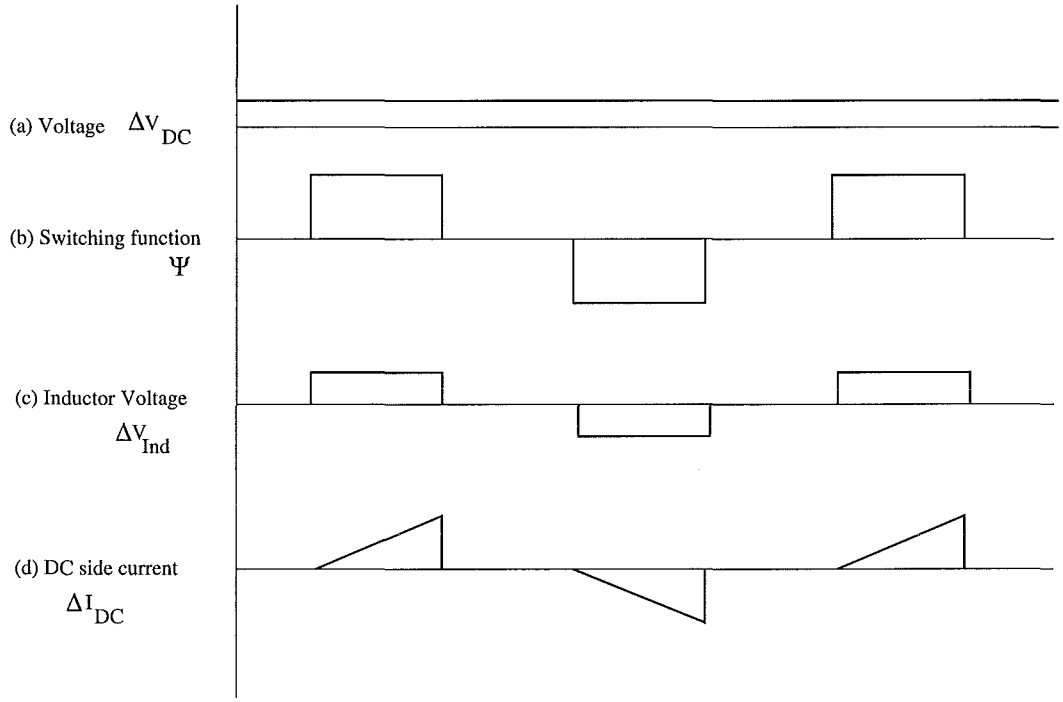

Figure 6.16 Waveforms showing the construction of AC side voltage to DC side current transfer for zero frequency input voltage.

switching pulses then the PAM waveform and the zero frequency components added. The FTM for each component transfer is generated and these are then added to create the total transfer FTM.

The ΔV_{AC} to ΔI_{AC} transfer components and construction are shown in Table 6.2. Notice that the same Fourier series are used as in the ΔV_{AC} to ΔI_{DC} but the signs of the negative half cycle switching pulse, the negative half cycle PAM and the negative half cycle zero frequency current are changed.

The same component parts also make up the other two transfers. The ΔV_{DC} to ΔI_{AC} transfer is the same as the ΔV_{AC} to ΔI_{DC} transfer so Table 6.1 gives the time shifts and signs. Similarly the ΔV_{AC} to ΔI_{AC} transfer is the same as the ΔV_{DC} to ΔI_{DC} transfer so Table 6.2 is appropriate. The symmetry in the transfers is due to the symmetry between the AC and DC sides. Such symmetry does not occur in three-phase rectifiers where commutation and the three-phase nature of the device means that transfers from the AC side differ from their DC side counterparts [Osauskas and Wood 2001, Wood 1993].

In summary, the four component base switching transfers of the single-phase rectifier are combinations of a number of frequency transfer functions. The four can be combined to form the total transfers due to the base switching of the rectifier.

Waveform	Fourier series equation	Sign	Time shift
Pseudo steady state current, Figure 6.14(b)	(6.7)	+1	0
Positive half cycle switching pulse, Figure 5.2(a)	(5.1)	+1	$\frac{\theta_1+\theta_2}{2}$
Negative half cycle switching pulse, Figure 5.2(a)	(5.1)	-1	$\frac{\theta_1+\theta_2}{2}+\pi$
Positive half cycle $PAM(\omega_0 t)$, Figure 6.14(f)	(6.10)	+1	θ_1
Negative half cycle $PAM(\omega_0 t)$, Figure 6.14(e)	(6.10)	-1	$\theta_1+\pi$
Positive half cycle zero frequency current, Figure 6.16(d)	(6.12)	+1	θ_1
Negative half cycle zero frequency current, Figure 6.16(d)	(6.12)	-1	$\theta_1+\pi$

Table 6.1 ΔV_{AC} to ΔI_{DC} transfer components.

6.5 SWITCHING INSTANT MODULATION TRANSFERS

In the introduction to this chapter the switching instant modulation was identified as a mechanism for a perturbing voltage to effect the rectifier behaviour. Analysis of the effects of the switching instant variation is carried out in this section. The first step is to determine the switching instant variation.

6.5.1 Determining turn on switching instant modulation

The change in each switching instant angle is determined by linearising the switching condition about the operating point. The condition governing the turn on switching instant is shown in Figure 6.17.

The condition for the turn on switching instant when ΔV_{AC} is added to the base AC voltage is (6.13).

$$V_{AC} + \Delta V_{AC} - V_{DCBUS} = 0 \tag{6.13}$$

The base case AC voltage is (6.14).

$$V_{AC} = M \sin \omega_0 t \tag{6.14}$$

Re-arranging (6.13) and substituting $\omega_0 t = \theta_1$ gives (6.15).

$$M \sin \theta_1 + \Delta V_{AC} = V_{DCBUS} \tag{6.15}$$

Waveform	Fourier series equation	sign	time shift
Pseudo steady state current, Figure 6.14(b)	(6.7)	+1	0
Positive half cycle switching pulse, Figure 5.2(a)	(5.1)	+1	$\frac{\theta_1+\theta_2}{2}$
Negative half cycle switching pulse, Figure 5.2(a)	(5.1)	+1	$\frac{\theta_1+\theta_2}{2}+\pi$
Positive half cycle $PAM(\omega_0 t)$, Figure 6.14(f)	(6.10)	+1	θ_1
Negative half cycle $PAM(\omega_0 t)$, Figure 6.14(e)	(6.10)	+1	$\theta_1+\pi$
Positive half cycle zero frequency current, Figure 6.16(d)	(6.12)	+1	θ_1
Negative half cycle zero frequency current, Figure 6.16(d)	(6.12)	+1	$\theta_1+\pi$

Table 6.2 ΔV_{AC} to ΔI_{AC} transfer components.

Letting $\theta_1 = \theta_1 + \Delta\theta_1$ and substituting this in (6.15) gives

$$M \sin(\theta_1 + \Delta\theta_1) + \Delta V_{AC} = V_{DCBUS} \tag{6.16}$$

Upon expansion the $\sin(\theta_1 + \Delta\theta_1)$ becomes (6.17)

$$\sin(\theta_1 + \Delta\theta_1) = \sin\theta_1 \cos\Delta\theta_1 + \cos\theta_1 \sin\Delta\theta_1 \tag{6.17}$$

Then using the linearising approximations, (6.18) and (6.19), that are valid so long as $\Delta\theta_1$ is sufficiently small gives (6.20). $\Delta\theta_1$ is assumed to be small when ΔV_{AC} has a small magnitude.

$$\sin\Delta\theta_1 \simeq \Delta\theta_1 \tag{6.18}$$

$$\cos\Delta\theta_1 \simeq 1 \tag{6.19}$$

$$M \sin\theta_1 + M \cos\theta_1 \Delta\theta_1 + \Delta V_{AC} = V_{DCBUS} \tag{6.20}$$

This linearisation uses the tangent at the switching instant, Figure 6.17, as an approximation to the small signal slope of the base voltage at this point. At the turn on switching instant the DC bus voltage and the AC voltage are the same (6.21).

$$V_{DCBUS} = V_{AC} = M \sin\theta_1 \tag{6.21}$$

This means (6.22)

$$M \cos\theta_1 \Delta\theta_1 + \Delta V_{AC} = 0 \tag{6.22}$$

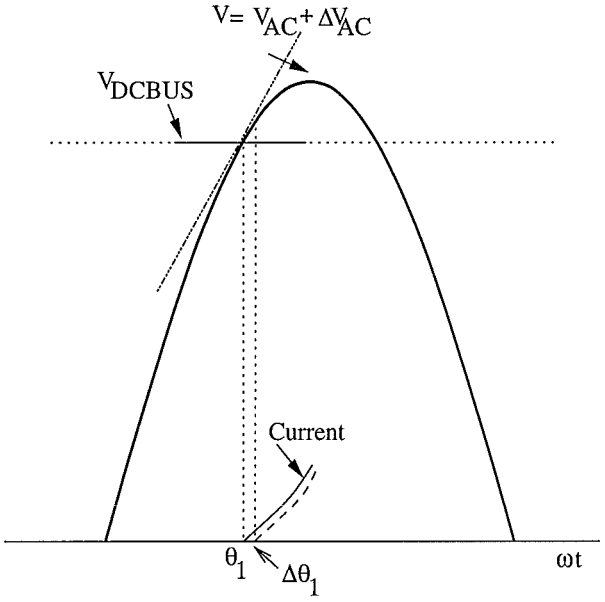

Figure 6.17 Condition determining turn on switching instant variation.

Re-arranging (6.22) gives (6.23)

$$\Delta\theta_1 = \frac{-\Delta V_{AC}}{M\cos\theta_1} \tag{6.23}$$

which is the change, $\Delta\theta_1$, in the turn on switching instant, defined by the angle θ_1, for a given perturbing voltage ΔV_{AC} and fundamental magnitude M.

6.5.2 Effective frequency of switching instant modulation

The unperturbed switching of the single-phase rectifier occurs at twice the fundamental frequency. When an AC side perturbing voltage, $\Delta V_{AC} = V_k \sin(k\omega_0 t + \delta_k)$, is applied the effect of that voltage on the switching instant modulation is determined by the interaction of the rectifier's twice fundamental switching and ΔV_{AC}. Figure 6.18 shows how the switching action of the rectifier samples ΔV_{AC} at twice the fundamental frequency. The value of ΔV_{AC} that determines the switching instant variation is the value at each unperturbed switching instant. This value of ΔV_{AC} at three successive switching instants is evaluated in Figure 6.18 in order to find the frequency and phase of the change in the switching instant angle. (The negative half cycle of the AC voltage is shown inverted and the sign of ΔV_{AC} at the $\pi + \theta_1$ switching instant is negated for clarity. This is equivalent to actual rectifier operation.) As the sampling occurs at twice fundamental frequency a modulation or frequency shift occurs meaning that the effective switching instant modulation frequency is different from the frequency of ΔV_{AC}. In order to determine this frequency the values of ΔV_{AC} from (6.24) are shown for successive turn on switching instants in (6.25) through (6.27).

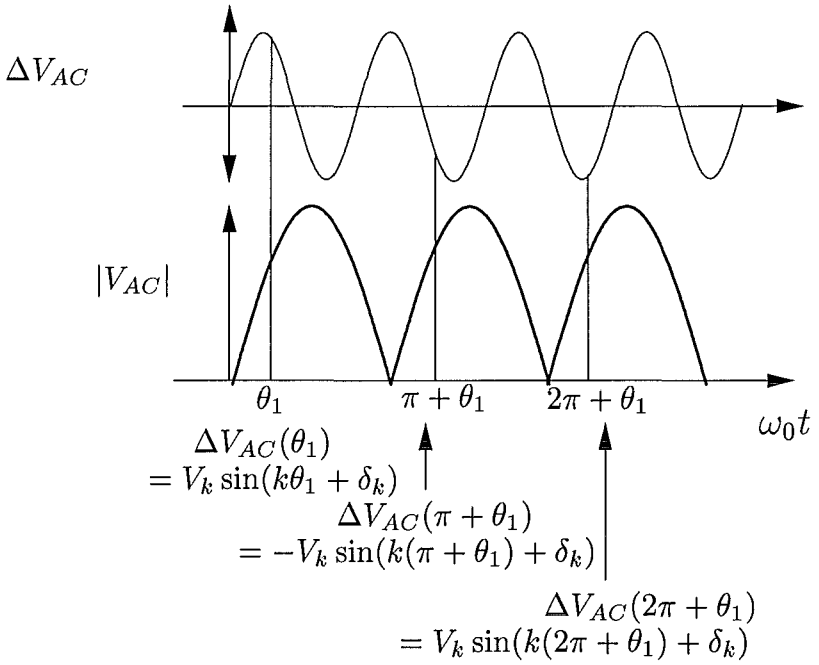

Figure 6.18 Sampling to determine the effective frequency of switching instant modulation.

$$\Delta V_{AC} = V_k \sin(k\omega_0 t + \delta_k) \tag{6.24}$$

for $\omega_0 t = \theta_1$

$$\Delta V_{AC} = V_k \sin(k\theta_1 + \delta_k) \tag{6.25}$$

for $\omega_0 t = \pi + \theta_1$

$$\Delta V_{AC} = V_k \sin(k\theta_1 + \delta_k + k\pi \pm \pi) \tag{6.26}$$

for $\omega_0 t = 2\pi + \theta_1$

$$\Delta V_{AC} = V_k \sin(k\theta_1 + \delta_k + 2k\pi) \tag{6.27}$$

Any function that produces these values at these switching instants is a valid effective switching instant modulation. One such function is (6.28).

$$\Delta V_{AC_{effective}} = V_k \sin\left((k-1)\omega_0 t + \theta_1 + \delta_k\right) \tag{6.28}$$

This means that an AC side perturbing voltage ΔV_{AC} of frequency $k\omega_0$ effects the switching instant at a frequency $(k-1)\omega_0$. However, as this result is from possibly sub nyquist rate sampling (which is the situation shown in Figure 6.18) other expressions that produce a valid $\Delta V_{AC_{effective}}$ can be developed. The choice of the effective frequency is arbitrary because an effective switching instant modulation can be found involving frequency $(k-3)\omega_0$, $(k-5)\omega_0$, $(k+1)\omega_0$ or any other frequency an odd multiple of ω_0 different to k. Each of these functions generates the same value for the

switching instant modulation at each switching instant. That is when the switching instant modulation value is used in a switching instant modulation spectrum, (6.3), the resultant frequency components are the same. The $(k-1)\omega_0$ function is used for calculation purposes.

6.5.3 Turn on switching instant modulation validation

The switching instant modulation caused by the applied voltage ΔV_{AC} was measured using a time domain variable time step MATLAB/Simulink simulation of the rectifier. The variable time step allows the switching instant to be accurately calculated without error caused by time quantisation that can occur in fixed time step simulations. A 0.5 % sinusoidal voltage ($V_k = 0.5V$) of frequency 143Hz and phase 0 radians was added to the 50Hz 50 V peak fundamental voltage. The DC bus voltage is 42 Vdc, $\theta_1 = 0.9486$ and $\theta_2 = 2.4544$. The effect of ΔV_{AC} on the turn on switching instants is shown in Figure 6.19 by the light bars. As can be seen these are well approximated by the dark bars which are calculated using (6.28) and (6.23). Each angular variation occurs at the same time instant but they are shown side by side in Figure 6.19 for clarity. The mean absolute error in the switching instants is less than 4% for this case. This shows that the linearisation is highly accurate. Similar accurate results are also obtained for other perturbing frequencies.

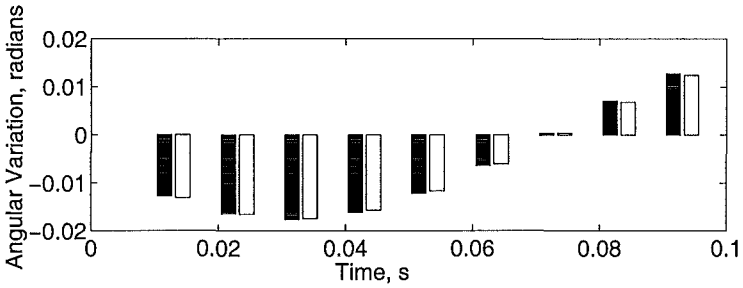

Figure 6.19 Turn on switching instant modulation validation for 143Hz applied voltage (Dark bars indicate analytic results and light bars simulated results).

6.5.4 Turn off switching instant modulation

The turn off switching instant modulation is determined by equating the integral of the voltage applied to the DC side inductor to zero. That is, the DC side current returns to zero, the condition for the switch off, when the total integral volt-seconds is zero. Figure 6.20 shows the AC side and DC side voltages that determine this switching. The integral of the voltage across the inductor is (6.29)

$$\int_{\theta_1}^{\theta_2+\Delta\theta_2} (V_{AC} + \Delta V_{AC} - V_{DCBUS}) d\theta = 0 \qquad (6.29)$$

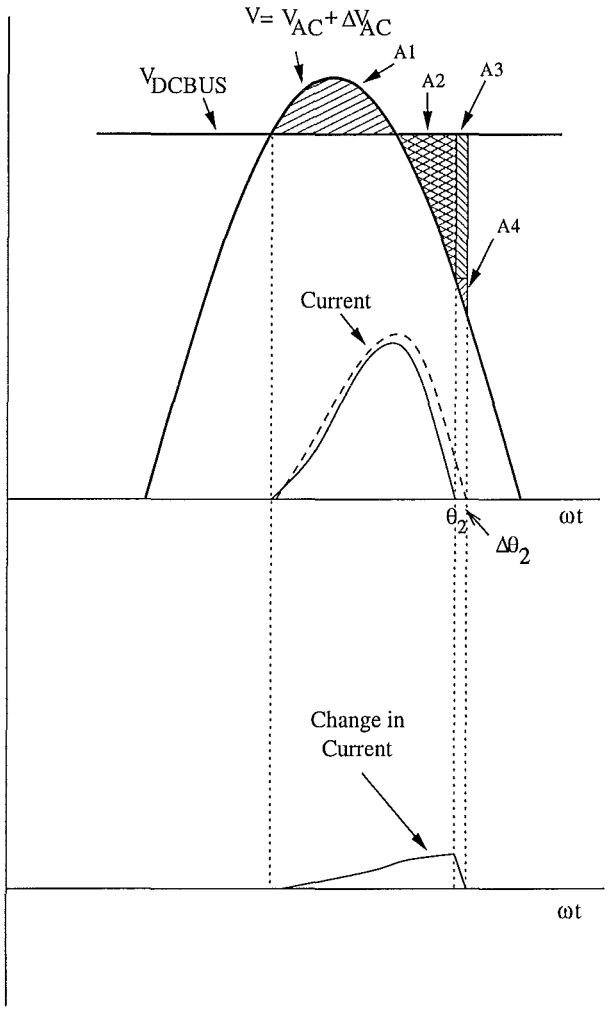

Figure 6.20 Condition determining turn off switching instant variation.

The modulation of θ_2 does not depend on the modulation of θ_1 as the contribution to the integral from the modulation of θ_1 is negligibly small (or equivalently second order as will be shown in section 6.5.6). By separating the contributions in (6.29) and rearranging the limits the individual effects can be found.

$$\int_{\theta_1}^{\theta_2} (V_{AC} - V_{DCBUS}) d\theta \quad + \tag{6.30}$$

$$\int_{\theta_2}^{\theta_2+\Delta\theta_2} \Delta V_{AC} d\theta \quad + \tag{6.31}$$

$$\int_{\theta_2}^{\theta_2+\Delta\theta_2} (V_{AC} - V_{DCBUS}) d\theta \quad + \tag{6.32}$$

$$\int_{\theta_1}^{\theta_2} \Delta V_{AC} d\theta \quad = \quad 0 \tag{6.33}$$

The applied perturbing voltage ΔV_{AC} is (6.34).

$$\Delta V_{AC} = V_k \sin(k\omega_0 t + \delta_k) \tag{6.34}$$

The AC fundamental voltage is (6.35).

$$V_{AC} = M \sin \omega_0 t \tag{6.35}$$

and the DC bus voltage is assumed to be constant (6.36).

$$V_{DCBUS} = M \sin \theta_1 \tag{6.36}$$

The term from (6.30), which corresponds to area A1 and A2 in Figure 6.20, is zero as this is the situation that determines the turn off switching instant in the case where no ΔV_{AC} is present (the base case).

The effect of ΔV_{AC} in the interval from θ_2 to $\theta_2 + \Delta\theta_2$ is

$$\int_{\theta_2}^{\theta_2+\Delta\theta_2} \Delta V_{AC} d\theta = \left[\frac{-V_k}{k} \cos(k\theta + \delta_k)\right]_{\theta_2}^{\theta_2+\Delta\theta_2} \tag{6.37}$$

$$= \frac{-V_k}{k} \sin(k\theta_2 + \delta_k) \sin k\Delta\theta_2 \tag{6.38}$$
$$+ \frac{-V_k}{k} \cos(k\theta_2 + \delta_k) \cos k\Delta\theta_2$$
$$- \frac{-V_k}{k} \cos(k\theta_2 + \delta_k)$$

So long as $k\Delta\theta_2$ is sufficiently small the two cosine terms add to zero. The $\frac{\sin k\Delta\theta_2}{k}$ contribution is proportional to $\Delta\theta_2$ when $\Delta\theta_2 \to 0$. The multiplication by the small V_k means that the contribution of this integral is a small quantity multiplied by a small quantity and so can be ignored as a second order effect.

The contribution of the difference between V_{AC} and V_{DCBUS} in the interval θ_2 to $\theta_2 + \Delta\theta_2$ (6.32), which corresponds to area A3 and A4 in Figure 6.20, is (6.39).

$$\int_{\theta_2}^{\theta_2+\Delta\theta_2} (V_{AC} - V_{DCBUS}) d\theta = [-M \cos\theta - M\theta \sin\theta_1]_{\theta_2}^{\theta_2+\Delta\theta_2} \tag{6.39}$$

By grouping the terms and making the small value approximations (6.18) and (6.19) the contribution of this term is

$$\Delta\theta_2 M(\sin\theta_2 - \sin\theta_1) \tag{6.40}$$

The final term, (6.31), is the effect of ΔV_{AC} during the interval θ_1 to θ_2.

$$\begin{aligned} \int_{\theta_1}^{\theta_2} \Delta V_{AC} d\theta &= \left[-\frac{V_k}{k} \cos(k\theta + \delta_k) \right]_{\theta_1}^{\theta_2} \\ &= \frac{V_k}{k} \left[\cos(k\theta_1 + \delta_k) - \cos(k\theta_2 + \delta_k) \right] \end{aligned} \tag{6.41}$$

At the turn off switching instant $\omega_0 t = \theta_2$ and $\theta_1 = \omega_0 t - \theta_2 + \theta_1$ so substituting for θ_1 and θ_2 then simplifying gives

$$\tfrac{2V_k}{k} \sin(k\omega_0 t + \delta_k - \tfrac{k\theta_2}{2} + \tfrac{k\theta_1}{2}) \sin(\tfrac{k\theta_1}{2} - \tfrac{k\theta_2}{2}) \tag{6.42}$$

Using the same sampling approach as previously described in (6.24) through (6.27) gives the effective frequency and phase of the turn off switching instant modulation due to applied ΔV_{AC} (6.34). By taking the two non-zero integral results, (6.40) and the sampled (6.42), and making their sum zero the turn off switching instant modulation $\Delta\theta_2$ is (6.43).

$$\Delta\theta_2 = \frac{2V_k \sin\left(\frac{k\theta_1 - k\theta_2}{2}\right)}{kM(\sin\theta_2 - \sin\theta_1)} \sin((k-1)\omega_o t + \theta_2 + \delta_k + \frac{k\theta_1 - k\theta_2}{2}) \tag{6.43}$$

$$= \frac{2V_k \sin\left(\frac{k\theta_1 - k\theta_2}{2}\right)}{k\left(V_{AC_{\omega_0 t=\theta_2}} - V_{DCBUS_{\omega_0 t=\theta_2}}\right)} \sin((k-1)\omega_o t + \theta_2 + \delta_k + \frac{k\theta_1 - k\theta_2}{2}) \tag{6.44}$$

Note that $\Delta\theta_2$ does not depend on the inductance value L except through the dependence of the operating point θ_1 and θ_2 on the inductance. Noting in (6.43) that for a constant DC bus voltage, $M \sin\theta_1$ is the value of the base DC bus voltage at the turn off switching instant and that $M \sin\theta_2$ is the base AC voltage at the same time allows the rear switching instant to be written as equation (6.44). Inspecting Figure 6.20 at the rear switching instant provides confirmation. When the DC side circuit has a capacitor rather than a constant zero frequency voltage the DC bus voltage at the turn off switching instant $V_{DCBUS_{\omega_0 t=\theta_1}}$ must be used to determine the rear switching instant variation.

Equation (6.43) is in the form of a $\frac{\sin k}{k}$ so the zero frequency response can be found by taking the limit as k tends to zero. However it is possible to use another method to confirm the result found by taking the limit. In the same way as the base switching response to zero frequency ΔV_{AC} was evaluated (section 6.4) it is necessary to separately determine the rear switching modulation when a zero frequency is applied on the AC side. Consider the effect of the zero frequency voltage when transferred to the DC side of the rectifier as shown in Figure 6.21. As ΔV_{AC} is a constant at zero

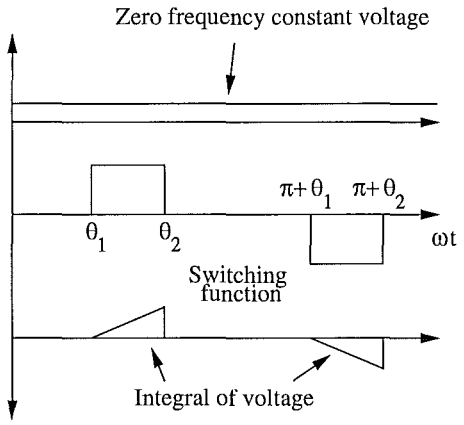

Figure 6.21 Waveforms to determine switching instant modulation caused by zero frequency voltage on the AC side.

frequency its integral in the period θ_1 to θ_2 is

$$\begin{aligned} \int_{\theta_1}^{\theta_2} \Delta V_{AC} d\theta &= [V_k]_{\theta_1}^{\theta_2} \\ &= V_k [\theta_2 - \theta_1] \end{aligned} \tag{6.45}$$

In the period $\theta_1 + \pi$ to $\theta_2 + \pi$ the integral has the negative of this value. By adding (6.45) and (6.40) as previously, the resulting rear switching instant modulation for a zero frequency on the AC side is

$$\Delta\theta_2 = \frac{-V_k [\theta_2 - \theta_1]}{M(\sin\theta_2 - \sin\theta_1)} \sin(\omega_o t + \theta_2) \tag{6.46}$$

Validation is shown in Figures 6.22(a) and 6.22(b) with the simulated variation (lighter bars) matching those calculated (darker bars) with (6.43). The operating condition is the same as that for the previous turn on switching instant example in Figure 6.19. The frequency of the perturbing voltage for Figure 6.22(a) is 73Hz at phase 0 and the magnitude $V_k = 0.5$. ($V_k \simeq 1\%$ of the fundamental magnitude.). Figure 6.22(b) shows the switching instant modulation for a zero frequency perturbing voltage on the AC side.

6.5.5 Switching instant variation from DC side voltage variation

The switching instant variation that occurs due to DC side voltage variation is calculated in exactly the same fashion as that for the AC side voltage variation with the perturbing voltage added to the DC side voltage rather than the AC side voltage. There is, however, no associated frequency change (see section 6.5.2). The turn on switching

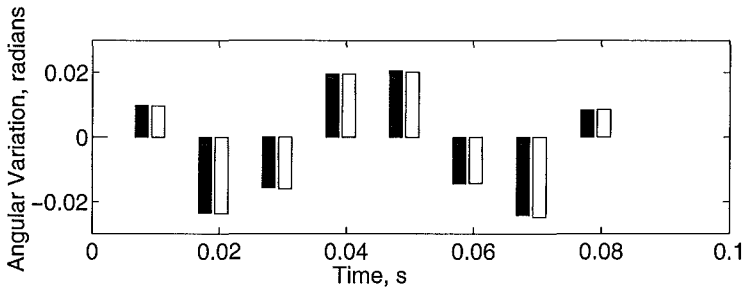

(a) 73 Hz applied AC side perturbing voltage.

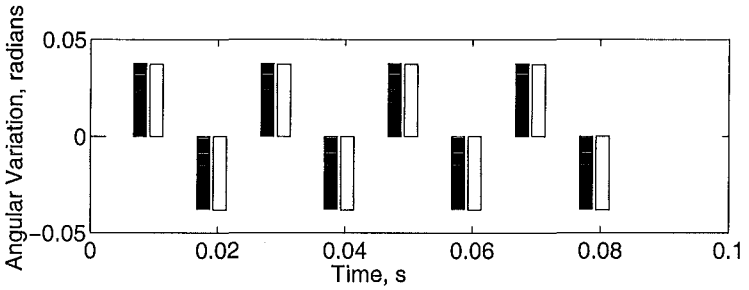

(b) 0Hz applied AC side perturbing voltage.

Figure 6.22 Turn off switching instant modulation validation. (Dark bars analytic results, light bars simulated results).

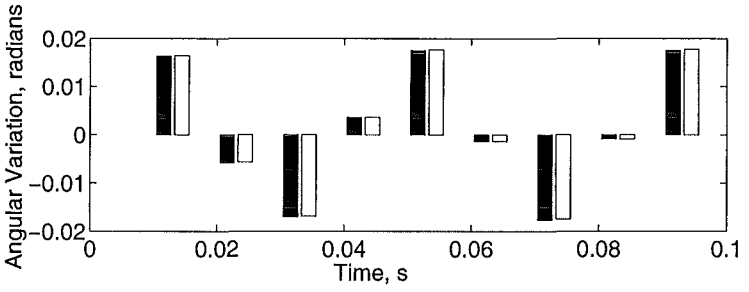

Figure 6.23 Front switching instant modulation validation for DC side 24Hz perturbing voltage. (Dark bars analytic, light bars simulated.)

instant variation due to a DC side voltage is (6.47).

$$\Delta\theta_1 = \frac{\Delta V_{DCBUS}}{M \cos\theta_1} \tag{6.47}$$

Figure 6.23 shows the analytic and simulated turn on switching instant modulation for a DC side voltage perturbation at 24Hz.

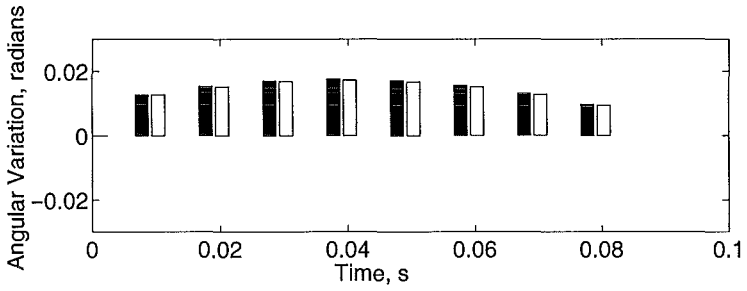

Figure 6.24 Rear switching instant modulation validation for DC side 104Hz perturbing voltage. (Dark bar analytic, Light bar simulated).

The turn off switching instant variation from a DC side voltage of (6.48) is (6.49)

$$\Delta V_{DCBUS} = V_k \sin(k\omega_0 t + \delta_k) \tag{6.48}$$

$$\begin{aligned} \Delta\theta_2 &= \frac{2V_k \sin\left(\frac{k\theta_1 - k\theta_2}{2}\right)}{kM(\sin\theta_2 - \sin\theta_1)} \sin(k\omega_o t + \delta_k + \frac{k\theta_1 - k\theta_2}{2}) \qquad (6.49) \\ &= \frac{2V_k \sin\left(\frac{k\theta_1 - k\theta_2}{2}\right)}{k\left(V_{AC_{\omega_0 t=\theta_2}} - V_{DCBUS_{\omega_0 t=\theta_2}}\right)} \sin(k\omega_o t + \delta_k + \frac{k\theta_1 - k\theta_2}{2}) \qquad (6.50) \end{aligned}$$

Figure 6.24 shows the analytic and simulated turn off, or rear, switching instant modulation match.

The voltage perturbations effect the switching instants. The current that is caused by this variation then needs to be determined.

6.5.6 Effect of switching instant modulation on currents

The effect of the switching instant variation on the current can be appreciated by considering Figure 6.25. The base voltage waveform is shown in Figure 6.25(a). The voltage waveform when the front switching instant is varied is shown in Figure 6.25(b). The difference between the two is shown in Figure 6.25(c). Consider the triangular area of this waveform. The width of the triangle is the switching instant variation which is (repeated from section 6.5.1) (6.51).

$$\Delta\theta_1 = \frac{-\Delta V_{AC}}{M\cos\theta_1} \tag{6.51}$$

The height of the triangular area is the voltage perturbation value at the base switching instant. However, the switching instant variation depends on the voltage perturbation

so the area of the triangle, or equivalently the integral, is (6.52)

$$\begin{aligned}\int_{\theta_1}^{\theta 1+\Delta\theta_1} \Delta V_{AC} d\theta &= \frac{1}{2}\Delta\theta_1 \Delta V_{AC_{\omega_0 t=\theta_1}} \\ &= \frac{1}{2}\Delta\theta_1 \Delta\theta_1 M \cos\theta_1 \\ &= \frac{1}{2} M \cos\theta_1 {\Delta\theta_1}^2\end{aligned} \tag{6.52}$$

As $\Delta\theta_1$ has a sinusoidal variation then $(\Delta\theta_1)^2$ has frequency components and magnitude as shown in (6.53).

$$\begin{aligned}{\Delta\theta_1}^2 &= \sin(k\omega_0 t + \delta_k)\sin(k\omega_0 t + \delta_k) \\ &= |\Delta\theta_1|^2 \left(\frac{1}{2} - \frac{1}{2}\cos(2k\omega_0 t + 2\delta_k)\right)\end{aligned} \tag{6.53}$$

This indicates that when a small quantity is squared the resulting magnitude is significantly smaller than the original small quantity.

The current waveform in the interval between the base switching instant and the perturbed switching instant is shown on an exaggerated scale in Figure 6.25(d). Also shown is the constant current offset that flows as the result of the current change during the switching variation. This offset is time varying much like the PAM waveform used in the base switching transfer described in section 6.4. However, the integral of the voltage during the switching instant variation interval $\Delta\theta_1$ to $\theta_1 + \Delta\theta_1$ is proportional to the square of the angular variation. This means that the amplitude of the current offset also varies with the square of the angular variation. As a result the amplitude is extremely small and the frequency of variation is not that of the switching instant but rather zero frequency and twice that of the switching instant.

The base current, perturbed current and the difference current waveforms from the time domain simulation for the negative half cycle conduction period are shown in Figure 6.5.6. An annotated detail view of the same waveforms near the turn on switching is shown in Figure 6.5.6. The small area shown shaded corresponds to the current waveform of Figure 6.25(d). The step in the current can be seen in the height of the triangle. It is important to realise that this step effect is second order and so is negligibly small.

At the rear switching instant the variation in the switching instant gives rise to the inductor voltage change as shown in Figure 6.28(c). The area of this voltage waveform is proportional to the variation of the switching instant because the height of the pulse is equal to the difference between the base AC voltage at the turn off switching instant and the base DC voltage at the same time. The total current variation in Figure 6.28(d)

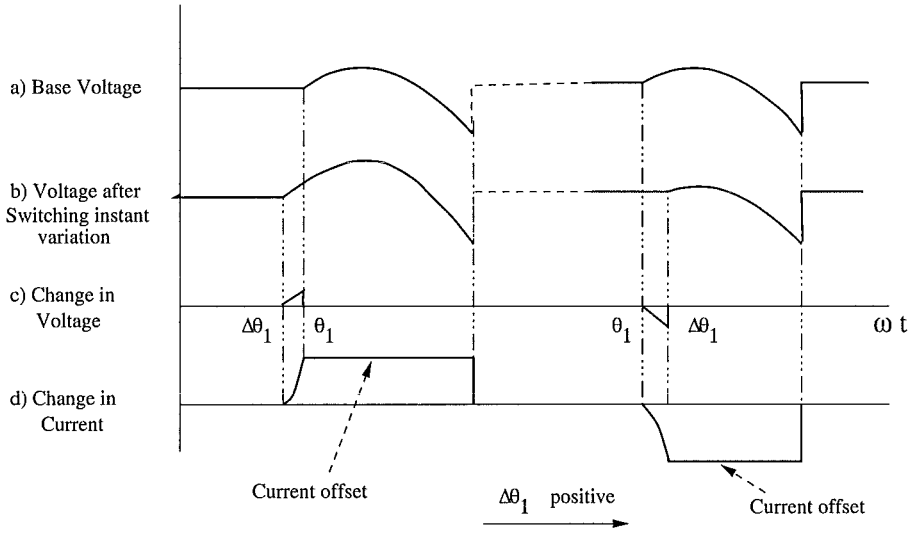

Figure 6.25 Voltage and current waveforms when varying the turn on switching instant.

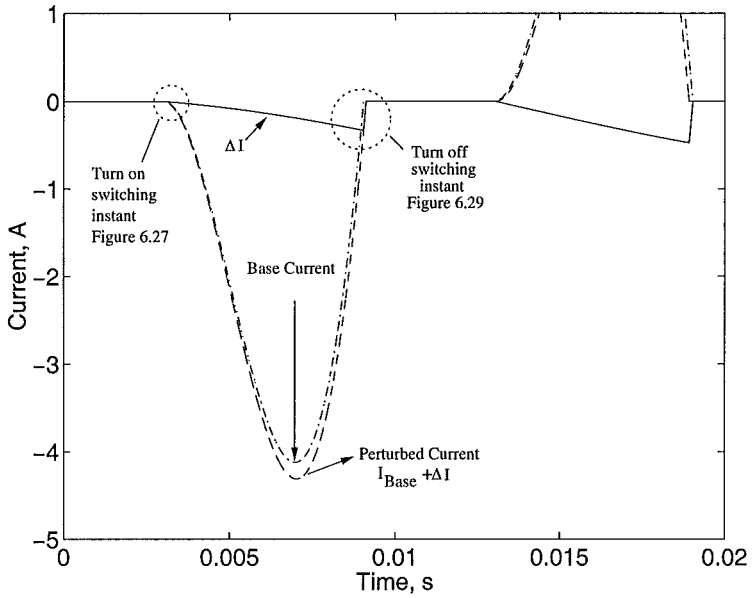

Figure 6.26 Currents during the conduction period of the single-phase rectifier. Dot-dashed line represents base case current, dashed line perturbed current and solid line ΔI

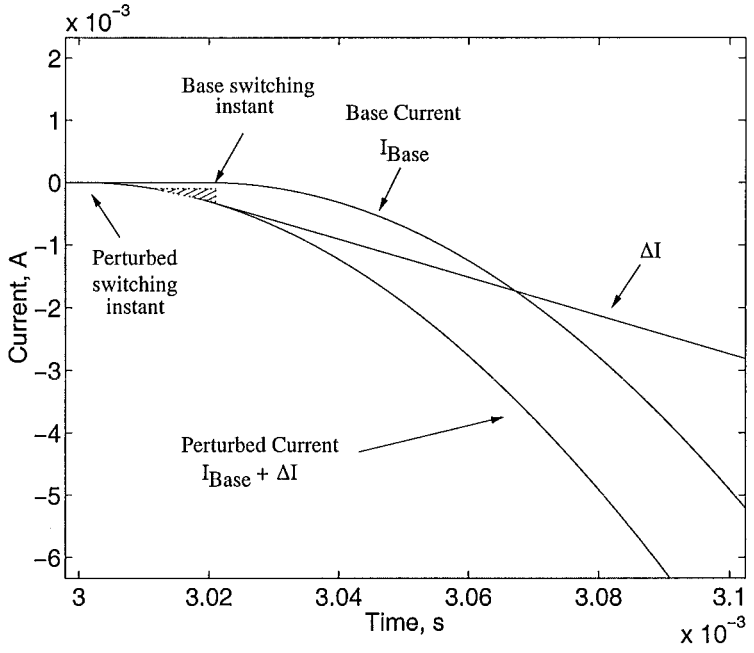

Figure 6.27 Current variation when front switching instant varies. Shaded area shows the change in the current due to the switching instant variation. This area has a second order relationship to the applied voltage distortion.

shows how a voltage perturbation can change the current during the base switching period. The switching instant modulation generates the correct amount of voltage-time integral to return the current to zero. (This is the method described to return the current to zero in the voltage partition description of the rectifier in section 6.3.3.) The current at the beginning of the turn off switching instant, which is proportional to the integral of the perturbing voltage, determines the variation of the switching instant variation. Obviously if the current is zero there is no switching instant variation and if the current is large then the switching instant variation is also large. Therefore the current waveform for rear switching instant variation, Figure 6.28(e), has a width that is proportional to its height. This means that once again the result is second order with frequency components arising at zero frequency and twice the frequency of the switching variation. The magnitude of this second order effect is once again considerably smaller than that of first order effects such as the transfer from the base switching.

By re-examining the current waveforms of Figure 6.5.6 it is apparent that the turn on switching instant effect is negligibly small compared to the current due to the base switching. The same conclusion can be drawn from the turn off switching instant modulation effect. This means that it is not necessary to include the effects of the switching instant variation in order to determine a linear first order FTM model of the single-phase rectifier.

In summary, the effects of the switching instant modulation on the currents in

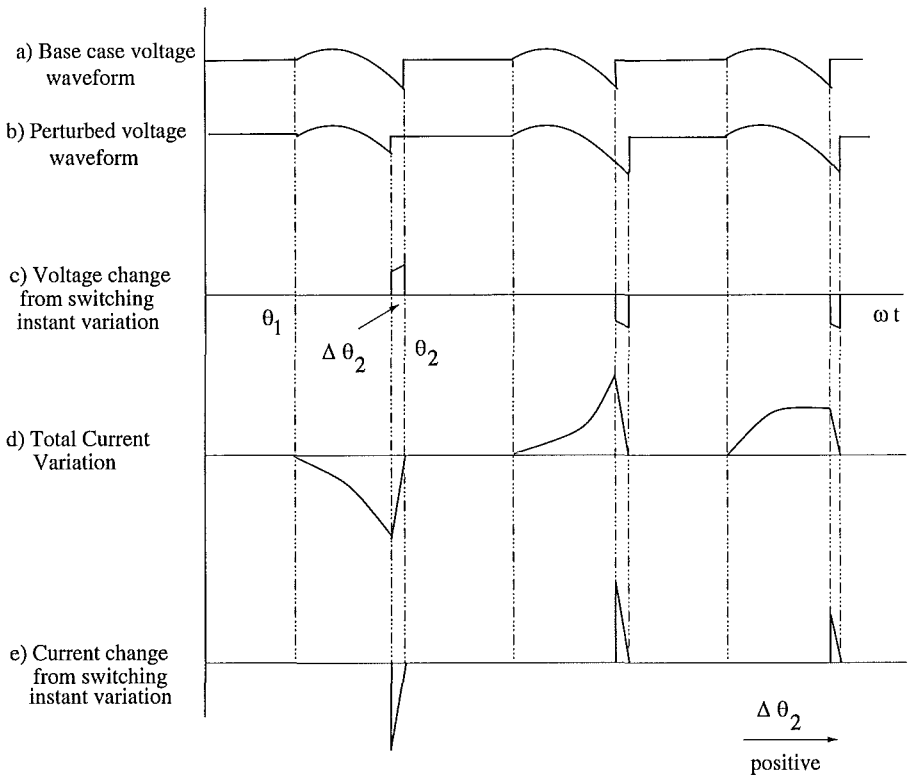

Figure 6.28 Effect on current of modulating the turn off switching instant.

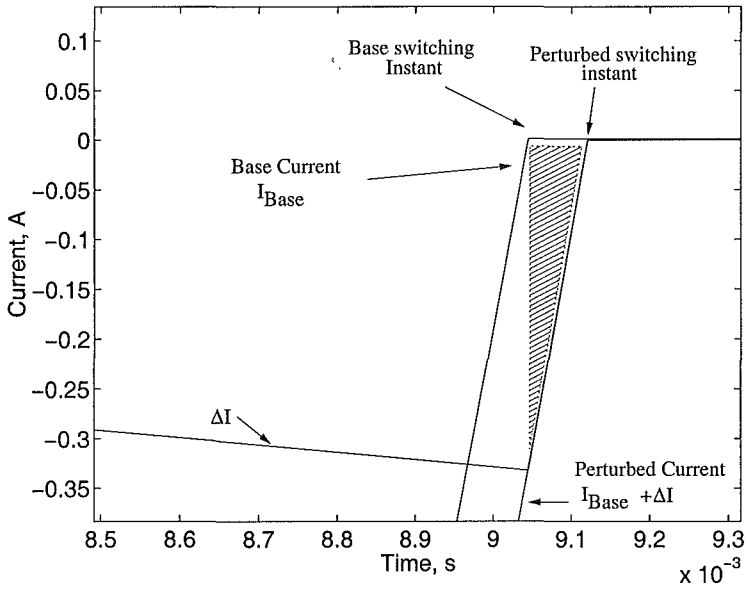

Figure 6.29 Current waveforms when rear switching instant varies. Shaded area is triangular showing that rear switching instant variation has a second order effect.

the single-phase rectifier are second order by nature. This means that the magnitude of the effect is considerably smaller, to the point of being negligible, than that due to the base switching transfer. The effect of the turn on switching modulation is a negligible second order pulse amplitude modulated waveform added to the current. The turn off switching modulation makes the current return to zero ensuring discontinuous conduction and so the current waveform that results has a width proportional to its height and is therefore also a second order effect. These second order effects will be noticable if large perturbations are applied but for suitably small signals the transfers to these second order frequencies will be small. The validity or otherwise of ignoring the switching instant modulation transfers can be seen by comparing time domain simulation results to those from the analysis.

6.6 VALIDATION OF TRANSFERS FROM VOLTAGE TO CURRENT WITH SIMULATION

In order to verify the accuracy and validity of the analysis a rectifier simulation is used. This simulation is implemented using MATLAB/Simulink. Time domain waveforms of a number of test cases are generated with the simulation. An FFT of the waveform is then compared to the spectrum generated by the analysis encoded into FTM form. See Appendix D for the method of encoding the Fourier series into FTM form.

6.6.1 ΔV_{AC} to ΔI_{DC} - The C transfer

The FTM representing the transfer from the AC side voltage to the DC side current is constructed as per Table 6.1. The FTM bandwidth is chosen to be 2500Hz. Two examples, each with different frequency input voltage, of the accuracy of the analysis for this transfer are given in the following pages. Similar examples for the three other transfers, $\mathbf{A} = \Delta V_{AC}$ to ΔI_{AC}, $\mathbf{B} = \Delta V_{DC}$ to ΔI_{AC} and $\mathbf{D} = \Delta V_{DC}$ to ΔI_{DC}, are in Appendix E. Figure 6.30(a) shows the DC side current waveform that flows in the rectifier when a zero frequency voltage with magnitude of 0.5 V is added to the base case fundamental voltage. The current waveform synthesised from the FTM spectra is shown in Figure 6.30(b) and a more detailed view of the two waveforms is shown in Figure 6.30(c). The waveforms are the same except for the higher frequency differences caused by the limited FTM bandwidth.

The magnitude of the spectrum of the time domain waveform is shown in Figure 6.31(a) while Figure 6.31(b) shows the spectrum from the FTM. The detailed comparison of Figures 6.31(c) (magnitude) and 6.31(d) (phase) shows the accuracy of the analysis and so the appropriateness of ignoring the switching instant modulation. In the spectrum of the simulated current it is apparent that there are components at 100Hz, 200Hz and the continuing even harmonics of the fundamental frequency. These

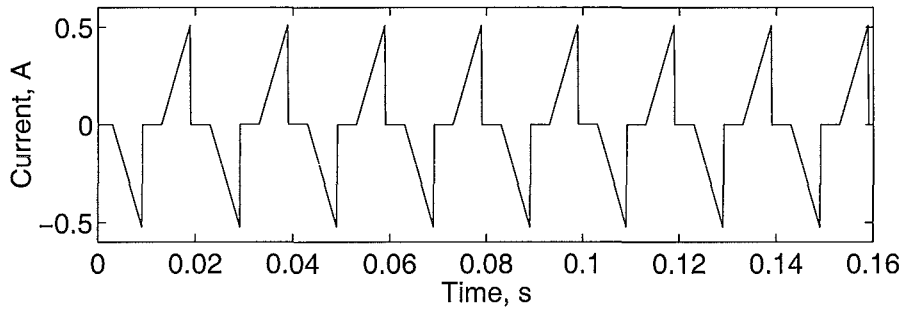

(a) Time domain simulation waveform

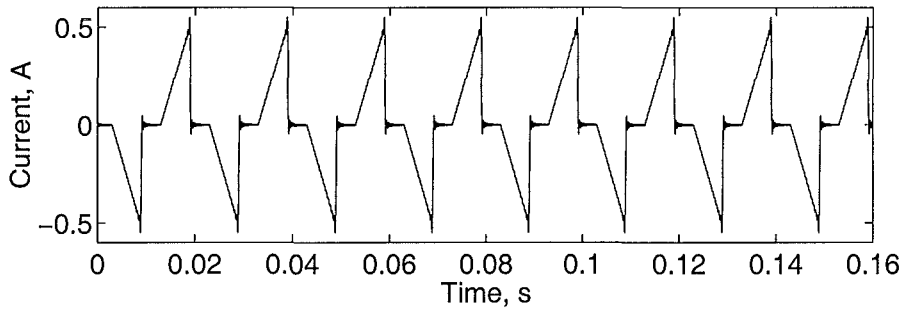

(b) FTM synthesised waveform (FTM bandwidth 2500Hz)

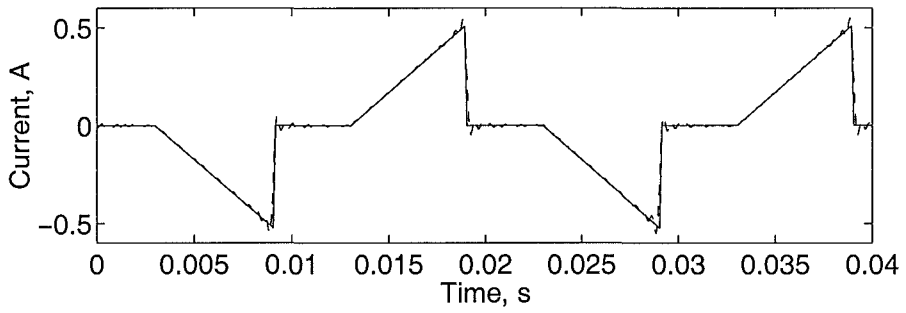

(c) Zoom on time domain (solid line) and FTM waveform (dashed line) (FTM bandwidth 2500Hz)

Figure 6.30 Current waveforms for ΔV_{AC} to ΔI_{DC} transfers for $kf_0 = 0$ Hz.

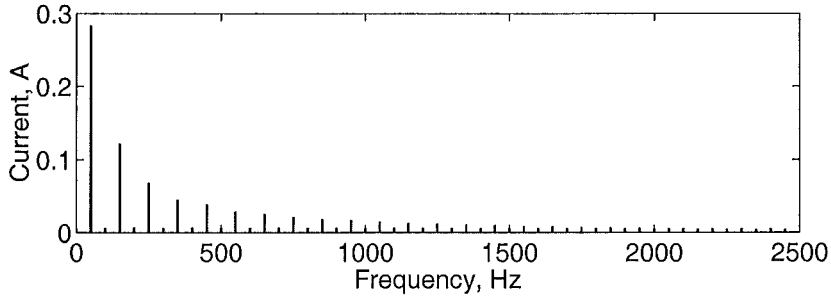

(a) Spectrum from time domain simulation (magnitude)

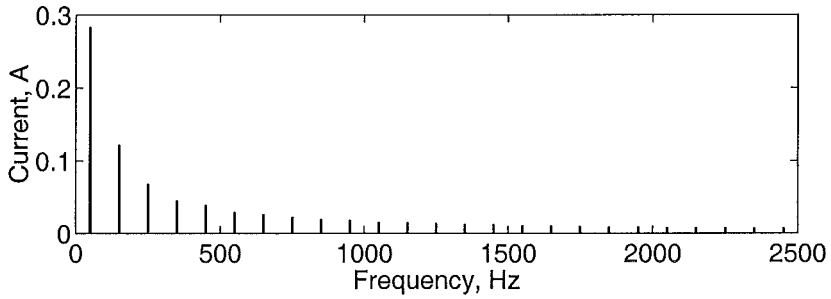

(b) FTM Spectrum (Magnitude)

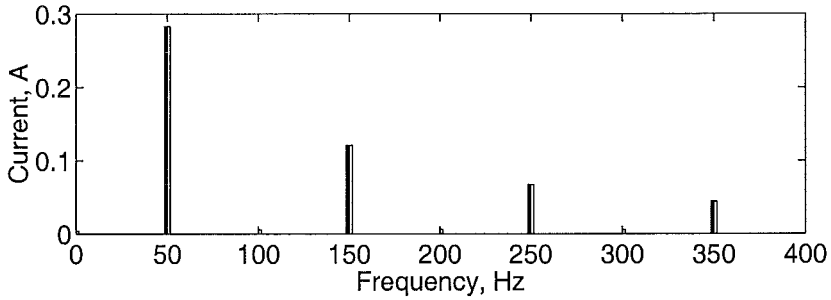

(c) Detailed comparison of magnitudes (Dark bars represent FTM, light bars time domain simulation)

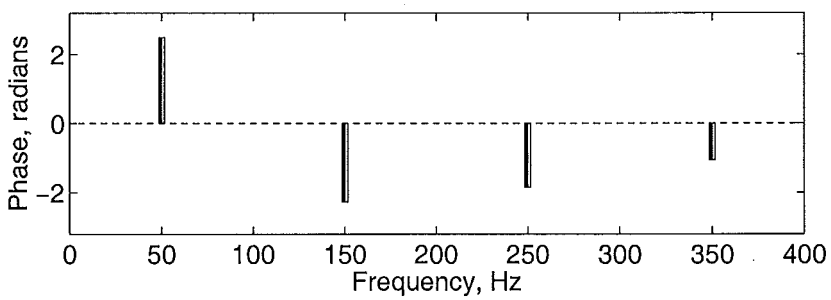

(d) Detailed comparison of phases (Dark bars represent FTM, light bars time domain simulation)

Figure 6.31 Spectra of current for ΔV_{AC} to ΔI_{DC} transfers for $kf_0 = 0$ Hz.

are the frequencies at which second order effects would be expected. However the appearance of these components is not entirely due to the second order effects because the simulation has fixed time step. This is done to allow the processing of the simulation results with an FFT. The fixed time step means that the effect of the switching instant modulation is amplified as the possible switching times are quantised. This means that the current cannot go to zero when required if the actual turn off time does not coincide with the discrete time and so the current typically is not exactly zero at the turn off switching instant. This leads to a non zero offset in the simulation current when it is supposed to be zero. Since the rectifier switches at 100Hz the time quantisation effect appears as the 100Hz, 200Hz and continuing even harmonic effect. This is not to say that there are not second order effects, or zero order effects due to the bessel function of kind zero in equation (6.3), occurring but the magnitude of these effects suggested by the switching instant spectrum equation (6.3) is smaller than those shown in Figure 6.31(a). The existence of the same even harmonic frequency components in Figure 6.33(c) where the expected second order effects are not apparent reinforces the conclusion that these effects are due, in part, to the time quantisation in the simulation. Investigation showed that this time quantisation effect dominates simulation results if the applied perturbation voltages are very small. As the perturbation size is increased the relative magnitude of the quantisation effect becomes less and the true second order effects are more noticeable.

When a voltage of 0.5V with frequency of 18.75Hz is applied, the simulated DC side current waveform is shown in Figure 6.32(a). The FTM result is shown in Figure 6.32(b) and the detailed comparison is shown in Figure 6.32(c). The match is good. The magnitude of the spectra of the current from the simulation is shown in Figure 6.33(a). Figure 6.32(b) shows that same current synthesised from the FTM. Detailed low frequency spectral comparison is shown in Figures 6.33(c) and 6.32(c) for magnitude and phase respectively. Again the match is excellent with the difference between the two results being less than 2%. Similar waveforms and spectrum showing the ΔV_{AC} to ΔI_{AC} (or $\mathbf{A}$) transfer, the ΔV_{DC} to ΔI_{AC} (or $\mathbf{B}$) transfer, and the ΔV_{DC} to ΔI_{DC} (or $\mathbf{D}$) transfer are included in Appendix E.

The individual transfers that are shown to be accurate in this section and in Appendix E can be combined to realise the total device transfer.

6.7 TOTAL SINGLE-PHASE RECTIFIER TRANSFER

Each of the FTMs in (6.5) is of the form of an admittance since current is the result of voltage being multiplied by a constant. The effect of the DC side RC filter is incorporated by adding its admittance (which is classically linear in that when a single-frequency is applied only that same frequency appears in its response) to the DC side transfer $\mathbf{D}$ so that $\mathbf{D}' = \mathbf{D} + \mathbf{Y}_{\mathbf{DCFilter}}$. The total transfer of the AC side

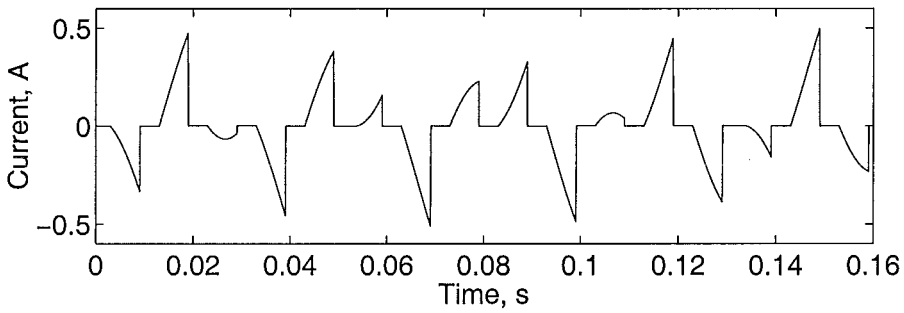

(a) Time domain simulation waveform

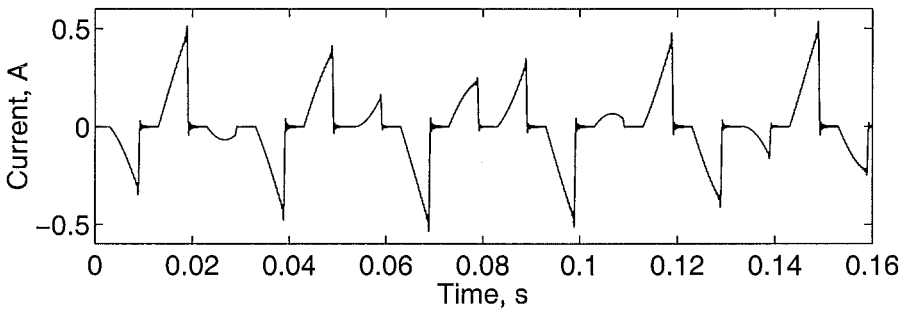

(b) FTM synthesised waveform (FTM bandwidth 2500Hz)

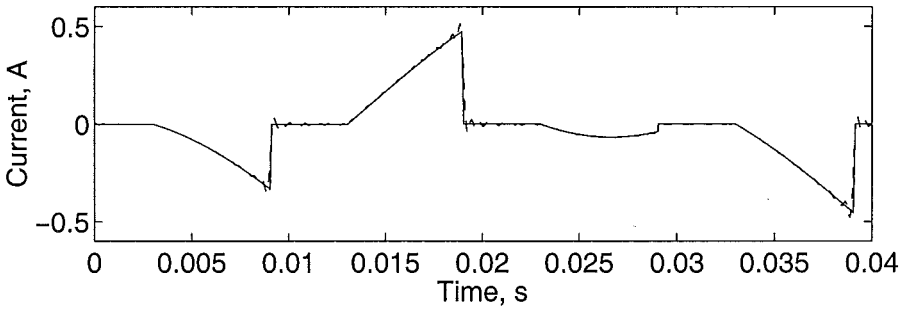

(c) Zoom on time domain (solid line) and FTM waveform (dashed line) (FTM bandwidth 2500Hz)

Figure 6.32 Current waveforms for ΔV_{AC} to ΔI_{DC} transfer for $kf_0 = 18.75$ Hz.

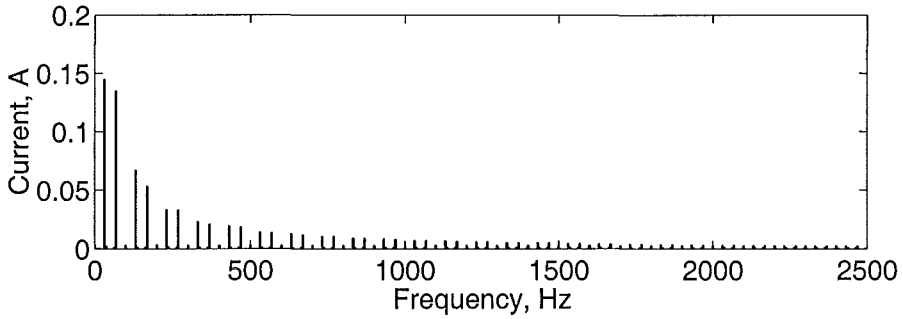

(a) Spectrum from time domain simulation (magnitude)

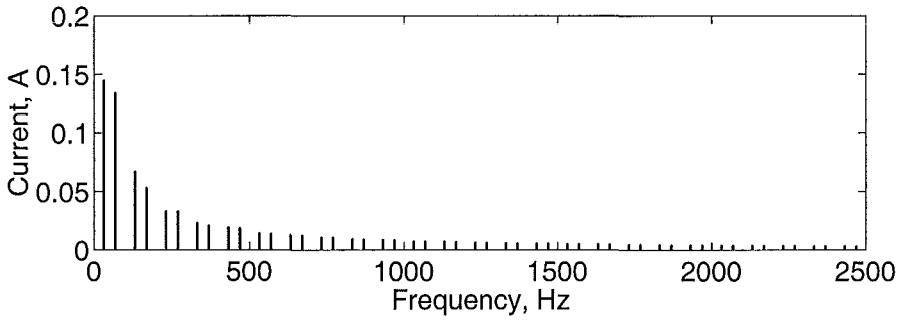

(b) FTM Spectrum (magnitude)

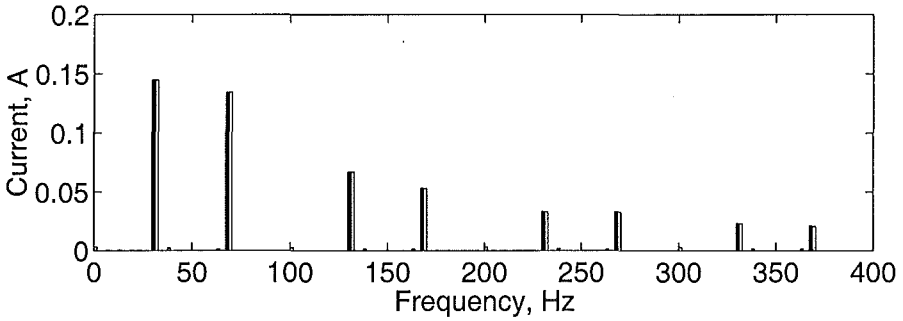

(c) Detailed comparison of magnitudes (Dark bars FTM, light bars time domain simulation)

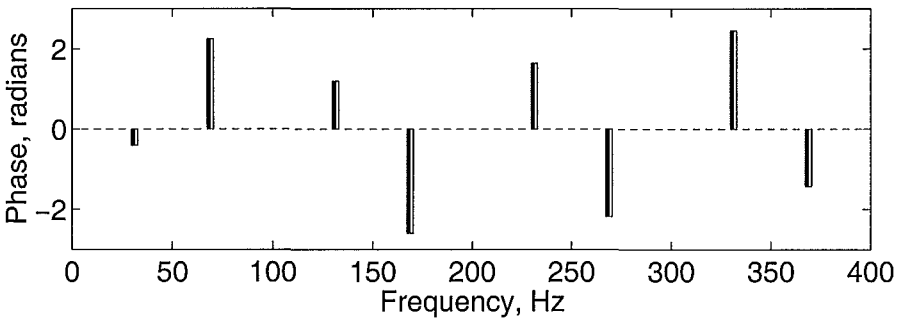

(d) Detailed comparison of phases (Dark bars FTM, light bars time domain simulation)

Figure 6.33 Spectra of current for ΔV_{AC} to ΔI_{DC} transfer for kf_0 18.75 Hz.

voltage ΔV_{AC} to the AC current is given by eliminating ΔI_{DC} and ΔV_{DC} to give (6.54) [Smith *et al.* 1998].

$$\Delta I_{AC} = (\mathbf{A} - \mathbf{B}\mathbf{D'}^{-1}\mathbf{C})\Delta V_{AC} \tag{6.54}$$

The total transfer is the single-phase rectifier admittance in FTM form, Y_{Load}.

$$Y_{Load} = \mathbf{A} - \mathbf{B}\mathbf{D'}^{-1}\mathbf{C} \tag{6.55}$$

This transfer matrix completely characterises the first order effects that occur in the single-phase rectifier and so can be used to accurately represent the voltage to current transfer behaviour of the rectifier.

6.7.1 Confirmation of transfer by time domain simulation

The behaviour and characteristics of the complete analytic model of the single-phase rectifier are compared to time domain simulation results from PSCAD-EMTDC. The power system simulation package PSCAD-EMTDC provides fixed step time domain simulation base on trapezoidal integration [Dommel 1969]. A small voltage perturbation is added to the fundamental voltage source as previously shown at the start of this chapter in Figure 6.1. The DC side filter has an inductor L = 5.8mH, capacitor C= 2000 μF and a resistor R=100Ω. Appendix F gives the PSCAD-EMTDC circuit used in the simulation.

Figure 6.34(a) shows the 6.25Hz perturbing voltage waveform (the dashed sinusoid), the current from the time domain simulation (solid line) and the current from synthesis of the analytic model FTM (dashed line). The excellent accuracy of the analytic model makes it very difficult to notice any difference in the time domain waveforms. A similar comparison for a 12.5Hz voltage perturbation (the dashed sinusoid) is shown in Figure 6.34(b). Once again the accuracy is excellent. The magnitude and phase of the spectrums of both the analytic (dark bars) and the simulated (light bars) in Figures 6.34(c) and 6.34(d) reinforce the accuracy of the approach with the magnitudes matching to approximately 4% and the phase well inside a 10% error.

Figure 6.35(a) shows the magnitude of the ratio of the current to the voltage for both the analytic model (solid line) and the simulation (dashed line). This single-input single-output (SISO) transfer is the ratio of the rectifier current at the same frequency as the applied voltage perturbation. It is used to show that the analytic model and the simulation match. Figure 6.35(b) shows the phase of the SISO transfer from voltage to current. The match is excellent with the two phase plots indistinguishable and the magnitude having a small error of less than 5% at low frequencies. The match is excellent even at the frequencies where magnitude-phase dependence is apparent. This can be clearly seen in at 100Hz in Figure 6.35(a) where the *spike* shape is not due to an

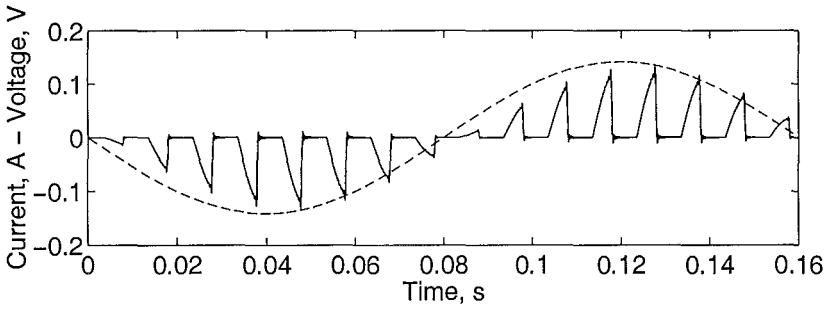

(a) Single-phase rectifier current (solid and dotted lines) for 6.25Hz voltage perturbation (dotted sinusoid).

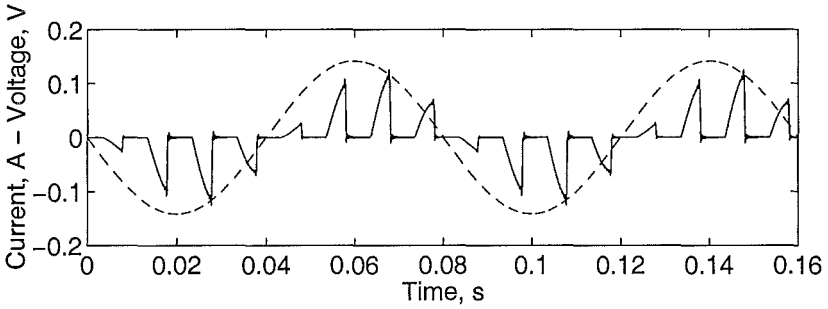

(b) Single-phase rectifier current (solid and dotted lines) for 12.5Hz voltage perturbation (dotted sinusoid).

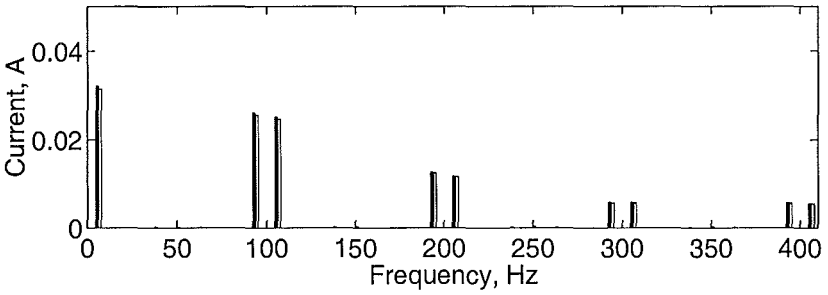

(c) Rectifier current magnitude spectra (Analytic dark bars, simulated light bars).

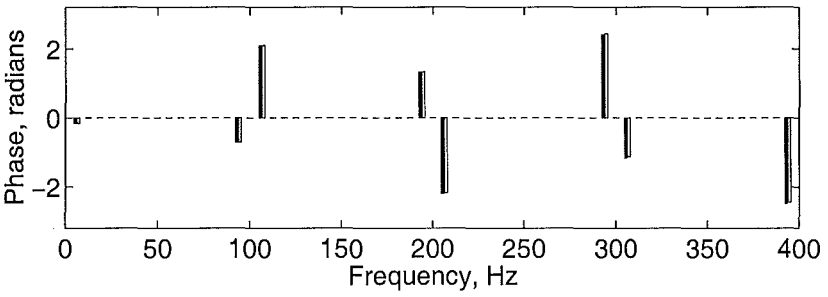

(d) Rectifier current spectral phases (Analytic dark bars, simulated light bars).

Figure 6.34 Confirmation of accuracy of complete model by comparison to PSCAD-EMTDC simulation.

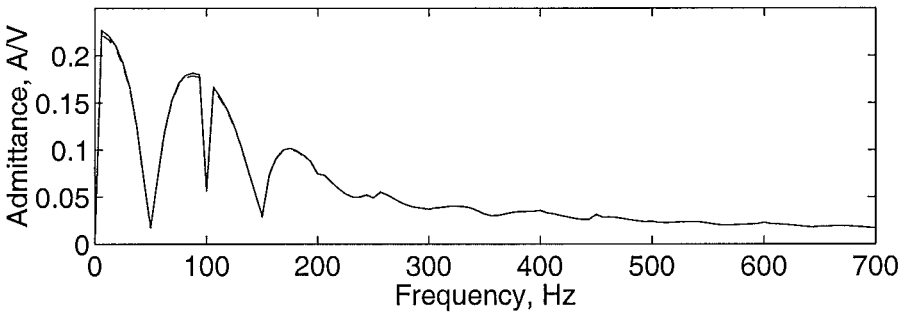

(a) SISO match magnitude.

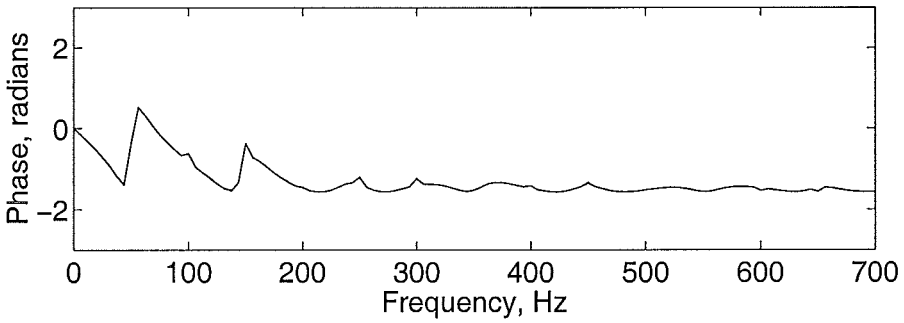

(b) SISO match phase.

Figure 6.35 Single frequency transfer confirmation of accuracy of complete model. (Dotted line - simulation, solid line analytic.)

extremely high Q resonance but is due to magnitude-phase dependence and the limited frequency resolution (6.25Hz) of the data.

6.8 SUMMARY

A complete, highly accurate, small-signal frequency domain model of a single-phase rectifier is developed. Rectifier operation is divided into the base case and the response to a small-signal perturbation. This small-signal response is determined because it provides information on the sensitivity of the rectifier.

A switching function approach is used to describe the way the AC and DC side are connected. Two mechanisms were initially identified as having effects in the rectifier. These are the transfer due to the base switching and that due to the switching instant modulation. The base switching transfers are developed by choosing a voltage input to current output model of the rectifier. This model is suitable as it can enforce the zero current on the AC and DC sides when the circuits external to the rectifier are arbitrary. By combining the pseudo steady state current, the base switching and a suitable pulse amplitude modulated waveform the FTM for the AC side voltage perturbation to DC side current response is constructed. Transfers for the other FTMs are constructed in the same manner.

The transfers due to the switching instant modulation are analysed by first generating suitable linearisations for the switching instant variation caused by the applied perturbation. These are shown to be accurate by comparison to time domain simulation. The effect of the switching instant variation on the model output current is then developed. This effect was found to be second order so its magnitude is negligible when compared to first order effects such as the base switching transfer. This means that the switching instant effect can be ignored in the single-phase rectifier model.

Each individual analytic transfer, or partial differential, is compared to the transfer from time domain simulation and all are found to be accurate. By combining the FTMs into a total system sensitivity matrix the total transfer for the single-phase rectifier is developed. This total transfer was compared to time domain simulation results from PSCAD-EMTDC. The resulting wave form and spectral comparisons show high accuracy in the combined analytic FTM model. A same frequency single-input single-output comparison of the voltage to current transfer also shows good accuracy. The SISO transfer is equivalent to the describing function of the response.

Overall, the FTM model of the single-phase rectifier shows a high level of accuracy. This shows the effectiveness and appropriateness of the partial differential approach of generating each transfer in isolation then combining them. The accuracy of the total transfer shows that the single-phase rectifier can be effectively accurately and perhaps most importantly linearly represented by FTM in the frequency domain without loosing any of the device characteristics. This means that including the characteristics of

the single-phase rectifier into a power system can be achieved by solving a single linear matrix equation. Such a method provides a convenient and fast way to analyse power conditioner systems where the loads are non-linear rectifiers like the single-phase rectifier. In the next chapter the experimental system is used to make measurements to confirm that the FTM model is a suitable and accurate way to model the single-phase rectifier.

Chapter 7

EXPERIMENTAL MEASUREMENTS AND SHUNT ACTIVE FILTER OPERATION

7.1 INTRODUCTION

The installation and use of shunt active filters and other power conditioners is becoming more common. Their use is increasing principally in order to manage the power quality of the AC system. This power quality is becoming more important as the number of sensitive, usually non-linear loads, that are connected increases. The AC system that results is one that is increasingly less like a single frequency power transfer network and more like a system of interconnected linear and non-linear load devices, generators, transmission and power conditioners. With the increase in their numbers the effects that non-linear loads and power conditioner devices have on the power system are becoming important. This is compounded by the deregulation of power systems around the world and the shift in emphasis from building infrastructure to an environment where the expansion of generation, transmission and distribution networks is difficult. As a result of this, it is necessary to control the power system to increase the power flow without increasing the installed transmission or distribution capacity.

The single-phase rectifier is a very common non-linear load. In order to determine its behaviour when connected to the AC system and also to some form of power conditioner the previous chapter developed a theoretical analytic model and showed that the model is accurate with comparison to time domain simulation. This chapter presents experimental results with measurements of a single-phase rectifier taken using the DSP based system previously described in Chapter 4. These measurements are made to confirm the accuracy of the analysis of Chapter 6.

A number of SAF systems are based on digital or microprocessor based controllers. This means the experimental system in Chapter 4 is typical of a SAF apart from having perhaps larger RAM memory and more processing power. The ability to make reasonable measurements to confirm the analysis with a relatively simple sensor system shows the possibilities for perhaps utilising power conditioners in measurements and perhaps even in control adaptation or design.

7.2 EXPERIMENTAL SYSTEM OPERATION

The experimental setup to take measurements is shown in Figure 7.1. The AC supply voltage V_S connects through the system impedance Z_{Sys} to the rectifier load and the SAF converter. The SAF system measures the load current and can make the current necessary to perform active filtering, I_{AF} and the perturbing current I_{inj}. The base rectifier load current is I_L and the small signal change caused by the perturbation is ΔI_L. The DC side filter of the rectifier has the typical inductor/capacitor/resistor filter.

The initial proposed method of measuring the load characteristics was to determine the change in the load current, ΔI_L, for a change in the terminal voltage ΔV_{AC} as was used in the simulation confirmation of the total analytic model in section 6.7.1. However as the SAF converter system is shunt connected it is difficult to create a current injection I_{Inj} that produces a single frequency ΔV_{AC}. This single frequency perturbation is desirable because it then makes the measurement a single-frequency input to multiple-frequency output. It is intuitively difficult to deal with a multiple frequency to multiple frequency transfer. When a single frequency current is injected and the voltage is measured, the voltage is a signal with a number of frequency components. Some of these voltage frequency components result from the load current change, ΔI_L, flowing in the system impedance and so they are the product of a small signal with a small impedance. This makes them difficult to measure accurately as they fall below the noise floor of the measurement equipment. Therefore the experimental system measures the transfer from the injected current to the change in the load current. This ensures that the input, the injected current, has only one frequency and the output is large enough to be relatively easily measured.

To make the measurements a number of current perturbations at different frequencies and phases are injected successively and the load current in each case is measured after the system has come to steady state. After each measurement with a perturbation a measurement without a perturbation is made. This means that each measurement has a base case that was taken at almost exactly the same time. The system switching converter is operated as a controlled current source switching at a frequency significantly higher (approximately 10kHz) relative to the perturbing or SAF currents that are typically below 1kHz. The system can be operated as a shunt active filter and can inject a perturbing current while doing so. It can also be operated solely as a perturbing current source. It is therefore possible to determine the effects of the perturbation on the rectifier and also the effect of the perturbation on the rectifier when the SAF operates. Initial measurements are for the case where the SAF does not operate.

During base case operation, which means zero perturbing current, the switching converter is run to maintain the AF bus voltage. Running the switching converter when the base case is measured ensures that the operating point does not change between

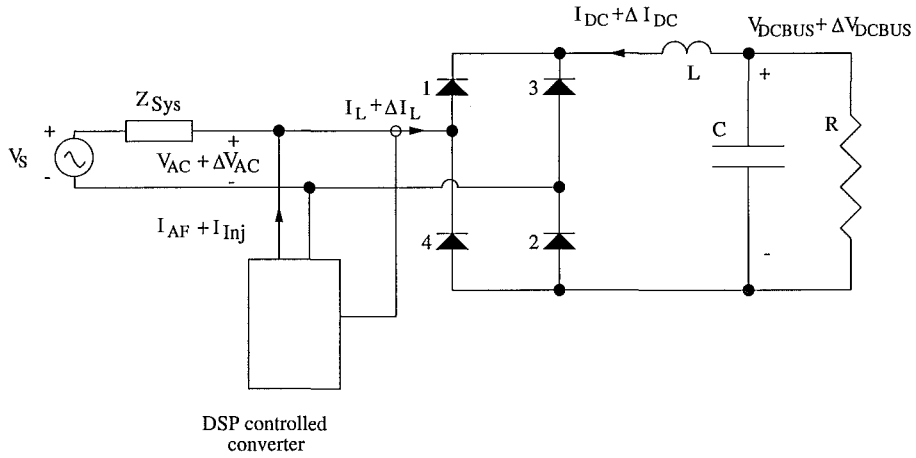

Figure 7.1 Experimental system schematic diagram.

the perturbed case and the base case. Each measurement is collected and uploaded to the PC for post-processing with MATLAB. The inter measurement accuracy of the system is in the order of five percent. That is the result of two measurements made successively of the same situation can have a difference of a maximum of five percent.

7.2.1 Measurement results example

Confirmation of the analytic and simulation results and other measurements is performed by measuring the injected current to load current transfer. The experimental system is connected to a single-phase rectifier load and the converter system generates successive single frequency constant amplitude current injections. Figure 7.2(a) shows the perturbed single-phase rectifier current waveform, $I_L + \Delta I_L$, measured by the experimental system. Figure 7.2(b) shows the base case single-phase rectifier current, I_L. As the system is not performing shunt active filtering the measurement is for the rectifier/AC system combination only.

The single-phase rectifier current has the typical peaked discontinuous shape that is expected. The controlled converter is made to produce a single frequency current injection at 25Hz with magnitude 0.365Amps. Figure 7.2(a) shows the perturbed rectifier current. The difference between the perturbed and base case current is noticeable and measurable and is shown in Figure 7.2(c). The waveform has significant noise present but the shape can be appreciated and its frequency components can be found with an FFT. In processing the results the FFT is performed on the total perturbed waveform, Figure 7.2(a), rather than on the difference waveform of Figure 7.2(c). This reduces the noise present in the signal as it is unlikely that the noise is correlated between the two measurements. The base harmonic currents are present in the resulting FFT but so long as the perturbation is not at a harmonic frequency then these base harmonics will be constant. This allows the separation of the small signal response case from

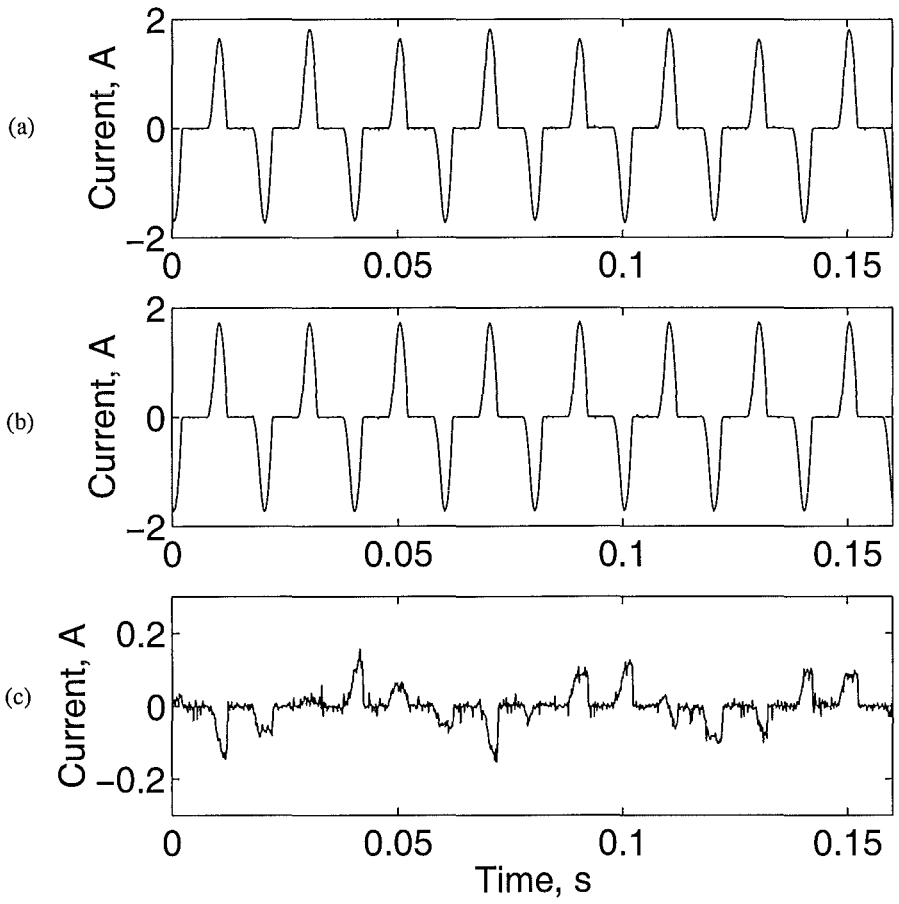

Figure 7.2 Example experimental current waveforms for the single-phase rectifier when I_{Inj} is 25Hz. (a) Perturbed rectifier current $I_L + \Delta I_L$. (b) Unperturbed base rectifier current I_L. (c) ΔI_L difference between (a) and (b).

the base case by simply nulling the fundamental frequency harmonic components of the FFT of the perturbed current (Figure 7.2(a)). This is not possible for harmonic current perturbations in which case the FFT of the change in the current ΔI_L is used. This means that the measurements at harmonic frequencies are perhaps more noisy than those at non-harmonic frequencies.

7.3 THE SINGLE-PHASE RECTIFIER RESPONSE - COMPARISON TO THEORETICAL PREDICTIONS

The experimental system block diagram is shown in Figure 7.3. Analysis is made using standard feedback loop analysis taking care of the order of the matrix operations (See Appendix H for the mathematical working). The small perturbation input I_{Inj} is used to determine the transfer. The transfer from input I_{Inj} to the measured change in the output load current ΔI_L is given by (7.1) where **I** is the identity matrix.

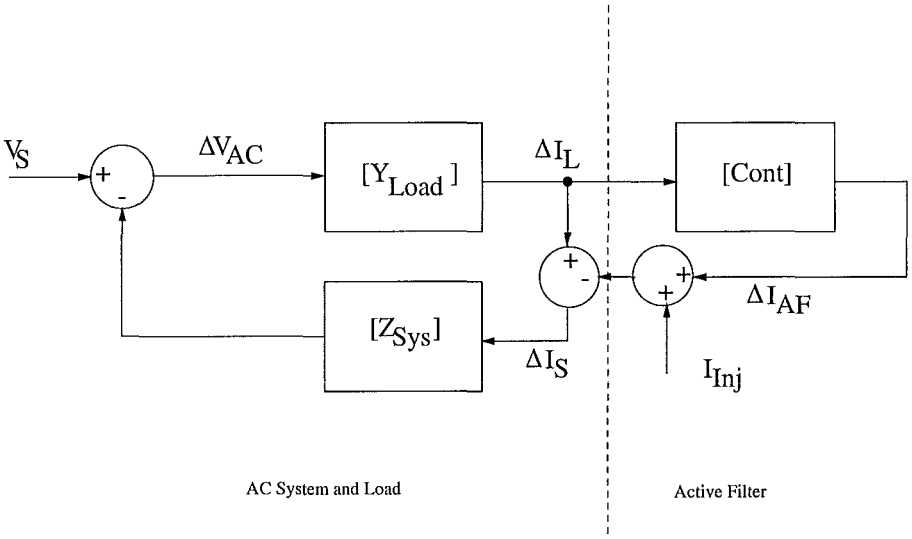

Figure 7.3 Experimental system block diagram showing injected current $Iinj$ and the resulting changes marked with Δ.

$$\Delta I_L = [\mathbf{Y_{Load}}][\mathbf{Z_{Sys}}]\,[\mathbf{I} + [\mathbf{I} - \mathbf{Cont}][\mathbf{Y_{Load}}][\mathbf{Z_{Sys}}]]^{-1}\, I_{Inj} \tag{7.1}$$

The component parts of the total system are represented with an FTM. These FTMs are substitued into (7.1) to give the total transfer. The required FTMs are the AC system, the power converter and the controller and that for the load.

7.3.1 AC system FTM

The total AC system is a large interconnected network made up of generators, transmission lines and transformers. The AC system impedance that results from these components is linear and time invariant in the short term. It is true that the AC system can vary in both topology and character as component parts are switched but these variations are assumed to occur at frequencies lower than those used to make the measurements. Also there are components in the AC transmission system that are non-linear. These include the magnetising reactance of transformers, static VAr compensation systems and other non-linear loads. However the system impedance of AC systems is generally considered linear [Arrillaga *et al.* 1985]. In order to compare current-input current-output measurements against those predicted by the theory, equation (7.1), it is necessary to have an accurate estimate of the AC system impedance Z_{Sys}. Z_{Sys} is measured by removing the rectifier load and injecting a single frequency current. The voltage at the same frequency is measured and the ratio of the voltage and current is the system impedance or admittance. In order to remove the effect of noisy measurements a low order polynomial is fit to the data using a singular value decomposition [Todd *et al.* 1997]. The system impedance measured and used in this chapter is shown in Appendix G. The impedance is assumed to be constant throughout

the experiments described in this chapter.

7.3.2 Load, Power converter and SAF controller FTM

The single-phase rectifier load FTM [Y_{Load}], in (7.1), is given from the analysis in chapter 6. SAF power conditioner controllers, represented by the FTM [$Cont$] in (7.1), are all linear. The function of the power conditioner converter is to amplify the signal level output of the SAF control system to the required current level. It is typical to use a switching power converter to generate the required SAF current as switching converters have minimal power loss [Round 1992, Ingram and Round 1999]. Switching is a non-linear operation but in order to minimise the effects of the switching it is usual to switch at a high frequency and to minimise the size of the output inductors. The fast switching produces a switching frequency current ripple but the low pass effect of the output inductors ensures this ripple is small. A fast current control loop linearises the response from input current demand to the current output [Brod and Novotny 1985]. This means that so long as the bandwidth and slew rate limits of the converter are not exceeded the response is linear [Ingram and Round 1999] and can be represented as an FTM with unity gain.

7.3.3 Comparison of results

Previously the single-phase rectifier analytic model was shown to correctly predict the results of PSCAD-EMTDC time domain simulation (see section 6.7.1). Figure 7.4(upper - noisy red waveform) shows the experimental load current waveform, ΔI_L, measurements of the single-phase rectifier load with a current injection of 18.75Hz (Figure 7.4(lower)). Also shown (smooth blue line) is the current waveform predicted by equation (7.1) with the appropriate FTMs. While there are some differences between the two waveforms it can be seen that the experimental current is very much like the analytic current.

Figure 7.5(a)(upper) shows the load current change when the 200Hz sinewave current of the lower subfigure is injected. Once again both the measured (noisy red waveform) and the analytically produced waveforms (shown by the blue line) are shown. There is a good match between the measured and the analytic waveforms. When a cosine waveform, shown in Figure 7.5(b)(lower) is injected, the rectifier current waveform changes, having upward pulses rather than downward pulses as in Figure 7.5(a). The rectifier current's, ΔI_L, zero frequency (average) value in Figure 7.5(a) is negative while that Figure 7.5(b) is positive. This is the magnitude-phase dependent behaviour that was outlined in section 5.3.6.3. Its existence shows that the magnitude-phase dependence of the single-phase rectifier at harmonic frequencies is measurable and noticeable and that including it with the tensor representation produces an accurate model.

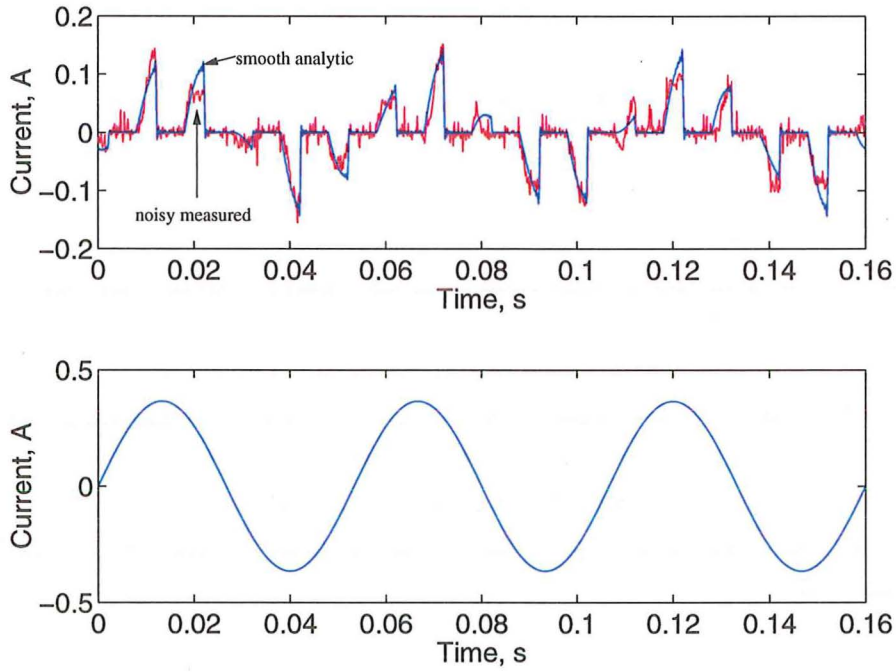

Figure 7.4 Rectifier current ΔI_L (Noisy red waveform (upper) represents measured current, smooth blue waveform (upper)- analytic current) and injected 18.75Hz current (lower).

Another example of the model effectiveness is shown by Figure 7.6 for an injected current of 31.75Hz. The noisy red measured current waveforms in Figure 7.6(a) show close resemblance to those from the model (shown by the smooth blue waveform).

The spectral comparisons shown in Figure 7.6(b) show that there is some difference between the measured current and the analytic model current. The difference in the magnitudes is in the order of 15%. This is probably caused by one or more of four effects. Firstly, the relatively large amount of noise present in the system due to the power electronic converter switching means that the uncertainty from one measurement to another is at times in the order of 5%. Secondly, the model is sensitive to base case operating point inaccuracies, especially in the turn off switching instant angle, θ_2. The operating point is determined from the experimental measurements and this data's sampled nature means that it is difficult to exactly gauge the turn on and turn off switching instants. The third effect is the variability of the AC system impedance, which is assumed to be constant but can change. The final possible area of uncertainty is the base case distortion of the AC supply voltage. Appendix G shows that the base case voltage has some harmonic distortion. When all these possible causes of error are considered the match is reasonably good. The phase of the spectrum, in Figure 7.6(b), shows that even with the effects of the noisy measurements, the inaccuracies of the AC system measurement and the unknowns of the base case the phase is generally accurate to within 1 radian. With better measurements the actual cause of the uncertainty will become apparent. It should be noted that as phase is continuous the wrapped phase

values at approximately 280Hz and 1230Hz are almost the same.

Figure 7.7 shows the load current spectrum for the injection of a 25Hz current. The accuracy in this measurement is higher than the previous spectrum, Figure 7.6(b), with the maximum magnitude error being approximately 5% and the absolute phase error consistently reaching 1 radian only at frequencies above approximately 800Hz. This higher accuracy is possibly the result of the inter measurement variation. Overall, the results presented in this section show that the analytic model correctly predicts the actual experimentally measured behaviour of the single-phase rectifier load. The waveforms of the rectifier current show good resemblance to those that the analytic model predicts. The spectral comparisons, which are a far more demanding test of the accuracy, also show good correlation between the experimental and the analytic model results. This accuracy shows the validity of the model and means that the model can be used to determine the behaviour of the rectifier in other situations. One such area is the forward transfer of a SAF.

7.3.4 Measured SISO transfer of single-phase rectifier load

It is difficult to gain an overall appreciation of the single-phase rectifier characteristics because the spectrum results, as shown in Figures 7.7 and Figures 7.6(b), are single input multiple output (SIMO). This SIMO type of transfer makes intuitive understanding of the device characteristics difficult and also prevents the transfer being used in a classical control analysis. It is common in non-linear system analysis to form the describing function of a device [Nagrath and Gopal 1982]. Describing functions retain only the signal that occurs at the same frequency as the applied signal. Typically a describing function depends on both the frequency and magnitude of the applied signal. In the case of the analytic model only first order effects are represented, meaning there is no magnitude dependence. Thus the describing function is the ratio of the load current's spectral component to the injected current at the same frequency. Magnitude-phase dependence cannot be accurately represented with a describing function system description because as the phase of the input changes the output magnitude changes.

Figure 7.8 shows the single-input single-output (SISO) describing function transfer for the single phase rectifier. The dashed line shows the measured result and the solid line the behaviour predicted by the model. The measured and analytic describing functions match well considering the possible error sources in the measurements. The magnitude error is less than 10% at frequencies below 200Hz. The error rises with increasing frequency reaching 50% at 900Hz. In order to ensure that the non-ideal behaviour of the DC filter components were not the cause of the difference these components were measured and their actual frequency characteristics used in the model. Very little difference in the analytic model results between the two representation of the DC filter components led to the use of the ideal component representation. The

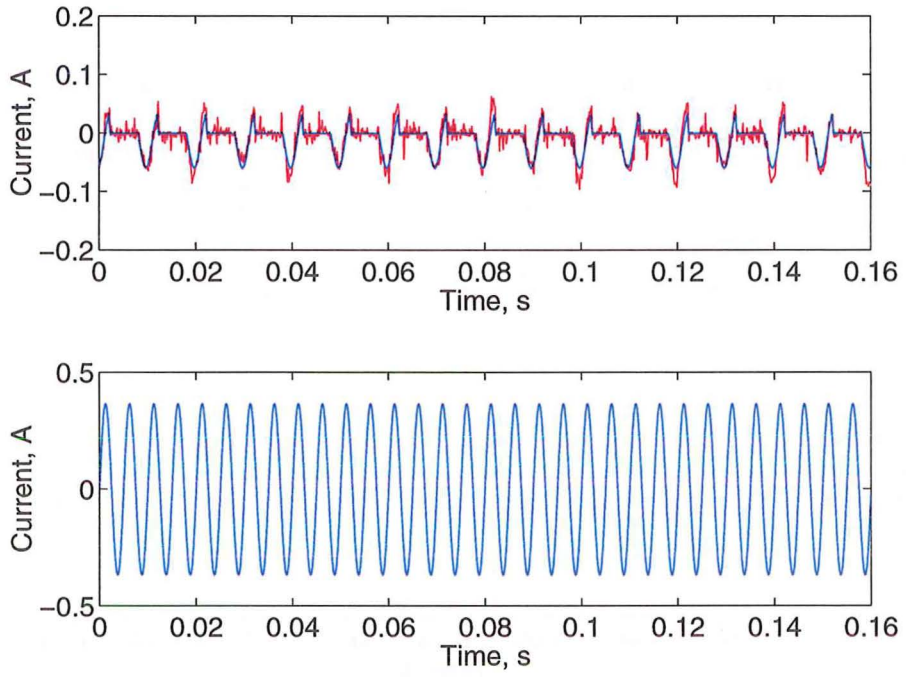

(a) Sinewave injected current.

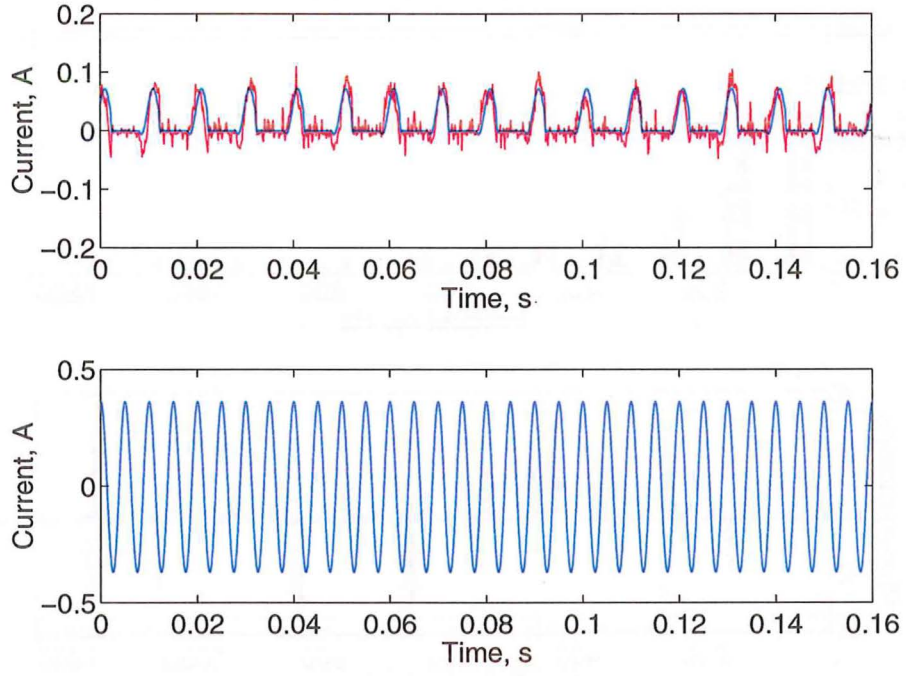

(b) Cosinewave injected current.

Figure 7.5 Load current ΔI_L (in upper subfigures noisy red represents measured and smooth blue represents analytic) and injected current (in lower subfigures) waveforms for 200Hz injected current sine (a) and cosine (b) waveforms at different phase.

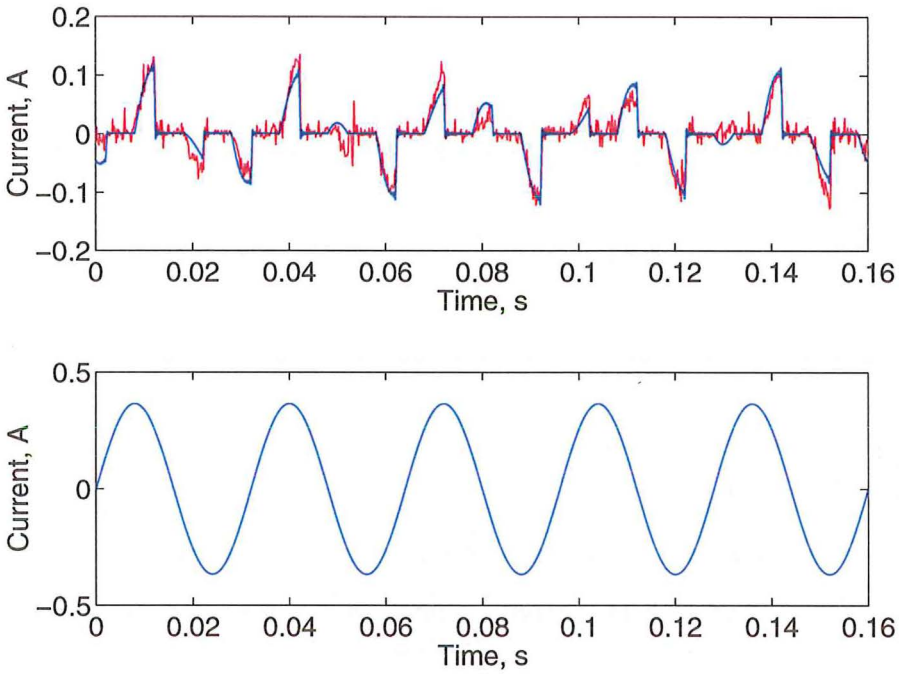

(a) Current waveforms. (Noisy red measured, smooth blue analytic model).

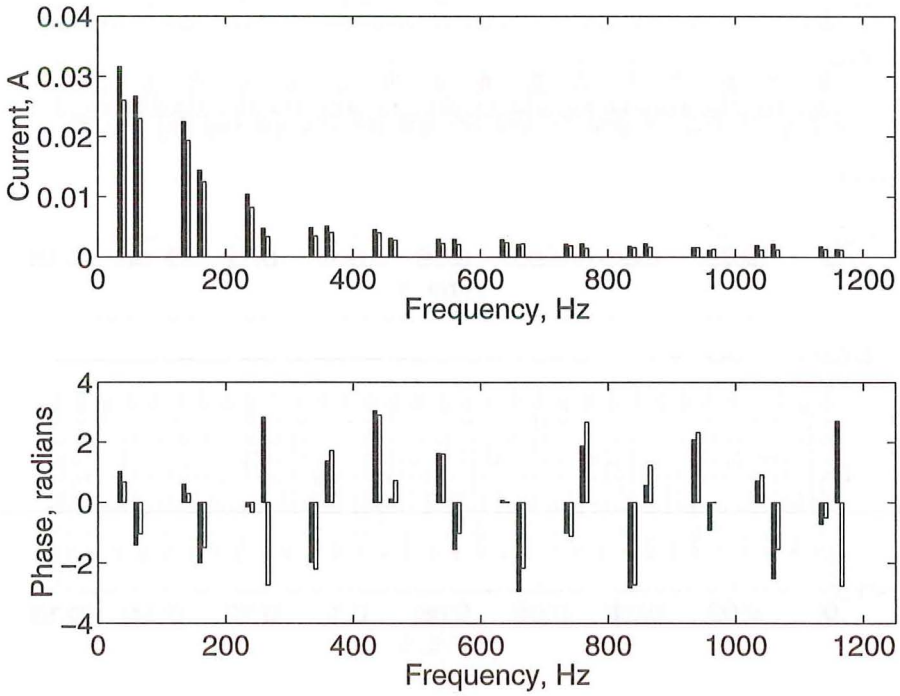

(b) Current spectra. (Dark bars measured, light bars analytic model)

Figure 7.6 Measured and analytic load currents for 31.75Hz injected perturbing current.

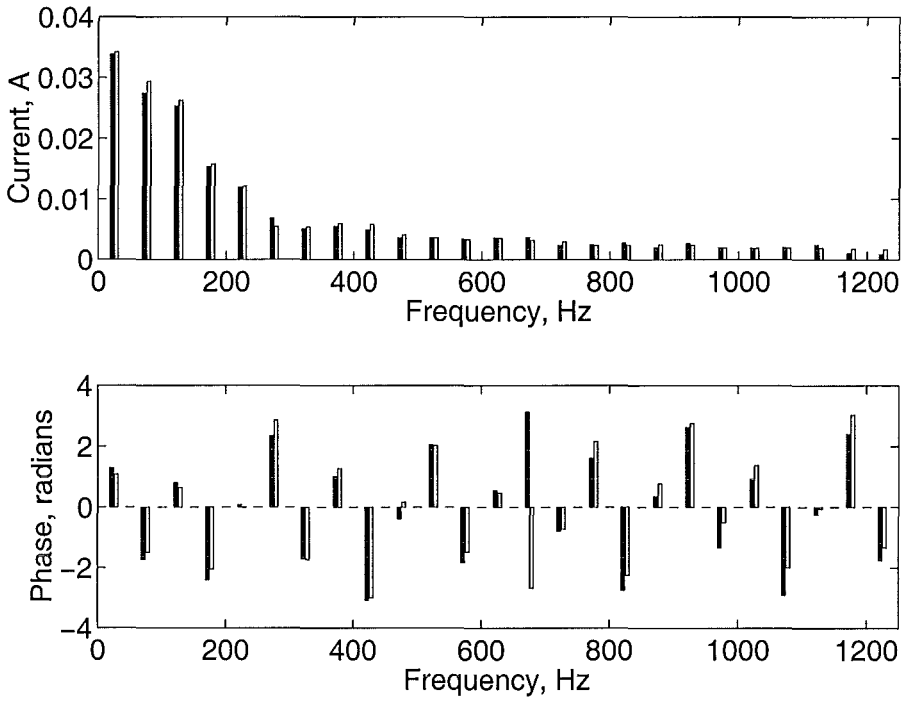

Figure 7.7 Spectrum of load current change for current injection of 25Hz.

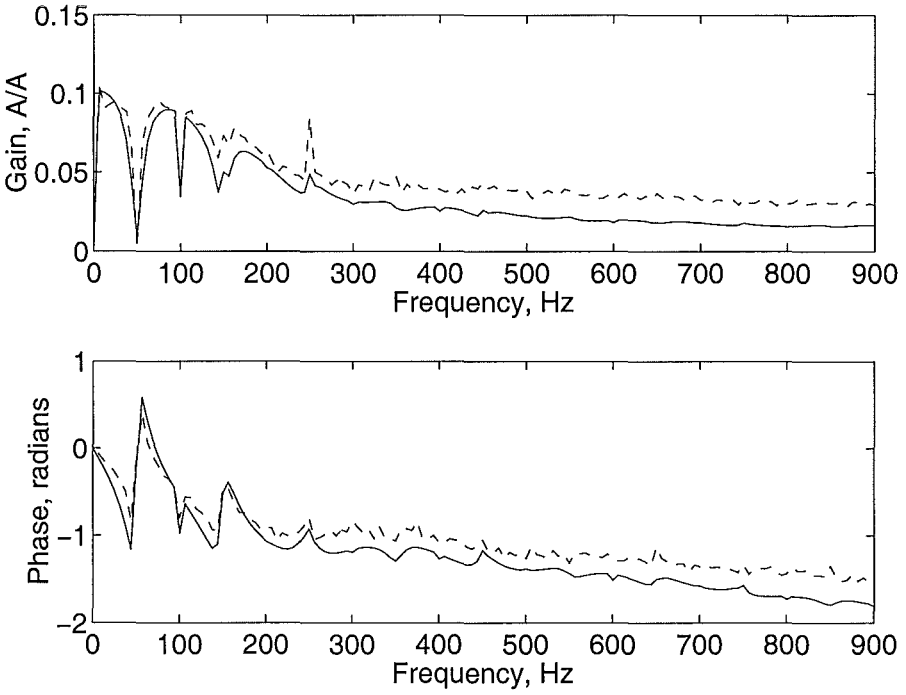

Figure 7.8 Describing function of injected current perturbation to load current change for single phase rectifier. (Dashed - measured experimental, solid - analytic.

cause of the differences in the theoretical and measured magnitudes may be measurement noise or perhaps AC system impedance inaccuracies. The phase angle match is excellent at low frequencies with the rapid phase change features at 50Hz and 150Hz being noticeable points of good agreement. As the frequency rises a small phase difference occurs. The reason for this may be the result of noisy measurements. At points where the rectifier exhibits strong same frequency magnitude-phase dependence a spike occurs in the magnitude and phase plots. This can be seen in the magnitude plot at 100Hz in Figure 7.8 in both the measured and analytic SISO transfer.

Overall, the SISO transfers from the analytic model and the measurements have very much the same character. The feature match especially at frequencies below 400Hz shows that the analysis method of Chapter 6 produces an accurate FTM representation of the non-linear single-phase rectifier. This means that both the analysis and FTM representation method are suitable for further investigation of the single-phase rectifier and other non-linear loads.

7.3.5 Control implications of the SISO transfer

As can be seen from the system block diagram in Figure 7.3 the SISO describing function transfer from I_{Inj} to I_L shown in Figure 7.8 is the forward control transfer of a load current measurement SAF. Previously, describing function descriptions of AC line commutated rectifier type converters have been found to be suitable for robustness analysis and control design [Todd *et al.* 1997]. In [Todd *et al.* 1997] the control bandwidth was less than the Nyquist sampling limit however the switching rate of the single-phase rectifier is 100Hz giving a Nyquist sampling limit of 50Hz. This suggests that the SISO may not be suitable for control analysis. However this is not the case.

Consider the control action of a LCM SAF. The load current is measured, the harmonic or non fundamental current is isolated and injected to cancel the harmonic currents. This control action is classically linear in that it is a single frequency to single frequency transfer. This means that when a frequency occurs in the load current the control response of the SAF is at that very same frequency. The control action of the SAF may cause changes in the load response at a number of other frequencies but the frequency coupling nature of the single-phase rectifier couples these other frequencies back to the original frequency, meaning that the SISO approach is valid even above the Nyquist sampling limit. To further reinforce this, consider the injection of a 130Hz current by the converter. The single-phase rectifier's response has components at 130Hz, 30Hz, 70Hz and 170Hz ... etc. The system impedance couples the rectifier currents to voltages. These voltages at 30Hz 70Hz ... etc in turn each change the rectifier current at 130Hz. This describes how the transfer from 130Hz injected current to 130Hz load current includes the complete frequency transfer or coupling behaviour of the rectifier, AC system and SAF controller at all related, or coupled, frequencies. As a result the

SISO transfer is in fact suitable to describe the total behaviour of the system for control purposes.

When installing a SAF the key operation requirements are that the device operates in a stable fashion and that the device improves power quality. The stability of this specific case can be estimated by determining the gain and phase margins of the open loop transfer given by Figure 7.8. In this case the gain is always below one and the phase never reaches $-\pi$ so the operation is stable and robust. This is reasonable as the reported operation of SAFs does not include instability except when power factor correction capacitors are connected downstream. As the frequency domain plot of the forward SISO transfer for the SAF gives the ability to determine the stability and robustness of the SAF operation the FTM method and analytic model of the rectifier load are powerful tools for use with SAF and other power conditioner analysis and design. This removes the total dependence on time domain simulation. Also because frequency domain techniques inherently include the robustness of allowing easily for system variation this increases the confidence in the power conditioner operation.

7.4 EFFECT OF SAF ON SMALL-SIGNAL SINGLE-PHASE RECTIFIER TRANSFER

In Chapter 3 it was noted that the SAF operation can increase the sensitivity of the non-linear load by removing the frequency cross coupling that the system impedance provides. Alternatively the system impedance is made zero at all frequencies except the fundamental allowing external voltage disturbance from the AC system to transfer unattenuated by the system impedance to the load. Measurements made of the single-phase rectifier Figure 7.9 shows the transfer for the injected current to the load current when the SAF operates (solid line) and when it does not (dotted line). Note that the transfers have the same general character but that when the SAF is operating the transfer has higher magnitude by up to 25% at frequencies below 200Hz. The phase character does not change significantly when the SAF operates. As explained in section 7.2 the experimental system measures a current to current transfer but the sensitivity of the load to external voltage disturbance is the intuitive and conveniently analysed measure of the load sensitivity. Consider the typical operating condition of a load and the AC power system. The AC system must deliver power to the load without dropping excessive voltage. This means that the AC system impedance is low compared with that of the load so the AC system dominates the driving point impedance. By making the assumption that the AC system has the considerably lower impedance the injected perturbing current flows principally into the AC system so the voltage at the terminal is almost proportional to the perturbing current. This means that the injected current to load current transfer has approximately the same character as the sensitivity or voltage to current transfer of the non-linear load so long as the load has the greater

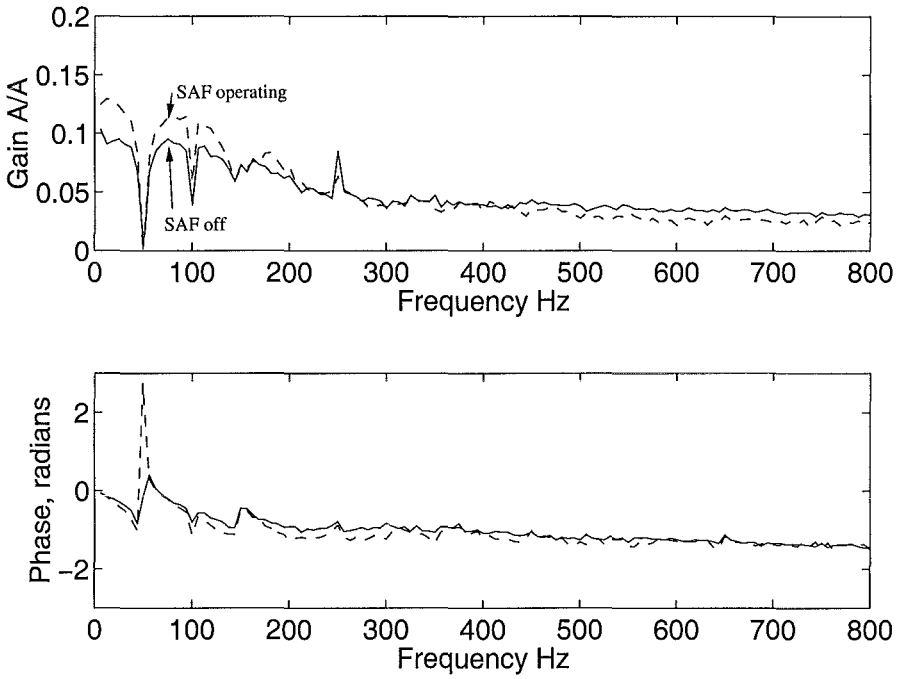

Figure 7.9 Single-phase rectifier injected current to load current transfer when the SAF operates (dotted) and when the SAF is not operating (solid).

impedance. This can be seen in the similarity of phase and magnitude features that occur in both the simulated voltage to current transfer from section 6.7.1 in Figure 6.34 and the measured transfers of Figure 7.9. As the sensitivity of the single-phase rectifier-load is well represented by the current to current transfer from Figure 7.9 it can be seen that SAF operation makes the single-phase rectifier load more sensitive to disturbance in the AC system .

7.5 SMALL SIGNAL TRANSFER COMPARISON BETWEEN LOADS

The effect of loads on AC power systems is generally not well known. That is to say that from a power systems point of view loads are not well modelled, understood or included in analysis. In the case of non-linear rectifier loads the lack of attention is perhaps due to the lack of problems that these loads have caused and the difficulty in analysis of non-linear systems. The representation of linear loads for use in power systems is also not an entirely complete area of knowledge either. It is true that induction motor characterisitics have been explored extensively for use with variable speed drives but the motor behaviour in response to AC power system disturbance is not entirely well characterised. The principle potential problem that loads can perhaps cause in AC power systems is the one of resonance. The AC power system is characterised by its fundamental frequency at which it can deliver real power and the low loss of the

distribution network. This low loss is generally necessary to maximise the economic gain provided by the AC power system.[1] Low loss means low resistance which in turn means low damping for oscillations. Therefore the AC power system is a driven resonant system with low damping to which shunt capacitors are often connected to maintain voltage levels. Each shunt capacitor changes the resonant frequency of the AC system. When a SAF is installed and operated in the load current measurement (LCM) manner the load's ability to dissipate energy at any frequency other than the fundamental is removed as was shown in section 3.6.2. In order to determine how much damping SAF operation removes the relative perturbing current to load current transfer for three loads is calculated. As rectifier loads are non-linear the SISO transfer for the single-phase rectifier connected to the AC system is used to allow a comparison to be made to the transfer of other linear loads. Consider a resistor load and a resistor-inductor load power factor of 0.9 lagging, both having almost the same real power dissipation as the experimental single-phase rectifier. These loads have fundamental frequency admittances of $0.016\frac{1}{\Omega}$ and $0.0168 - j0.074\frac{1}{\Omega}$ respectively. Figure 7.10 shows the SISO transfer from the injected current to the load current for each of the two example linear loads and the single-phase rectifier.

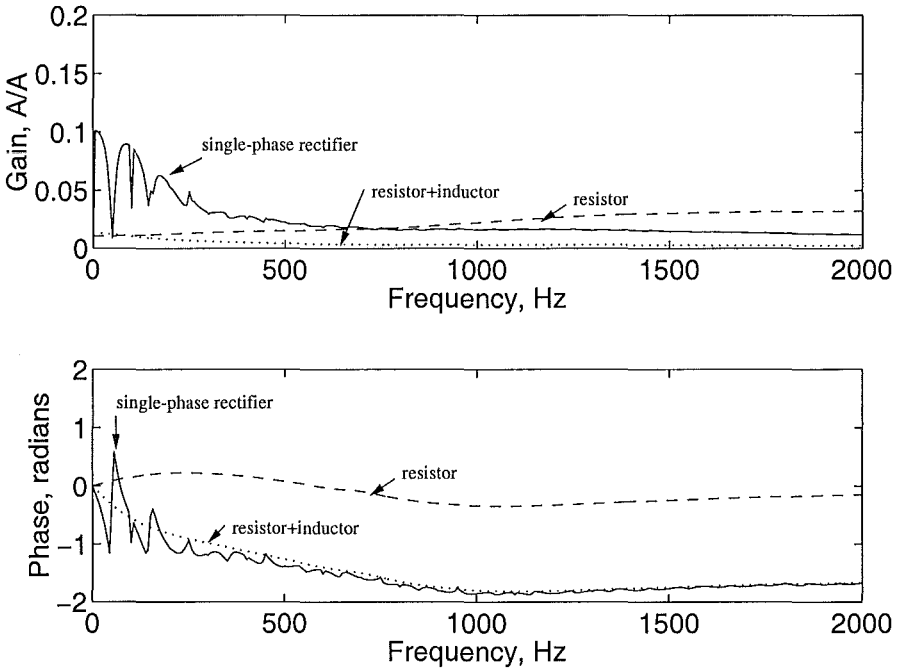

Figure 7.10 Injected current to load current SISO transfers of single-phase rectifier (solid), resistor load (dashed) and resistor-inductor load (dotted).

The transfers of these example linear loads show two things when compared to the single-phase rectifier. Firstly, the rectifier has a far greater transfer magnitude. This

[1] As with all economic solutions the cost of the ongoing power loss depends heavily on the way in which the future cost of the loss is discounted to the present cost.

means that it is significantly more sensitive to a disturbance from the power system than the R or R+L load. This is reasonable when the rectifiers operation is considered as the disturbance becomes larger. When the disturbance is sufficiently large the rectifier mode of operation changes, causing it perhaps to be dissapear electrically. This also means that the single-phase rectifier load contributes far more small signal damping to the power system than the equivalent power resitor or resistor inductor load. Since the SAF removes the damping provided by the load from the AC system and because the single-phase rectifier provides more damping than a resistor or resistor/inductor load, the SAF effect on the AC system when used with rectifier loads could remove significant power system damping perhaps to the point where the power system is not robust to disturbances. The phase of the R+L load's transfer is very much like that of the rectifier if the lower frequency phase changes are ignored. That means that from a power system point of view the single-phase rectifier provides damping at low frequencies and its admittance becomes inductive at higher frequencies. This can be deduced intuitively by considering that the load filter capacitor behaves as an open circuit at low frequencies so the current flows in the resistor. This occurs at any frequency on the AC side that appears as a zero or low frequency current. As the frequency increases the capacitor becomes a short circuit and then the DC side inductor dominates the impedance. Such intuitive frequency transfer thinking about the single-phase rectifier is useful but the conjugation and phase change associated with modulation means that the device is difficult to quantify intuitively.

This means that the effect of SAF on load performance has previously, if at all, been explored mainly with time domain simulation. However as the load FTM represents the sensitivity at all frequencies, including harmonic frequencies since the phase dependence is accurate, it can be used to determine how the SAF effects the steady state load current.

7.6 THE EFFECT OF SAF OPERATION ON THE RECTIFIER CURRENT

In applying a SAF the intention is to improve power quality by removing harmonic currents. The interaction of the SAF with the load has in the past been ignored principally for simplicities sake. As has been previously reported [Peng and Lai 1996] the SAF does change the current that flows into rectifier loads meaning that rectifiers have non zero sensitivity. This has been shown to be the case with the experimental measurements in the previous sections 7.5 and 7.3. The quantification of this effect is required because this allows the power quality improvement, if any, to be predicted. When the SAF operates, the single-phase rectifier load forms the forward part of the feedback transfer. The non-zero load sensitivity means that the SAF's injection of anti-phase harmonic currents into the AC system can change the current flowing into

the load [Luor 2000, Peng and Lai 1996]. The change in the single-phase rectifier load current that SAF operation causes is found using the FTM. As it is defined by the base case operation, the FTM can be used to calculate the base operation current.[2] That is when the base case fundamental voltage is used in the place of the perturbing input voltage the base case load current result. Therefore equation (7.2) gives the load current when the load FTM is correct for the operating point defined by the supply voltage V_S and system impedance Z_{Sys}. See Appendix H for the matrix algebra used to derive (7.2) and (7.3).

$$I_L = [\mathbf{Y_{Load}}](\mathbf{I} + [\mathbf{Z_{Sys}}][\mathbf{Y_{Load}}])^{-1} V_S \tag{7.2}$$

The current change caused by the SAF operation is found by calculating the load current when the SAF operates (7.3) and then subtracting the base case load current of (7.2). See Appendix H for the matrix algebra used to derive (7.2) and (7.3).

$$I_L = [\mathbf{Y_{Load}}](\mathbf{I} + [\mathbf{Z_{Sys}}][\mathbf{I} - [\mathbf{Cont}]][\mathbf{Y_{Load}}])^{-1} V_S \tag{7.3}$$

Figure 7.11 shows the PSCAD-EMTDC simulated single-phase rectifier current with and without the SAF operating. The circuit situation that gives rise to the currents shown in Figure 7.11 is quite extreme because the fundamental frequency AC system impedance magnitude is of the same order as that of the single-phase rectifier inductor. This means that the change on the rectifier AC terminal voltage caused by the SAF operation may violate the small-signal approximations used to develop the model. Appendix F shows the PSCAD circuit for the SAF simulation. The SAF operating current (the dashed line in Figure 7.11) has a higher peak and slightly narrower waveshape. This occurs because the SAF operation removes the frequency coupling provided by the AC system and makes the AC system impedance seem low at all frequencies apart from the fundamental. Alternatively SAF operation can be seen as removing the frequency cross coupling that the AC system impedance provides during normal operation or that no harmonic voltage is allowed to drop in the system impedance. By examining the change in the load current, Figure 7.12, it can be seen that the FTM model (dashed line) quite accurately predicts the current waveform from the PSCAD-EMTDC simulation (solid line). Figure 7.12 also shows the spectrum of the load current change from simulation and the FTM. One possible cause of the difference between the results is due to second order effects associated with switching instant modulation having exactly the same frequency as the first order effects. This means that the first order FTM representation of the single-phase rectifier cannot ever be entirely accurate in predicting the change in the load current caused by SAF operation. However second

[2]This situation is not usual for non-linear rectifier type loads and is probably the case for only rectifier loads with discontinuous currents. Generally it cannot be assumed that the base case operating condition can be calculated using the small signal transfers.

order effects are small so the inaccuracies they cause are an order of magnitude smaller than those from first order effects. The small inaccuracies in the operating point to which the analytic model is quite sensitive are most probably the main cause of error. Considering the possible error sources the agreement is reasonably good. An

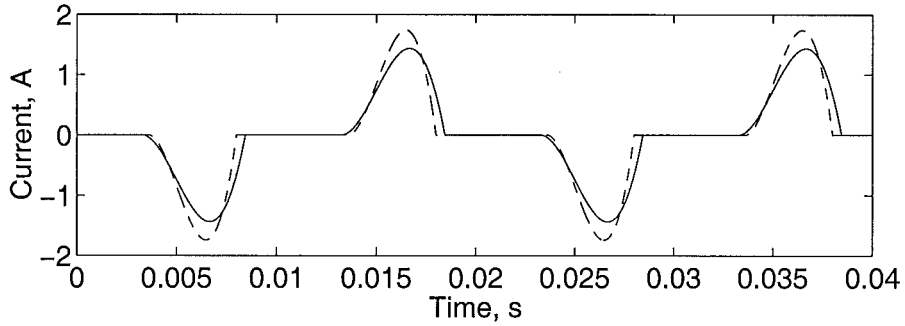

Figure 7.11 Single-phase rectifier load current when SAF operating (dashed line) and when the SAF is not operating (solid line). Both waveforms from PSCAD-EMTDC simulation.

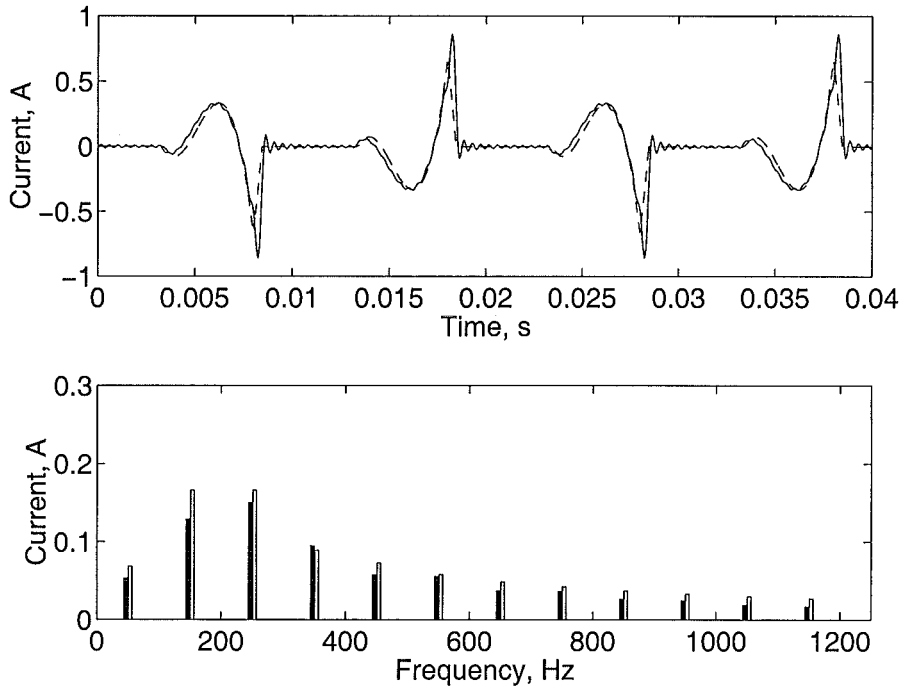

Figure 7.12 Change in single-phase rectifier load current caused by SAF operating for high system impedance. Upper figure dashed line - PSCAD-EMTDC, solid line from FTM of analytic model. Lower figure magnitude spectrum of current change. (Light bars analytic dark bars PSCAD-EMTDC)

alternative way to view the source of the error is to note that the analysis to produce the FTM model of the single-phase rectifier assumes constant operating conditions. It could be argued that the change in the load's terminal voltage that occurs when the SAF operates means that this assumption is no longer valid. As an example of the improved accuracy, Figure 7.13 shows the change in current for the situation where the fundamental frequency supply impedance is ten times smaller than the impedance

of the rectifier inductor. As is evident the analytic model predicts the change in the load current with a reasonably small error. This situation is perhaps the more realistic for real SAF operation. Figure 7.14 shows the experimentally measured single-phase

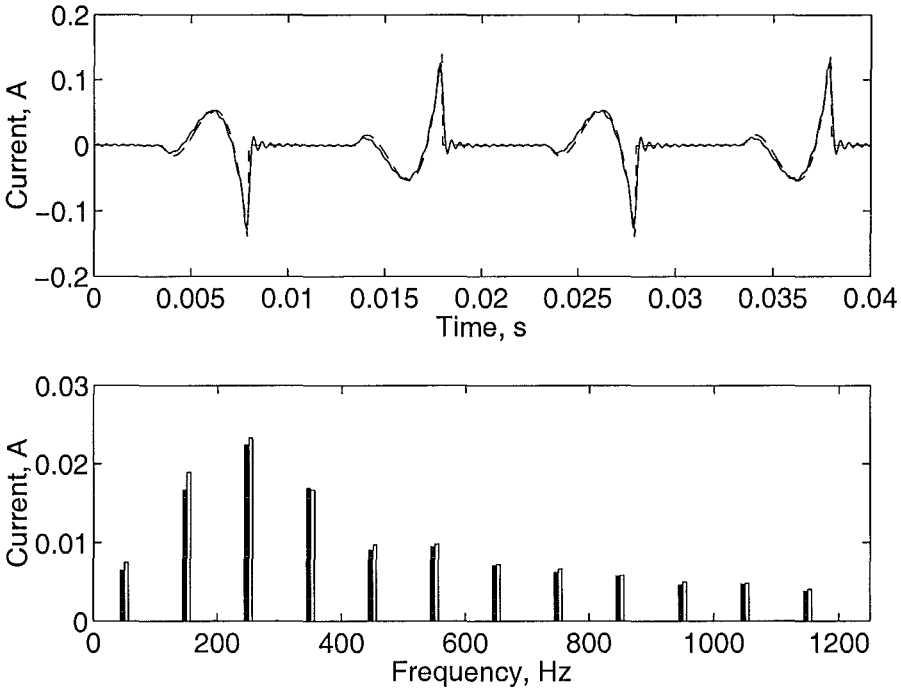

Figure 7.13 Change in single-phase rectifier load current caused by SAF operating for lower system impedance. Upper figure dashed line - PSCAD-EMTDC, solid line from FTM of analytic model. Lower figure magnitude spectrum of current change. (Light bars analytic, dark bars PSCAD-EMTDC)

rectifier load current when the SAF operates (upper figure dashed) and when it does not (upper figure solid). The change in the current, shown in the lower figure, has the same type of waveshape as that in the analytic and simulated waveforms of Figure 7.13. The difference between the waveforms is due to the difference in the rectifier operating point and the imperfect operation of the experimental SAF caused by the processing delays.

It is apparent that the inclusion of the second order effects in the model may be a way to improve the accuracy of the results. However, this is not a trivial matter because all second order effects depend on the square of the magnitude of the applied perturbation. This means that including them in the linear FTM requires the linearisation of the transfer for each perturbation magnitude, effectively making the perturbation magnitude part of the operating point. It may be that such an exercise proves fruitless. Perhaps a better approach is to go to some form of iterative solution [Bathurst 1998].

However the FTM model of the single-phase rectifier is very useful in determining the change in the single-phase rectifier current that SAF operation causes. The accuracy of the results in Figures 7.12 and 7.13 means the FTM is appropriate for use as a good quantitative guide to the SAF suitability, effectiveness and possible power quality

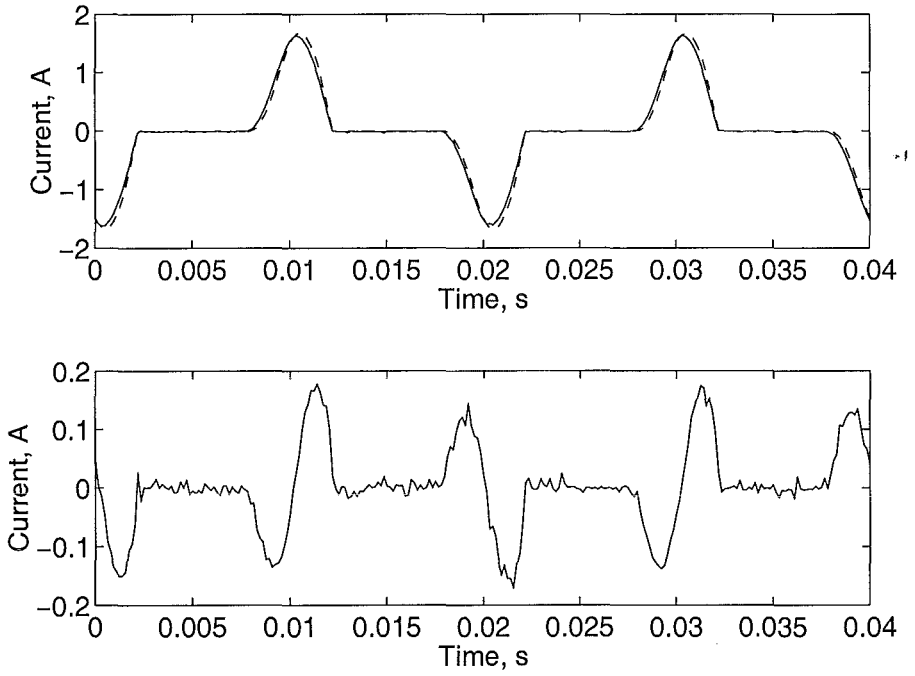

Figure 7.14 Experimentally measured change in single-phase rectifier load current caused by SAF operating for lower system impedance. Upper figure dashed line - SAF operating, solid line SAF not operating. Lower figure change in current)

improvement.

7.7 MEASURABILITY OF RECTIFIER TRANSFERS

Throughout the development of the experimental system to make measurements like those shown in Figure 7.2 there was a doubt as to whether it is possible to actually measure the characterisitics of the non-linear rectifiers. The principal concern is that whether the perturbing current I_{inj} is sufficiently large a signal to cause a measurable response in the load current. This concern has not been found to be valid and in fact the measurements have been made with only moderate regard to the noise rejection or range of the experimental system analogue to digital converters. It is true that the experimental time domain waveforms presented in this chapter are noisy but the use of the FFT to determine the frequency components has proved more than adequate to show both the validity of the analytic model and that the collection of the measurements is possible.

Since the AC system plays a large part in determining the size of the current to current transfer, the relative amount of perturbation current flowing into the load decreases as the AC system impedance decreases. This can been appreciated by setting $[Z_{Sys}]$ to zero in equation 7.1. This does not however mean that the measurements will be impossible to make, but rather that they are zero to the precision of the measurement. When the AC system is very strong ($[Z_{Sys}]$ very close to zero), the measured

transfer is close to zero meaning that the flow of harmonic currents in the system causes very little harmonic voltage drop. This in turn means that the operation of the SAF will have little effect on the load current as the voltage will not change significantly when the SAF operates. When the AC system is relatively weak having larger impedance, the measured current to current transfer will be larger as more of the injected current will flow into the load. Therefore the ability to measure a zero transfer caused by a very strong AC system is no less useful than the measurement of the non-zero transfer that will occur when the AC system has a higher impedance. In effect the measurement of a zero transfer means that the operation of the device with the SAF will be very close to the same as the device without the SAF. This means that it is probable that when the AC system is strong the application of the SAF is not be required as the effect of the load on the network is minimal. However when there are power quality problems due to weak AC systems the installation of the SAF is not a panacea but requires careful consideration of the interactions with the SAF, the load and AC system using the FTM method.

7.8 SUMMARY

The analytic model of the single-phase rectifier has been compared with experimental measurements of the injected current to the rectifier current transfer. Generally the measured results show good correlation to those from the analytic model and when the sources of uncertainty and error in the measurements are considered the model is very predictive.

The experimental system used to make the measurements is in no way extraordinary in its complexity, specification or accuracy. Even so it was possible to measure the performance of the single-phase rectifier remarkably well. Such measurements that are well predicted by theory give a strong insight into the behaviour of this particular non-linear load within the AC power system and also with a shunt active filter power conditioner.

The SISO transfer of the single-phase rectifier which gives a describing function transfer that allows the non-linear device to be described as an equivalent linear time invariant device, shows that for the specific operating condition the SAF, AC system and rectifier form a stable system. This transfer is confirmed by experimental measurement. Measurements when the SAF operates shows the increase in the sensitivity of the rectifier that was predicted in Chapter 3. The change was in the order of a 10% increase at the lower frequencies.

In order to give an indication of the relative sensitivity of the single-phase rectifier to other loads, two linear test loads were compared with the analytic model. The SISO current to current transfer of the single-phase rectifier is used to do the comparison.

The results show that the single-phase rectifier is in fact significantly more sensitive in the small-signal than resistive and resistive-inductive at frequencies below 750Hz.

The use of the FTM to predict the change in the load current that SAF operation causes shows good results. The accuracy to 20% means that the FTM can be used as a very good indicator of the effect of the SAF. The error is less when the relative impedance of the rectifier load is small compared to the system impedance. This is usually the situation in a power system.

Not all non-linear rectifier loads are single-phase where SAF are used. In fact the three-phase SAF is very well suited to operating with three-phase rectifier loads. Therefore the behaviour of three-phase rectifiers is also important. The following chapter presents a set of measurements made for a three-phase rectifier using the experimental system.

Chapter 8

THREE-PHASE RECTIFIER FREQUENCY TRANSFER MEASUREMENTS

8.1 INTRODUCTION

The vast majority of the electrical power in the world is generated, transported and utilised as three-phase currents and voltages. Three-phase generation, transmission and utilisation is used because it allows constant instantaneous power transport. This ensures that constant speed rotating loads can have constant torque. A large number of non-linear three-phase loads have three-phase rectifiers that are used to convert the three-phase AC voltage to a DC voltage. One example is the induction motor speed drive that typically has a three-phase diode bridge rectifier or three-phase thyristor bridge rectifier usually controlled only to provide soft charge of the DC bus and then turned on continuously. The three-phase SAF system presented in Chapter 4 is used in Chapter 7 to make measurements of the single-phase rectifier that confirm the analytic model developed in Chapter 6. The FTM method base model of the single-phase rectifier proved to be accurate and convenient. The three-phase experimental system can also be used to make measurements of three-phase rectifiers and this will allow confirmation that the three-phase rectifier has a frequency coupling transfer much like the single-phase recitifier.

The use of the same FTM method to represent the three-phase rectifier so its interaction with the power system can be explored and analysed is of considerable interest especially with the increased installation of SAFs and other power conditioners. Establishing that the FTM approach is suitable for three-phase rectifiers is the principal aim of this chapter.

8.2 THREE-PHASE RECTIFIER OPERATION

The primary function of a three-phase rectifier is to convert the fundamental frequency positive sequence voltage to a zero frequency voltage on the DC side of the rectifier. Typically three-phase rectifier operation means that fifth harmonic negative

sequence and seventh harmonic positive sequence currents flow in the AC side current along with the positive sequence fundamental current. The harmonic spectrum of the AC side current has negative sequence components at frequencies $(6n-1)\omega_0 t$ $n = 1, 2, 3...$ and positive sequence harmonics at frequencies $(6n+1)\omega_0 t$ $n = 0, 1, 2, 3...$ [Arrillaga *et al.* 1985]. Examination of the frequency modulation behaviour of controlled thyristor three-phase rectifiers using the FTM method has been performed for HVDC situations [Wood *et al.* 1998].

Three-phase rectifiers can be viewed as frequency modulators in the same way as the single-phase rectifier is in Chapter 5 and Chapter 6. The frequency driving the single-phase rectifier switching is the fundamental while that driving the three-phase rectifier is the fundamental positive sequence. The three-phase rectifier switching action couples or transfers the AC side positive sequence voltage to the DC side zero frequency effectively performing a negative fundamental frequency shift. In a similar but slightly different fashion the DC side current at zero frequency is transferred to fundamental positive sequence current, negative sequence fifth harmonic current and positive sequence seventh harmonic current and also the continuing positive and negative sequence components. This indicates that the three-phase rectifier performs a negative fundamental frequency shift sequence coupling from an AC side voltage or current $(k_{AC})\omega_0$ to the DC side frequency of $(k_{DC})\omega_0 = (k_{AC}-1)\omega_0$. It also performs negative $(6n+1)\omega_0$ and positive $(6n-1)\omega$ AC side to DC side frequency shifts for $n = 1, 2, 3, ...$ which gives rise to the characteristic DC side harmonics at $6n$. The DC side frequency transfers back through the rectifier to two frequencies of $(1+k_{DC})\omega_0$ and $(1-k_{DC})\omega_0$ on the AC side [Wood *et al.* 1998, Bathurst 1998]. A negative AC side frequency indicates that the component is negative sequence. This means that for a three-phase AC system in sequence components a negative frequency has meaning and is not the same as a phase conjugated positive frequency (see section 5.3.3). As the three-phase rectifier transfers sequence components the use of sequence representation of the system voltages and currents is a good choice [Smith *et al.* 1998]. That is not to say that variables in individual phase form or in an orthogonal two-phase form cannot be successfully used to represent the three-phase rectifier behaviour. However, the choice of these other forms leads to FTMs that are not at all sparse and so do not contribute significantly to the understanding of the three-phase rectifier operation or behaviour [Smith *et al.* 1998, Bathurst 1998].

This chapter presents measurements of a three-phase perturbing current to the three-phase rectifier current transfer made using the experimental system which is reconfigured from the single-phase measurement mode used in Chapter 7 to a three-phase sequence measurement system. As previously, a number of single frequency (and sequence), constant amplitude currents are injected successively and the current that flows in the rectifier is measured. However, as the rectifier current is three-phase and the expectation is that the device will couple sequence components, it is necessary to

have some method of measuring and isolating the sequence components. A three-phase FFT provides such a method.

8.3 THREE-PHASE FAST FOURIER TRANSFORMS

In order to make measurements of three-phase quantities it is appropriate and convenient to use either sequence, orthogonal $\alpha\beta$ or rotated dq components. In a three wire three-phase system there can be no zero sequence component so the system is completely represented as a two-phase system. A sequence transform resolves a three wire three-phase system into two sequences which rotate in opposite directions. These two sequences are the positive and negative sequence of the three-phase system. In the experimental system the the three-phase variables are measured and a two-phase equivalent system formed. The two-phase system is used in the SAF controller implementation and the converter DC bus control.

However, the two-phase variables represent the same real situation as the three-phase variables and one is a linear combination of the other. This means that determining the frequency components of the three-phase system can be achieved by working with the two-phase equivalent. Consider the situation where a single frequency positive sequence three-phase system is transformed to an equivalent two-phase system. The three-phase system is represented in (8.1).

$$\begin{aligned} a &= M\sin(\omega_0 t + \delta) \\ b &= M\sin(\omega_0 t + \delta - \frac{2\pi}{3}) \\ c &= M\sin(\omega_0 t + \delta - \frac{4\pi}{3}) \end{aligned} \tag{8.1}$$

When a three-phase to two-phase transform (8.2) is used, the resulting two-phase representation is (8.3).

$$\begin{bmatrix} \alpha \\ \beta \end{bmatrix} = \sqrt{\frac{2}{3}} \begin{bmatrix} 1 & -\frac{1}{2} & -\frac{1}{2} \\ 0 & \frac{\sqrt{3}}{2} & -\frac{\sqrt{3}}{2} \end{bmatrix} \begin{bmatrix} a \\ b \\ c \end{bmatrix} \tag{8.2}$$

$$\begin{aligned} \alpha &= \sqrt{\frac{3}{2}} M\sin(\omega_0 t + \delta) \\ \beta &= -\sqrt{\frac{3}{2}} M\cos(\omega_0 t + \delta) \end{aligned} \tag{8.3}$$

The phase sequence is reversed by changing the sign of the frequency ω_0 (8.4).

$$\begin{aligned} a &= M\sin(-\omega_0 t + \delta) \\ b &= M\sin(-\omega_0 t + \delta - \frac{2\pi}{3}) \\ c &= M\sin(-\omega_0 t + \delta - \frac{4\pi}{3}) \end{aligned} \tag{8.4}$$

This gives the resulting two-phase system (8.5).

$$\begin{aligned} \alpha &= -\sqrt{\frac{3}{2}}M\sin(\omega_0 t - \delta) \\ \beta &= -\sqrt{\frac{3}{2}}M\cos(\omega_0 t - \delta) \end{aligned} \tag{8.5}$$

Plotting the positive and negative sequence two-phase systems on a complex plane, as in Figure 8.1, with α and $-\beta$ as the imaginary and real parts respectively, shows the locus mapped by each of the signals is circular. The loci of the positive and negative sequence signals with $\delta = 0$ both have the same starting point. That is when $\delta = 0$ equations (8.3) and (8.5) have the same value for $t = 0$. From equations (8.3) and (8.5) it can be seen that the direction that the locus rotates depends on the sequence of the three-phase system.

A complex FFT operates on any time varying complex variable effectively performing a FFT of a locus or shape [Brigham 1988]. The complex exponential representing a positive frequency signal is (8.6).

$$e^{j(\omega_0 t+\delta)} = \cos(\omega_0 t + \delta) + j\sin(\omega_0 t + \delta) \tag{8.6}$$

If ω_0 is made negative, corresponding to a signal with negative frequency, then the complex exponential is (8.7).

$$\begin{aligned} e^{j(-\omega_0 t+\delta)} &= \cos(-\omega_0 t + \delta) + j\sin(-\omega_0 t + \delta) \\ &= \cos(\omega_0 t - \delta) - j\sin(\omega_0 t - \delta) \end{aligned} \tag{8.7}$$

The Fourier transform of (8.6) is $\delta(\omega - \omega_0)$ and that of (8.7) is $\delta(\omega + \omega_0)$. This shows the difference between negative and positive frequencies and that a FFT can determine the direction of rotation of a complex signal. By making α the imaginary component of a complex signal and $-\beta$ its real component, the complex signal is of the form of

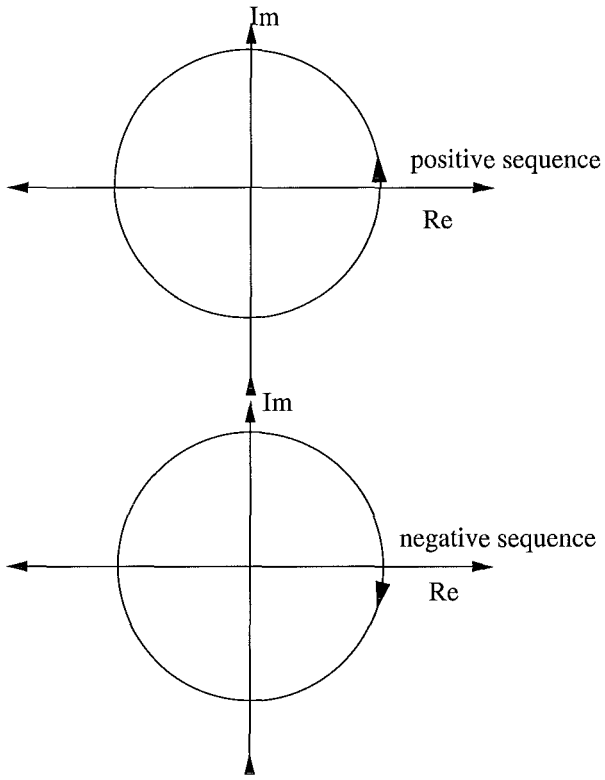

Figure 8.1 Positive and negative sequences in two-phase plane

(8.8) for a positive sequence signal and (8.9) for a negative sequence signal.

$$-\beta + j\alpha = \sqrt{\frac{3}{2}}M\cos(\omega_0 t + \delta) + j\sqrt{\frac{3}{2}}M\sin(\omega_0 t + \delta) \tag{8.8}$$

$$-\beta - j\alpha = \sqrt{\frac{3}{2}}M\cos(\omega_0 t - \delta) - j\sqrt{\frac{3}{2}}M\sin(\omega_0 t - \delta) \tag{8.9}$$

Equations (8.8) and (8.9) have exactly the same form as the complex exponentials in (8.6) and (8.7). This means that by using the orthogonal two-phase $\alpha\beta$ transform of a three-phase system and then taking the FFT of the complex signal formed from the two-phase representation, the sequence components of the three-phase signals can be determined. Therefore, the experimental system can perform complex sequence FFTs of the three-phase measurements. The coding of a complex FFT using a pre-existing real value FFT routine is described in Appendix A. This sequence FFT is used to measure the behaviour of the three-phase rectifier.

8.4 THREE-PHASE RECTIFIER TRANSFER MEASUREMENTS

Three-phase rectifiers operate in two modes. These are the continuous current mode, where the current on the DC side is continuous and at no time has zero value, and the discontinuous current mode where the current does at times fall to and have zero

value.

8.4.1 Discontinuous current mode

The measured three AC side rectifier currents for the discontinuous current mode are shown in the Figure 8.2(upper). Figure 8.2(lower) shows the three AC currents when the rectifier operation is perturbed by an injected positive sequence current of 25Hz. The effect of the perturbation is noticeable by closely comparing the waveforms. The

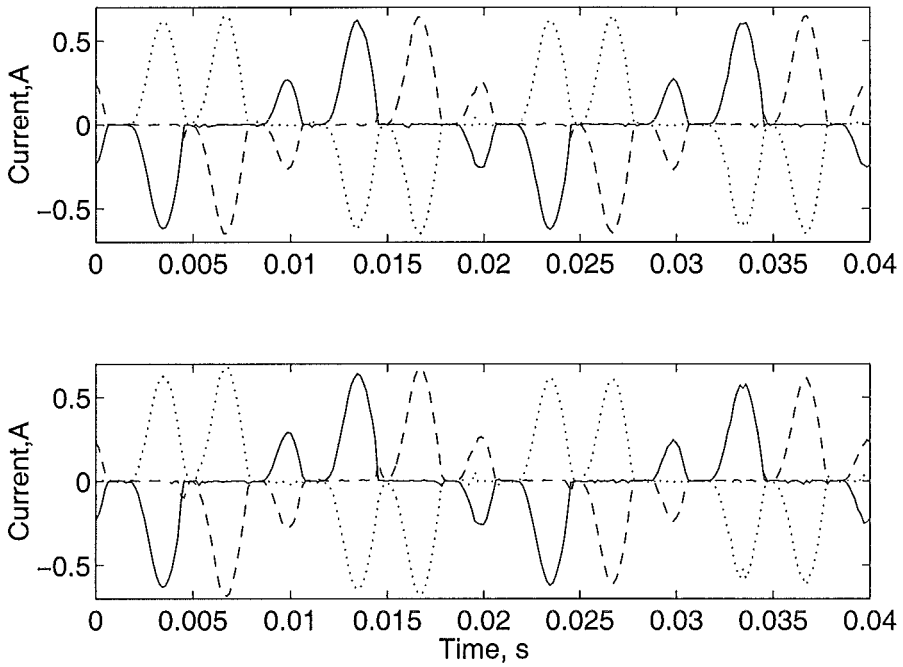

Figure 8.2 Experimentally measured base case (upper) and perturbed (lower) current waveforms for three-phase rectifier in discontinuous conduction mode. (Solid line - a phase, dashed line - b phase, dotted line - c phase.)

spectrum components that occur in the load current when the 25Hz positive sequence perturbation are shown by the sequence FFT result in Figure 8.3. This spectrum has not had the base case suppressed so the fundamental harmonic currents of the base case are shown along with the frequency components caused by the injected current. These harmonic currents occur at frequencies that are multiples of the 50Hz fundamental. The fundamental frequency positive sequence current occurs at 50Hz. The negative sequence current, which indicates that the load is not completely balanced, has a frequency of -50Hz. The expected harmonic currents at positive sequence seventh harmonic (frequency 350Hz) and the negative sequence fifth harmonic negative sequence (frequency -250Hz) are the largest spectral components after the fundamental positive sequence component. There are other harmonics present at all positive and negative harmonic frequencies. These are smaller than the fifth negative and seventh positive sequence and are the result of the imbalance in both the load and the supply

voltage [Smith *et al.* 1998, Bathurst 1998]. The 25Hz injected perturbing current produces the 25Hz and 75Hz components which are sum and difference frequencies of the resulting DC side current with the fundamental positive sequence. The same sum and difference effect can be seen at both the fifth negative sequence and seventh positive sequence. There are other sum and difference terms either side of 650Hz and -550Hz, these being the next characteristic frequency harmonics. Also, there are modulation products with the non-characteristic harmonics that result from the rectifier and system voltage imbalance. These frequencies can be seen in the spectrum as the small unlabelled components at non-harmonic frequencies.

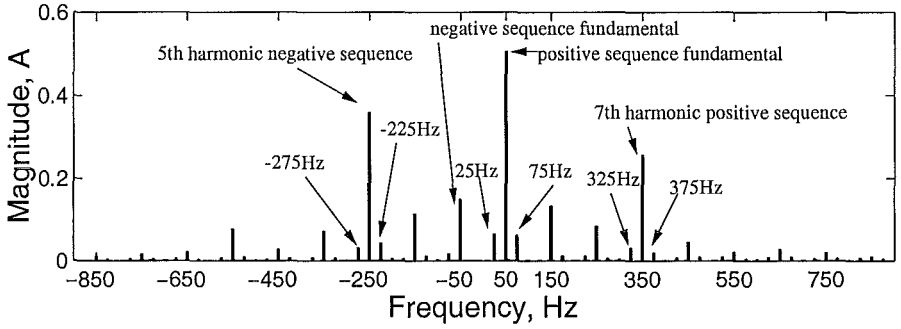

Figure 8.3 Sequence spectrum of experimentally measured three-phase load current operating in discontinuous mode with injected perturbing current at 25Hz positive sequence.

The coupling of frequencies by a single-phase rectifier can be well represented by the lattice diagram of the FTM as was demonstrated in Chapter 5. Figure 8.4 shows the three-phase rectifier lattice with columns made up of the experimentally measured sequence FFT magnitudes. The horizontal axis is the positive sequence input frequency and the vertical axis is the output such that the lattice FTM has the same matrix-type orientation, with the zero-zero point at the top left, used throughout this thesis. The harmonic frequencies are once again not suppressed and appear as the horizontal lines. The components above a magnitude threshold are retained. This magnitude threshold is chosen to give the best noise rejection while retaining sufficient information for clarity. The disappearance of the horizontal line representing the $-850Hz$ (negative) sequence component as the perturbing input frequency is increased is perhaps because the operating point changes slightly between the low and high frequency perturbations. It may even be the case that the real power drawn by the converter when making the high frequency perturbations is sufficient to move this harmonic current from above the display threshold to below that threshold. The diagonal lines in Figure 8.4 are the equivalent of the FTM and show the sequence coupling nature of the three-phase rectifier. Diagonal lines A and B show the components that result from the fundamental positive sequence switching interacting with the injected perturbation and then the resulting DC side current being transferred to the AC side. The fact that these lines continue for a significant length shows that these components are relatively large at

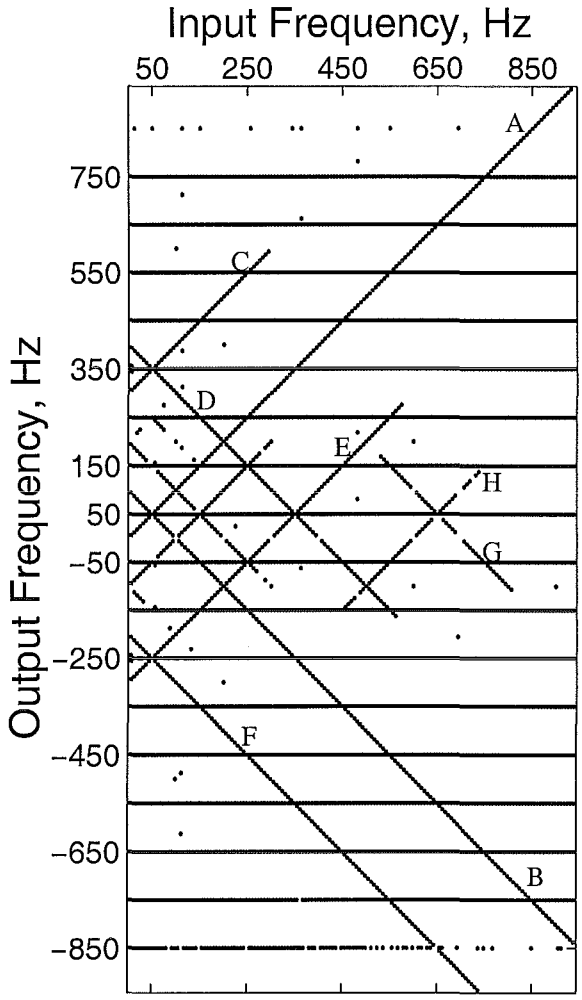

Figure 8.4 Experimentally measured three-phase rectifier discontinuous current mode lattice for positive sequence perturbing current. (Rectifier FTM is equivalent to diagonal lines only. Horizontal lines are the base case which is not removed).

low frequencies as the low pass nature of the DC side filter attenuates the higher frequencies. Lines C and D are from the interaction of the positive sequence seventh and the perturbation, while E and F are for the fifth harmonic negative sequence. The G and H coupling lines occur as a result of the perturbation's interaction with the 13th harmonic positive sequence and the 11th harmonic negative sequence. The other unlabelled lines are the result of the perturbation interacting with the non-characteristic harmonic behaviour of the three-phase rectifier.

The diagonal lines in Figure 8.4 all have slope of minus one or one. This means that the frequencies that are measured are all first order frequencies. Therefore, the discontinuous current three-phase rectifier has a response that is completely dominated by first order frequencies. As first order transfers do not change with the magnitude of the perturbation, the constant FTM approach is appropriate and suitable to represent the three-phase rectifier. The FTM approach and variants of it have been used in

representing three-phase rectifiers for HVDC transmission analysis [Larson *et al.* 1989, Wood 1993, Wood *et al.* 1998, Smith *et al.* 1998].

The sequence coupling behaviour of the discontinuous conduction three-phase rectifier with a negative sequence perturbing current injection is shown in Figure 8.5. The FTM coupling line labelling is the same as the positive sequence FTM of Figure 8.4. Consider the line labelled A in Figure 8.5. This line continues across the zero frequency axis and onto the positive sequence part of the lattice, as shown by the line labelled A in Figure 8.4. The other lines also continue across the zero frequency axis in the manner shown by the labels. This shows how the sequence coupling nature of the three-phase

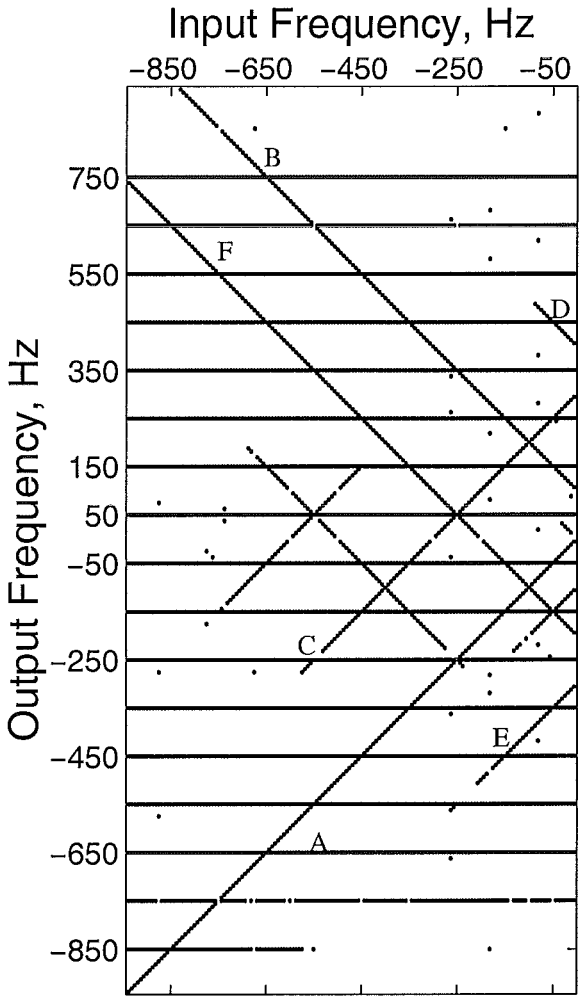

Figure 8.5 Experimentally measured three-phase rectifier discontinuous current mode lattice for negative sequence perturbing current. (Rectifier FTM is equivalent to diagonal lines only. Horizontal lines are the base case which is not removed).

rectifier is continuous across the zero frequency axis and that the response to a certain frequency negative sequence perturbation is at a frequency different to the response to a positive sequence perturbation at the same frequency. This means that the positive sequence and negative sequence behaviour of a three-phase rectifier are not the same.

Note that a negative sequence perturbation couples (see the B line in Figure 8.5) to positive sequence third harmonic current. As this third harmonic current is not zero sequence it can propagate through the delta winding of the supply transformer into the transmission and distribution system. This refutes the commonly held view that there cannot be third harmonic currents in three-phase three wire systems. The existence of non zero sequence third harmonic currents when there is a negative sequence perturbation should be noted when using three-phase rectifiers.

The discontinuous current mode is however uncommon in three-phase rectifiers and it is typical to operate three-phase rectifiers in continuous current mode.

8.4.2 Continuous current mode

The single-phase rectifier's discontinuous current means that the initial conditions for each conduction state are always the same (Chapter 6) . This means that in its analysis there is no need to incorporate the dependence of a conduction state on the preceding state (see section 6.3.1). When the three-phase rectifier operates in continuous conduction mode the constant initial condition for each conduction period or mode is not a valid assumption because the behaviour in one conduction period can effect the behaviour in the next. Also, the commutation from one phase to the other may perhaps cause differences from the discontinuous conduction behaviour described in section 8.4.1.

Typically the three-phase rectifier is operated in continuous current mode as this makes best use of the semiconductors by minimising the crest factor and also minimises the harmonic distortion in the AC side currents. The three AC side current waveforms are shown in Figure 8.6. The rectifier is made to operate in the continuous mode by increasing the DC side load. The current is continuous on the DC side of the rectifier and so there are commutations when the current switches from one phase to the other. This can be seen where one current rapidly rises and another rapidly falls.

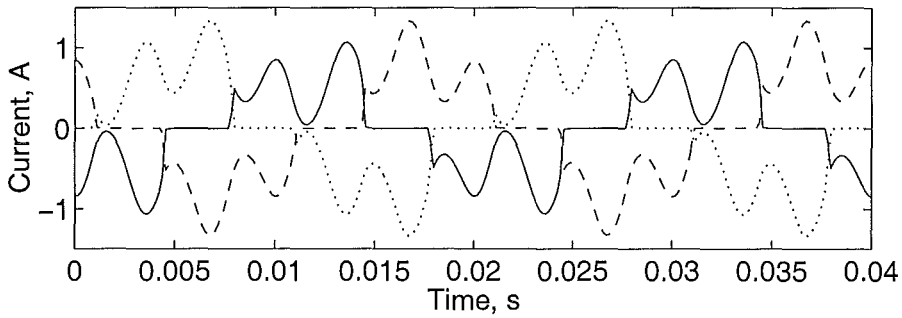

Figure 8.6 Experimentally measured current waveforms for three-phase rectifier in continuous conduction mode. (Solid line - a phase, dashed line - b phase, dotted line - c phase.)

The sequence coupling FTM lattice for positive sequence perturbation is shown in Figure 8.7. The same pattern is evident for the continuous conduction as for the

discontinuous conduction lattice (Figure 8.4). As with the discontinuous mode the interaction of the injected current and the fundamental positive sequence switching can be seen in lines labelled A and B. The C and D coupling lines result from the positive sequence seventh harmonic interaction while the E and F lines are due to the negative sequence fifth harmonic. It is evident that the continuous conduction is perhaps the slightly less sensitive of the two conduction modes. This conclusion can be drawn from the fact that the resulting current coupling lines from the interaction of the perturbation with the positive sequence seventh harmonic frequency do not extend as far up in frequency as those for the discontinuous current case in Figure 8.4. This sensitivity change does not prevent the experimental system making measurements that are well above the FFT noise floor, as is apparent in Figures 8.3 and 8.7.

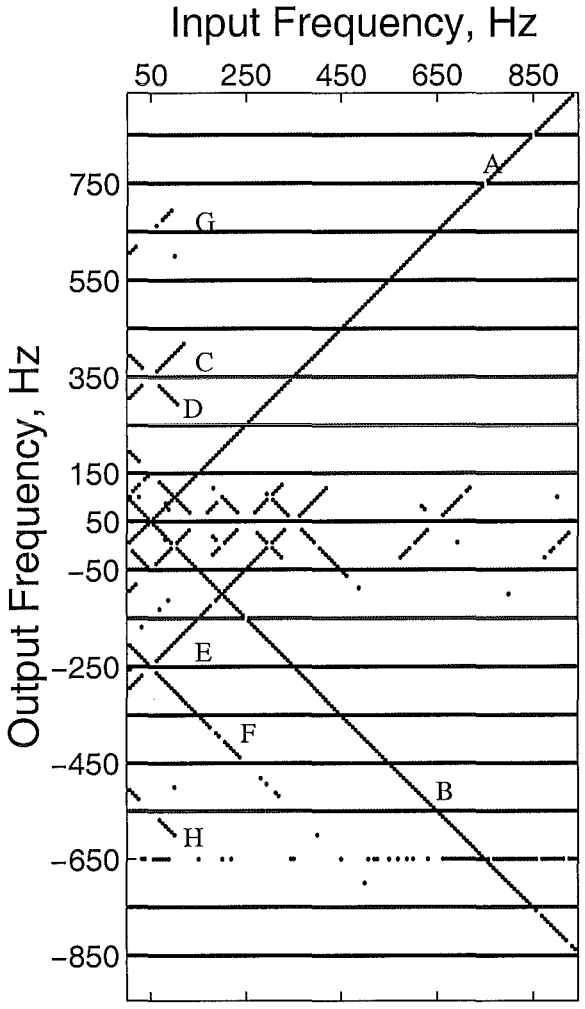

Figure 8.7 Experimentally measured three-phase rectifier continuous current mode lattice for positive sequence perturbing current. (Rectifier FTM is equivalent to diagonal lines only. Horizontal lines are the base case which is not removed).

When the injected perturbing current has negative sequence frequency the lattice of the FTM is as shown in Figure 8.8. The pattern of frequency coupling is once again

the same as that for the discontinuous current mode. The continuous nature of the frequency coupling behaviour can be seen in the way the labelled diagonal coupling lines continue across from the positive sequence lattice to the negative sequence lattice diagram. This shows that the FTM approach is appropriate and suitable for the three-

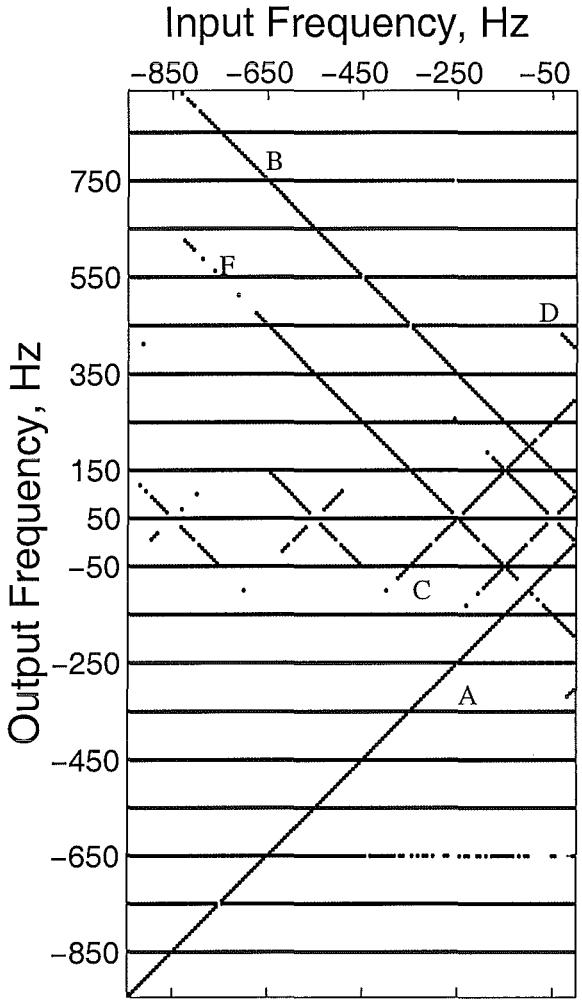

Figure 8.8 Experimentally measured three-phase rectifier continuous current mode lattice for negative sequence perturbing current. (Rectifier FTM is equivalent to diagonal lines only. Horizontal lines are the base case which is not removed).

phase rectifier operating in either the discontinuous or continuous current mode.

8.5 SUMMARY

The experimental system has been used to measure the response of a three-phase rectifier. In order to allow the best representation of the frequency coupling behaviour the measurements have been made using sequence components. Perturbing currents of negative or positive sequence are injected and the three-phase rectifier load current response measured. The sequence components of this current are found using a sequence

FFT that operates on a complex signal formed from the two-phase equivalent of the three-phase variables.

The sequence FFTs of the three-phase rectifier for both discontinuous and continuous current show that the device is indeed a sequence coupling device and that the frequencies that result are first order in nature. This is shown by the slope of the frequency coupling lines being either one or minus one. First order frequency coupling indicates that the three-phase rectifier can be well modelled by a constant FTM in the same way as the single-phase rectifier. This FTM approach has been previously used for three-phase HVDC converter rectifiers. There is little difference between the behaviour of the discontinuous and continuous modes of operation except that the device is slightly less sensitivity when in continuous conduction mode. The representation of negative sequence components with negative frequencies means that the frequency coupling behaviour of the three-phase rectifier is continuous across zero frequency. As a result it should be possible to represent the total negative and positive sequence behaviour of three-phase rectifiers with FTMs. The three-phase rectifier's response to a negative sequence injected perturbing current does not contain the same frequencies as the response to a positive sequence perturbing current of the same nominal frequency and hence the negative and positive sequence response of the rectifier are different.

Chapter 9

FUTURE WORK

9.1 INTRODUCTION

The research presented in this thesis opens up a number of other and related areas for future research. This chapter suggests some of the directions that research could be pursued further or extended.

9.2 USING NON-LINEAR LOADS CONTROL TRANSFERS FOR SAF CONTROLLER DESIGN

The SISO transfer of the SAF when connected to the single-phase rectifier gives a method to determine that the SAF will operate in a stable manner. Using the FTM to determine how much, if any, the load current will change when the SAF operates allows the SAF designer or applications engineer to make a quantitative assessment of effectiveness of the SAF. The FTM contains a large amount of information about the load. Utilising this information in SAF controller design involves the incorporation of the non-linear, frequency and phase dependent load characteristics. This is most probably not a simple task. However, the load non-linearity can be represented by additive or multiplicative model uncertainty in modern control approaches. Such approaches have been made in the past but they have not used accurate load information. It may be that using this modern control approach will provide the ability to design controllers that allow for the sensitivity of the load and so may allow further improvement in power quality.

9.3 ANALYSIS AND MEASUREMENT OF OTHER LOADS

With increased use of power electronics to provide flexibility and energy efficiency the modern AC power system is increasingly becoming a collection of non-linear loads connected to a lightly damped transmission and distribution system. The behaviour of new loads, be they linear or non-linear, will to some degree be influenced by the existing loads connected to the AC system. This means that for any load the AC

system impedance will appear to have the form of a cross-coupled FTM. That is, the impedance seen by a load is the AC system impedance in parallel with the other, possibly non-linear, loads connected to the system. The situation where two or more non-linear loads are connected close electrically could be the cause of power quality problems not predicted by standard linear harmonic penetration analysis. As has been shown for large HVDC converters there is the possibility that rectifier loads can be the pivotal component in lightly damped or unstable system resonances. The possibility of a similar instability occurring in the distribution or supply network cannot be entirely ruled out. As an example, consider the common variable speed induction motor drive. Typically the induction motor load draws near constant power. The AC connection of the drive is typically through a six pulse diode rectifier. The effect of the constant power motor load is that if the AC voltage rises the rectifier AC current will fall. This is a negative resistance effectively producing negative damping. By analysing and modelling the rectifier drive system with an FTM the AC side behaviour of the motor drive can be predicted. The behaviour of the system can be measured by installing a suitably modified SAF at a variable speed motor drive installation. This measurement of the total system, including all the loads, will enable further understanding of non-linear rectifier effects in power systems.

The influence of the AC system impedance on any measurements made is significant. As AC system characteristics can vary with time, measurements can have a variability which may limit their usefulness. This can be eliminated as a cause of uncertainty by utilising an isolated generating system of known system impedance. Such a system is possible with wide bandwidth power amplifiers operating connected, through passive components to set the system impedance, to the non-linear load. Using a simulator, such as a real time digital simulator (RTDS), the amplifiers can be made to generate arbitrary waveforms so the operation of non-linear loads can be explored for both completely sinusoidal and distorted, non-sinusoidal AC system voltages. These isolated types of measurements can be used to confirm the analytic models, while those taken connected to the real AC system show the actual operating conditions.

The experimental system developed as part of this work or one similar to it is suitable to make measurements in both isolated and AC network connected situations.

9.4 ONLINE ADAPTATION OF SAF CONTROL

In this work the control system of the SAF has not been an area of emphasis. Sufficed to say that there are numerous SAF control strategies all attempting to perform some form of filtering. However, the one area in the controller design of SAF and other power conditioners that has not received much attention until recently, is the incorporation of the effect of the load into the design. The FTM representation of the single-phase rectifier load gives a total characterisation of the load and the measurements made show

that is is possible to determine a representative load FTM by making perturbations in the injected SAF current. Once a measurement is made it may be possible to alter controller parameters to improve the operation of the SAF or power conditioner. Such an adaptive scheme is possible but controller adaption effectively becomes part of the controller behaviour so it may be that caution and measurement inaccuracies prevent the rapid retuning of the SAF controller. Perhaps the simplest approach to adaptive control is the use of two controllers with the adaption switching between the two controllers or changing the mix of the two.

9.5 POSSIBLE METHODS FOR IDENTIFYING NON-LINEAR LOADS

The experimental measurements presented in Chapters 7 and 8 show that the experimental system described in Chapter 4 can make measurements that contain large amounts of information about the non-linear load. One way to utilise this information is in the identification of the load. This could be the identification of the type of load or one or a number of its features. It could also be the complete characterisation of the load to be used as a signature of the load.

9.5.1 Harmonic and inter-harmonic spectra as load signatures

The load current harmonic spectrum gives a large amount of information as to which type of load the SAF is connected. The single-phase rectifier current has the classic odd harmonic spectrum while the six pulse three-phase rectifier has a current spectrum that contains the first positive sequence, fifth negative sequence, seventh positive sequence, eleventh negative sequence and thirteen positive sequence... etc harmonics. These allow the simple recognition by a human being of the type of device. The possibility that the SAF could perform this function is one that may have some benefit. Consider the SAF detecting that it was connected to a single-phase rectifier. The sensitivity of the rectifier can be allowed for by the SAF by switching to a suitable control strategy. If the power conditioner makes a small perturbing current injections at a given frequency the frequency of the load current change indicates the type of load. Admittedly the behaviour of only the single-phase rectifier and the three-phase rectifier has been presented in this thesis, but the preponderance of these two load types means that a SAF that can identify them and somehow use this information could provide improved performance.

The SAF can at any time measure its own forward control transfer at any frequency. This allows the device itself to determine when operation is unstable. This is typically when the downstream impedance is capacitive. At such time the SAF can change its control strategy, perhaps moving to a voltage measurement system. Such an feature

ensures the SAF will not cause power quality degradation in the case that there are power factor correction capacitors downstream.

9.5.2 Phase dependency in perturbation responses

Non-linear rectifier loads have a phase dependency that can be measured. This was shown in the experimental results of Chapter 7. The phase dependency of the various frequency to frequency transfers can be measured by the SAF and as only non-linear loads have this harmonic frequency phase dependence the type and size of the non-linear load can be determined.

9.5.3 Change in load current when the SAF operates

The simplest measure of the non-linear load's sensitivity to SAF operation is to operate the SAF and measure what happens to the load current. This before and after strategy to measuring the load is a low cost way of measuring the load's behaviour as it requires only the difference between two currents to be computed. Continual measurement of the sensitivity requires continual adjustment of the SAF operation either by switching it on and off or by adjusting the level of the SAF operation. This may mean that changes in the load's behaviour because of an operating change or switching may not be detected. The choice of how often to measure the load's sensitivity may not be a trivial problem but the measurement itself does provide load sensitivity information.

9.6 THE EFFECTS OF NON-LINEAR LOADS AND SAFS IN AC SYSTEMS

It was noted in Chapter 3 that the load current measurement SAF effectively isolates any downstream load from the AC system preventing that load contributing to the damping of the AC system. The comparison between two linear loads and the single-phase rectifier in section 7.5 shows that the non-linear single-phase rectifier has a relatively low SISO impedance and contributes to system damping, especially at low frequencies. This means that power systems with non-linear loads attached may be made to be less stable when SAF are installed as the relatively large damping from the non-linear loads is removed. This effect requires investigation along with the identification of the source of low voltage supply level AC power system damping.

9.7 SAF STABILITY PROOFS

The SISO describing function transfer of a non-linear load gives (see section 7.3.5), it seems, adequate information to determine that the SAF will operate in a stable fashion. However, the concept that the operation of the SAF and the rectifier together

will always be stable cannot be proven by frequency domain plots that represent a single operating point. Proving stability requires a formal proof along the lines of a Liapurnov function or an exploration of the passivity of the system. Such an investigation is the domain of the specialist control theorist. While perhaps useful the investigation may end up only repeating the experience of the induction motor drive industry where stable sensorless torque control motor drives were used for a long while without formal proof that they were necessarily and always stable. However, proofs are enormously valuable as absolute building blocks for future research.

Chapter 10

CONCLUSIONS

As the cost of inadequate AC power system performance to the end user has increased, the quality of the electrical power has received close attention. This focus on power quality is occurring at the same time as power system operation is changing from a utility type approach to one where competition is used to force improved economic performance. Generally as power systems are operated closer to their limits the power quality has decreased. This has meant that the local solution to power quality problems, be they transient or steady state, is becoming more and more popular. One way to solve power quality problems is with a shunt active filter power conditioning device which typically removes harmonic currents that are generated by a non-linear rectifier type load. These rectifiers are becoming more and more common and their behaviour is typically neglected when the shunt active filter is used. In fact most, if not all, shunt active filter research is concerned with the control system to determine which parts of the load current to remove or retain.

Viewing the interconnection of the rectifier load, the AC system and the shunt active filter as a control system allows the interaction and mutual effects of the component parts of the total system to be determined. This small-signal control system approach identifies that the, possibly non-linear, load sensitivity is part of the forward control transfer of the SAF transfer. As all loads including non-linear rectifiers are sensitive to terminal voltage variation modelling the loads accurately allows their effect to be incorporated into the SAF operation and perhaps design. The connection of a capacitor in the downstream or load position of the current measurement SAF causes the total interconnected shunt active filter, AC system and load to be unstable. The existence of this instability means that the interaction of the SAF and non-linear loads could be unstable if the load can present a capacitive impedance. Also SAF operation removes the damping the load provides to the AC system. If loads provide a significant portion of the AC system damping this may have implications for AC system stability as more SAFs are installed.

The measurement of the non-linear load behaviour is accomplished by using a DSP controlled converter system. This is operated as both a SAF and as a source of small-

signal perturbing signals. These perturbing signals excite the small signal response of the interconnected AC system, SAF and non-linear load system. These are measured and the data stored in the DSP memory. FFTs of the data are then performed to determine the frequency components present in the response. The experimental system includes a central DSP processor connected to a FPGA that controls the output current by switching an IGBT bridge, manages the data collection and monitors faults. The SAF control and the collection and processing of the measurements is implemented in the DSP software. These experimental measurements are uploaded to a PC where they are displayed and stored to disk for post-processing.

The frequency domain is used to accurately represent the non-linear rectifier load. In the frequency domain the non-linear modulation becomes a linear frequency coupling or transfer. By extending each frequency transfer so the real and imaginary components are represented separately, modulation can be accurately represented by a two by two matrix or tensor. The tensor approach allows the accurate representation of the magnitude-phase dependence that occurs in rectifier loads, which cannot be represented by a complex multiplication. This linearised FTM representation of the switching of the rectifier is an accurate and suitable approach to the analysis and modelling of rectifiers.

The frequency domain FTM analysis of single-phase rectifier is accomplished by using a small perturbing signal to find the response of the rectifier. The total rectifier transfer is developed by using partial transfers which are the partial differentials of the variables. This approach means each transfer is determined separately simplifying the analysis. The AC side and DC side voltages are used as the inputs and this means the AC side and DC side currents are the outputs. The analysis is structured this way because the currents are discontinuous. Two mechanisms are identified as playing parts in the total transfer of the single-phase rectifier. These are the base switching and the the switching instant variation. The analysis of the base switching effect is made by developing the voltage to current transfer matrices using a number of component waveforms and combining their Fourier series. Suitably accurate first order linearisations to determine the switching instant modulation effects are made. However, the switching instant modulation effects are found to be second order only. This means that they do not occur at frequencies that relate to the switching instant variation frequency but rather to twice this frequency. It also means that these effects are considerably smaller than the first order effects. Therefore the switching instant effects can be ignored in the analysis of the single-phase rectifier. Each partial transfer is confirmed by time domain simulation. The total transfer of the single-phase rectifier is formed from the partial transfers and the DC side filter admittance. The analytic transfer is confirmed as being accurate by comparison to time domain simulation.

Further validation of the analytic approach and results is provided by the experimental measurements of single-phase rectifier behaviour, which show good agreement

with those predicted by the analytic model. The measurements show that is is possible to make experimental measurements of a single-phase rectifier load. A single frequency input single frequency output describing function of the SAF forward transfer indicates the total system is stable and SAF operation confirms this. When the SAF is operating this describing function transfer has increased magnitude at frequencies below 200Hz. This shows that SAF operation increases the sensitivity of the single-phase rectifier load.

Comparison of the single frequency transfer to that of linear loads with the same power consumption shows that the single-phase rectifier load has considerably higher sensitivity which indicates that the damping provided by non-linear loads could be relatively large. The analytic FTM method correctly predicts the change in load current that SAF operation causes so it is suitable to predict the effect that the SAF has on the single-phase rectifier load current. When sequence perturbing currents are injected to make measurements of three-phase rectifiers in both discontinuous and continuous conduction the results show that the FTM method is suitable to represent three-phase rectifiers. The results measured using the three-phase sequence FFT shows that the three-phase rectifier is best viewed as a sequence coupling device. The results also show that analytic models for three-phase rectifiers based on the small signal FTM approach can be generated in the same way as for a single-phase rectifier. The development of this complete, linear, analytically correct, model of a single-phase rectifier allows the interaction of this non-linear load with the power system and the increasingly used SAF to be analysed and explored.

Appendix A

USING A REAL VALUE FFT ROUTINE TO GENERATE A COMPLEX FFT

The FFT operation is linear and so by superposition the FFT of the sum of two signals is the sum of the FFTs of the same signals (A.1).

$$\mathbf{FFT}(A + jB) = \mathbf{FFT}(A) + j\mathbf{FFT}(B) \tag{A.1}$$

Each FFT result has a real and complex part (A.3).

$$\mathbf{FFT}(A) = Re\mathbf{FFT}(A) + jIm\mathbf{FFT}(A) \tag{A.2}$$

$$\mathbf{FFT}(B) = Re\mathbf{FFT}(B) + jIm\mathbf{FFT}(B) \tag{A.3}$$

This means that equation (A.1) can be implemented in the code using (A.4).

$$\begin{aligned} \mathbf{FFT}(A + jB) &= \mathbf{FFT}(A) + j\mathbf{FFT}(B) \\ &= Re\mathbf{FFT}(A) + jIm\mathbf{FFT}(A) + j(Re\mathbf{FFT}(B) + jIm\mathbf{FFT}(B)) \\ &= Re\mathbf{FFT}(A) - Im\mathbf{FFT}(B) + j(Im\mathbf{FFT}(A) + Re\mathbf{FFT}(B)) \end{aligned} \tag{A.4}$$

In order to use pre-existing real value FFT code, a complex FFT was constructed. This uses the linearity of the FFT to allow two real FFTs to be calculated and the resulting complex results to be combined to perform the complex FFT.

Appendix B

FOURIER SERIES AND WAVEFORM MANIPULATION

B.1 INTRODUCTION

Throughout this thesis waveforms have been described by Fourier series. The Fourier series is the time domain representation of the Fourier transform for repetitive wave shapes.

B.2 FOURIER SERIES OF A SAMPLING FUNCTION

The time domain train of impulses with occuring at angles $0, 2\pi..2n\pi$ at frequency of ω_0 that is typically used to perform the sampling function has the Fourier series shown in equation (B.1).

$$SF(\omega_0 t) = \frac{1}{2\pi} + \frac{1}{\pi}\sum_{m=1}^{\infty} \sin(m\omega_0 t + \frac{\pi}{2}) \tag{B.1}$$

B.3 TIME SHIFTING OF WAVEFORMS

When a waveform is time shifted the new Fourier series is found by substituting with a new time variable for the old time variable. As an example consider the waveform described by the Fourier series in (B.1) time shifted by the time $t_0 = \frac{\theta_1}{\omega_0}$

$$\begin{aligned} SF(\omega_0 t) &= \frac{1}{2\pi} + \frac{1}{\pi}\sum_{m=1}^{\infty} \sin(m\omega_0(t - t_0) + \frac{\pi}{2}) \\ &= \frac{1}{2\pi} + \frac{1}{\pi}\sum_{m=1}^{\infty} \sin(m\omega_0 t - m\theta_1 + \frac{\pi}{2}) \end{aligned} \tag{B.2}$$

This shift by the angle of the base switching instant is typical of the Fourier series manipulations performed throughout this thesis. Any other time shift can be accomplished by similar substitution.

B.4 SWITCHING WAVEFORM FOURIER SERIES

The Fourier transform is linear which means that the Fourier series of a sum is the sum of the component Fourier series. This approach is used to determine the direct transfers for the single-phase rectifier. The switching function is the sum of two waveforms. These are both of the same form but they have different time shifts and signs. Figure B.1 shows the base waveform (a) and the final switching function (d). The base switching function pulse has Fourier series (B.3).

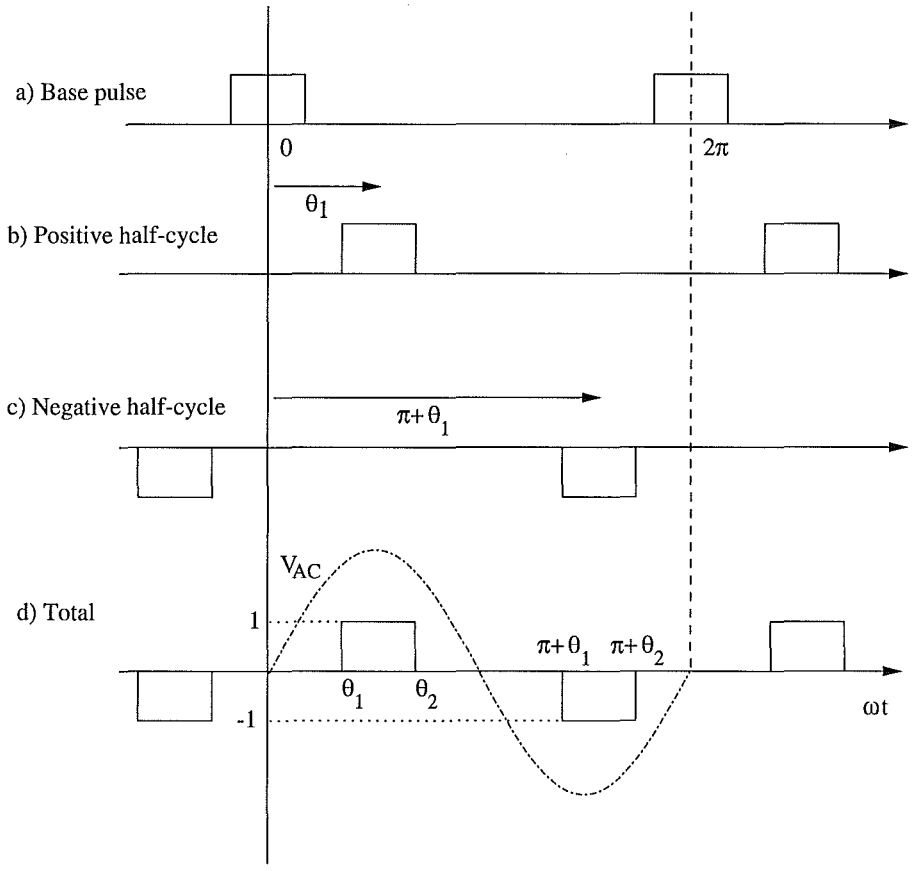

Figure B.1 Single-phase switching function development showing time shifting and sign change.

$$\begin{aligned}\Psi_{Base} &= \frac{1}{2\pi}(\theta_2 - \theta_1) \\ &+ \sum_{m=1}^{m=\infty} \frac{2}{m\pi} \sin\left(\frac{m\theta_2 - m\theta_1}{2}\right) \sin(m\omega_0 t + \frac{\pi}{2})\end{aligned} \tag{B.3}$$

In order to time shift the waveform, the new time of $(t - t_0)$ is substituted for t in (B.3) which with $t_0 = \frac{\theta_1+\theta_2}{2\omega_0}$ gives (B.4).

$$\begin{aligned}\Psi_{Shifted} &= \frac{1}{2\pi}(m\theta_2 - m\theta_1) \\ &+ \sum_{m=1}^{m=\infty} \frac{2}{m\pi} \sin\left(\frac{m\theta_2 - m\theta_1}{2}\right) \sin(m\omega_0 t - m\frac{\theta_1+\theta_2}{2} + \frac{\pi}{2}) \end{aligned} \quad \text{(B.4)}$$

The negative half cycle switching pulse, Figure B.1(c), is created by shifting the base waveform by $\pi + \theta_1$ and multiplying by -1. By adding these two shifted Fourier series the total switching function series is found (B.5)

$$\begin{aligned}\Psi_{Total} &= \frac{4}{m\pi} \sin\left(\frac{m\theta_1 - m\theta_2}{2}\right) \sin\left(m\omega_0 t - m\frac{\theta_1+\theta_2}{2} + \frac{\pi}{2}\right) \\ &\quad for\ m = 1, 3, 5, 7... \\ \Psi_{Total} &= 0 \\ &\quad for\ m = 0, 2, 4, 6...\end{aligned} \quad \text{(B.5)}$$

B.5 PULSE AMPLITUDE MODULATED SPECTRUM DEVELOPMENT

The pulse amplitude modulated (PAM) waveforms are generated by sampling the pulse height waveform (B.6) at the appropriate instant with a sampling function or train of impulses (B.2).

$$h = b\sin(k\omega t + \delta_k) \quad \text{(B.6)}$$

The result is a impulse train with its height the value of (B.6) at the sampling instants. The Fourier series of the waveform from multiplying (B.6) by the impulse train of (B.1) shifted by θ_1 is (B.7).

$$\begin{aligned}SF(\omega_0 t) &= \frac{b}{2\pi} \sin(k\omega_0 t + \delta_k) \\ &+ \frac{b}{2\pi} \sum_{m=1}^{\infty} \sin((m+k)\omega_0 t - m\theta_1 + \delta_k) \\ &- \frac{b}{2\pi} \sum_{m=1}^{\infty} \sin((m-k)\omega_0 t - m\theta_1 - \delta_k)\end{aligned} \quad \text{(B.7)}$$

The square pulse shape is added by convolving (B.7) with a suitable pulse (B.3) the Fourier transform of which is shown in equation (B.8). Time domain convolution is equivalent to frequency domain multiplication of the Fourier transforms.

$$FT(\Psi_{Base}) = \frac{\sin(2\pi f \frac{\theta_2-\theta_1}{2})}{\pi f} \tag{B.8}$$

The Fourier transform of the sampled sinewave (B.7) is defined as $FT(SS)$. The Fourier transform of the base pulse (B.8) is then multiplied with $FT(SS)$ to give (B.9).

$$FT(PAM) = \frac{\sin(2\pi f \frac{\theta_2-\theta_1}{2})}{\pi f} * FT(SS) \tag{B.9}$$

$FT(SS)$ is of the form of $\delta(f - kf_0)$ which means that the contribution of the switching function term can be taken outside the inverse FT integral. This means that the Fourier series has the same frequency components as the sampled sinusoid Fourier series but their magnitudes are modified by the $\frac{sinx}{x}$ or sinc contribution of the base pulse FT. The waveform is then shifted by half the square pulse width to form the final PAM waveform in the correct place. The Fourier series of the PAM waveform is shown in (6.10).

$$\begin{aligned} PAM(\omega_0 t) = {} & \frac{bd}{2\pi}\text{sinc}(\frac{kd}{2\pi})\sin(k\omega_0 t - k(\frac{d}{2}) + \delta_k) \\ + {} & \frac{bd}{2\pi}\sum_{m=1}^{\infty}\text{sinc}((m+k)\frac{d}{2\pi})\sin((m+k)\omega_0 t - (m+k)(\frac{d}{2}) - m\theta_1 + \delta_k) \\ - {} & \frac{bd}{2\pi}\sum_{m=1}^{\infty}\text{sinc}((m-k)\frac{d}{2\pi})\sin((m-k)\omega_0 t - (m-k)(\frac{d}{2}) - m\theta_1 - \delta_k) \end{aligned}$$

$$\begin{aligned} \text{where } d &= \text{pulse width} \\ &= (\theta_2 - \theta_1) \end{aligned} \tag{B.10}$$

Appendix C

SWITCHING INSTANT MODULATION SPECTRA AND CONSDERATIONS

C.1 FIRST ORDER APPROXIMATION OF SWITCHING INSTANT MODULATION SPECTRUM

The spectrum of the switching instant modulation that the Fourier series, equation (C.1), shows contains frequencies that depend on both the harmonic order m and the order n of the Bessel function that determines the magnitude. For a switching instant variation of $b\cos(k\omega_0 t + \delta_k)$ the resulting spectrum is (C.1)

$$\begin{aligned}
\Psi_{Simod} &= \frac{2}{m\pi}\left[J_0(mb) - 1\right]\sin(m\omega_0 t - m\theta_1) \\
&- \frac{2}{\pi}\sum_{n=1}^{\infty}\frac{J_n(mb)}{m}\left[\sin(m+nk)\omega_0 t - m\theta_1 + n\delta_k - \frac{n\pi}{2}\right] \\
&- \frac{2}{\pi}\sum_{n=1}^{\infty}\frac{J_n(mb)}{m}\left[\sin(m-nk)\omega_0 t - m\theta_1 - n\delta_k - \frac{n\pi}{2}\right] \\
&\quad \text{for } m = 1, 3, 5.. \\
\Psi_{Simod} &= 0 \\
&\quad \text{for } m = 2, 4, 6..
\end{aligned} \tag{C.1}$$

If the spectrum is evaluated for $n = 1$ only then the spectrum becomes that of a train of impulses multiplied by the switching instant variation. The approximation is suitable because the first kind Bessel function's first order approximation is as shown in equation (C.2).

$$\frac{J_1(mb)}{m} = \frac{b}{2} \tag{C.2}$$

This means that the first order approximation to the switching instant modulation

spectrum is as shown in equation C.3

$$\begin{aligned} SIV_{1storder}(\omega_0 t) &= \left[\frac{1}{2\pi} + \frac{1}{\pi}\sum_{m=1}^{\infty}\sin(m\omega_0 t + \frac{\pi}{2})\right]\cos(k\omega_0 t + \delta_k + \frac{\pi}{2}) \\ &= \frac{1}{2\pi}\sin(k\omega_0 t + \delta_k + \frac{\pi}{2}) \\ &\quad + \frac{1}{2\pi}\sum_{m=1}^{\infty}\sin((m+k)\omega_0 t + \delta_k + \frac{\pi}{2}) \\ &\quad + \frac{1}{2\pi}\sum_{m=1}^{\infty}\sin((m-k)\omega_0 t - \delta_k + \frac{\pi}{2}) \end{aligned} \tag{C.3}$$

By noting the sign change and the phase change by π this is equivalent to equation (C.1). This means that if only first order frequencies are considered then the switching instant variation spectrum is equivalent to that a sinusoidally varying train of impulses.

C.1.1 Spectra of switching instant modulation - verification

In order to verify that the switching instant variation spectrum correctly represents the spectrum of the switching instant waveform, a switching instant modulator was coded into MATLAB. An example of the output is shown in Figure C.1.

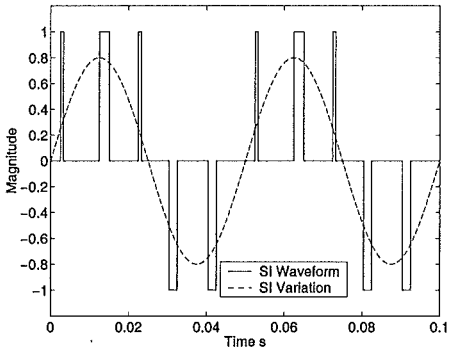

Figure C.1 Example DC side switching instant variation waveform - Variation is exaggerated to illustrate the effect

The FFT of this waveform, Figure C.1.1, has the same first order frequency components as the switching instant approximation coded into a FTM, Figure C.1.1. This shows the accuracy and suitability of the first order approximation. The difference between the two in Figure C.3 shows that the magnitude of the difference rises as the frequency increases but remains relatively small if compared to the magnitude of the first order frequency magnitudes.

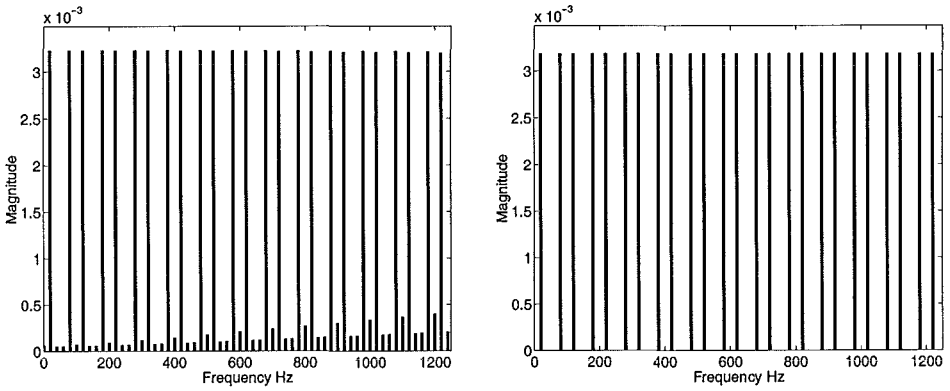

(a) From time domain (b) From FTM

Figure C.2 Switching instant variation spectra determine (magnitude)

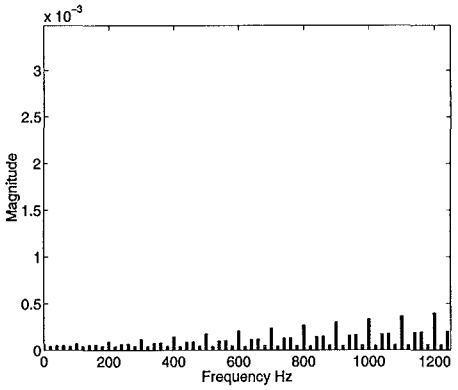

Figure C.3 Difference between FTM and FFT (magnitude of difference)

C.2 SECOND ORDER EFFECTS OF REAR SWITCHING INSTANT VARIATION.

A triangular shaped regularly positioned waveform where the height is proportional to the sinusoidally modulated width has an area that varies at twice the frequency of the width. However the assertion that this means that the waveform has no frequency component at the frequency of the width variation is perhaps not obvious. Consider the first order approximation to the switching instant modulation spectrum introduced above in section C.1. This represents the frequency components that have the larger magnitudes. By multiplying the Fourier series of the width variation by that of the height variation the total Fourier series can be found. Assuming the proportionality of the height and width is k_{prop} then the spectrum of the triangular waveform is equation (C.5).

$$k_{prop}\,[SIV_{1storder}(\omega_0 t)]^2 \;=\; \frac{1}{2\pi}\sin(k\omega_0 t + \delta_k + \frac{\pi}{2})$$

$$
\begin{aligned}
&+\frac{1}{2\pi}\sum_{m=1}^{\infty}\sin((m+k)\omega_0 t+\delta_k\frac{\pi}{2}) \\
&+\frac{1}{2\pi}\sum_{m=1}^{\infty}\sin((m-k)\omega_0 t-\delta_k+\frac{\pi}{2}) \qquad \text{(C.4)}\\
=\ & \frac{1}{4(\pi)^2}\sum_{m=1}^{\infty}(3\cos(0)-\frac{1}{2}\cos(2k\omega_0 t+2\delta_k) \\
+\ & 2\cos(m\omega_0 t)-2\cos((m+2k)\omega_0 t+2\delta_k) \\
+\ & \frac{1}{2}\cos((2m+2k)\omega_0 t+2\delta_k)) \qquad \text{(C.5)}
\end{aligned}
$$

This shows that the triangular shape with height varying proportionally to the sinusoidally varying width at frequency $k\omega_0 t$ has no frequency component at frequency $k\omega_0 t$.

Appendix D

CODING FOURIER SERIES INTO FREQUENCY TRANSFER MATRIX FORM

D.1 INTRODUCTION

The FTM is the method used to represent the frequency transfers in and around the rectifiers in this thesis. Converting frequency transfer information into FTM form is a relatively simple process.

D.2 FTM FORM OF FOURIERS SERIES

When an input signal (D.1)

$$\Delta = D_k \sin(k\omega_0 t + \delta_k) \tag{D.1}$$

gives rise to an output signal (D.2)

$$Sig = S_l \sin(l\omega_0 t + \delta_l + \delta_k) \tag{D.2}$$

the FTM sub-matrix, S, that relates the input signal phasor to the output signal phasor has the form

$$S = \frac{S_l}{D_k} \begin{bmatrix} \cos(\delta_l) & -\sin(\delta_l) \\ \sin(\delta_l) & \cos(\delta_l) \end{bmatrix} \tag{D.3}$$

If the output is dependent on the conjugate of the input signal

$$Sig = S_l \sin(l\omega_0 t + \delta_l - \delta_k) \tag{D.4}$$

then the the sub-matrix has the form

$$S = \frac{S_l}{D_k} \begin{bmatrix} \cos(\delta_l) & \sin(\delta_l) \\ \sin(\delta_l) & -\cos(\delta_l) \end{bmatrix} \tag{D.5}$$

Using these two identities allows the FTM for any transfer to be generated and it is simple matter to convert Fourier series information to FTM form. Placing the correct sub-matrix at the correct position in the FTM ensures that the transfer from the correct input frequency to the correct output frequency occurs.

D.3 MULTIPLICATION OF TWO COMPLEX NUMBERS

Consider the case where two complex numbers $(x + jy)$ and $(w + jz)$ are represented in polar form

$$x = r_1 \cos(\delta_1) \tag{D.6}$$

$$y = r_1 \sin(\delta_1) \tag{D.7}$$

$$w = r_2 \cos(\delta_2) \tag{D.8}$$

$$z = r_2 \sin(\delta_2) \tag{D.9}$$

The two complex numbers multiplication result is $xy - wz + j(xz + wy)$. Substituting (D.6) through (D.9) gives

$$\begin{aligned} xy - wz &= r_1 r_2 \cos(\delta_1)\cos(\delta_2) - r_1 r_2 \sin(\delta_1)\sin(\delta_2) \\ &= r_1 r_2 \left[\frac{1}{2}\cos(\delta_1 - \delta_2) + \frac{1}{2}\cos(\delta_1 + \delta_2) - \frac{1}{2}\cos(\delta_1 - \delta_2) + \frac{1}{2}\cos(\delta_1 - \delta_2)\right] \\ &= r_1 r_2 \cos(\delta_1 + \delta_2) \end{aligned} \tag{D.10}$$

and

$$\begin{aligned} xz + wy &= r_1 r_2 \sin(\delta_2)\cos(\delta_1) + r_1 r_2 \sin(\delta_1)\cos(\delta_2) \\ &= r_1 r_2 \left[\frac{1}{2}\sin(\delta_2 - \delta_1) + \frac{1}{2}\sin(\delta_2 + \delta_1) - \frac{1}{2}\sin(\delta_2 - \delta_1) + \frac{1}{2}\sin(\delta_2 + \delta_1)\right] \\ &= r_1 r_2 \sin(\delta_1 + \delta_2) \end{aligned} \tag{D.11}$$

Notice that these two results, (D.10) and (D.11), have an angle that is the sum of the angles of the two original signals. This shows that multiplying one complex number by another produces a result that has an angle that is the sum of the two contributing angles and so this means it is impossible to generate the difference between the angles that is required for a difference term.

Appendix E

TRANSFER SIMULATION RESULTS

E.1 INTRODUCTION

This appendix contains further results to confirm the accuracy of the single-phase rectifier analysis. The component transfers from the analysis are compared to those from time domain simulation with MATLAB/Simulink as previously in Chapter 6. There are two more examples for the ΔV_{AC} to ΔI_{DC} or C transfer and a single transfer example for each of the ΔV_{AC} to ΔI_{AC} or A, ΔV_{DC} to ΔI_{DC} or D, and ΔV_{DC} to ΔI_{AC} or B transfers.

E.2 ΔV_{AC} TO ΔI_{DC} - THE C TRANSFER

Figure 6.33(a) shows the simulated current for a 0.5V 106.25Hz voltage. This matches the current from the FTM which is shown in Figure E.1(b). The detailed comparison E.1(c) once again shows exceptionally good match. The spectral comparison shown in Figures E.2(a) through E.2(d) once again confirms the accuracy and effectiveness of the analysis.

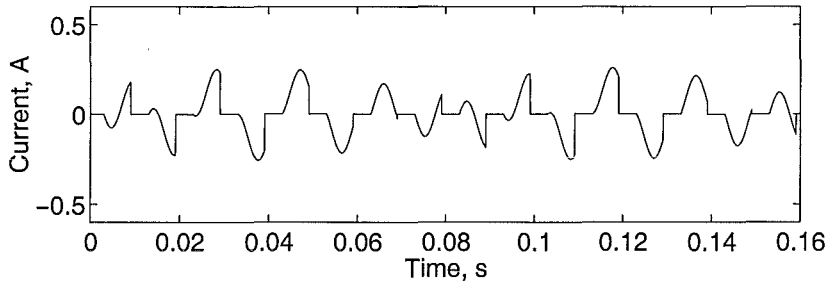

(a) Time domain simulation waveform

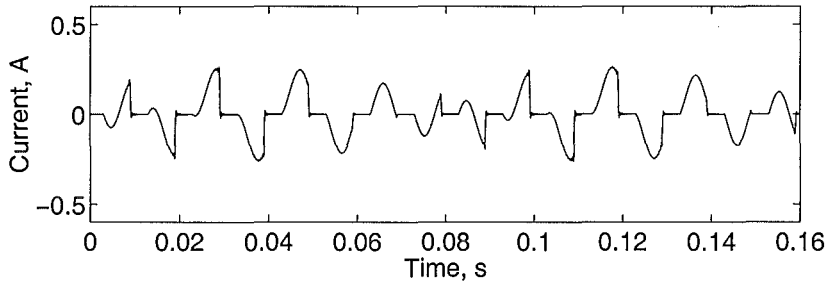

(b) FTM synthesised waveform (FTM bandwidth 2500Hz)

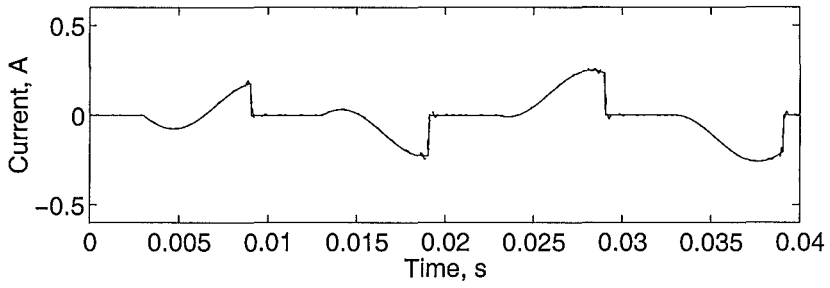

(c) Zoom on time domain (solid) and FTM waveform (dashed) (FTM bandwidth 2500Hz)

Figure E.1 Current waveforms for ΔV_{AC} to ΔI_{DC} transfers for $kf_0 = 106.25$ Hz.

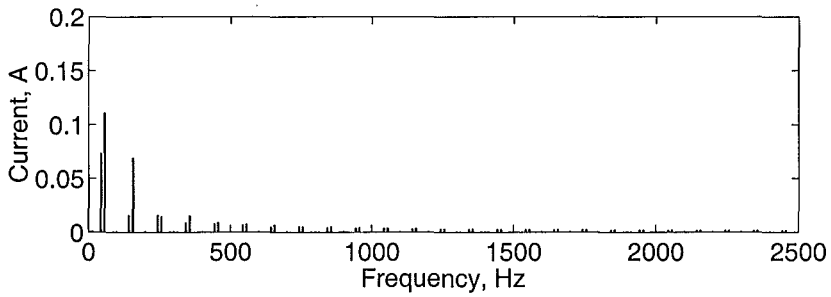

(a) Spectrum from time domain simulation (magnitude)

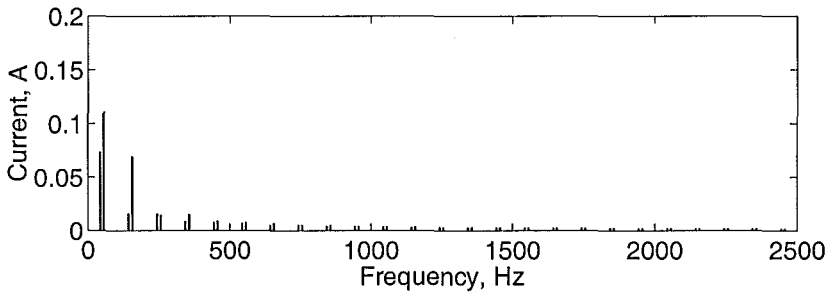

(b) FTM Spectrum (Magnitude)

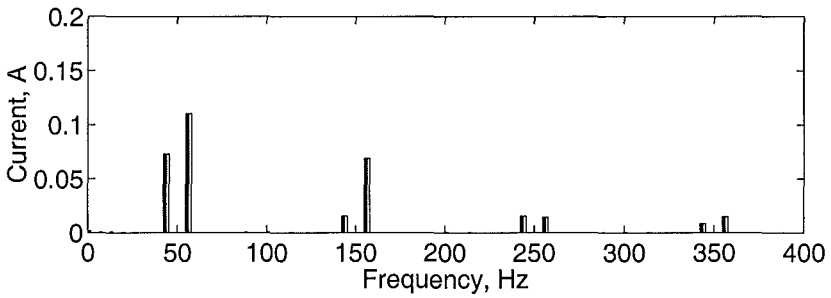

(c) Detailed comparison of magnitudes (Dark FTM light Time domain simulation)

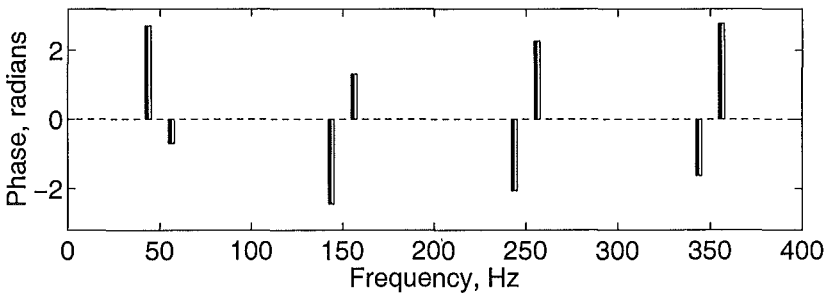

(d) Detailed comparison of phases (Dark FTM light Time domain simulation)

Figure E.2 Spectra of current waveforms for ΔV_{AC} to ΔI_{DC} transfers for $kf_0 = 106.25$ Hz.

E.3 ΔV_{AC} TO ΔI_{AC} - THE A TRANSFER

Figures E.3(a), E.3(b) and E.3(c) shows the time domain waveforms for a voltage at 106.25Hz with a magnitude of 0.5V. The spectrum results of E.4(a) through E.4(d) show the appropriateness of the analysis method.

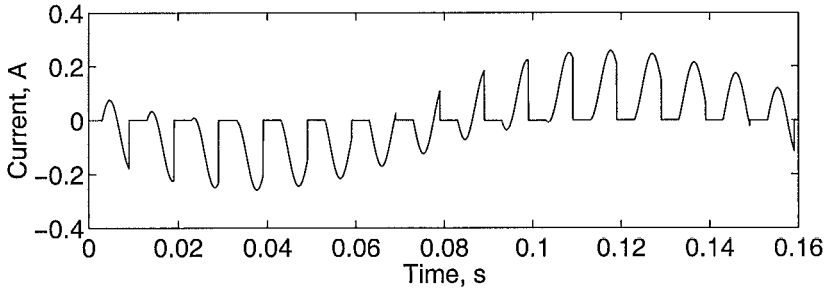

(a) Time domain simulation waveform

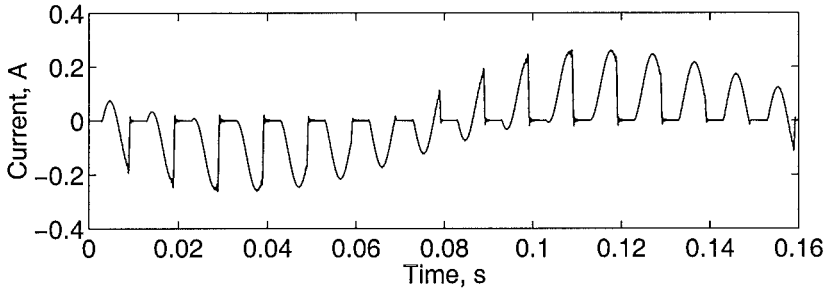

(b) FTM synthesised waveform (FTM bandwidth 2500Hz)

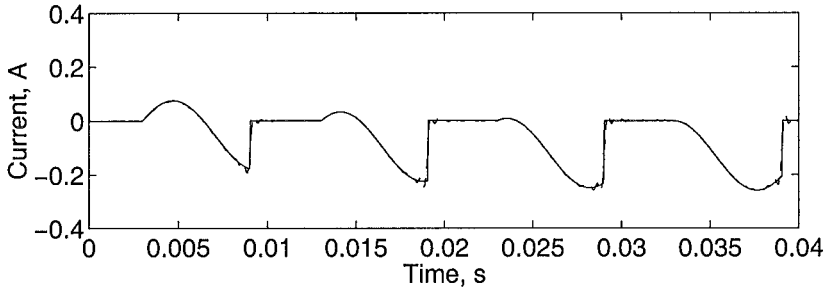

(c) Zoom on time domain (solid) and FTM waveform (dashed) (FTM bandwidth 2500Hz)

Figure E.3 Current waveforms for ΔV_{AC} to ΔI_{AC} transfers for $kf_0 = 106.25$ Hz.

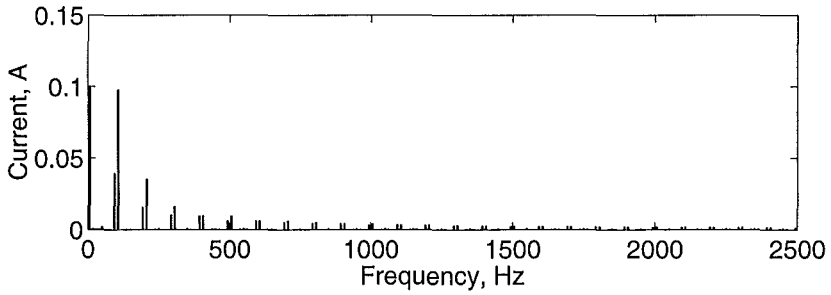

(a) Spectrum from time domain simulation (magnitude)

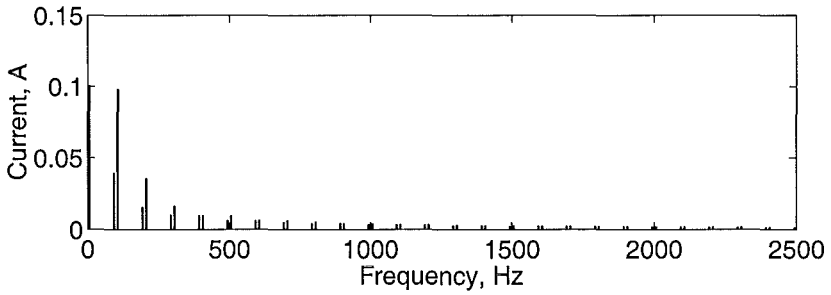

(b) FTM Spectrum (Magnitude)

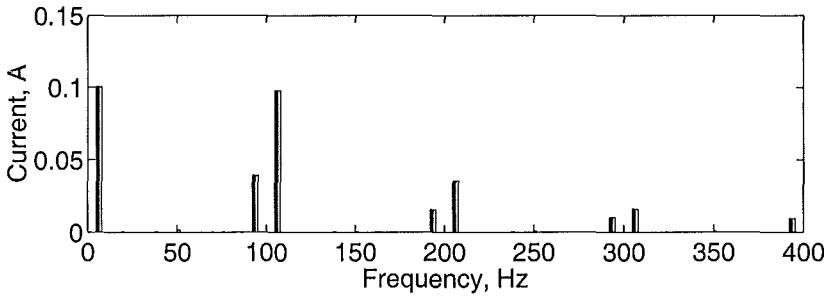

(c) Detailed comparison of magnitudes (Dark FTM light Time domain simulation)

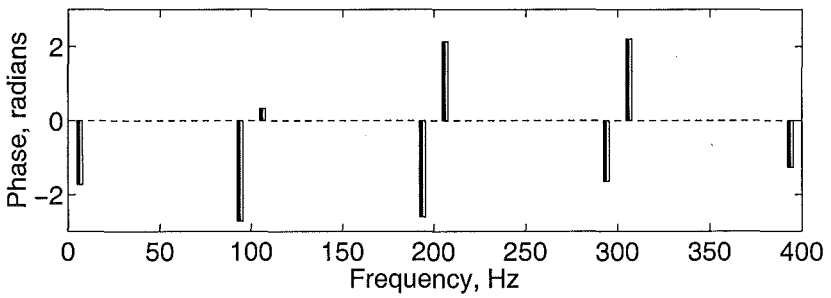

(d) Detailed comparison of phases (Dark FTM light Time domain simulation)

Figure E.4 Spectra of current waveforms for ΔV_{AC} to ΔI_{AC} transfers for $kf_0 = 106.25$. Hz

E.4 ΔV_{DC} TO ΔI_{DC} - THE D TRANSFER

Similar time domain waveform results for a voltage of 75Hz are shown in Figures E.5(a), E.5(b), E.5(c). The spectral comparisons, Figures E.6(a) through E.6(d) shows that the analysis is accurate for this the ΔV_{DC} to ΔI_{DC} transfer also.

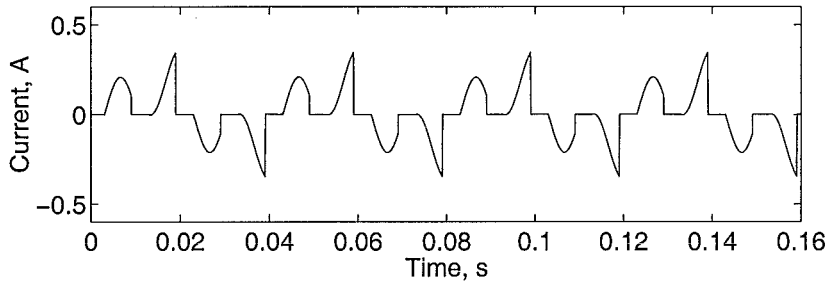

(a) Time domain simulation waveform

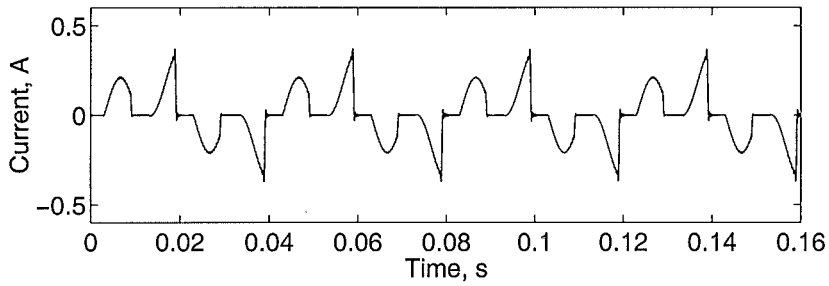

(b) FTM synthesised waveform (FTM bandwidth 2500Hz)

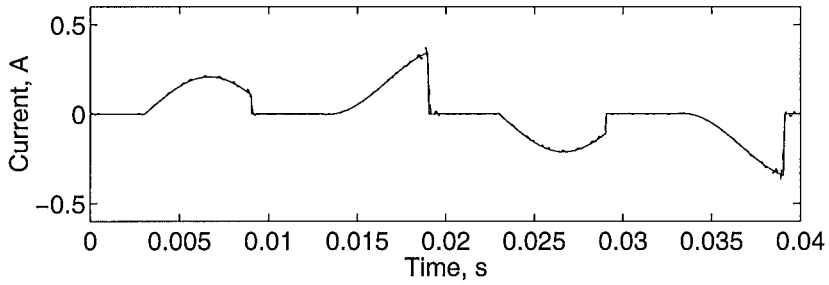

(c) Zoom on time domain (solid) and FTM waveform (dashed) (FTM bandwidth 2500Hz)

Figure E.5 Current waveforms for ΔV_{DC} to ΔI_{DC} transfers for $kf_0 = 75$ Hz.

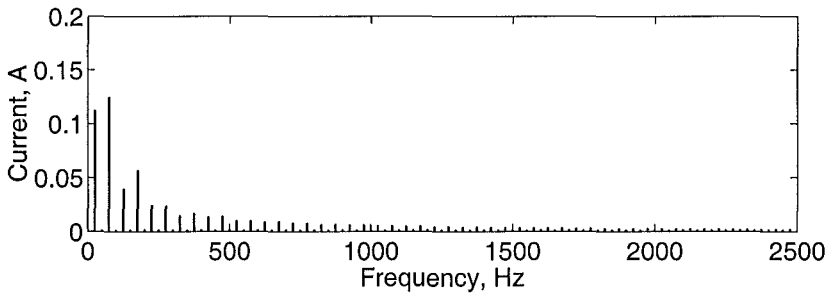

(a) Spectrum from time domain simulation (magnitude)

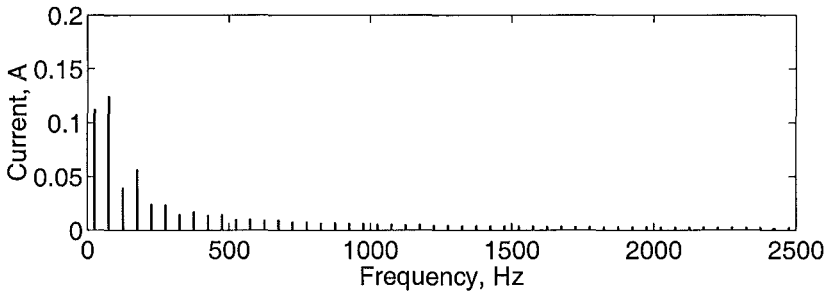

(b) FTM Spectrum (Magnitude)

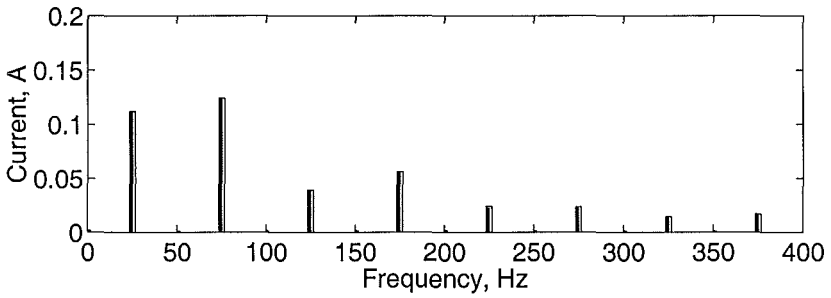

(c) Detailed comparison of magnitudes (Dark FTM light Time domain simulation)

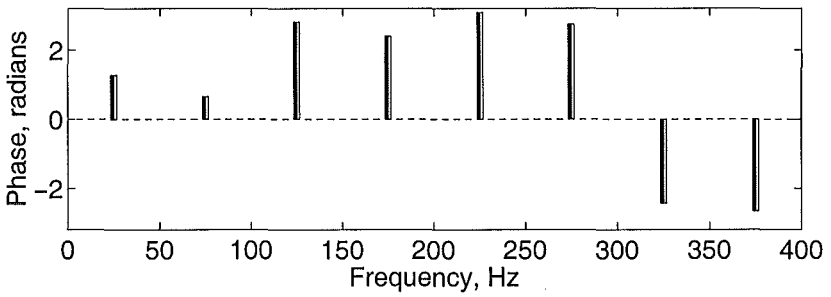

(d) Detailed comparison of phases (Dark FTM light Time domain simulation)

Figure E.6 Spectra of current waveforms for ΔV_{DC} to ΔI_{DC} transfers for $kf_0 = 106.25$. Hz

E.5 ΔV_{DC} TO ΔI_{AC} - THE B TRANSFER

Finally to confirm the ΔV_{DC} to ΔI_{AC} transfer the AC side current waveform is shown for DC side voltage of 0.5V and frequency of 106.25 Hz in Figures E.7(a). The comparison between the spectra is shown in Figures E.8(a) through E.8(d).

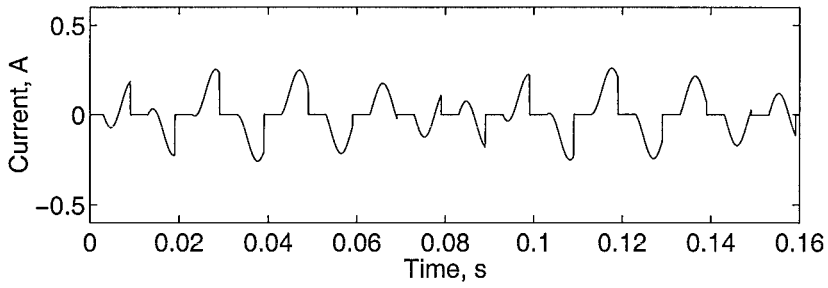

(a) Time domain simulation waveform

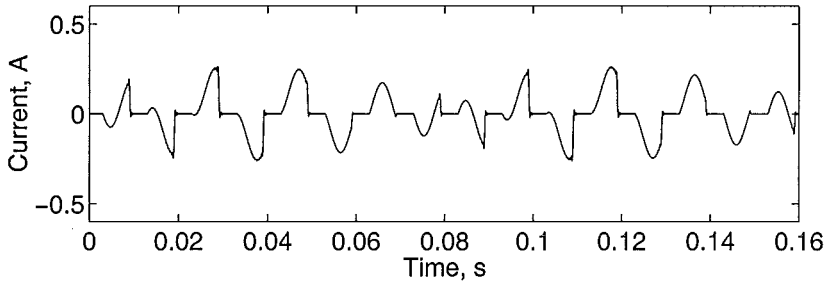

(b) FTM synthesised waveform (FTM bandwidth 2500Hz)

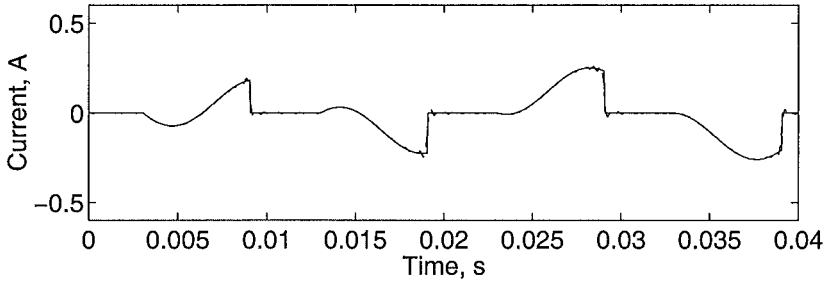

(c) Zoom on time domain (solid) and FTM waveform (dashed) (FTM bandwidth 2500Hz)

Figure E.7 Current waveforms for ΔV_{DC} to ΔI_{AC} transfers for $kf_0 = 106.25$ Hz.

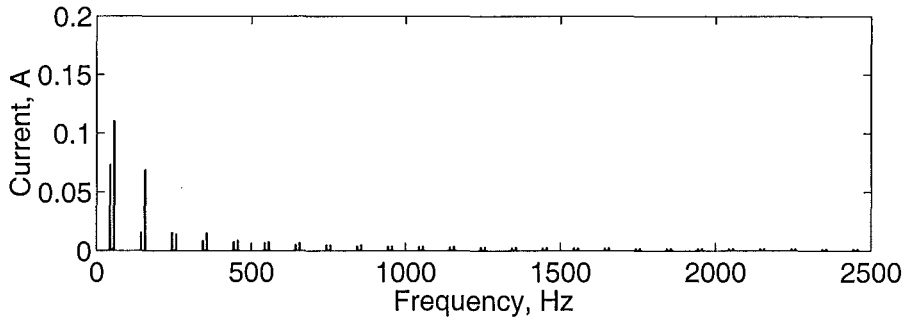

(a) Spectrum from time domain simulation (magnitude)

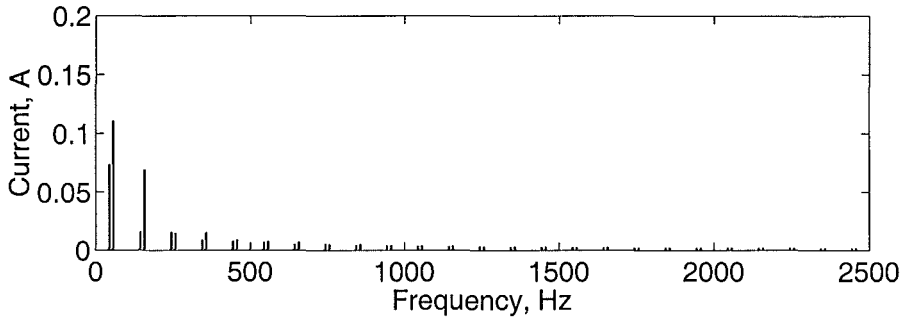

(b) FTM Spectrum (Magnitude)

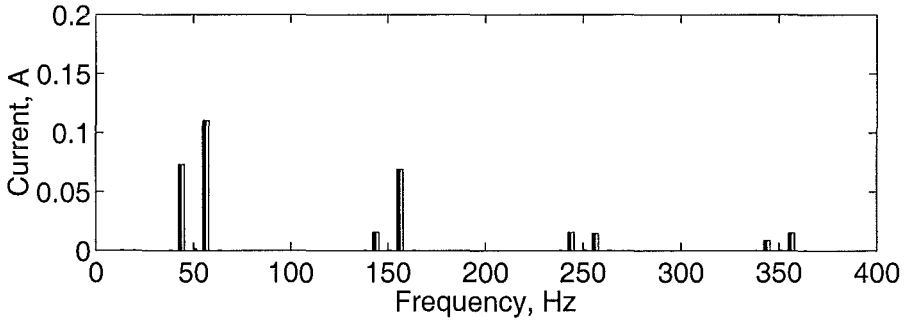

(c) Detailed comparison of magnitudes (Dark FTM light Time domain simulation)

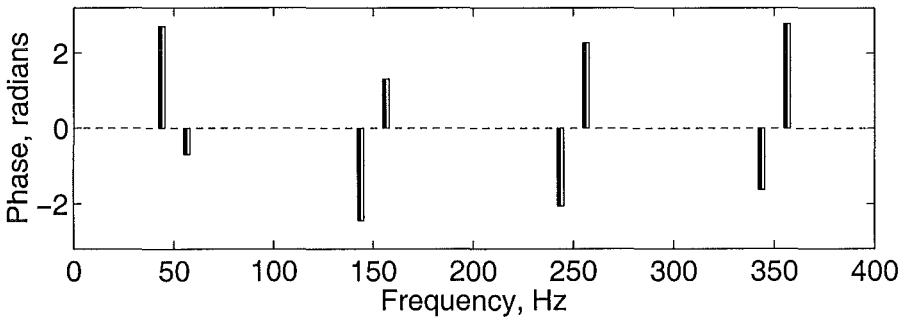

(d) Detailed comparison of phases (Dark FTM light Time domain simulation)

Figure E.8 Spectra of current waveforms for ΔV_{DC} to ΔI_{AC} transfers for $kf_0 = 106.25$. Hz

Appendix F

PSCAD CIRCUIT OF EMTDC SIMULATION

The PSCAD/EMTDC circuit of the simulation used to determine the behaviour of the single-phase rectifier and therefore confirm the analytic results is shown in Figure F.1. This shows the voltage source, the rectifier and the variable frequency voltage source used to generate the perturbing voltage. Figure F.2 shows the PSCAD/EMTDC circuit of the rectifier/SAF system used in confirming the effect of SAF operation on the rectifier.

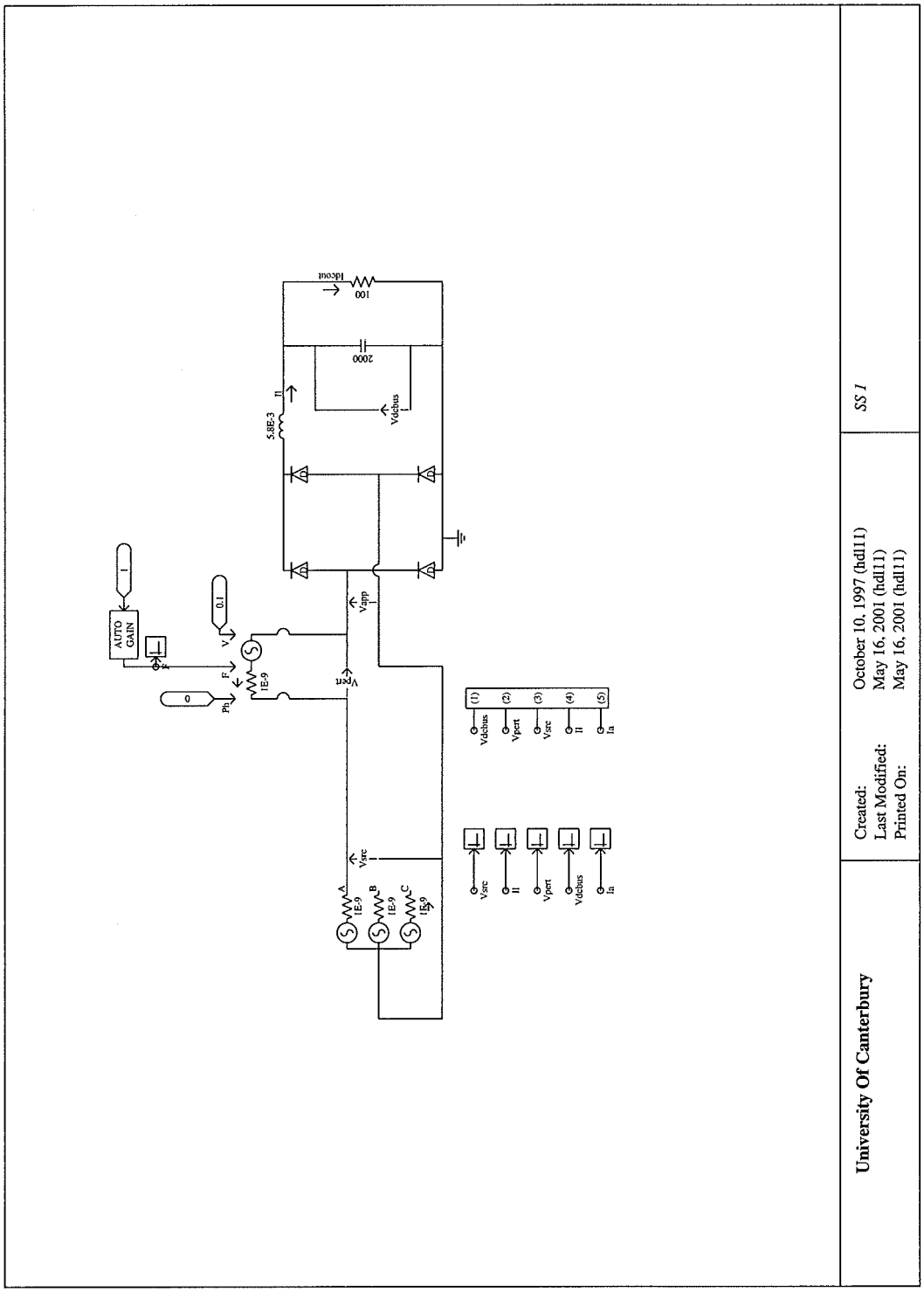

Figure F.1 PSCAD circuit of single-phase rectifier simulation to show the model validity

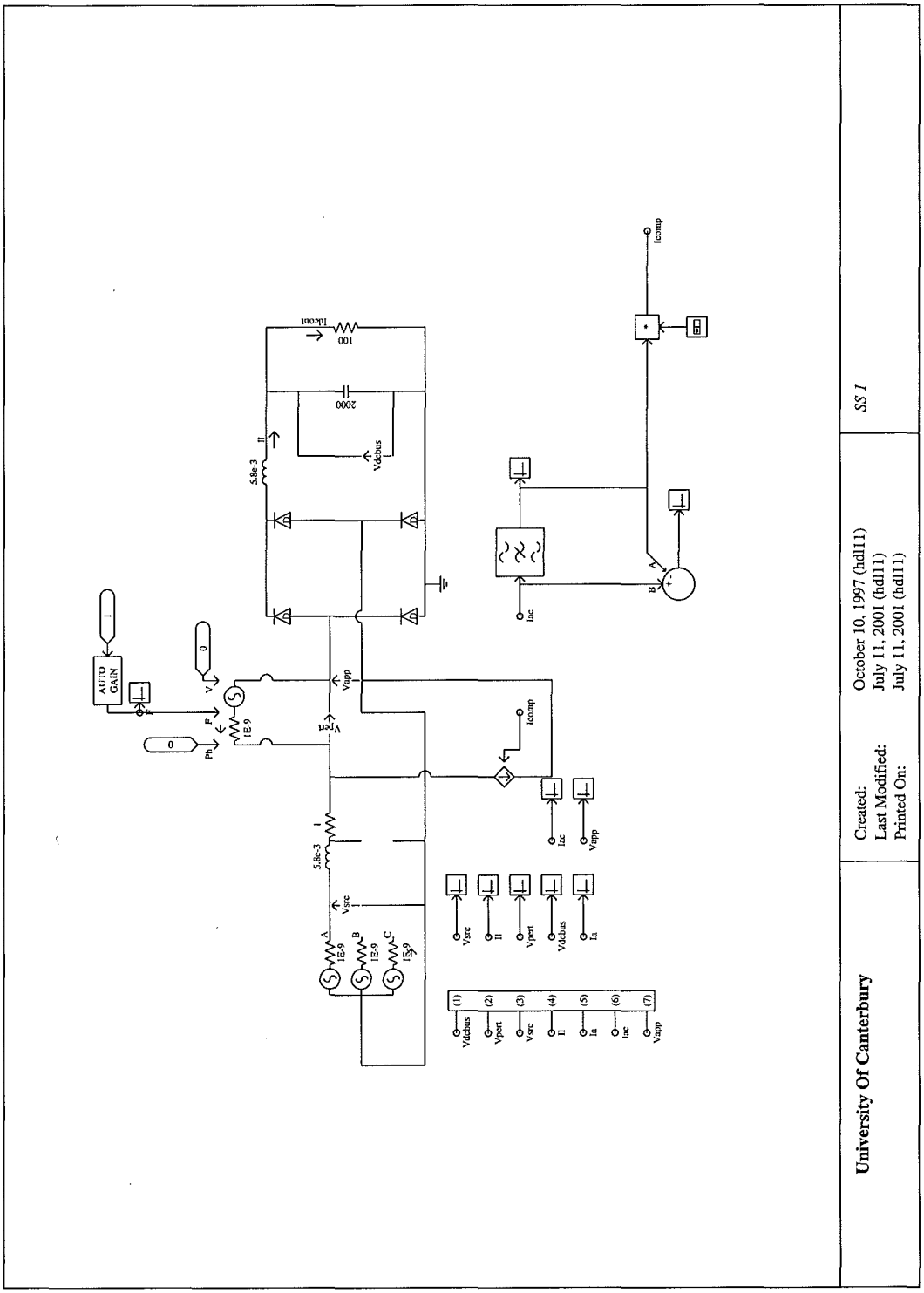

Figure F.2 PSCAD circuit of single-phase rectifier and SAF simulation to show the analysis validity in predicting the effect of the SAF on the load.

Appendix G

AC SYSTEM IMPEDANCE

G.1 MEASURED SYSTEM IMPEDANCE

The system impedance measured with the DSP controlled coverter system is shown in Figure G.1.

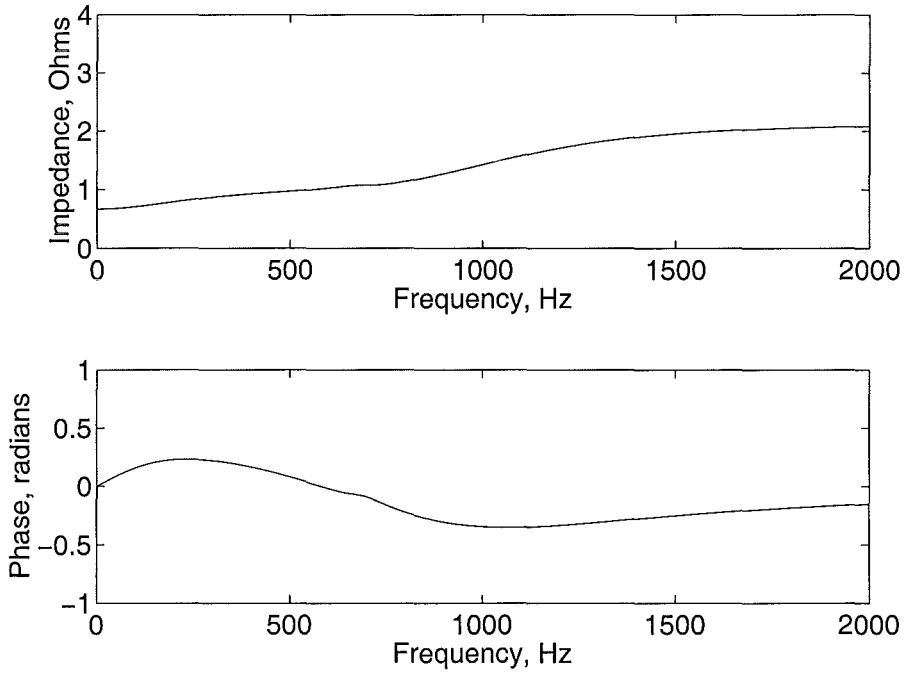

Figure G.1 AC system impedance used in experimental measurements.

G.2 BASE AC VOLTAGE WAVEFORM

The AC system voltage is shown in Figure G.2. This shows the distortion present due to other non-linear loads connected to the network.

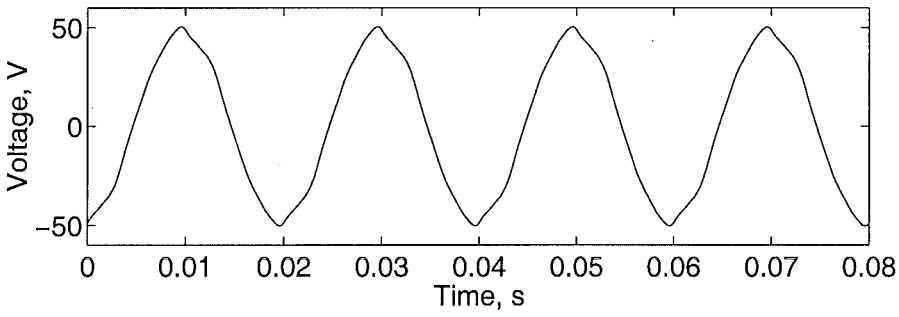

Figure G.2 AC system voltage waveform.

Appendix H

MATRIX ALGEBRA

H.1 INTRODUCTION

Throughout this thesis the component parts of the system are represented with frequency transfer matrices (FTM). The manipulation of matrices to arrive at the identities and results of Chapters 6 and 7 are included here for clarity.

H.2 PERTURBING CURRENT INPUT TO LOAD CURRENT CHANGE

Consider the system block diagram in Figure H.1.

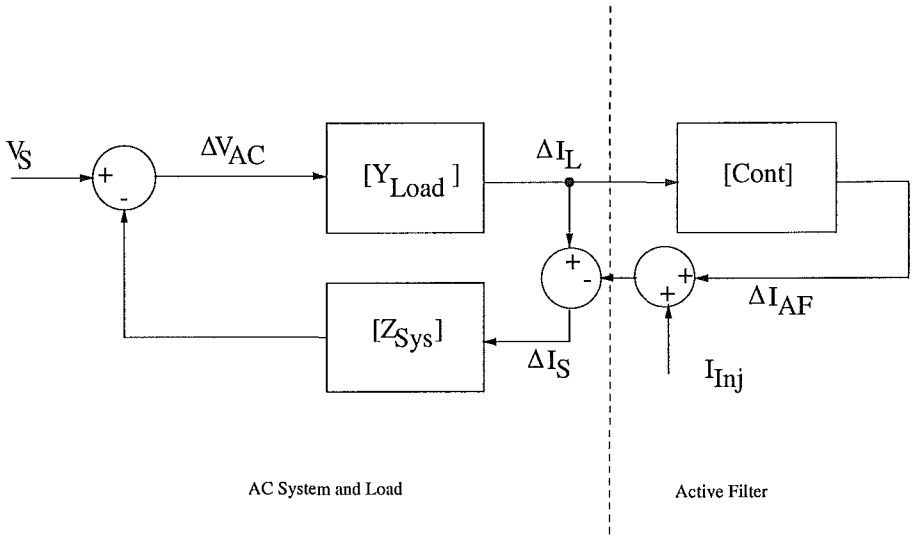

Figure H.1 Active filter small signal block diagram.

Ignoring the Δs for convenience the supply current is given by (H.1).

$$I_S = -I_{Inj} + [\mathbf{I} - \mathbf{Cont}]I_L \tag{H.1}$$

The load current is (H.2)

$$I_L = -[\mathbf{Y_{Load}}][\mathbf{Z_{Sys}}]I_S \tag{H.2}$$

Substituting and rearranging gives (H.3).

$$I_S = -[\mathbf{I} + [\mathbf{I} - \mathbf{Cont}][\mathbf{Y_{Load}}][\mathbf{Z_{Sys}}]]^{-1} I_{Inj} \tag{H.3}$$

The substituting using (H.2) gives equation (H.4).

$$\Delta I_L = [\mathbf{Y_{Load}}][\mathbf{Z_{Sys}}]\,[\mathbf{I} + [\mathbf{I} - \mathbf{Cont}][\mathbf{Y_{Load}}][\mathbf{Z_{Sys}}]]^{-1} I_{Inj} \tag{H.4}$$

This is the transfer from the injected perturbing current to the change in the load current.

H.3 CHANGE IN LOAD CURRENT CAUSED BY SAF OPERATION

Consider again the system Figure H.1. Assume for the moment that $[Cont]$ is zero this being the case when the SAF is not operating. Once again ignoring the Δs for convenience the load current is (H.5).

$$I_L = [Y_{Load}]V_{AC} \tag{H.5}$$

By following round the loop formed by the load admittance and supply impedance and noting that I_S is the same as the load current I_L for no SAF, V_{AC} is found in terms of V_S (H.8.

$$V_{AC} = V_S - [Z_{Sys}]I_S \tag{H.6}$$
$$= V_S - [Z_{Sys}]I_L \tag{H.7}$$
$$= V_S - [Z_{Sys}][Y_{Load}]V_{AC} \tag{H.8}$$

Gathering V_{AC} terms and rearranging gives (H.10

$$(I + [Z_{Sys}][Y_{Load}])V_{AC} = V_S \tag{H.9}$$
$$V_{AC} = (I + [Z_{Sys}][Y_{Load}])^{-1}V_S \tag{H.10}$$

Substituting (H.5) into (H.10) gives (H.11)

$$I_L = [Y_{Load}](I + [Z_{Sys}][Y_{Load}])^{-1}V_S \tag{H.11}$$

When the SAF operates the analysis is the same until (H.10) where $[I - [Cont]]I_L$ is substituted for I_S instead of I_L (H.17).

$$\begin{aligned} V_{AC} &= V_S - [Z_{Sys}]I_S && \text{(H.15)} \\ &= V_S - [Z_{Sys}][I - [Cont]]I_L && \text{(H.16)} \\ &= V_S - [Z_{Sys}][I - [Cont]][Y_{Load}]V_{AC} && \text{(H.17)} \end{aligned}$$

Once again rearranging gives (H.19)

$$\begin{aligned} (I + [Z_{Sys}][Y_{Load}])V_{AC} &= V_S && \text{(H.18)} \\ V_{AC} &= (I + [Z_{Sys}][I - [Cont]][Y_{Load}])^{-1}V_S && \text{(H.19)} \end{aligned}$$

and the load current is therefore (H.20)

$$I_L = [Y_{Load}](I + [Z_{Sys}][I - [Cont]][Y_{Load}])^{-1}V_S \qquad \text{(H.20)}$$

The difference between the two load currents, (H.14) and (H.20), allows the calculation of the change in the load current that SAF operation causes.

REFERENCES

[Abi-Samra *et al.* 1996a]

N. Abi-Samra, A. Sohn, G. Gurlaske, and W. Malcom. Analysis of voltage sags on distribution systems -part 1. *Power Quality Solutions/Alternative Energy*, pp. 45–58, Las Vegas Nevada, 1996.

[Abi-Samra *et al.* 1996b]

N. Abi-Samra, A. Sohn, G. Gurlaske, and W. Malcom. Analysis of voltage sags on distribution systems -part 2. *Power Quality Solutions/Alternative Energy*, pp. 59–72, Las Vegas Nevada, 1996.

[Ainsworth 1967]

J.D. Ainsworth. Harmonic instability between controlled static converters and AC networks. *IEE Proceedings*, vol. 114, no. 7, pp. 949–957, July 1967.

[Akagi *et al.* 1984]

H. Akagi, Y. Kanazawa, and A. Nabae. Instantaneous reactive power compensators comprising switching devices without energy storage. *IEEE Transactions on Industry Applications*, vol. 20, no. 3, pp. 625–630, May 1984.

[Akagi *et al.* 1986]

H. Akagi, A. Nabae, and S. Atoh. Control strategy of active power filters using multiple voltage source PWM converters. *IEEE Transactions on Industry Applications*, vol. 22, no. 3, pp. 460–465, May 1986.

[Akagi 1992]

H. Akagi. Trends in active power line conditioners. *International Conference on Industrial Electronics, Control and Instrumentation*, pp. 19–24, San Diego, USA, November 1992.

[Akagi 1996a]

H. Akagi. New trends in active filters for power conditioning. *IEEE Transactions on Industry Applications*, vol. 32, no. 6, pp. 1312–1322, November 1996.

[Akagi 1996b]

H. Akagi. Performance and modelling of a shunt active filter for installation on

power distribution systems. *International Conference on Harmonics and Quality of Power*, pp. 254–259, Las Vegas, Nevada, USA, October 1996.

[Akagi 1997a]
H. Akagi. Control strategy and site selection of a shunt active filter for damping of harmonic propagation in power distribution systems. *IEEE Transactions on Power Delivery*, vol. 12, pp. 354–363, September 1997.

[Akagi 1997b]
H. Akagi. A shunt active filter based on voltage detection for harmonic damping thoughout a power distridution feeder. *European Power Electronics Conference*, volume 1, pp. 440–446, Trondheim, Norway, September 1997.

[Al-Haddad *et al.* 1999]
K. Al-Haddad, B. Sinngh, and A. Chadra. A review of active filters for power quality improvement. *IEEE Transactions on Industrial Electronics*, vol. 46, no. 5, pp. 960–971, October 1999.

[Aredes and Watanabe 1995]
M. Aredes and E. Watanabe. New control algorithms for series and shunt three-phase four-wire active power filters. *IEEE Transactions on Power Delivery*, vol. 10, no. 3, pp. 1649–1656, July 1995.

[Arrillaga *et al.* 1985]
J. Arrillaga, D.A. Bradley, and P.S. Bodger. *Power System Harmonics.* John Wiley and Sons, Chichester, 1985.

[Arrillaga *et al.* 2000]
J. Arrillaga, M. Bollen, and N. Watson. Power quality following deregulation. *Proceedings of the IEEE*, vol. 88, no. 2, pp. 246–253, February 2000.

[Arthur and Shanahan 1996]
R. Arthur and R. A. Shanahan. Neutral currents in three-phase wye systems. *International Conference on Harmonics and Quality of Power*, pp. 40–47, Las Vegas, Nevada, USA, October 1996.

[Bathurst 1998]
G. Bathurst. *Harmonic Domain Modelling of Power Systems.* Phd thesis, University of Canterbury, Christchurch, New Zealand, March 1998.

[Berizzi *et al.* 1996]
A. Berizzi, A. Silvestri, D. Zaninelli, and A. E. Emanuel. Optimum location of active filters in feeders with uniformly distributed nonlinear loads. *International Conference on Harmonics and Quality of Power*, pp. 637–642, Las Vegas, Nevada, USA, October 1996.

[Bernard 1997]
S. Bernard. Harmonic pollution. *Power Quality Online http://www.powerquality.com/art004/art1.html*, vol. 1, May 1997.

[Bhattacharya *et al.* 1991]
S. Bhattacharya, D.M. Divan, and B. Banerjee. Synchronous frame harmonic isolator. *European Power Electronics Conference*, pp. 3030–3035, Florence, Italy, 1991.

[Bollen *et al.* 1997]
M.H.J. Bollen, T. Tayjasanant, and G. Yalcinkaya. Assessment of the number of voltage sags experienced by a large industrial customer. *IEEE Transactions on Industry Appliactions*, vol. 33, no. 6, pp. 1465–1471, November 1997.

[Bose 1992]
B.K. Bose. Recent advances in power electronics. *IEEE Transactions on Power Electronics*, vol. 7, no. 2, pp. 1–16, January 1992.

[Brigham 1988]
E. O. Brigham. *The Fast Fourier Transform.* Prentice and Hall, Englewood Cliffs, NJ, USA, 1988.

[Brod and Novotny 1985]
D.M. Brod and D.W. Novotny. Current control of VSI-PWM inverters. *IEEE Transactions on Industry Applications*, vol. 21, no. 3, pp. 562–570, May 1985.

[Cavallini and Montanari 1994]
A. Cavallini and G.C. Montanari. Compensation strategies for shunt active-filter control. *IEEE Transactions on Power Electronics*, vol. 9, no. 6, pp. 587–593, November 1994.

[Choe and Park 1988]
G.H. Choe and M.H. Park. A new injection method for AC harmonic elimination by active power filter. *IEEE Transactions on Industrial Electronics*, vol. 35, no. 1, pp. 141–147, January 1988.

[Cuk 1984]
S. Cuk. Survey of switch mode power supplies. *IEE Conference on Power Electronics and Variable Speed Drives*, pp. 83–94, London, UK, May 1984.

[Dommel 1969]
H.W. Dommel. Digital computer simulation of electromagnetic transients in single and multiphase networks. *IEEE Transactions on Power Apparatus and Systems*, vol. 88, no. 4, pp. 388–399, April 1969.

[Duke and Round 1990]

R. M. Duke and S. D. Round. Novel use of a synthetic sinusoid in the measurement of power system harmonics. *Conference on Power Electronics and Motion Control*, volume 2, pp. 368–373, Budapest, Hungary, October 1990.

[Duke and Round 1993]

R.M. Duke and S.D. Round. The steady state performance of a controlled current active filter. *IEEE Transactions on Power Electronics*, vol. 8, no. 3, pp. 140–146, April 1993.

[Duke *et al.* 1990]

R.M. Duke, S.D. Round, and K.C. Henderson. An active filter for current distortion compensation in power systems. *International Conference on Harmonics in Power Systems*, Budapest, Hungary, October 1990.

[Encinas 1989]

J. Encinas. *Phase Locked Loops.* Chapman and Hill, London, UK., 1989.

[Enslin and Van Harmelan 1990]

J.H.R. Enslin and G.L. Van Harmelan. Real-time dynamic control of dynamic power filters in supplies with high contamination. *Twenty First Annual Power Electronics Specilaists Conference*, volume 2, pp. 887–895, San Antonio, Texas, USA, June 1990.

[Grady *et al.* 1990]

W. M. Grady, M. J. Samotyj, and A. H. Noyola. A survey of active power line conditioning methodologies. *IEEE Transactions on Power Delivery*, vol. 5, no. 3, pp. 1536–1542, June 1990.

[Grady *et al.* 1991]

W.M. Grady, M.J. Samotyi, and A.H. Noyola. Minimizing network harmonic voltage distortion with an active power line conditioner. *IEEE Transactions on Power Delivery*, vol. 6, no. 4, pp. 1690–1697, October 1991.

[Hafner *et al.* 1997]

J. Hafner, M. Aredes, and K. Heumann. A shunt active filter applied to high voltage distribution lines. *IEEE Transactions on Power Delivery*, vol. 12, no. 1, pp. 266–272, January 1997.

[Heydt 1991]

G.T. Heydt. *Electric Power Quality.* Stars in a Circle Publications, West Lafayette, Indiana, USA, 1991.

[Horn *et al.* 1996]

A. Horn, L.A. Pittoriono, and J.H.R. Enslin. Evaluation of active power filter control algorithms under non-sinusoidal and unbalanced conduitions. *7th International*

Conference on Harmonics and Quality of Power, pp. 217–224, Las Vegas, Nevada, October 1996.

[IEC 1995]
IEC. *EMC. Part 3.2 Limits for harmonic current emissions (Equipment less than or equal to 16A per phase).* International Electrotechnical Committee, 1995.

[IEEE 1983]
IEEE. Working group on power system harmonics: Power system harmonics: an overview. *IEEE Transactions on Power Apparatus and Systems*, vol. 102, no. 8, pp. 2455–2460, August 1983.

[IEEE 1992]
IEEE. *IEEE Recomended practices and requirements for harmonic control in electric power systems.* Institute of Electrical and Electronic Engineers, 1992.

[Ingram and Round 1999]
D.M.E. Ingram and S.D. Round. A fully controlled digital hysteresis controller for an active power filter. *International Journal of Electronics*, vol. 86, no. 10, pp. 1217–1232, 1999.

[Ingram 1998]
D. M. E. I. Ingram. An evaluation of harmonic isolation techniques for three-phase active filtering. Masters thesis, University of Canterbury, Christchurch, New Zealand, March 1998.

[Jalali and Lasseter 1994]
S. G. Jalali and R.H. Lasseter. A study of nonlinear harmonic interaction between a single-phase line commutated converter and a power system. *IEEE Transactions on Power Delivery*, vol. 9, no. 3, pp. 1616–1624, July 1994.

[Kazmierkowski and Dzieniakowski 1994]
M.P. Kazmierkowski and M.A. Dzieniakowski. Review of current regulation techniques for three phase pwm inverters. *International Confernence on Industrial Electronics, Control and Instrumentation*, pp. 567–574, Bologna, Italy, 1994.

[Kazmierkowski and Malesani 1999]
M.P. Kazmierkowski and L. Malesani. Guest editorial. *IEEE Transactions on Industrial Electronics*, vol. 45, no. 5, p. 689, October 1999.

[Koval and Hughes 1997]
D.O. Koval and M.B. Hughes. Canadian national power quality survey: Frequency of industrial and commercial voltage sags. *IEEE Transactions on Industry Applications*, vol. 33, no. 3, pp. 622–627, May 1997.

[Kwon *et al.* 1999]

B.H. Kwon, B.D. Min, and J.H. Youm. An improved space-vector-base hysteresis current controller. *IEEE Transactions on Industrial Electronics*, vol. 45, no. 5, pp. 752–760, October 1999.

[Lai and Key 1997]

J. Lai and T.S. Key. Effectiveness of harmonic mitigation equipment for commercial office buildings. *IEEE Transactions on Industry Applications*, vol. 33, no. 4, pp. 1104–1110, July 1997.

[Laird *et al.* 2000]

H. D. Laird, S. D. Round, and R. M. Duke. A frequency domain model of an uncontrolled single-phase voltage source rectifier. *IEEE Transactions on Industrial Electronics.*, vol. 47, no. 3, pp. 525–532, June 2000.

[Larson *et al.* 1989]

E.V. Larson, D.H. Baker, and J.C. McIver. Low order harmonic interaction on AC/DC systems. *IEEE Transactions on Power Delivery*, vol. 4, no. 1, pp. 493–501, January 1989.

[Linder *et al.* 1997]

S. Linder, S. Klaka, M. Frecker, E. Carrol, and H. Zeller. A new range of reverse conducting gate commutated thyristors for high-voltage medium power applications. *European Power Electronics Conference*, volume 1, pp. 1.117–1.124, Trondheim, Norway, 1997.

[Luor 2000]

T.S. Luor. Influence of load characteristics on the application of passive and active harmonic filters. *Ninth International Conference on Harmonics and Quality of Power*, pp. 128–133, Orlando, Florida, USA, October 2000.

[Malesani *et al.* 1988]

L. Malesani, P. Mattavelli, and S. Buso. On the application of active filters to generic loads. *Eigtht International Conference on Harmonics and Quality of Power*, pp. 310–319, Athens, Greece, October 1988.

[McEachern *et al.* 1995]

A. McEachern, W. M. Grady, W. A. Moncrief, G.T. Heydt, and M. McGranaghan. Revenue and harmonics: An evaluation of some proposed rate structures. *IEEE Transactions on Power Delivery*, vol. 10, no. 1, pp. 474–481, January 1995.

[Michaels 1997]

K.M. Michaels. Sensible approaches to diagnosing power quality problems. *IEEE Transactions on Industry Appliactions*, vol. 33, no. 4, pp. 1125–1130, July 1997.

[Mollerstedt and Berhardsson 2000]
E. Mollerstedt and B. Berhardsson. A harmonic transfer function model for a diode converter train. *IEEE PES Winter Meeting*, Singapore, January 2000.

[Moran *et al.* 1995]
L.A. Moran, J.W. Dixon, and R.R. Wallace. A three-phase active power filter operating with fixed switching frequency for reactive power and current harmonic compensation. *IEEE Transactions on Industrial Applications*, vol. 42, no. 4, pp. 402–408, 1995.

[Nagrath and Gopal 1982]
I.J. Nagrath and M. Gopal. *Control systems engineering.* John Wiley and Sons, Chichester, UK, 1982.

[Osauskas and Wood 2001]
C.M.O. Osauskas and A.R. Wood. A small signal model of an HVDC converter. Accepted for publication in IEE Proceedings on Generation, Tramssion and Distributionisn April, 2001.

[Palethorpe *et al.* 2000]
B. Palethorpe, M. Sumner, and D.W.P Thomas. Power system impedance measurement using a power electronic converter. *Ninth International Conference on Harmonics and Quality of Power*, pp. 208–213, Orlando, Florida, USA, October 2000.

[Peng and Lai 1996]
F. Z. Peng and J. S. Lai. Application considerations and compensation characteristics of shunt active and series active filters in power systems. *International Conference on Harmonics and Quality of Power*, pp. 12–20, Las Vegas, Nevada, USA, 1996.

[Quinn *et al.* 1993]
C.A. Quinn, Mohan N, and H.A. Mehta. A four wire, current-controlled converter provides harmonic neutralisation in three phase, four wire systems. *Applied Power Electronics Conference*, pp. 829–836, San Diego, California, USA, 1993.

[Ramirez 1985]
R.W. Ramirez. *The FFT Fundamentals and Concepts.* Prentice and Hall, Englewood Cliffs, NJ, USA., 1985.

[Redl *et al.* 1996]
R. Redl, P. Tenti, and J.D. van Wyk. Power electronics polluting effect. *IEEE Spectrum*, vol. 34, no. 5, pp. 161–177, May 1996.

[Round and Ingram 1997]

S. D. Round and D. M. E. Ingram. An evaluation of techniques for determining active filter compensating currents in unbalanced systems. *European Power Electronics Conference*, volume 4, pp. 4.767–4.772, Trondheim, Norway, September 1997.

[Round *et al.* 1998a]

S. D. Round, H. D. Laird, R. M. Duke, and Tuck C. An improved three level shunt active filter. *International Conference on Power Electronics Drives and Energy Systems for Industrial Growth*, pp. 12–20, Perth, Western Australia, December 1998.

[Round *et al.* 1998b]

S. D. Round, H. D. Laird, R. M. Duke, and A. Gardiner. The steady state and transient performance of a shunt active filter using measured site data. *International Conference on Harmonics and Quality of Power*, pp. 395–400, Athens, Greece, October 1998.

[Round 1992]

S.D. Round. *Real time optimisation of an active filter's performance and application to the power system.* Phd thesis, University of Canterbury, Christchurch, New Zealand, September 1992.

[Sakui and Fujita 1994]

M. Sakui and H. Fujita. An analytic method for calculating harmonic currents of a three-phase diode-bridge rectifier with DC filter. *IEEE Transactions on Power Electronics*, vol. 9, no. 6, pp. 631–637, November 1994.

[Sasaki and Machida 1971]

H. Sasaki and T. Machida. A new method to eliminate AC harmonic currents by magnetic flux compensation - considerations on basic designs. *IEEE Transactions on Power Apparatus and Systems*, vol. 90, no. 5, pp. 2009–2019, September 1971.

[Sato *et al.* 2000]

Y. Sato, T. Kawase, M. Akiyama, and T. Kataoka. A control strategy for general purpose active filters based on voltage detection. *IEEE Transactions on Industry Applications*, vol. 36, no. 5, pp. 1405–1412, September 2000.

[Shaughnessy 1997]

T. Shaughnessy. Power factor, harmonics and harmonic filters. *IEEE Transactions on Power Apparatus and Systems*, vol. 90, pp. 2009–2019, June 1997.

[Siebert 1986]

W.M. Siebert. *Circuits, Signals and Systems.* MIT Press, Cambridge, Massachusetts, USA, 1986.

[Smith *et al.* 1998]

B. C. Smith, N. R. Watson, A. R. Wood, and J. Arrillaga. Harmonic tensor linearistion of HVDC converters. *IEEE Transactions on Power Delivery*, vol. 13, no. 4, pp. 1244–1250, October 1998.

[Sonnenschein *et al.* 1996]

M. Sonnenschein, M. Weinhold, and R. Zurowski. Shunt-connected power conditioner for improvement of power quality in distribution networks. *International Conference on Harmonics and Quality of Power*, pp. 27–32, Las Vegas, Nevada, USA, October 1996.

[Srianthumrong and Sangwongwanich 1988]

S. Srianthumrong and S. Sangwongwanich. An active power filter with harmonic detection method based on recursive DFT. *International Conference on Harmonics and Quality of Power*, pp. 127–132, Athens, Greece, October 1988.

[Staudt 1996]

V. Staudt. Dynamic parallel compensation of active non-linear loads using the FBD-method. *International Conference on Harmonics and Quality of Power*, pp. 21–26, Las Vegas, Nevada, USA, October 1996.

[Stefani *et al.* 1994]

R. Stefani, C. Savant, B. Shahian, and G. Hostetter. *Feedback Control Systems.* Saunders College Publishing, 1994.

[Sullivan *et al.* 1997]

M. J. Sullivan, T. Vardell, and M. Johnson. Power interuption costs to industrial and commercial consumers of electricity. *IEEE Transactions on Industry Applications*, vol. 33, no. 6, pp. 1448–1458, November 1997.

[Swcharz *et al.* 1966]

M. Swcharz, W.R. Bennet, and S. Stein. *Communications Systems and Techniques.* McGraw Hill., Chichester, 1966.

[Talacek and Watson 1999]

P. Talacek and N.R. Watson. Valuation of harmonic injections. Accepted for publication in IEEE Transactions on Power Systems, April 1999.

[Texas Instruments 1989]

Texas Instruments. *Digital Signal Processing Applications with the TMS320 Family.* Texas Instruments, Houston, Texas, 1989.

[Texas Instruments 1994]

Texas Instruments. *TMS320C30 User's Guide.* Texas Instruments, Houston, Texas, 1994.

[Todd *et al.* 1997]
S. Todd, A. R. Wood, and P. S. Bodger. An s-domain model of an HVDC converter. *IEEE Transactions on Power Delivery*, vol. 12, no. 4, pp. 1723–1729, October 1997.

[Verdelho and Marques 1999]
P. Verdelho and G.D. Marques. Four-wire current-regulated PWM voltage converter. *IEEE Transactions on Industrial Electronics*, vol. 45, no. 5, pp. 761–770, October 1999.

[Verghese and Mukherji 1981]
G. Verghese and U. Mukherji. Extended averaging and control proceedures. *Power Electronics Specialists Conference*, pp. 329–336, Boulder, Colorado, USA, June 1981.

[Watanabe *et al.* 1993]
E. Watanabe, R. Stephan, and M. Aredes. New concepts of instantaneous active and reactive powers in electrical systems with generic loads. *IEEE Transactions on Power Delivery*, vol. 8, no. 2, pp. 697–703, April 1993.

[Williams and Hoft 1991]
S.M. Williams and R.G. Hoft. Implementation of current source inverter for power line conditioning. *IEEE Transactions on Industry Applications*, vol. 27, no. 4, pp. 773–779, August 1991.

[Wood and Arrillaga 1995]
A.R. Wood and J. Arrillaga. HVDC convertor waveform distortion: A frequency domain approach. *IEE Proceedings on Generation, Transmission and Distribution*, vol. 142, no. 1, pp. 88–96, January 1995.

[Wood *et al.* 1998]
A.R. Wood, D.J. Hume, and J. Arrillaga. Cross modulation of harmonics in HVDC schemes. Technical Report W.G 14-25, CIGRE, 1998.

[Wood 1993]
A Wood. *An Analysis of Non-Ideal HVDC Convertor Behaviour in the Frequency Domain, and A New Control Proposal.* Phd thesis, Canterbury University, Christchurch, New Zealand, November 1993.

[Xilinx Corporation 1998]
Xilinx Corporation. *The Programmable Logic Book.* Xilinx, 1998.